EXPERIMENTAL STUDIES OF ION-NEUTRAL CHEMISTRY RELATED TO THE EXTRATERRESTRIAL ENVIRONMENT

A Thesis
Presented for the Degree
of Doctor of Philosophy in Chemistry
In the
University of Canterbury

by
Samuel Joseph Edwards

University of Canterbury
2009

TABLE OF CONTENTS

Title Page i
Table of Contents ii
Acknowledgements vi
List of Figures viii
List of Tables xi
Abstract xiii

1. Introduction. 1
1.1. The Occurrence of Ions in Terrestrial and Extraterrestrial Environments. 1
1.2. The Interstellar Medium. 1
1.2.1. The Composition of Interstellar Clouds (ISCs). 2
1.2.2 The Origin of Molecules in ISCs. 4
1.2.3 Ion-neutral Reactions. 5
1.2.4 Dust Grain Chemistry. 8
1.2.5 Modeling ISCs. 10
1.3. Titan. 12
1.3.1. The *Voyager* 1 Mission to Saturn and Titan. 13
1.3.2. Chemistry in the Atmosphere. 17
1.3.3. Models of Titan's Atmosphere. 20
1.3.4. The *Cassini* Mission. 24
1.4. Instrumentation. 27
1.5. Ion-molecule Collision Theory. 29
1.6. Introduction to Current Research. 29

2. Experimental. 32
2.1. Introduction. 32
2.2. The SIFT Instrument. 32
2.2.1. Introduction. 34
2.2.2. The Flowing Afterglow Ion Source. 34
2.2.3. The Ion Selection Region. 36
2.2.4. The Venturi. 38
2.2.5. The Flow Tube. 40
2.2.6. The Analysis and Counting Region. 42
2.3. Ancillary Systems. 44
2.3.1. Helium Gas Flow System. 44
2.3.2. The Glass Gas Handling Line. 44
2.3.3. SIFT Protection Circuitry. 45
2.4. SIFT Kinetics. 46
2.4.1. Theory. 46
2.4.2. Carrier gas and ion velocity. 47
2.4.3. The Practical Measurement of Rate Coefficients. 47
2.4.4. Mass Discrimination and Diffusion Enhancement. 50

2.5. Reagents and Physical Conditions. 52

3. Attempts to Generate Atomic Carbon for Reaction. 54
3.1. Introduction. 54
3.2. $C + H_3^+$ - A Key Reaction in Interstellar Space. 56
3.3. The Study of Ion-Atom Reactions. 57
3.4. Generating Atomic Species and Establishing their Concentration in the Gas Phase. 58
3.5. Atom Recombination. 59
3.6. Methods which can be used to Generate Atomic Carbon. 60
3.7. The Detection of Atomic Carbon. 62
3.7.1. Introduction. 62
3.7.2. Generating H_3^+ in the SIFT. 63
3.7.3. $C_6H_6^+$ as a Monitor Ion for Atomic Carbon. 64
3.8. The Design of the Carbon Atom Source. 65
3.8.1. Introduction. 65
3.8.2. Operation. 65
3.8.3. Early Modifications. 67
3.8.4. Experiments and Results. 67
3.8.5. Alternative Detection Methods. 71
3.9. Radio Frequency Discharge. 71
3.9.1. RF Experiments. 72
3.10. Carbon Suboxide. 72
3.10.1. Carbon Suboxide as a Source of Carbon Atoms. 72
3.10.2. Carbon Suboxide Synthesis. 73
3.10.3. Results of Carbon Suboxide Experiments. 74
3.11. Summary of Discharge Work. 75
3.12. Photolysis Experiments. 75
3.12.1. VUV Flash Photolysis. 75
3.12.2. Laser Photolysis. 76
3.13. Conclusions. 80

4. Cyanodiacetylene – HC_5N. 82
4.1. Introduction. 82
4.2. Experimental. 85
4.2.1. The Preparation of HC_5N. 85
4.2.2. Characterization of HC_5N Preparation Products. 86
4.2.3. Other Experimental Details. 89
4.3. Results. 89
4.4. Discussion. 92
4.4.1. Ion Chemistry. 92
4.4.2. The Proton Affinity of HC_5N. 94
4.5. Conclusion. 95

5. Methylenimine and Propionitrile. 97
5.1. Introduction. 97

5.1.1. Results of the *Cassini-Huygens* Mission. 97
5.1.2. Methylenimine - CH_2NH. 99
5.1.3. Propionitrile – C_2H_5CN. 100
5.1.4. Summary. 101
5.2. Experimental. 101
5.2.1. The Generation of Methylenimine. 103
5.3. Results. 105
5.4. Discussion. 109
5.4.1. Methylamine. 109
5.4.2. Methylenimine. 109
5.4.3. The Estimation of Relative Rates for Methylenimine. 110
5.4.4. Propionitrile. 112
5.5. Conclusion. 113

6. Minor Projects. 115
6.1. $C_3H_3^+$. 115
6.1.1. Experimental. 116
6.1.2. Results and Discussion. 117
6.1.3. Summary. 118
6.2. Proton Affinities. 118
6.2.1. Introduction. 118
6.2.2. Experimental. 122
6.2.3. Results and Discussion. 123
6.2.4. Conclusions. 125
6.3. Miscellaneous Ion-Molecule Reactions. 125
6.3.1. Introduction. 125
6.3.2. Experimental. 126
6.3.3. Results and Discussion. 126
6.3.4. Summary. 128

7. Lithium Ion Chemistry. 129
7.1. SIFT-MS and the Quantitation of Analytes. 129
7.2. Experimental. 132
7.2.1. Lithium Ion Source 132
7.3. Results and Discussion. 135
7.4. The Reactivity of $Li^+.X$ in the Presence of H_2O. 137
7.5. The Suitability of Li^+ as a SIFT-MS Reagent. 142

8. LabVIEW. 145
8.1. Introduction. 145
8.2. The Operation of *Sift for Windows*. 146
8.2.1. Mass Spectra. 146
8.2.2. Rate Coefficient Determination. 147
8.3. Experimental. 151
8.4. Program Development. 155
8.4.1. DAQ Considerations. 155

8.4.2. Operation of the Mass Scanner. 157
8.4.3. The Measurement of Kinetics. 160
8.5. A Summary of the New Software. 163

9. **Conclusion.** 165
9.1. Summary of Results. 165
9.1.1. Atomic Carbon. 165
9.1.2. Titan's Ion Chemistry. 166
9.1.3. Other Topics. 168
9.2. Suggestions for Further Work. 169

References 172

ACKNOWLEDGEMENTS

It is an inescapable fact that although this thesis is my own work it could never have been completed without the help of others. The brevity of the acknowledgement given below to those who have helped me should not be construed as a lack of gratitude. I am indebted to many people for their help during the four years of my Ph.D and my Honours year before that.

Firstly I must thank my academic supervisors: Professor Murray McEwan, Dr Colin Freeman and Dr Paul Wilson.

I feel fortunate to have had Murray as my principal advisor during my PhD and my Honours year before that. Murray has been a source of endless information and advice. Perhaps the greatest asset to my work has been Murray's relentless optimism. I began this work knowing that experimental science can be fickle and that patience and perseverance were important if any success was to be had. Murray's optimism (particularly with respect to the atomic carbon project) has been a great source of motivation throughout my PhD.

Next I must thank Colin for the encouragement and for always being available to help. I always enjoyed the lengthy discussions (usually about sporting events) which extended many of my lunch hours beyond reasonable limits, bringing home time that little bit closer. I am most indebted to Colin for proof-reading this book (although apparently he accepts no liability for any of the errors within).

I should also thank Colin and Murray for inviting me to Tuesday morning badminton. This was always a pleasant start to the day and is something I will miss.

Special credit must go to Dr Wilson for teaching me so many valuable lessons during my Honours year and the first two years of my PhD, including laboratory 'best practice'; where to find the best games on the internet; and lastly but most usefully how to operate and maintain the SIFT. Paul's sardonic wit was always in plentiful supply when my experiments were unsuccessful. In spite of this Paul invariably provided the solutions to even the most insoluble experimental problems and for this I am thankful. Your accumulated knowledge was greatly missed when you moved to Syft Technologies but I am grateful that your advice was always available by phone or email.

I must also thank the other staff at Syft who have helped me directly during this thesis: Dr Daniel Milligan, Dr Barry Prince and Dr Greg Francis.

I am indebted to the chemistry department's technical staff without whom none of the experiments outlined in this thesis would have been possible. In no particular order, thanks to: Rob, Wayne, Danny, Nick, Sandy, Roger, Steve and Russell.

Thank you to the Tertiary Education Commission for the provision of a Doctoral Scholarship during the first three years of my PhD.

I would like to thank Mum and Dad for providing food and shelter for the past year or so and for the constant encouragement throughout my University studies. I would not have got this far without your support. Thanks to Granny and Granddad for letting me park in your driveway for the past six or so years (since the University began charging for parking). This has certainly saved me a few long walks. Thanks for the sultana pasties too. I must also thank my sister Jean for showing the way for so many years. Finally, thanks to Julia for the support and for waiting so patiently for me to finish. I really appreciate it.

LIST OF FIGURES

1.1. The small molecular cloud Barnard 68 (B68) is sufficiently dense to extinguish background starlight. 2

1.2. Layers of haze in Titan's atmosphere give the moon its characteristic orange colour. 13

1.3. Images of Titan's surface taken in the near IR by the Hubble Space Telescope show an irregular surface. 14

1.4. IR emission spectrum from Titan recorded by the IRIS instrument aboard the *Voyager* 1 spacecraft. 15

1.5. Temperature and density profile of Titan's atmosphere constructed from the results of the *Voyager* mission. 16

1.6. An artist's impression of the *Huygens Probe* detaching from the *Cassini Orbiter* above Titan, with Saturn in the background. 25

1.7. Mass spectrum of Titan's upper atmosphere as recorded by the *Cassini* INMS. 27

1.8. Schematic diagram of a typical flowing afterglow apparatus. 28

2.1. Schematic diagram of the University of Canterbury Selected Ion Flow Tube (SIFT). 33

2.2. The microwave discharge ion source in operation. 35

2.3. Bird's-eye view of ion selection region. 37

2.4. A schematic diagram of the Venturi injector. 39

2.5. The SIFT Flow Tube. 40

2.6. The neutral inlet assembly. 41

2.7. Four of the SIFT's backing pumps located in the pump room. 43

2.8. Mass scan demonstrating the reaction of H_3O^+ (m/z 19) precursor ions with HC_5N which generates HC_5NH^+ (m/z 76). 48

2.9. Semi-logarithmic decay of lithium ion signal with increasing acetylene flow showing corresponding increase of product ions. 49

2.10. Extrapolation of product ion signals as a percentage of total product ions to zero neutral flow confirms $Li^+.C_2H_2$ as the true primary product of the reaction. 50

2.11. A typical plot obtained from a mass discrimination experiment with the UC SIFT. 52

3.1. The design of the first generation carbon atom source. 66

3.2. Second generation carbon atom source made entirely of Pyrex. 68

3.3. The third generation carbon atom source was adapted from the second generation source to allow the microwave discharge to be positioned closer to the flow tube. 69

3.4. Typical mass spectrum showing evidence of O atoms but not C atoms. 70

3.5. Schematic diagram of the equipment designed to examine the laser photolysis of carbon suboxide. 77

4.1. Chemical ionization spectrum generated from reaction of the products collected at -78 º C with H_3O^+. 87

4.2. Chemical ionization spectrum generated from reaction of the products collected at -78 º C with O_2^+. 87

4.3. Chemical ionization spectrum generated from the reaction of HC_5N collected at -30 º C with H_3O^+. 88

4.4. Chemical ionization spectrum generated from the reaction of HC_5N collected at -30 º C with O_2^+. 88

5.1 Ion mass spectra recorded by the *Cassini* spacecraft in Titan's upper atmosphere taken from reference [44]. 98

5.2. Mass spectrum illustrating the reaction of methylenimine (in the presence of methylamine) with $HCNH^+$. 111

5.3. Mass spectrum illustrating the reaction of pure methylamine with $HCNH^+$. 111

7.1. Lithium ion source based on thermionic emission from a coated filament. 133
7.2. A mineral sample of lithium β-eucryptite in a quartz matrix. 133
7.3. Typical emission spectrum obtained from a filament coated with lithium β-eucryptite illustrating the presence of other alkali metal ions in the mineral sample. 134
7.4. Product mass spectrum for the reaction of Li^+ with acetylene showing secondary clustering. 138

8.1. A mass spectrum recorded by *Sift for Windows* for the reaction between H_3O^+ (m/z 19) and C_2H_5CN generating $C_2H_5CNH^+$ (m/z 56). 147
8.2. The first panel of data displayed by *Sift for Windows* during a rate coefficient measurement is a semi-logarithmic plot of ion signal against neutral flow. 149
8.3. The second panel displays a plot of the product ion ratios at each neutral flow. 150
8.4. The third panel provides a summary of the data collected, the experimental conditions and the calculated results. 151
8.5. The SCB-68 connector block with four input/output wires connected. 152
8.6. Front panel as seen in the LabVIEW development environment. 153
8.7. Block Diagram as seen in the LabVIEW development environment. 154
8.8. User inputs required to initiate the measurement of a mass spectrum. 157
8.9. The GUI of the mass spectrum function. 158
8.10. Mass spectrum obtained with the new LabVIEW software. 159
8.11. Correlation between nominal ion position measured by the LabVIEW program and the expected ion mass. 160
8.12. The control panel for a kinetics experiment. 161
8.13. The GUI of the rate coefficient program. 162

LIST OF TABLES

1.1. The abundance of some atomic and molecular species relative to the total abundance of H nuclei in the direction of the diffuse cloud ζOpiuchi. 3

1.2. Typical fractional abundance of selected molecules in dense ISCs relative to $H_2 = 1$. 4

1.3. Volume mixing ratios in Titan's stratosphere for some key molecules observed by Voyager 1 [21]. 15

2.1. Typical regional standard operating pressures for the SIFT in Torr. 53

4.1. A summary of the reactivity of HC_5N with ions having a transferable proton. 90

4.2. A summary of the reactivity of HC_5N with ions without a transferable proton. 91

4.3. Trends in reaction chemistry for C^+ with cyanopolyynes. 93

4.4. Trends in reaction chemistry for N^+ with cyanopolyynes. 94

4.5. Neutrals employed to investigate the proton affinity of HC_5N. 95

5.1. The reactivity of methylamine, CH_3NH_2, with selected ions. 106

5.2. The reactivity of methylenimine, CH_2NH, with selected ions. 107

5.3. The reactivity of propionitrile, C_2H_5CN, with selected ions. 108

6.1. Ion-molecule reactions occurring in the atmosphere of Titan of which $C_3H_3^+$ is a product. 116

6.2. The reactivity of selected hydrocarbon and nitrile species with ions important to the chemistry of Titan. 127

7.1. Measured pseudo-bimolecular rate coefficients for the association of Li^+ with the given reactant at 294 K. 136

7.2. Li^+.X bond dissociation energies (for the loss of one ligand) for $Li^+.(H_2O)_n$ and a selection of Li^+.X products from Table 7.1. 139

ABSTRACT

Kinetic data is presented for a variety of ion-neutral reactions which are relevant to the atmosphere of Titan and to the chemistry occurring in interstellar clouds. The data were recorded with a Selected Ion Flow Tube (SIFT) operating at room temperature (294 ± 4 K) and at a pressure of 0.46 Torr.

Results of the recent *Cassini-Huygens* mission to Saturn and Titan have identified several species in the atmosphere of Titan not predicted by pre-*Cassini* models of the atmosphere. In order to determine the fate of three of these species (methylenimine, propionitrile and cyanodiacetylene) in Titan's ionosphere, their reactivity with the principal ions in Titan's upper ionosphere has been examined. As expected, collision rate proton transfer reactions dominate the chemistry with association channels also observed with many of the hydrocarbon ions. The results of the *Cassini* mission also identified several individual reactions as being of potential importance to models of Titan's atmosphere and this chemistry has also been examined. The above studies are also relevant to the interstellar medium where each of the neutral reactants have also been detected.

The results of some proton transfer equilibrium studies are also presented. The gas phase basicities of propyne and acetylene have been determined to be 681 kJ mol^{-1} and 617.4 kJ mol^{-1} respectively. Their relative proton affinities can be estimated from these values. A combined experimental/theoretical study of the proton affinity of cyanodiacetylene (HC_5N) has enabled this value to be estimated at 770 ± 20 kJ mol^{-1}.

Details of an attempt to complete the first laboratory measurement of the crucial reaction between H_3^+ and atomic carbon are presented. The generation of atomic carbon in sufficient quantities for reaction in the SIFT was not possible with the microwave discharge source used. Other generation methods have also been explored with the laser photolysis of carbon suboxide expected to provide a possible solution to the problems encountered.

The results of an investigation into the applicability of lithium ions (Li^+) to SIFT-MS are presented. The lithium ions associated with each of the twenty-one neutral analytes examined to form pseudo-molecular ions. The association reactions were rapid

($k \sim 10^{-9}$ cm^3 s^{-1}) for large hydrocarbons but were much slower for smaller analytes ($k < 10^{-11}$ cm^3 s^{-1}). In order to clarify some unusual experimental observations, the effect of water molecules on the observed chemistry has been examined in detail. The measured chemistry has important consequences for the applicability of Li^+ to SIFT-MS where the presence and detection of an identifiable ion of the analyte is essential.

Details of new SIFT operating software which can be run on a modern computer are given. Mass spectra and kinetic data recorded with the new software are also presented.

CHAPTER 1.

INTRODUCTION

1.1 The Occurrence of Ions in Terrestrial and Extraterrestrial Environments

The interaction of ions with neutral molecules is evident in countless chemical environments on Earth including oceans, flames and in living systems. Ions are very useful entities. Without Earth's ionosphere (the region of the upper atmosphere where neutral molecules are ionised by solar UV radiation) short wavelength radio waves could not be transmitted across the globe. The development of a rocket-borne mass spectrometer by Johnson *et al*. in 1958 provided the first *in situ* measurement of Earth's ionosphere and identified the true nature of the environment [1]. The chemistry in Earth's upper atmosphere, which is dominated by bimolecular positive ion-molecule reactions, is now well understood [2]. Inspired by this work and seeking further challenges, scientists subsequently turned their interest to the role of ions in planetary atmospheres and interstellar space. In the following decades the critical role of ions in molecule synthesis in extraterrestrial planetary atmospheres and in the interstellar medium has been revealed.

1.2 The Interstellar Medium

Interstellar space is an apt description of the immense regions between stars in our galaxy as the vast majority of mass in our galaxy is concentrated in stars. Even though particle densities are very low, the size of the interstellar medium (ISM) means that it actually contains a considerable quantity of gas and dust particles. In some regions these particles are agglomerated into what are known as interstellar clouds (ISCs). ISCs have much higher gas and particle densities than the rest of the ISM. Usually invisible to the

eye, some clouds are sufficiently large (they can be many light years across) and dense to extinguish all visible background starlight. An example is shown in Figure 1.1.

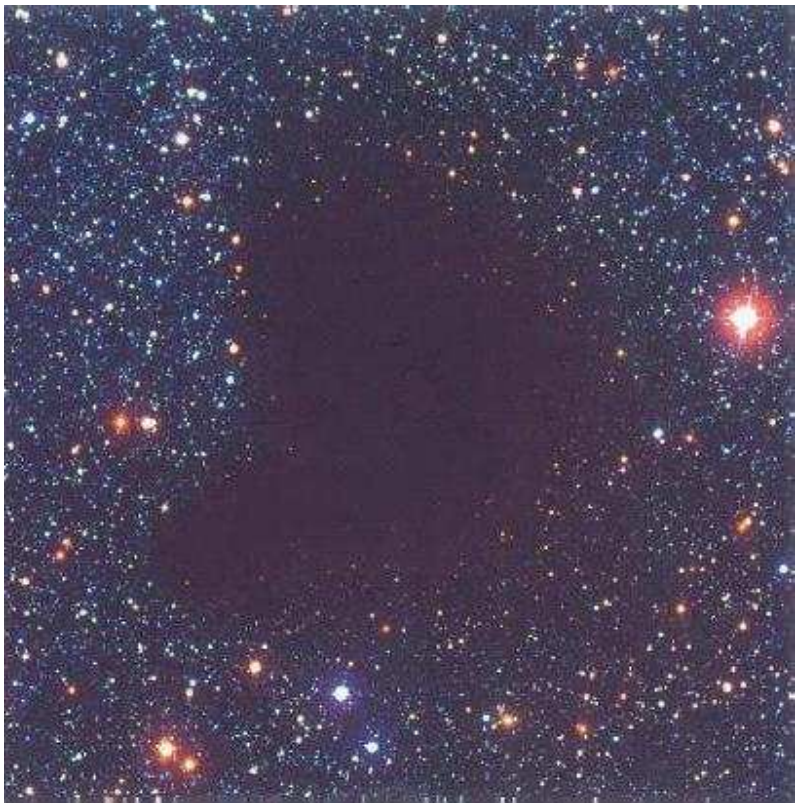

Figure 1.1. *The small molecular cloud Barnard 68 (B68) is sufficiently dense to extinguish background starlight. ISCs such as B68 are of interest to astronomers because they are the birthplace of stars.*

1.2.1 The Composition of Interstellar Clouds (ISCs)

There are two types of interstellar cloud. Although both are classified by their (averaged) physical characteristics it should be noted that ISCs are largely inhomogeneous. **Diffuse** interstellar clouds have gas densities between 10^1 and 10^3 cm^{-3} and have internal temperatures between 50 and 100 K. **Dense** clouds have higher gas densities of 10^3 to 10^6 cm^{-3} and are cooler than diffuse clouds with temperatures usually between 10 and 50 K. These definitions vary slightly in the literature and it is common to refer to clouds having attributes intermediate between these as *translucent* to avoid confusion.

In the late 1930s the diatomic molecules CH, CN and CH^+ were unexpectedly discovered in diffuse ISCs [3]. Their detection was surprising because interstellar space

was thought to be too harsh an environment for molecules to survive. Inspired by these results further investigations of ISCs were conducted and today nearly 140 molecules have been identified [4]. Hydrogen is by far the most abundant interstellar molecule with the next most abundant molecule (carbon monoxide, CO) being between four and five orders of magnitude less common.

Identification of atoms and molecules in ISCs requires knowledge of their laboratory spectra. Diffuse ISCs are transparent to ultraviolet and visible radiation. They can thus be probed by optical absorption spectroscopy utilising background stars as light sources. The first three molecules identified in ISCs were all discovered by visible absorption spectroscopy using Earth-based telescopes. A greater variety of molecular species was not detected until the advent of satellite based UV absorption spectrometers. Hydrogen molecules were always thought to be abundant in ISCs but their detection is non-trivial because they have no permanent dipole moment [5]. Detection was not made until 1970 when a rocket borne spectrometer was able to measure an ultraviolet spectrum in the direction of the star ξPer [6].

Spectroscopic examination of diffuse clouds has shown them to contain mostly atomic and molecular hydrogen. Other molecules are usually present in much lower abundances than hydrogen (H_2). Only basic diatomic molecules are observed in diffuse ISCs. Larger species are susceptible to photo-destruction in the environment which is unprotected from stellar UV radiation.

Table 1.1. *The abundance of some atomic and molecular species relative to the total abundance of H nuclei in the direction of the diffuse cloud ζOpiuchi. (Taken from reference* [6]*)*

Chemical Species	Relative Abundance
H	0.37
Li	5.2×10^{-11}
C	1.6×10^{-4}
N	7.2×10^{-5}
O	5.0×10^{-4}
H_2	0.32
CH	2.4×10^{-8}
CH^+	6.6×10^{-9}
CN	6.2×10^{-9}
OH	3.6×10^{-8}

Approximately one in ten thousand species is ionised in diffuse clouds. The degree of ionisation is greater than in dense clouds because diffuse clouds are more exposed to ionising radiation [7]. Cosmic rays (CRs) can penetrate dense clouds and are the main source of ionisation in the interior of these clouds. Cosmic rays are highly energetic particles (mostly protons) formed in supernovae which travel through the universe at high speed.

Dense clouds are opaque to UV/visible radiation and cannot be examined by absorption spectroscopy. They are instead probed by IR emission spectroscopy or radio astronomy. Dense clouds are dark in the visible but are transparent to radio waves. Radio astronomers can detect thousands of sharp emission features in the radio region of the spectrum which can be assigned to rotational transitions of molecules.

Dense ISCs are often described as 'molecular clouds'. Because there is sufficient dust to shield the interior from most radiation, species of greater size and complexity may survive.

Table 1.2. *Typical fractional abundance of selected molecules in dense ISCs relative to H_2 = 1. (Taken from reference* [6]*)*

Chemical Species	Fractional Abundance
H_2	1.0
CH	10^{-8}
CH^+	10^{-8}
CN	10^{-9}
CO	10^{-5}
C_2	10^{-8}
HCN	10^{-9}
NH_3	10^{-8}
HC_3N	10^{-9}
CH_3OH	10^{-9}

1.2.2 The Origin of Molecules in ISCs

Following the unexpected discovery of molecules in the ISM attention turned to an explanation of their origin. The temperature and gas densities in ISCs place severe limitations on the chemistry that can occur there. It is natural to suppose that under such conditions molecules may have been formed in other environments and transported to ISCs rather than being formed *in situ*. However, the transport of molecules formed in other environments (such as the out-flowing atmospheres of giant stars) to ISCs is made

impossible by stellar UV radiation which would quickly destroy the molecules. It is now accepted that these molecules are synthesised in ISCs by gas phase reactions as well as reactions on the surfaces of dust particles.

The environmental conditions prevailing in ISCs impose significant limitations on the gas phase chemistry that can occur. Firstly, because ISCs are so sparse only binary reactions are possible. Secondly, at low temperatures only exothermic reactions are viable, and thirdly, reactions must have little or no activation energy requirements if they are to be rapid. In addition to these constraints, there is no sink for the excess energy produced by an exothermic reaction. Consider the generic molecule-forming reaction **(1.1)** below between two atomic species, A and B. In most laboratory experiments the product (AB*) is stabilised by collision with a third body (M, usually helium) which absorbs the excess energy from the exothermic reaction. If collisional stabilisation does not occur the complex will immediately dissociate and a molecule (AB) will not be formed.

$$A + B \leftrightarrow AB^* + M \rightarrow AB + M^* \qquad \textbf{(1.1)}$$

Simple exothermic binary reactions require some way of losing this excess energy (to stabilise the product) that is unavailable in ISCs. The emission of an infra-red photon has been postulated as the stabilising mechanism that permits such reactions in ISCs. This is known as radiative association and is illustrated by reaction **(1.2)**.

$$A + B \rightarrow AB^* \rightarrow AB + h\upsilon \qquad \textbf{(1.2)}$$

This type of reaction cannot initiate molecule formation in ISCs because its efficiency is very low for atomic reactants. The lifetime of the excited species must be quite long for photon emission to occur and only larger (polyatomic) species having many degrees of freedom can survive sufficiently long for stabilisation to take place.

1.2.3 Ion-neutral Reactions

Ion-neutral reactions are not inhibited by the stringent criteria outlined above. They have no appreciable activation energy and are known to be fast at low temperatures when exothermic. Gas phase ion-neutral collision rates are commonly 100 times faster than comparable neutral-neutral reactions (which usually have activation energy barriers) although certain classes of neutral-neutral reactions, for example atom-radical reactions, can occur rapidly at very low temperature [8].

A small fraction of the species in interstellar clouds are ionised (~10^{-4} in diffuse clouds) by energetic photons or cosmic rays. Positively charged ions predominate although some negative ions have recently been discovered [9].

Beginning with the formation of H_3^+, ion-neutral chemistry can provide the variety and complexity of molecules observed in ISCs. H_3^+ is formed in two steps beginning with the CR ionisation of hydrogen molecules (which are assumed to be formed by grain surface chemistry, see Section 1.1.4).

$$H_2 + CR \rightarrow H_2^+ \qquad \textbf{(1.3a)}$$

$$H_2^+ + H_2 \rightarrow H_3^+ + H \qquad \textbf{(1.3b)}$$

Once H_3^+ is formed a rich ion-neutral chemistry is initiated. H_3^+ is unreactive with the most common interstellar molecule, H_2, but will react with the most abundant atomic species: carbon, nitrogen and oxygen. For example:

$$H_3^+ + O \rightarrow OH^+ + H_2 \qquad \textbf{(1.4)}$$

$$OH^+ + H_2 \rightarrow H_2O^+ + H \qquad \textbf{(1.5)}$$

$$H_2O^+ + H_2 \rightarrow H_3O^+ + H \qquad \textbf{(1.6)}$$

The simple reaction sequence **(1.4-1.6)** generates one diatomic and two polyatomic ions. A similar reaction sequence is observed for atomic nitrogen leading to the ammonium ion (NH_4^+). Ion-electron recombination is the main process by which new neutral molecules are formed from these ions.

$$HCO^+ + e \rightarrow H + CO \qquad \textbf{(1.7)}$$

Ion-electron recombination reactions such as **(1.7)** are rapid and highly exothermic. This exothermicity usually results in dissociation (they are commonly referred to as dissociative recombination reactions), so at least a tri-atomic ion is usually needed to generate a new molecular species. Dissociative recombination reactions are less frequent than ion-neutral reactions due to the low density of electrons in ISCs relative to neutral reactants. The electron density is mostly the result of ionisation of neutrals [5].

Carbon atoms are incorporated in three quarters of known interstellar molecules and it is currently assumed that all hydrocarbons stem from reaction **(1.8)**, the primary hydrocarbon forming reaction in the ISM.

$$H_3^+ + C \rightarrow CH^+ + H_2 \qquad \textbf{(1.8)}$$

$$CH^+ + H_2 \rightarrow CH_2^+ + H \qquad \textbf{(1.9)}$$

$$CH_2^+ + H_2 \rightarrow CH_3^+ + H \qquad \textbf{(1.10)}$$

$$CH_3^+ + H_2 \rightarrow CH_5^+ + h\upsilon \qquad \textbf{(1.11)}$$

Despite its importance a successful experimental examination of **(1.8)** has not been undertaken and the (calculated) product(s) and rate of reaction are still uncertain [10-13]. The lack of an experimental study arises from the difficulty in generating sufficient gas phase atomic carbon to permit the measurement of kinetics.

Reaction **(1.11)** proceeds via radiative association since H-atom transfer to CH_3^+ (analogous to reactions **(1.9)** and **(1.10)**) is endothermic. Although methane (CH_4) can be formed from the dissociative recombination of CH_5^+ with an electron, the main product of the reaction is in fact CH_3 (70%) with CH_2 (20%) the other major product [14]. Methane is commonly formed from the reaction of CH_5^+ with carbon monoxide:

$$CH_5^+ + CO \rightarrow HCO^+ + CH_4 \qquad \textbf{(1.12)}$$

Carbon monoxide is the second most abundant interstellar molecule behind hydrogen. There are multiple routes leading to its formation, for example:

$$CH_3^+ + O \rightarrow HCO^+ + H_2 \qquad \textbf{(1.13)}$$

$$HCO^+ + e^- \rightarrow CO + H \qquad \textbf{(1.14)}$$

Cosmic ray ionisation is not limited to hydrogen molecules and the ionisation of other atomic species increases the number of ion-neutral reactions possible [15].

$$C^+ + CH_4 \rightarrow C_2H_2^+ + H_2 \qquad \textbf{(1.15a)}$$

$$\rightarrow C_2H_3^+ + H \qquad \textbf{(1.15b)}$$

$$CH_3^+ + N \rightarrow HCNH^+ + H \qquad \textbf{(1.16)}$$

The products of reactions **(1.1-1.16)** (be they neutral or ionic) may react with one of the many other ionic and neutral species present. Dissociative recombination of the product ions may also lead to new neutral molecules which can then participate in ion-neutral reactions. Evidently a huge array of ions and molecules can be formed by ion-neutral chemistry even under the conditions prevailing in ISCs. Once H_3^+ is formed from molecular hydrogen a series of ion-atom reactions initiate the chemistry. The chemistry quickly becomes complex once new ions and molecules are formed as new ion-neutral reaction pathways become available. Molecular hydrogen is fundamental to the formation

of every molecule via this chemistry yet no efficient gas phase synthesis for hydrogen exists. Instead it is assumed that this important molecule is formed on the surfaces of dust grains.

1.2.4 Dust Grain Chemistry

Dust grains contribute around 1% of the total mass of ISCs and have a (low) number density in dense clouds of 1.3×10^{-12} cm^{-3} relative to hydrogen [16]. It is known that dust grains are silicate and graphite based however they are not well characterised [6]. Optical studies are limited the estimation of dust grain size based on the variation of starlight extinction at wavelengths ranging from the IR to the UV [16]. These studies indicate that dust grains range in size from 1 nm to around 10 μm with the median size being around 1 μm. Smaller grains are thought to be near spherical whilst larger grains are irregular in shape. Dust grains are very 'sticky' at the low temperatures of ISCs and gases adsorb efficiently to their surfaces. The species that adsorb to grains are identified by the depletion of atomic species in diffuse ISCs from their standard cosmic abundance [16]. This also gives an indication of the species of which the grains are composed.

Chemical reactions between adsorbed species on the surface of grains have been proposed as a way of forming molecules in the harsh conditions of ISCs. Two mechanisms have been proposed by which molecules are formed on grains. Both assume that the grain surface is chemically inactive. The ubiquitous hydrogen molecule is thought to be created by this chemistry. In the following paragraphs the formation of hydrogen molecules by each of the two mechanisms is described.

The first mechanism proposes that weakly adsorbed hydrogen atoms are free to diffuse across the surface dust grains and react with other adsorbed species. Hydrogen is the most abundant species in ISCs and the most likely reaction partner. The grain acts as the third body (as in reaction **(1.1)**) absorbing the energy released by the reaction and stabilising the product molecule. The molecule can desorb into the gas phase if a sufficient amount of the exothermicity from the reaction is directed to translational motion perpendicular to the grain surface [17]. This is known as the Langmuir-Hinshelwood mechanism for molecule formation on a grain surface. Unfortunately the number of reactions that can proceed in this manner is limited because the only species able to migrate across dust grains at ISC temperatures are H, H_2 and He [6]. Hydrogen

formation by this mechanism is considered rapid, however the temperature range over which the diffusive mechanism can operate is limited. If the temperature is too low diffusion does not occur and if the temperature is too high the hydrogen atoms evaporate before a reaction can occur.

If the migration of absorbed species across a grain surface is not possible hydrogen atoms are fixed in their position on the grain surface. A reaction can only occur if a gas phase hydrogen atom collides directly with the adsorbed atom. If a collision does occur the excess energy from the collision and reaction contributes to desorption of the hydrogen molecule. This is the Eley-Rideal mechanism for hydrogen formation.

Both the Langmuir-Hinshelwood mechanism and the Eley-Rideal mechanism have been shown experimentally to be feasible routes to the formation of H_2, however the exact importance of each is unknown [6].

Grain chemistry is not limited to hydrogen atoms. It is likely that the collision of gas phase atoms (other than hydrogen), ions and molecules with grains will induce some chemistry. However, grain chemistry cannot significantly increase the abundance of complex molecules in the gas phase. Because larger molecules have more degrees of freedom in which to distribute the energy released by an exothermic reaction, they absorb the excess energy internally and less is available for desorption into the gas phase. Desorption of larger molecules is therefore much less likely. Once formed, larger molecules could only be desorbed by highly energetic collisions between the grain and another ISC particle. Such collisions are infrequent and thus grain surface chemistry is not likely to be an efficient route to the formation of large gas phase molecules. The formation of molecules which could not escape into the gas phase would lead to the gradual build-up of molecules on the surface of grains. The observation of ice mantles comprised of carbon dioxide, carbon monoxide, water and methanol on dust grains by the Infrared Space Observatory [17] appears to verify this supposition. The species in these ice mantles are not complex and reflect the limited chemistry that can occur at very low temperatures.

To summarise: grain surface chemistry does not provide a fast, efficient route to the formation of molecules except for H_2.

1.2.5 Modeling ISCs

Spectroscopic observations of ISCs provide data from which countless important conclusions can be drawn. This gives astronomers and astrochemists a basic knowledge of the environment but provides a far from complete picture. The best way to gain an improved understanding of the physical conditions and chemistry is to make direct measurements. This is precisely how scientists enhanced their knowledge of Earth's atmosphere, and subsequently other planets and satellites in our solar system. Unfortunately direct analysis of ISCs is not practical because they are many light years from Earth. The best alternative to an *in situ* measurement is a detailed model of the chemistry. The principal objective of a chemical model is to match the observed abundances of the dominant molecular species.

A model of the chemistry occurring in an ISC must incorporate all of the known physical and chemical properties of the cloud. These include: the initial species present and their abundance; cloud size, shape, temperature and density; the intensity of the ultraviolet radiation field; the rate of photo-ionisation; the CR ionisation rate; and most importantly a complete list of formation and loss routes for every species, including kinetics. Because of the volume of reactions possible, models are invariably complex. It is quite common to begin with a simplified model which includes only the most abundant species, to which complexity can be added later. Models normally focus on obtaining agreement between calculated data and measured fractional abundances in a particular ISC. The model of Black and Dalgarno is an example of this approach with the authors focusing on matching the observed abundances in the diffuse cloud located between Earth and the star ζOpiuchi [18]. Because of the inhomogeneities in ISCs a comparison between model and observed cloud properties is not a trivial exercise. The observational measurements give densities along a particular line of sight and say nothing of actual ISC morphology [6].

Models of ISCs can be either time-dependent or equilibrium-based. Equilibrium models assume that the lifetime of the cloud is sufficiently long that equilibrium can be reached and at this point the abundance of every species in the model is effectively static. Equilibrium is reached after between 10^3 and 10^5 years in most cloud models [6]. Time-dependent models are considerably more demanding to create but the provision of data

on the evolution of each species is more useful than equilibrium data. Comparisons between time-dependent model data and observed data can be used to determine cloud age.

In Herbst and Klemperer's chemical model of a dense ISC, molecule formation is based primarily on gas phase ion-molecule reactions [15]. Over 50 ion-molecule reactions were included and for the 35 species studied, steady-state abundances were predicted to occur after around 10^5 years. Some neutral-neutral reactions between radicals and atoms are also included as these can be fast at low temperatures [8, 19]. Although dust grains play only a minor role in their model (with condensation of molecules onto grain surfaces not considered), the shielding capacity of the dust is critical to the formation of molecules. The success of Herbst and Klemperer's model in reproducing the observed abundances in ISCs such as Orion A confirmed that (positive) ion-molecule reactions were the most important mechanism for the formation of molecules in ISCs [15].

Of the ion-molecule reactions included in the model of Herbst and Klemperer, laboratory kinetics had been measured directly for only half. The remaining rate coefficients were estimated. This highlights a key problem in modelling ISC chemistry – models are frequently limited by a lack of experimental data.

The chemistry in dense clouds is quite different to that occurring in diffuse clouds. In diffuse ISCs photo processes have a considerable influence on the chemistry. This includes increasing the degree of ionisation of species other than hydrogen such as carbon, and the destruction of molecules. The increased prevalence of electrons (from the increased ionisation levels) in diffuse clouds inhibits the formation of larger molecules as dissociative recombination rates are increased in importance. The overall effect of these processes on the chemistry is significant and diffuse clouds are much less 'molecular' than dense clouds. Hydrogen molecules are the most important precursors to ISC chemistry which is very limited in their absence [5]. Hydrogen atoms are entirely locked up in hydrogen molecules in dense clouds and this immediately enhances the chemistry that can occur.

The accuracy of a model is limited only by the data from which it is constructed. This means that a complete understanding is not possible unless all possible formation

and destruction routes for each species are included. Consequently models can be made more accurate as new laboratory data becomes available. van Dischoeck and Black exploited a much larger range of chemical reactions to create an improved model of diffuse ISCs [20].

A model's accuracy is critically dependent on accurate kinetic information. This is particularly true for reactions which initiate the chemistry such as the reactions of H_3^+ with atomic species. Because of experimental difficulties, reaction **(1.8)** has not been examined in the laboratory and the products of the reaction are uncertain. An experimental examination of this reaction is vital and was attempted as part of this thesis.

Another environment in which ion chemistry plays a considerable role in molecule formation is within our solar system, in particular in the atmosphere of Titan.

1.3 Titan

Scientific interest in the nature and chemistry of planetary atmospheres motivated the shift in attention from Earth's atmosphere - analysed in considerable depth during the 1960s and 1970s - to that of Titan, Saturn's largest moon. Titan is unique in the solar system as the only moon having a substantial atmosphere. It is also the only body in our solar system, other than Earth, to have a significant, nitrogen-based atmosphere.

Titan was first discovered by Dutch astronomer Christiaan Huygens in 1655. Titan's diameter of 5150 km is approximately 70% larger than Earth's moon. Huygens believed Titan to be the largest of the planetary satellites, but the distinction in fact belongs to Jupiter's largest moon Ganymede. The error is understandable with Titan's hazy atmosphere creating the illusion of its superior size. Titan orbits Saturn at a distance of 1.2 million km and one Titanian year is nearly thirty times longer than an Earth year.

It was not until nearly 300 years after its discovery that Titan's atmosphere was identified by the Earth based measurements of Kuiper [21]. Kuiper was able to identify methane in an infrared emission spectrum of Titan and to provide an estimate of the density of the Titanian atmosphere [21]. The discovery of a methane-containing atmosphere sparked interest in Titan but early investigations were hampered by the impenetrability of Titan's characteristic orange haze.

Although much is now known of Titan and its atmosphere, little was known of its composition or the prevailing physical conditions prior to the *Voyager* missions.

1.3.1 The *Voyager* 1 Mission to Saturn and Titan

The *Voyager* 1 and 2 spacecraft were the first large spacecraft to travel to the outer solar system (and beyond). Their mission objective was to perform thorough scientific analyses of Jupiter and Saturn's atmospheric characteristics. The *Voyager* 1 spacecraft also encountered Titan, passing just 4394 km from the moon in November 1980 [22]. During its brief encounter with Titan the eleven scientific instruments aboard *Voyager* 1 recorded and relayed sufficient data to reveal the nature and conditions prevalent in Titan's atmosphere [22]. *Voyager* 2 encountered Titan in August 1981, but at a much greater distance [22].

The *Voyager* data has provided the foundation for all subsequent studies of Titan. Titan's atmosphere extends nearly 2000 km from its surface. Cameras aboard *Voyager* 1 showed the entire moon to be covered with a thick orange haze which obscured the surface.

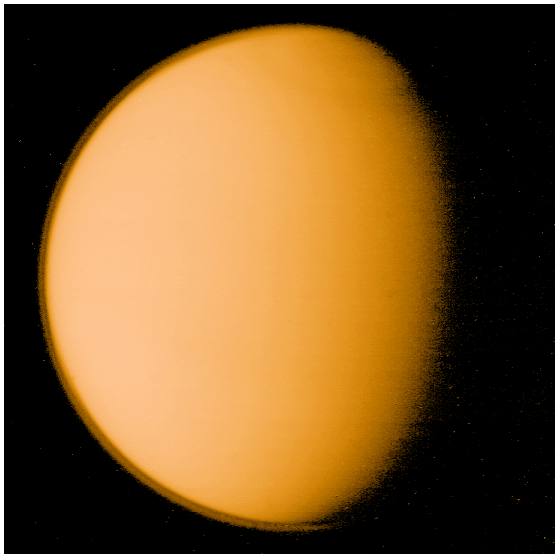

Figure 1.2. *Layers of haze in Titan's atmosphere give the moon its characteristic orange colour. This image was recorded by a camera aboard Voyager 1* [23].

The composition of the atmosphere identified by the *Voyager* results intersected the two pre-*Voyager* models of Titan's atmosphere. The first of the models favoured a methane-based atmosphere with a surface temperature of 86 K and a surface pressure of 20 mbar [24]. The second model correctly assumed nitrogen to be the dominant neutral

species but anticipated a much higher surface pressure of 20 bars with the surface temperature ~ 200 K [25]. *Voyager* data established Titan's surface temperature to be 94 ± 1.5 K, with the surface pressure around 50% greater than on Earth at 1.5 bar. The ultraviolet spectrometer (UVS) aboard the spacecraft identified nitrogen as the major atmospheric constituent, comprising 90-98 % of the atmosphere depending on altitude, with the most abundant minor constituent being methane (between 2% and 8% of the atmosphere depending on altitude) [22, 26].

These physical conditions led to speculation that liquid methane or ethane may be present in lakes or oceans on Titan's surface, and that atmospheric clouds of hydrocarbons may rain down on the surface. Infrared images of Titan's surface taken by the Hubble Space Telescope show that the surface is not uniform, but has large 'dark' areas which absorb IR radiation. This has been interpreted as resulting from a sea of liquid hydrocarbons. One of the most spectacular observations of the *Cassini-Huygens* mission (described later) relates to this.

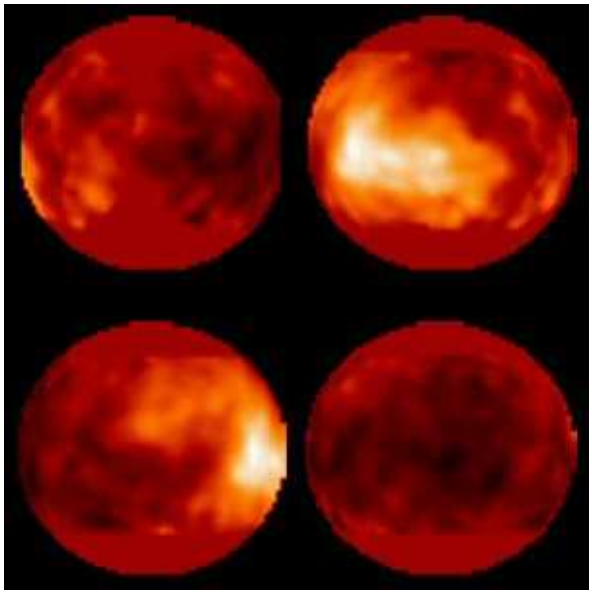

Figure 1.3. *Images of Titan's surface taken in the near IR by the Hubble Space Telescope show an irregular surface.*

The most significant measurements of Titan's atmosphere were obtained by *Voyager*'s infrared interferometer and radiometer (IRIS). This instrument examined emission from the atmosphere between 200 and 1400 cm^{-1}. A variety of **minor** atmospheric constituents were observed, some of which had not previously been detected by Earth based measurements. Molecules detected on Titan by the *Voyager* instruments

(UVS and IRIS) include: N_2, H_2, CH_4, C_2H_2, C_2H_4, C_2H_6, C_3H_6, HCN, HC_3N, C_2N_2, C_4H_2, CH_3CCH, C_3H_8 and CO_2.

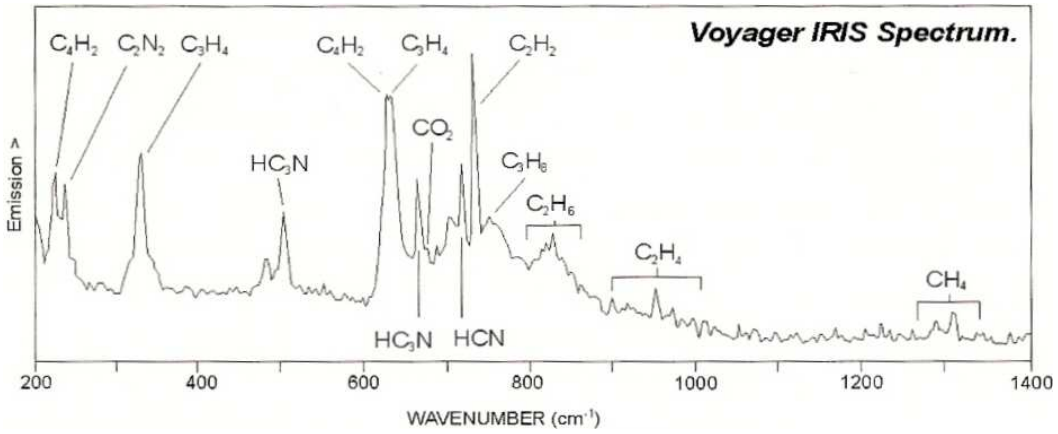

Figure 1.4. *IR emission spectrum from Titan recorded by the IRIS instrument aboard the Voyager 1 spacecraft (taken from* [22]*).*

A notable omission from the species detected in Titan's atmosphere is molecular oxygen. Carbon dioxide was detected by the *Voyager* mission and CO and H_2O have since been discovered in Titan's atmosphere. The oxygen atoms in CO and CO_2 are thought to originate from H_2O delivered to the atmosphere by external sources, such as icy meteorites. The limited level of oxygen has important consequences for the chemistry occurring in Titan's atmosphere (described later).

The relative abundance of each species was estimated following their identification in the atmosphere. These are principally stratospheric abundances because this is the region of Titan's atmosphere that is probed by IR spectroscopy.

Table 1.3. *Volume mixing ratios in Titan's stratosphere for some key molecules observed by Voyager 1* [27].

Molecule	Volume Mixing Ratio
CH_4	$1\text{-}3 \times 10^{-2}$
H_2	2×10^{-3}
C_2H_6	2×10^{-5}
C_2H_2	2×10^{-6}
C_2H_4	4×10^{-7}
C_3H_8	$2\text{-}4 \times 10^{-6}$
C_4H_2	$10^{-8}\text{-}10^{-7}$
HCN	2×10^{-7}
HC_3N	$10^{-8}\text{-}10^{-7}$
C_2N_2	$10^{-8}\text{-}10^{-7}$
CO	6×10^{-5}

Titan's atmosphere is thought to be comprised almost entirely of nitrogen however the mean molecular weight in Titan's atmosphere is greater than it would be for pure nitrogen, at 28.6 amu. This suggests there is a moderate amount of some heavier species in the atmosphere. Argon has been proposed as the most likely solution to this discrepancy although argon has yet to be detected directly in the atmosphere. Estimates of the mole fraction of argon in the atmosphere have varied wildly from zero to 30%. The upper limit for the (estimated) argon mole fraction has decreased over the years and currently sits around 10%, although there may be none at all [22].

Radio occultation experiments permitted the calculation of vertical density distributions in Titan's atmosphere. This experiment involved measuring the rate of attenuation of *Voyager*'s radio signal as it passes behind Titan, and the opposite effect as it re-emerged. This provides two vertical refractivity profiles which can be converted to density profiles (assuming that the atmosphere is entirely nitrogen) [22]. Further calculations can convert the altitude density profiles to temperature versus mean molecular weight profiles [22].

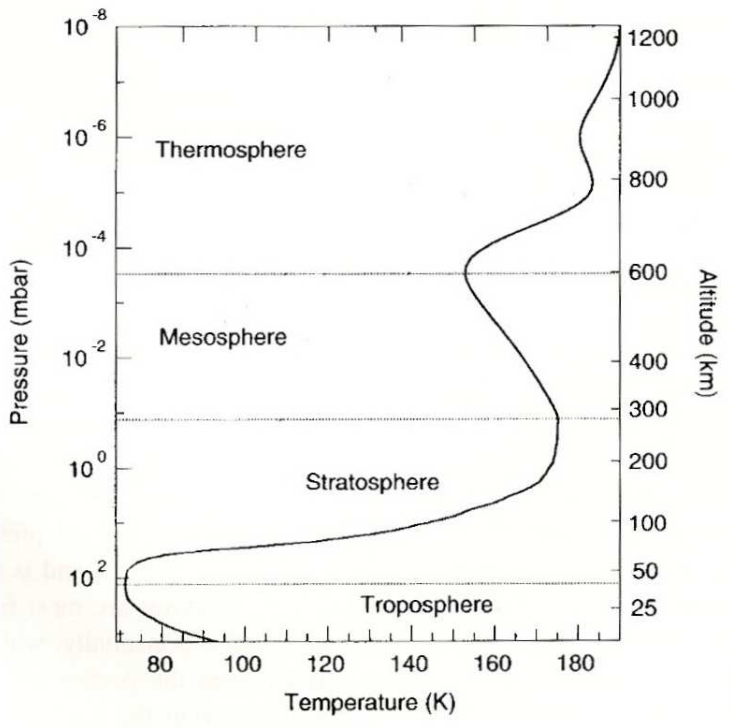

Figure 1.5. *Temperature and density profile of Titan's atmosphere constructed from the results of the Voyager mission* [22].

Titan's atmosphere extends far further from its surface than Earth's atmosphere, but like Earth, the atmosphere is classified by layers based on temperature characteristics. The troposphere of Titan extends to around 40 km from the surface in contrast to Earth where the tropopause lies only 15 km above the surface. At 40 km the atmospheric temperature, which has been decreasing with increasing altitude, reaches a minimum (the tropopause) before beginning to rise again. In the stratosphere (from the tropopause up to 300 km) the temperature rises with altitude. Above the stratopause (at 300 km) is the mesosphere where the temperature begins to fall again until reaching a minimum at an altitude of 600 km. Above the mesopause (at 600 km) is the thermosphere. As the name suggests this is the warmest region of the atmosphere, due to the penetration of extreme UV radiation. This radiation ionises and dissociates molecules releasing kinetic energy which heats this part of the atmosphere. The temperature in Titan's thermosphere increases from around 150 K at the mesopause to 190 K at 1200 km. Above 1200 km the atmosphere gradually thins as it extends to the exopause, the limit of the atmosphere, at an altitude of around 3500 km [22].

Recently *in situ* measurements of Titan's atmosphere by the *Huygens Probe* (described later) have shown Figure 1.5 to be accurate at altitudes up to around 500 km [28]. Above 500 km the temperature variation is inconsistent with the *Voyager* derived data, but the atmospheric pressure does fall away as expected.

1.3.2 Chemistry in the Atmosphere

It is generally accepted that most of the minor constituents of Titan's atmosphere were formed from nitrogen and methane by photochemical processes [27]. There are two routes by which molecules are synthesized in Titan's atmosphere, both of which occur primarily in the upper atmosphere.

Early studies of chemistry in Titan's atmosphere focused on neutral-neutral reactions initiated by the dissociation of nitrogen and methane. In the mesosphere and thermosphere, methane and nitrogen are dissociated by extreme solar ultra-violet (EUV) radiation, high energy electrons from Saturn's magnetosphere and (much less so) by cosmic rays.

The key reactions are:

$N_2 + e^- \rightarrow N + N(^2D) + e^-$ **(1.17)**

$N_2 + h\upsilon \rightarrow 2N(^2D)$ **(1.18)**

$CH_4 + h\upsilon \rightarrow CH_3 + H$ **(1.19a)**

$\rightarrow CH_3^* + H \rightarrow CH + H + H_2$ **(1.19b)**

$\rightarrow CH + H + H_2$ **(1.19c)**

N and $N(^2D)$ represent the ground (^4S) and first excited states of nitrogen respectively. At wavelengths above 136 nm reactions **(1.19b)** and **(1.19c)** are not energetically possible making CH_3 the only product of the methane dissociation **(1.19a)** [29]. The atoms and radicals produced by reactions **(1.17-1.19)** react with the main atmospheric constituents to form new molecules.

$CH + CH_4 \rightarrow C_2H_4 + H$ **(1.20)**

$N + CH_4 \rightarrow NH + CH_3$ **(1.21)**

$N + CH_3 \rightarrow H_2CN + H$ **(1.22)**

$CH_3 + CH_3 + M \rightarrow C_2H_6 + M$ **(1.23)**

Bimolecular neutral-neutral reactions such as **(1.20-1.22)** typically have rate coefficients of the order of 10^{-11} cm^3 s^{-1} at the temperature of Titan's upper atmosphere [29]. The termolecular association reaction **(1.23)**, in which M is a third body (N_2 in Titan's atmosphere) which can accept the excess energy from the reaction and thus stabilise the product, is efficient only at altitudes below 800 km [29]. The products of these reactions can participate in further reactions. This cycle continues forming an elaborate array of molecules by chemistry which begins with just methane and nitrogen. Comprehensive lists of the possible neutral-neutral reactions including kinetics can be found elsewhere [22, 29, 30].

Planets which have an atmosphere usually also possess an ionosphere. Earth's ionosphere is distinguished by the presence of ions and electrons formed by the incidence of solar UV radiation on the neutral species in the thermosphere. Earth's ionosphere is divided into four layers, based loosely on ion density, with the peak ion density (where there are around one million electrons per cubic centimetre) located at an altitude of 300 km.

Like Earth, Titan has an ionosphere. The *Voyager* mission provided little information about Titan's ionosphere other than to identify that it existed and was significant. The ionosphere of Titan is slightly different to Earth's. Firstly Titan has no intrinsic magnetic field [22] and is thus not shielded from Saturn's magnetosphere, through which most of Titan's orbit passes [31]. The result is that Titan's upper atmosphere is bombarded by high energy electrons from Saturn's magnetosphere which ionise the neutral atmosphere. Ionisation is also effected by solar EUV photons and by photo-electrons thus produced. The effect of ionising solar radiation on Titan's atmosphere is reduced by comparison with Earth because Titan is further from the sun.

Radio occultation experiments allowed upper limits to be set for the electron (and correspondingly the ion) density in the upper atmosphere. Lindal *et al*. put the limits at 3000 cm^{-3} on the evening-side of Titan and 5000 cm^{-3} on the morning-side [32]. Two limits are proposed because Titan always presents the same face to Saturn, i.e. it is gravitationally locked [33]. As a result each of the sides of Titan are subjected to different sources and degrees of ionisation. Ions on the day-side are mostly generated by photo-ionisation whilst the night-side is primarily subjected to magnetospheric electron ionisation [31, 34]. Re-analysis of the *Voyager* data by Bird *et al*. [35] found the night-side electron density to peak at 2400 ± 1100 cm^{-3} at an altitude of 1180 ± 150 km. This places the ionosphere well up in the thermosphere where the temperature is around 190 K and the pressure 10^{-8} mbar.

Cosmic ray (CR) ionisation is negligible in the upper atmosphere relative to the above sources of ionisation. CRs do however have an effect on chemistry at lower altitudes as the penetrating power of the CRs is sufficient that they can reach deep within the atmosphere to regions inaccessible to other sources of radiation. Capone *et al*. have modelled the effect of CR ionisation at altitudes between 50 and 400 km and found that a significant ionosphere can develop [36, 37]. This lower region of Titan's atmosphere is not considered in this thesis.

It is in the (upper) ionosphere that additional chemical pathways to molecule formation can be found. Ionisation in the upper atmosphere generates N_2^+ and N^+ in approximately equal abundance. A network of ion-molecule reactions is initiated by the reactions of these ions with the next most abundant molecule in the atmosphere, methane.

$N_2^+ + CH_4 \rightarrow CH_2^+ + N_2 + H_2$ 0.09 **(1.24a)**

$\rightarrow CH_3^+ + N_2 + H$ 0.91 **(1.24b)**

$k = 1.14 \times 10^{-9}$ cm^3 s^{-1} [38]

$N^+ + CH_4 \rightarrow CH_3^+ + NH$ 0.50 **(1.25a)**

$\rightarrow CH_4^+ + N$ 0.05 **(1.25b)**

$\rightarrow HCNH^+ + H_2$ 0.36 **(1.25c)**

$\rightarrow HCN^+ + H_2 + H$ 0.36 **(1.25d)**

$k = 1.15 \times 10^{-9}$ cm^3 s^{-1} [38]

The product ions of reactions **(1.24)** and **(1.25)** are unreactive with N_2 and go on to react further with methane and other hydrocarbon species which are present in the atmosphere (produced by neutral chemistry). New ions are formed and the chemistry becomes complex very quickly. Ion-molecule reactions are considerably faster than analogous neutral-neutral reactions with most exothermic reactions proceeding at close to the collision rate (~10^{-9} cm^3 s^{-1}). The reducing nature of Titan's atmosphere means that the ionisation flows from the ions produced initially to neutral molecules with high proton affinities. New neutral species are formed by ion-electron recombination reactions. The product ions which do not recombine with an electron continue to react with neutral species until (eventually) product ions form which are unreactive with the major neutral constituents of the atmosphere. The only loss mechanism for these species is ion-electron recombination. These 'terminal ions' accumulate over time relative to more reactive ions.

Newly formed molecules diffuse to lower altitudes where they mix evenly with the atmosphere and contribute to the molecular abundances observed by the *Voyager* spacecraft. As the molecules diffuse through the stratosphere they are condensed. The aerosol layer formed by the condensation of molecules in the stratosphere is the source of Titan's characteristic orange haze.

1.3.3 Models of Titan's Atmosphere

Evidently there are two distinct types of chemistry occurring in the upper atmosphere of Titan, one based on neutral-neutral reactions and the other on ion-molecule reactions. The *Voyager* spacecraft provided evidence that both were occurring, but did little to establish the relative importance of each.

Without an *in situ* measurement of Titan's upper atmosphere, the only way to gain an understanding of the environment and of the species present is to model the chemistry occurring. This was the approach to Titan of many scientists since the *Voyager* mission, with interest in the atmosphere building as the *Cassini-Huygens* mission (Section 1.5.6) approached.

To build a model of the chemistry occurring in an atmosphere it is necessary to know: the initial species present; the reactions occurring; the products of these reactions; the rate of formation and destruction of each of the species present; and the physical parameters which govern the chemistry. Laboratory data for each process is essential to the construction of an accurate model. When laboratory data is unavailable for an important reaction it is common to make an estimate of the reaction rate. A model is not complete until every species and reaction is accounted for. Consequently models can quickly become extremely elaborate as more species are included. Once a model is constructed the results are compared with observed molecular abundances and various parameters are then adjusted to give the best fit with the observed data.

Because the chemistry in Titan's upper atmosphere is dominated by just two species, N_2 and CH_4, a basic understanding of the chemistry can be achieved from a few simple reaction schemes based on their chemistry. Early models of Titan included only the dominant species and the key minor constituents. The earliest models of Titan's atmosphere (pre-*Voyager*) were based solely on (neutral) hydrocarbon chemistry as nitrogen had not yet been identified in the atmosphere [36, 39]. With the *Voyager* results determining the atmosphere to be almost entirely nitrogen, with only a small amount of methane, new models of the chemistry were needed. Adding nitrogen to the atmosphere drastically increases the complexity of the possible chemistry and the number and nature of species produced.

The first model to give a broad perspective of the neutral chemistry occurring on Titan was the one-dimensional, time-dependent photochemical model of Yung, Allen and Pinto (hereafter YAP) [27] which was updated in 1987 with improved nitrile chemistry [40]. Beginning with the dissociation of methane and nitrogen, the model accurately accounted for the formation of all of the minor species observed by the *Voyager*. One of the most intriguing aspects of the atmosphere (identified by the model) is the continual

loss of H and H_2 from the upper atmosphere [22]. Whilst larger molecules diffuse to lower altitudes, hydrogen atoms and molecules are sufficiently light to diffuse upwards and to escape the atmosphere. Both species are derived from the dissociation of methane (see reaction **(1.19)**). If hydrogen is continually escaping from the atmosphere it becomes difficult to explain how the methane abundance is sustained in the atmosphere. This observation led to hypotheses that liquid methane (or ethane) lakes or oceans on the surface of Titan might act as reservoirs for methane in the atmosphere.

The YAP model was reasonably successful in predicting the observed abundances of the minor atmospheric species from simple photochemical schemes, although the lack of high quality kinetics data was lamented by the authors. Updated models were necessary when it became clear that the YAP model overestimated the concentrations of the minor atmospheric constituents. Photochemical models incorporating updated laboratory chemistry were developed by Toublanc *et al*. (1995) [30] and Lara *et al*. (1996) [29].

Models of Titan's ionosphere require a starting point i.e. a background neutral atmosphere in which the ion chemistry is initiated and the evolution examined. Several investigators employed the results of the YAP model as the basis for their models of Titan's ionospheric chemistry. Although it was not the first model of Titan's ionosphere, the model of Ip published in 1990 included more detail than previous models [41]. The mixing ratios (concentrations) derived by YAP for the ten most abundant neutrals in the upper atmosphere were employed as the background atmosphere for this model. These mixing ratios extended to only 1200 km above Titan's surface, so they were extrapolated to higher altitudes by Ip to cover higher regions of the atmosphere [41]. Laboratory data for the ion-molecule reactions were taken from the ion-neutral reaction database of Anicich and Huntress [42] and a model of Titan's ionosphere at high altitude (above 800 km) was developed. The model considered magnetospheric electrons as the dominant ionisation source. The dominant ions near the ionospheric peak (around 1240 km) were found to be N_2^+, N^+, CH_3^+, $C_2H_5^+$ and $HCNH^+$.

The 1992 equilibrium model of Titan's ionosphere produced by Keller, Cravens and Gan evaluated the ionospheric chemistry above 700 km [31]. Cosmic ray ionisation was neglected as it was assumed to be negligible in the upper atmosphere by comparison

with solar EUV and magnetospheric electron ionisation. The model found $HCNH^+$ to be the most abundant ion [31]. A key conclusion from this model was that magnetospheric electrons were a minor source of ionisation.

The 1997 ionospheric model of Fox and Yelle [43] was constructed with the background atmosphere of Strobel *et al*. [44] (with some mixing ratios taken from YAP) and the relevant ion-neutral reactions of Anicich and Huntress [42]. Magnetospheric electron ionisation was ignored and the model accounts only for photo-ionisation and secondary photo-electron impact ionisation. The model of Fox and Yelle contrasted with other ionospheric models in that $HCNH^+$ was not found to be the major ionic species. Instead hydrocarbon ions were found to dominate the upper atmosphere with the $C_xH_y^+$ 'pseudo-ion' established as dominant ionic species.

$HCNH^+$ was at this time considered a terminal ion in Titan's atmosphere. With no efficient reaction pathways available the only loss route for this ion was ion-electron recombination and the ion was therefore expected to accumulate relative to other more reactive ions. However, Fox and Yelle included two ion-molecule reactions not previously included in models of Titan's ionosphere:

$HCNH^+ + HC_3N \rightarrow H_2C_3N^+ + HCN \quad k = 3.4 \times 10^{-9}\ cm^3\ s^{-1}$ **(1.26)** [34]

$HCNH^+ + C_4H_2 \rightarrow C_4H_3^+ + HCN \quad k = 1.6 \times 10^{-9}\ cm^3\ s^{-1}$ **(1.27)** [34]

Although the neutral reactants in **(1.26)** and **(1.27)** are not abundant in Titan's atmosphere their concentration is sufficient to have a discernible effect on the chemistry, thus reducing the abundance of $HCNH^+$. Whilst this goes some way to explaining the unexpected result that $HCNH^+$ was not the most abundant ion, it is also likely that differences in the neutral model of Fox and Yelle (relative to other models) that formed the basis of their ionospheric model contributed to the result that $HCNH^+$ was not the dominant ionic species.

A new era in ionospheric models of Titan was heralded by the publication in 1997 of a new database of ion-molecule reactions relevant to Titan's atmosphere by Anicich and McEwan [45]. It has already been noted that a model cannot be considered complete until the entire range of possible reactions are included. The Anicich and McEwan database contained far more ion-molecule reactions than had been included in previous models. Cravens *et al*. ran the code for their 1992 model [31] using the Anicich and

McEwan database of reactions and generated $HCNH^+$ as the dominant ionic species as before [34].

In 2000 Banaszkiewicz *et al*. [46] published an updated version of the 1996 model (Lara *et al*. [29]) of Titan's neutral atmosphere. In addition to their neutral photochemical model they created a model of the ionospheric chemistry (based on the mixing ratios predicted their neutral model). By coupling the neutral only model with the ionospheric model, the interdependence of two molecule formation routes in Titan's atmosphere was exposed. Atmospheric densities of neutral species were significantly affected by the ion chemistry. In particular the methane mixing ratio in the upper atmosphere was greatly altered. Other species to be radically affected were CH_3CCH, HC_3N and CH_3CN.

In 2004 Wilson and Atreya published a similar model in which the coupling of the neutral and ion chemistry was examined [26]. The model included updated chemistry and explored more variables than previous models. The authors found photo-electron impact ionisation to be the only source of ionisation below 1000 km. Above this altitude photoionisation was predominant. Like previous models, this model predicted $HCNH^+$ to be the dominant ion above 1000 km.

The models discussed above do not represent a complete list of models of Titan's neutral and atmospheric chemistry; rather they are a representative sample of models which were important at their time of publication. Titan is a difficult environment to model because the chemistry is not uniform throughout the atmosphere. In spite of this the models outlined above have proved remarkably accurate in matching the observations provided by the *Voyager* IRIS and UVS instruments. The insight they provide into Titan's environment is useful, but their true accuracy cannot be known without a direct *in situ* measurement of the atmosphere.

1.3.4 The *Cassini-Huygens* Mission

On 15 October 1997 the *Cassini* spacecraft was launched on its mission to survey the Saturnian system. The spacecraft was named after Jean Dominique Cassini, the 17th century astronomer who discovered four of Saturn's moons and was the first to identify the presence of more than one ring around Saturn. The objective of the *Cassini-Huygens* mission was to undertake a complete investigation of the planet, its rings and some of its

31 moons, in the hope of gathering further insight into the nature and evolution of planets.

Saturn is an interesting system because the rings and moons are reminiscent of the early solar system, where dust and particles orbited the sun. As part of the mission the spacecraft encountered Titan more than forty times. One of the key mission objectives was to undertake a more sophisticated examination of Titan than was completed by the *Voyager* missions. Twelve of the eighteen scientific instruments aboard the spacecraft were carried by the *Cassini Orbiter* itself with the remainder, part of the detachable *Huygens Probe*.

The *Huygens Probe* is named after Christian Huygens, the discoverer of Titan, who also identified the two 'handles' of Saturn as rings. The *Probe*'s mission was to detach from the main spacecraft and descend with a parachute through the atmosphere of Titan, performing detailed observations of the atmosphere during the descent.

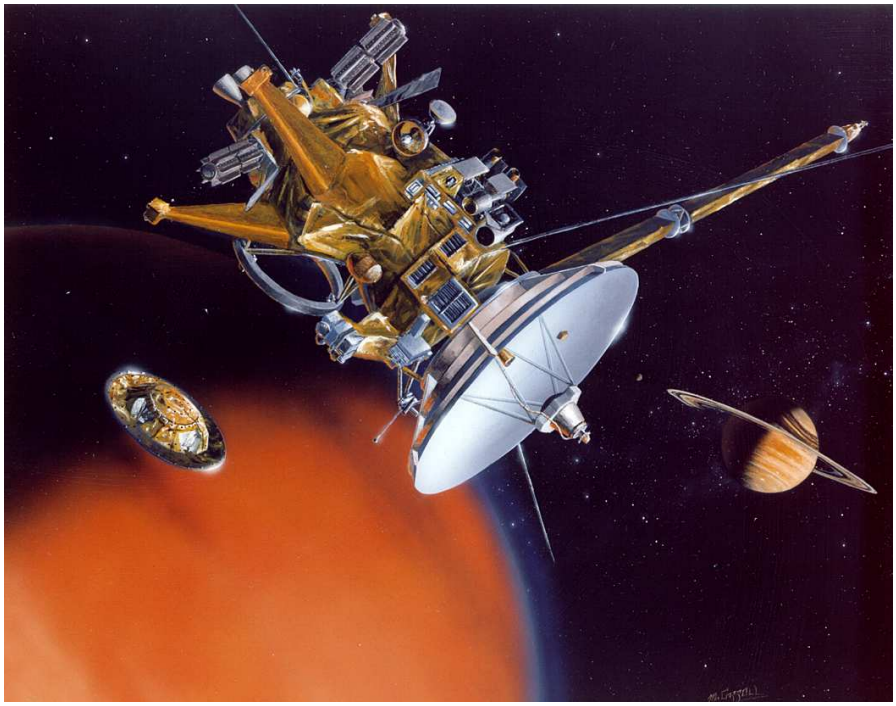

Figure 1.6. *An artist's impression of the Huygens Probe detaching from the Cassini Orbiter above Titan, with Saturn in the background. The Huygens Probe has a diameter of 2.7 metres and weighs 320 kg. The Cassini Orbiter measures 6.7 m by 4 m and weighs 5712 kg.*

This *Cassini-Huygens* mission was successfully completed on 14 January 2005 and many results from the mission have been published [28, 47]. The instrumentation aboard the *Huygens Probe* recorded a full atmospheric structure profile from an altitude of 1400 km down to the surface. The surface temperature was measured as 93.7 K and the surface pressure 1470 mbar [47]. Both values agree well with *Voyager* results.

The principal objectives of the *Cassini-Huygens* mission with respect to Titan were to determine: the mass composition of the atmosphere including abundances; the vertical and horizontal distribution of species in the atmosphere; the prevailing physical conditions; the nature of Titan's surface; and to scrutinize ionisation in the upper atmosphere and its impact on neutral species.

The radar instrument aboard the *Cassini Orbiter* recently provided one of the most astonishing discoveries of the *Cassini-Huygens* mission – that Titan does indeed have areas of liquid on its surface [48]. This makes Titan the only body other than Earth to have liquid on its surface.

Of the instruments aboard the *Cassini* spacecraft the most important to this research is the Ion and Neutral Mass Spectrometer (INMS) [49]. The instrument can operate in two modes sampling either neutral or ionic atmospheric constituents. An electron impact source is employed to ionise the neutral atmospheric species inside the sample inlet. This is disengaged to sample the ionosphere. The quadrupole mass filter within the instrument can analyze a mass range of 1 to 99 amu.

The primary objective of the INMS instrument was to identify gaseous neutrals and low energy ions (less than 100 eV) in the upper atmosphere and to examine the interaction of Saturn's magnetospheric electrons with the upper atmosphere. In order to understand the results obtained by the INMS an accurate model of Titan's neutral atmosphere and ionosphere is essential. Indeed the *Cassini-Huygens* mission provided much of the motivation behind the development of models of Titan.

Preliminary results from the *Cassini-Huygens* mission to Titan have been published in a special issue of Science [50]. Recently results of the INMS ionospheric measurements have been published [51]. The results confirm many of the characteristics predicted by models of the ionosphere.

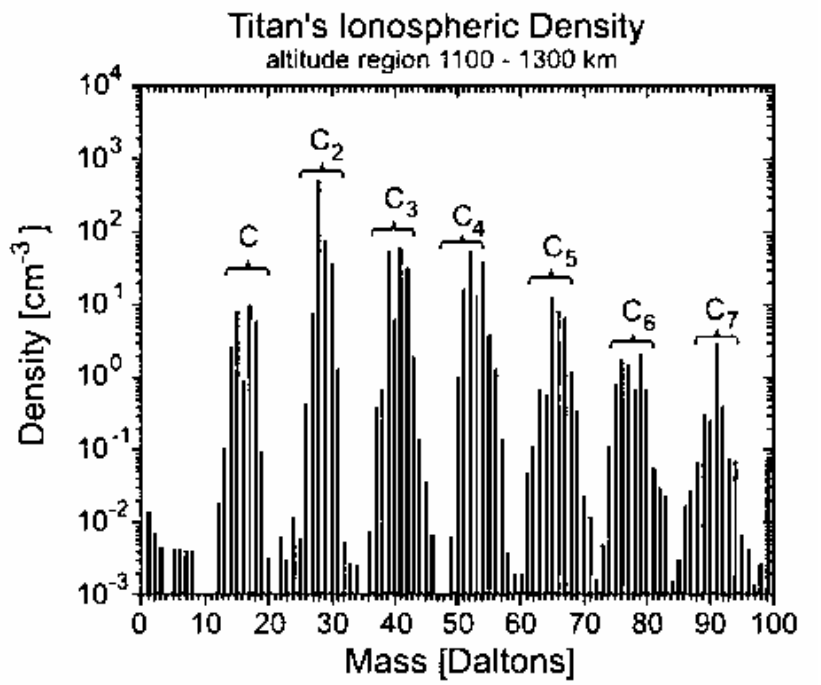

Figure 1.7. *Mass spectrum of Titan's upper atmosphere as recorded by the Cassini INMS* [52].

As expected $HCNH^+$ (m/z 28) is the dominant ionic species present (the largest peak in Figure 1.7). The mass spectra recorded by the INMS were surprisingly complex with many more ionic species being observed than predicted by pre-*Cassini* models of the atmosphere. In particular, many more nitrogen containing species were present. A key theme in this thesis is the measurement of ion-molecule reactions (including kinetics and product branching ratios) for species not previously included in models of Titan's atmosphere.

1.4 Instrumentation

The quantitative laboratory study of ion-molecule reaction kinetics was instigated by the need for laboratory data to support studies of Earth's ionosphere. Both the flowing afterglow (FA) [53, 54] and the ion cyclotron resonance (ICR) [55] techniques were developed specifically for the measurement of ion-molecule kinetics and along with the flow-drift tube (FDT) were the primary means by which gas phase ion-chemistry was examined for nearly two decades. The ICR allows measurements at lower pressures than the FA technique and is particularly useful for examining association reactions. The FA

technique allows ion chemistry to be examined at thermal energies, which is critical if the data is to be related to ionospheric chemistry. The collision-dominated afterglow plasma in the flow tube means that the reactants possess a Maxwellian distribution of kinetic energies. Below is a schematic diagram of the original FA apparatus.

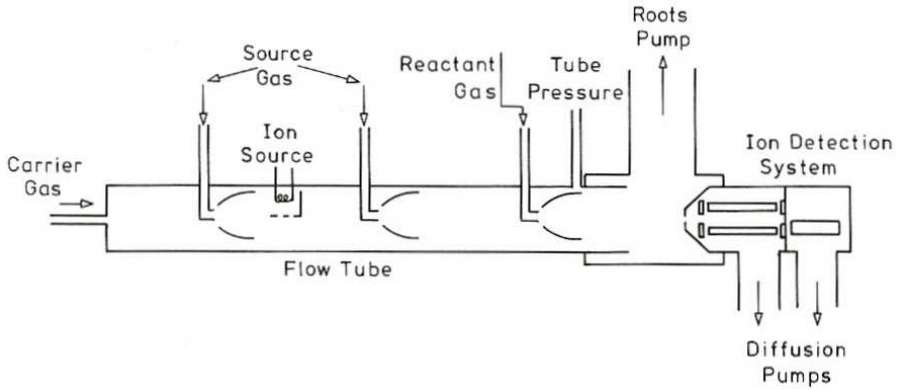

Figure 1.8. *Schematic diagram of a typical flowing afterglow apparatus* [56].

The principle of operation of a FA is as follows. Ions are generated (from an appropriate source gas) in a carrier gas (usually helium) which is drawn down the flow tube at high speed (~ 100 m s^{-1}) by a large Roots pump. The resulting plasma of ions and electrons is thermalized by the carrier gas as it travels along the flow tube. A measured flow of neutral reactant is admitted to the flow tube and reaction occurs for a fixed distance before the reactant and product ions are measured by the detection system. Reaction products and kinetics are established from analysis of the ion signals at a variety of neutral flows (See Section 2.4.3).

The FA apparatus is the forerunner to the selected ion flow tube (SIFT) instrument which has been utilised in this thesis. The separation of the ion source from the reaction region in the SIFT overcome many of the limitations imposed by the FA and FDT techniques. The ion chemistry for a single ionic species can now be examined in the absence of potentially interfering ions and the accuracy of product branching ratios is enhanced. A full description of the SIFT apparatus and its operation is given in the following chapter.

Laboratory studies of ion-molecule chemistry are usually made at room temperature rather than the very low temperatures present in ISCs or the comparatively warm temperatures in Titan's upper atmosphere. The data is however comparable to ISC

and Titanian ion chemistry as fast ion-molecule reactions tend to show minimal temperature dependence [57].

1.5 Ion-molecule Collision Theory

The theoretical treatment of ion-molecule reactions in tandem with experiments is essential to the understanding of both experimental results and the derivation of reaction mechanisms. Ion-molecule reaction rates are usually compared to the capture collision rate described by the well known Langevin expression:

$$k_c = 2\pi q\left(\frac{\alpha}{\mu}\right)^{1/2} \qquad \textbf{(1.28)}\ [58]$$

Here k_c is the capture collision rate in units of 10^{-9} cm^3 s^{-1}, q is the charge on the ion in units of $cm^{3/2}$ $g^{1/2}$ s^{-1}, α is the polarisability of the neutral in units of 10^{-24} cm^3 and μ is the reduced mass of the ion-molecule pair in grams. A measured reaction rate having a value close to the capture collision rate indicates that reaction occurs upon every collision whilst a slower rate is indicative of an energy barrier. The Langevin relationship works well for simple systems but underestimates rate coefficients for reactions between ions and polar molecules [58]. A more detailed theory is therefore needed for molecules which have a permanent dipole. The variational transition state theory of Su and Chesnavich was used in this work to calculate capture collision rates when the neutral reactant had a permanent dipole [59].

1.6 Introduction to Current Research

In ISCs, molecules are depleted by reactions, condensation on dust grains and (in diffuse clouds) by photo-dissociation, whilst ions are consumed mostly by reaction with neutrals and dissociative recombination reactions. The situation in the atmosphere of Titan is no less complex. The number of ion-molecule reactions that can potentially occur is enormous and all must be considered in models of these environments.

A complete understanding of Titan's atmosphere and of ISCs requires a comprehensive knowledge of the chemistry occurring. As new molecules are identified in the ISM, experimental data must be obtained for these species. The research in this thesis

examines a broad range of ion-molecule reactions relevant to ISCs and to the ionosphere of Titan that have not been measured previously. Models are heavily reliant on accurate laboratory data as estimated rate coefficients are not always reliable. As more ion-molecule reactions are examined and added to models their precision should be enhanced.

In the following chapters a range of experimental investigations into ion-molecule chemistry are described. With the exception of Chapters 7 and 8 the reactions investigated are relevant to the atmosphere of Titan and to the formation and reaction of complex molecules in ISCs.

In Chapter 2 details of the SIFT instrument employed to investigate the ion chemistry are outlined including the data collection software. Modifications to the apparatus necessary for individual experiments are outlined in the apposite chapters.

Chapter 3 describes a concerted effort to identify the ionic products of and to obtain an experimental rate coefficient for the gas phase reaction between H_3^+ and carbon atoms. An experimental investigation of this reaction is fundamental to solving the long standing problem of the inexplicably high CH^+ concentration in ISCs.

Chapter 4 outlines the results of an investigation into the reactivity of neutral methylenimine and propionitrile. These molecules were identified by the *Cassini-Huygens* mission as being significant constituents of Titan's atmosphere that were not included in current models of the atmosphere and ionosphere. A comparison is made between the expected ion chemistry of methylenimine and propionitrile and the observed reactivity.

The reactivity of the molecule HC_5N with a series of interstellar ions is examined in Chapter 5. This compound is also thought to be present in the atmosphere of Titan although unambiguous identification of the molecule in this environment has not yet been made. In addition to the exploration of its reactivity with simple interstellar ions its reactivity with the principal ions in Titan's ionosphere was examined.

The results of three minor projects undertaken at various times during the past four years are given in Chapter 6. Most of the results are applicable to the atmosphere of Titan with some having relevance to ISC chemistry.

The research described in Chapter 7 is unrelated to planetary and interstellar atmospheres. The SIFT instrument can be applied to the detection of trace gases in atmospheric samples, using judiciously chosen reactant ions, by a technique known as selected-ion flow tube mass spectrometry (SIFT-MS). In Chapter 7 the applicability of Lithium cations (Li^+) to trace gas detection by SIFT-MS is evaluated.

Chapter 8 presents the results of a project in which the SIFT data collection software was re-written. Although the original software was impeccable the aged computer required for its operation had become unreliable. A comparison is made between data collected with the newly developed software and the old software.

Finally, in Chapter 9 the results outlined in the preceding chapters are summarised and suggestions for future work are presented.

CHAPTER 2.

EXPERIMENTAL

2.1 Introduction

The work reported herein was conducted on a Flowing Afterglow Selected-Ion Flow Tube (FA-SIFT) at the University of Canterbury (UC) between 2005 and 2008. This instrument has been continuously modified and improved since its inception in the early 1980s. Comprehensive details of these alterations have been given by numerous authors and will not be repeated here [60-63]. Notwithstanding its history of continuous evolution, no major alterations to the SIFT (as it is often abbreviated to) were necessary during the course of this research. The essential features of the apparatus will be discussed in the following sections.

2.2 The SIFT Instrument

There are four principal regions in the University of Canterbury FA-SIFT: the flowing afterglow ion source, the reactant ion selection region, the flow tube and the detection region. The ion selection region is often referred to as the 'upstream' end of the SIFT (relative to the flow tube) and the detection region 'downstream'. All of the components within these sections have been described in depth previously, so only essential details will be given here.

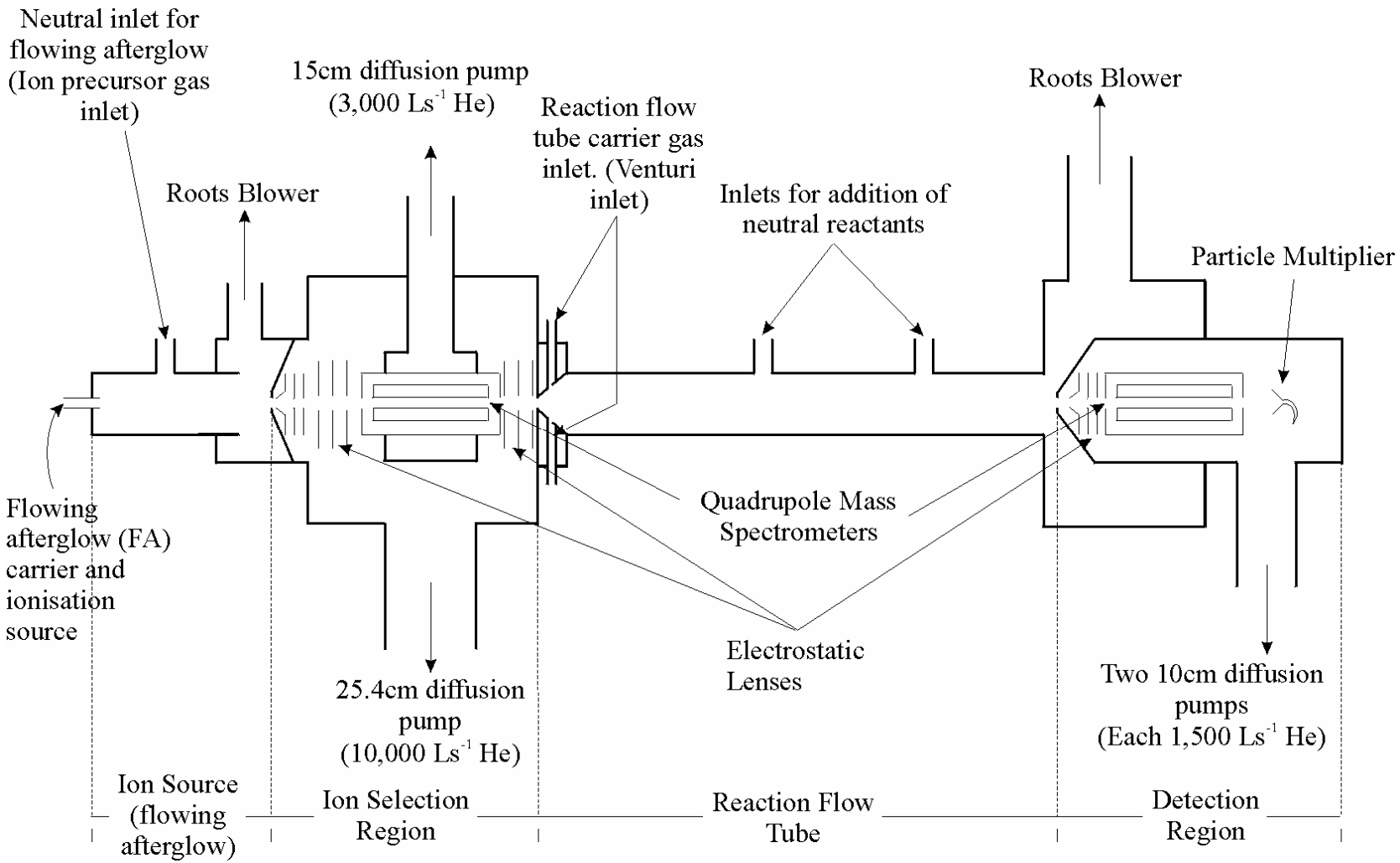

Figure 2.1. *Schematic diagram of the University of Canterbury Selected Ion Flow Tube (SIFT).*

2.2.1 Introduction

The Selected Ion Flow Tube (SIFT) was developed by Smith and Adams [64, 65] to overcome problems associated with the Flowing Afterglow (FA) (see Chapter 1). In particular, its development removed complications arising from the presence of species other than the reactant ion in the flow tube which complicated data analysis and regularly precluded the identification of true reaction products. By introducing an ion selection region between the ion source and the flow tube, ions of a single mass could be injected into the flow tube (FT) in the absence of interfering species.

A consequence of the introduction of a low pressure ion selection region - in this case a quadrupole mass filter - is reduced ion current. An efficient source of reactant ions is therefore required. Reagent ions are generated in a flowing afterglow in the UC SIFT. The FA is a versatile ion source capable of producing a wide variety of reagent ions.

Although the SIFT has the facility to produce ions from an electron impact source, all of the ions studied in this work were produced with a microwave discharge. An exception to this is the work reported in Chapter 7 which outlines the development of a lithium ion (Li^+) source which could be incorporated with the SIFT. The Li^+ ion source design did not require the FA. A detailed description of this ion source can be found in Chapter 7.

2.2.2 The Flowing Afterglow Ion Source

A microwave discharge is used to generate ions in a helium carrier gas which flow into a 205 mm long stainless steel flow tube (47.6 mm internal diameter (i.d.)) housed within a larger (125 mm i.d.) stainless steel tube. The flowing afterglow ion source mounts to the upstream quadrupole chamber via a 152.4 mm (6″) flange welded to the tip of the outer stainless steel tube. The flow tube extends to within ~ 50 mm of the nose cone (internal angle 134º) at the head of the downstream quadrupole chamber. At the apex of the nose cone is a thin molybdenum disc which transmits ions to the ion selection region through a 2 mm diameter orifice at its centre.

The FA carrier gas is pumped through a 152.4 mm (6″) diameter pumping line by an Edwards EH1200 mechanical booster pump backed by an Edwards E2M80 double stage high vacuum backing pump. The booster and backing pump combination is capable of pumping 3024 L s^{-1} at 0.3 mbar. Two gate valves separate the FA from the pumping

system, a manually operated 101.6 mm (4″) gate valve close to the FA and a pneumatically operated 152.4 mm (6″) gate valve immediately above the mechanical booster pump.

During pump down of the system (when the gate valves are closed), the ion source is isolated from the main SIFT pumping system except for the 2 mm orifice at the centre of the molybdenum disc. To improve pumping efficiency in the FA during this pump down, a bellows by-pass connecting the FA and the upstream quadrupole chamber is opened. The pressure in the FA ion source is monitored by a 0 to 10 Torr MKS 122AA capacitance manometer.

A Microtron 200 microwave power source operating at 2450 MHz and 75 W (with the same microwave cavity outlined in Scott's thesis [62]) generates the discharge. The discharge cavity encapsulates 12 mm outer diameter (o.d.) Pyrex tubing. The cavity is air cooled to prevent heat evolved by the discharge from melting the Pyrex discharge tube.

Previous workers have found it necessary to position the discharge tube at right angles to the axis of the quadrupole (Figure 2.2) [60]. Experiments demonstrated that photons generated in an on axis discharge were passing directly through the quadrupole chamber to the flow tube and photoionising impurities in the carrier gas, thus creating spurious ion signals. The addition of a Wood's horn below the discharge complements this adaptation by preventing the reflection of photons into the flow tube.

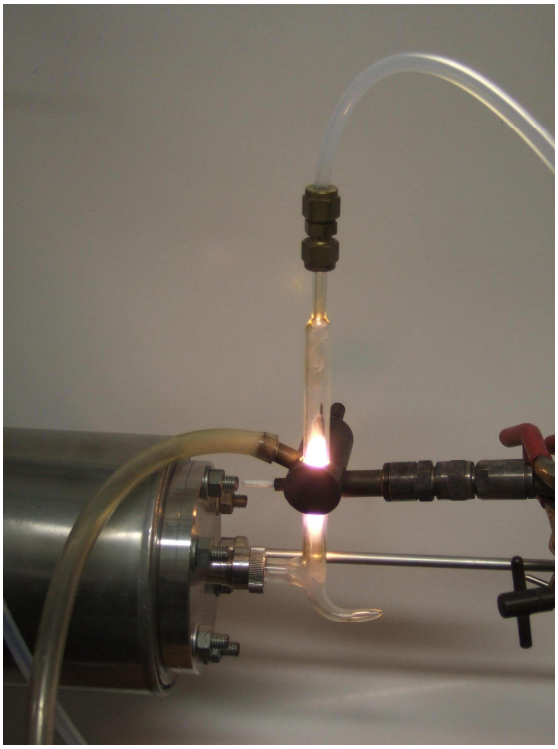

Figure 2.2. *The microwave discharge ion source in operation. A Wood's horn below the plasma prevents photons from entering the SIFT.*

The microwave discharge generates He^+ and metastable helium atoms (He 2^3S). Reactant ions are

produced by the addition of an appropriate neutral species ~200 mm downstream from the discharge. Appropriate flows of neutral (a gas or the vapour of a volatile liquid) are admitted through a Varian model 951-5100 variable leak valve. The gas or vapour is transported to the leak valve and FA inlet from the glass line (see Ancillary Systems, Section 2.3.2) by Teflon tubing.

2.2.3 The Ion Selection Region

A fraction of the ions generated in the flowing afterglow enter the upstream quadrupole chamber through an orifice in the molybdenum disc at the head of the nose cone. An array of six circular electrostatic lenses focuses these ions into a quadrupole mass filter programmed to transmit ions of a single mass. The transmitted beam of ions is collimated by three further electrostatic lenses (an Einzel type array) and injected into the high pressure flow tube through a dual annulus Venturi type injector. The stainless steel chamber housing the quadrupole and electrostatic lens assemblies is roughly cubic (~200 mm cubed) and is frequently referred to as the 'upstream quad box'. The pressure in this chamber is measured by a HFS 421 cold cathode ion gauge and microcontroller mounted to the top of the chamber.

The Quadrupole Mass Filters

The SIFT has two identical Extrel 7-270-9 quadrupole mass filters – one for reactant ion selection (upstream) and the other for analysis (downstream). Both quadrupoles consist of four 16 mm diameter, 220 mm long stainless steel rods set in ceramic supports. The mounted rods are fitted inside a cylindrical stainless steel case. Numerous 25 mm diameter holes have been drilled in the stainless steel case that sheathes the upstream quadrupole to improve pumping efficiency. Mounting plates at either end of the quadrupole case are utilised with the addition of two further electrostatic focusing lenses insulated from the case but not each other. Two Teflon supports help to align the quadrupole in the upstream chamber (visible in Figure 2.3), and also provide a rough seal between the quadrupole assembly and the rest of the chamber. The upstream quadrupole is driven by an Extranuclear power supply through a compatible Model 13 high-Q head.

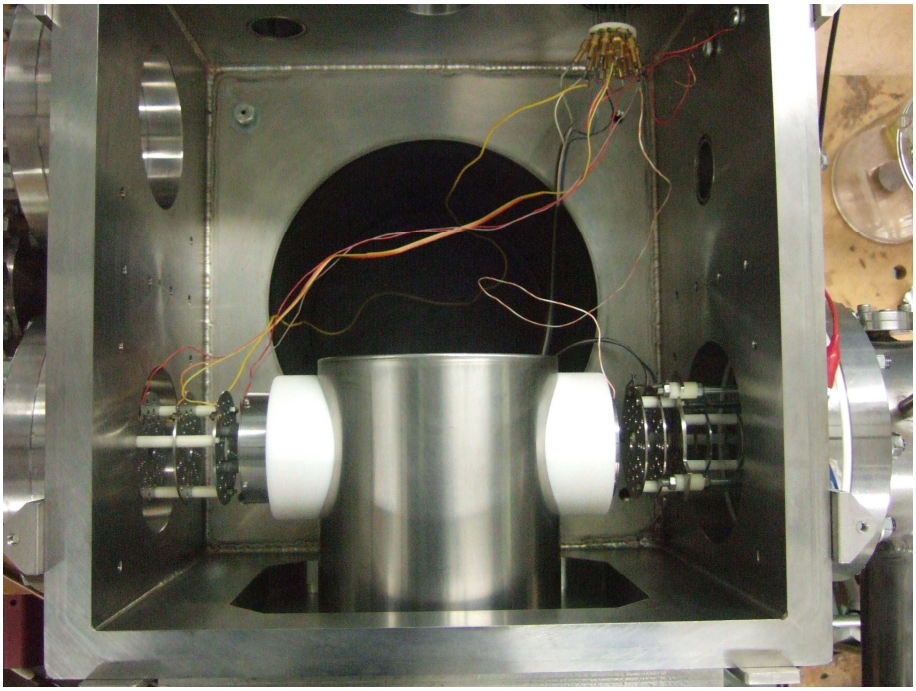

Figure 2.3. *A Bird's-eye view of the ion selection region. Ions traverse the chamber from right to left. Visible are the electrostatic lenses at either end of the quadrupole which is held in place by two Teflon supports. The chamber is pumped from below through the visible circular opening whilst the quadrupole is evacuated by its own pumping system - which operates perpendicular to both the flow of ions and the chamber's pumping system - through the stainless steel tubing in which it is mounted.*

Electrostatic Lens Assemblies

A sequence of six electrostatic lenses focuses the ion swarm transmitted by the upstream nose cone into the entrance aperture of the quadrupole. In addition to the electrostatic lenses at the front and rear of the quadrupole, a further three lenses (in the form of an Einzel array) guide ions transmitted by the quadrupole to the Venturi orifice. The lens system was designed using the SIMION 6.0 program by Petrie [61] as part of his thesis where more precise details than those given here can be found.

The first six lenses are mounted to the rear of the nose cone with the three lenses subsequent to the quadrupole being secured to the rear of the quadrupole assembly. Ceramic or Teflon spacers position the lenses as well as electrically isolating each lens from the rest of the assembly.

Pumping

Both the FA and the flow tube (FT) operate at relatively high pressure (0.3 to 0.5 Torr) in contrast to the high vacuum necessary for optimum quadrupole performance (< 1 x 10^{-5} Torr). Because the upstream quadrupole chamber is between two regions of high pressure, very high pumping speeds are necessary to maintain a high vacuum during operation.

A Varian VHS 400 (254 mm, 10″) oil diffusion pump (10000 L s^{-1}) backed by a Leybold-Haraeus Trivac D65B rotary pump (18 L s^{-1}) preserves a vacuum of ~5 x 10^{-5} Torr in the chamber during operation. A pneumatically operated Temescal gate valve at the base of the chamber automatically isolates the diffusion pump from the chamber if the pressure exceeds a preset limit (~ 2 x 10^{-4} Torr) as measured by the cold cathode ion gauge (see Protection Circuitry, Section 2.3.3). A series of louvres and a cryogenic trap cooled by liquid nitrogen prevent oil vapour from entering the quadrupole chamber.

The quadrupole is evacuated directly by a second oil diffusion pump, further reducing the pressure in the quadrupole relative to the chamber in which it is housed. The quadrupole is evacuated by a Varian VHS 6 (152.4 mm, 6″) oil diffusion pump (2400 L s^{-1}) backed by a Leybold-Haraeus Trivac D30A mechanical pump (12.7 L s^{-1}). As with the 254 mm diffusion pump, the 152.4 mm pump can be isolated from the quadrupole assembly by a pneumatic gate valve. A Duniway I-075-K ion gauge is used to measure the pressure in the region of the quadrupole which is usually ~1 x 10^{-5} Torr during operation.

Summary

In the ion selection region, a swarm of ions is focused into the entrance aperture of the quadrupole mass filter. The quadrupole is set to transmit ions of a single m/z ratio which are focused by an Einzel array of electrostatic lenses into the Venturi orifice and the flow tube.

2.2.4 The Venturi

The Venturi inlet separates the upstream quadrupole chamber from the flow tube and is vital to the efficient transmission of ions from the low pressure ion selection region to the high pressure flow tube. It is also the last electrostatic lens in the ion selection region, insulated from the flange to which it is mounted by a thin Teflon disc. The

function of the Venturi is to prevent the back-streaming of carrier gas into the upstream quadrupole chamber and hence to allow efficient transmission of ions to the flow tube.

Helium carrier gas is injected through a narrow circular annulus which rings the 2 mm ion injection orifice at the centre of the Venturi assembly. The annulus is 0.025mm wide and has an internal diameter of 8.7 mm. The width of the annulus is such that positioning is critical. A turbulent flow created by poor alignment will have severe implications for the passage of ions. Although the procedure for centering the annulus is simple, optimisation of the set-up is often difficult.

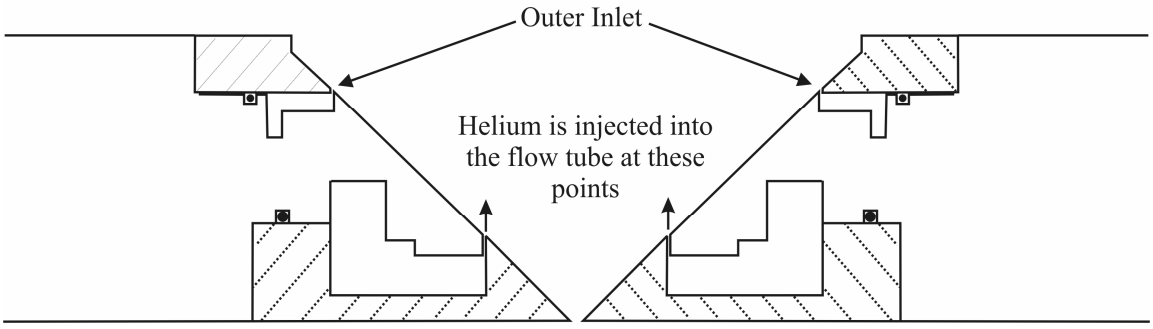

Figure 2.4. *A schematic diagram of the Venturi injector.*

To centre the Venturi, it is removed from the SIFT and laid flat with the injector facing upwards. A few drops of petroleum ether are allowed to fall around the edge of the annulus whilst a small flow of argon is passed upwards through the annulus. Visual inspection of the direction in which the pet ether is driven demonstrates the alignment of the annulus. If the gas is not dispersed evenly around the circular inlet, its position can be adjusted by tightening (or loosening) the eight mounting screws on the rear of the Venturi assembly. Multiple adjustments are commonly required to achieve a satisfactory alignment.

The University of Canterbury Venturi injector has a second annular slit (0.4 mm wide) at a much larger diameter of 37.1 mm. This does not act as a Venturi injector but assists in smoothing the transition from turbulent to laminar flow in the region around the inner annulus. The second annulus can also be used to increase the carrier gas flow without disrupting the Venturi's performance (which can be affected at critical flows). This annulus was not used in this work.

2.2.5 The Flow Tube

Ions injected into the FT through the Venturi orifice are thermalized by multiple collisions with the carrier gas. Collision induced dissociation is not uncommon when weakly bound ions are injected. In these situations it may be necessary to modify the injection conditions. Neutral species are admitted to the flow tube and react with the ions over a fixed distance where the reaction conditions are well defined. A small fraction of the reactant and product ions are then continuously sampled through an orifice at the head of the detector assembly.

Dimensions

The 1110 mm long flow tube is constructed from stainless steel tube with an internal diameter of 73 mm. The flow tube has 70 mm (2¾″) 'access' flanges at regular intervals along its length through which neutral reactants can be added. An 80 mm long, 148 mm wide section of bellows at the downstream end of the flow tube joins the flow tube to the downstream quadrupole chamber. The incorporation of this bellows section minimises the transmission of vibrations from the mechanical pumps to the rest of the system. The flow tube diameter is maintained within the (wider) segment by a stainless steel section concentric to the bellows which extends to within 40 mm of the downstream nose cone.

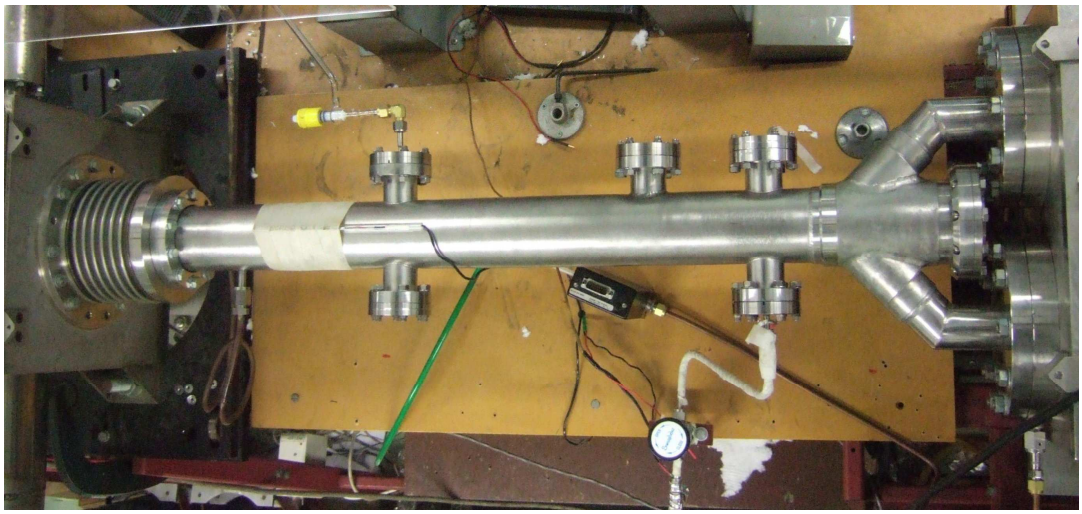

Figure 2.5. *The SIFT Flow Tube. Ions pass from right to left. Neutrals can be admitted through any of the ports visible on the axis. The main inlet which connects the glass line to the flow tube can be seen in the upper left. The yellow Young's tap is used to isolate the FT from the glass gas handling line. The inlet employed for trace gas analyses can be seen at the bottom right of the flow tube.*

The Admission of Neutral Reactant

The inlet 710 mm from the plane of the downstream nose cone has been adapted specifically for trace gas analyses. Small flows of air or breath samples (to be analysed) are admitted through a 50 mm long section of 25 gauge stainless steel hypodermic tubing. The narrow diameter tubing conductively limits the gas flow and is essentially a calibrated leak. A section of 6.35 mm (¼″) diameter stainless steel tubing guides the sample to the flow tube where it is injected into the centre of the gas flow. The inlet is electrically heated to prevent analyte gases from adsorbing to the walls of the inlet. A bellows valve between the narrow gauge tubing and the 6.35 mm tubing remains closed when the valve is not in use.

As this research was not primarily concerned with trace gas analysis this inlet was not used often. It was occasionally used to admit vapour flows of benzene, toluene and various ketones for the determination of mass discrimination factors (Section 2.4.4) and to admit lab air to the flow tube. Moisture in the laboratory air creates clusters with H_3O^+ reagent ions, ($H_3O^+.(H_2O)_n$ up to n=3), which are useful in calibrating the scale of mass spectra.

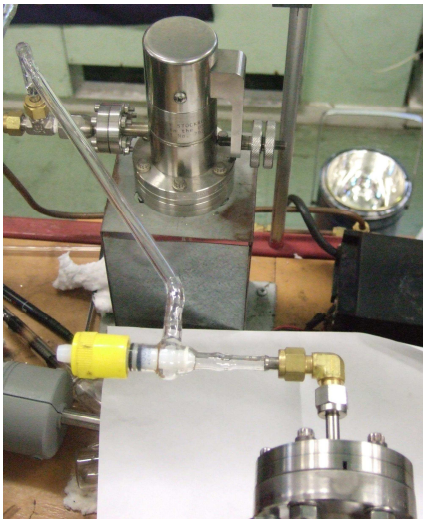

Figure 2.6. *The neutral inlet assembly. The gas handling line is connected to the Varian leak valve (background). Gases admitted through the valve flow through 6.35 mm (¼") glass tubing to the flow tube (foreground) where they are injected against the carrier gas flow through a 'shower-head' inlet.*

For reaction studies, one of two inlets coupled to the glass gas handling line (Section 2.3.2) via 6.35 mm (¼″) glass tubing is used to admit neutral species to the flow tube through a ring-type injector. The flow of gas to the FT is controlled by a Varian model 951-500 variable leak valve. The ring-type injectors face **upstream** in the flow tube to improve mixing of the neutral into the carrier gas flow. Reactant gases are often 'sticky' and readily adsorb to the walls of the inlet tubes. A small flow of helium is added to the flow of neutral reactant to reduce surface adsorption between the leak valve and the main flow tube region. For the vast majority of the rate constants measured in this work, the neutral was added through the port

located 504 mm upstream of the plane of the downstream nose cone. This inlet was modified for the production of CH_2NH as outlined in Chapter 5.

The second neutral inlet port, utilised in the work described in Chapters 6 and 7, is located 784 mm from the plane of the downstream nose cone.

2.2.6 The Analysis and Counting Region

A tiny but consistent fraction of the reactant and product ions in the flow tube is sampled through a small orifice in the downstream nose cone. Through this orifice lies the analysing quadrupole and particle multiplier. A full description of the downstream quadrupole, electrostatic lens assembly and ion detection system has been given previously and will not be repeated [60, 63]. The essential features are described next.

The Nose Cone and Analysing Assembly

The downstream nose cone consists of a 210 mm long tube (diameter 152 mm or 6″) with a conical section (with an internal angle of 126º) attached to its front end. The nose cone extends from the rear of the downstream quadrupole chamber to within 40 mm of the flow tube. A thin, 40 mm diameter molybdenum disc is affixed to the apex of the nose cone. The molybdenum disc is insulated from the nose cone so that it can be floated at different voltages. Ions are sampled through a 0.36 mm diameter orifice at the centre of the disc. The conical shape of the nose cone improves pumping efficiency around the molybdenum disc minimising turbulence near the ion sampling orifice.

Immediately behind the molybdenum disc, three electrostatic lenses form an Einzel array which guides the sampled ions into the quadrupole. As with the upstream quadrupole assembly there are two additional focusing electrostatic lenses at the front and rear of the quadrupole that cap the quadrupole assembly. The quadrupole is identical to that used upstream except that a model 12 high-Q Head is used in place of a model 15. The downstream quadrupole is coupled to a PC and controlled by purpose written software (see below and also in Chapter 8).

The Particle Multiplier

A continuous dynode particle multiplier, (De-Tech model XP-2122, gain 10.2 x 10^7 at 1900 V) is situated immediately behind the quadrupole exit. Depending on age and condition of the particle multiplier, operating voltages between 1600 and 2500 V were used. Electrical pulses from the particle multiplier are passed to an Advanced Research

Instruments model F-100-T preamplifier/discriminator which outputs TTL pulses. The preamplifier must be effectively grounded for noise free operation. The TTL pulses are fed to a PC lab card (Advantech PCL-812-PG) and a pulse counter/ratemeter circuit.

SIFT Data Analysis

Data generated in experiments is analysed and presented graphically in real time by *Sift for Windows*, a computer program developed specifically to measure the kinetics of SIFT experiments. The program was written by Dr Patrik Španěl who generously donated the program to the University of Canterbury SIFT laboratory in 1994.

The program is written in the Borland Pascal language and works well, however it runs on an old (circa. 1998) computer which has become increasingly unreliable and difficult to fix. To allow a more modern and reliable computer to be used, as part of this thesis the SIFT software has been rewritten with LabVIEW. Details of this as well as an in depth summary of *Sift for Windows* are given in Chapter 8.

All of the experimental rate measurements and mass spectra in this thesis were measured using *Sift for Windows* with the exception of some of those given in Chapter 8.

Figure 2.7. *Four of the SIFT's backing pumps located in the pump room.*

Downstream Pumping System

The flow tube is pumped by a high capacity Japan Vacuum Engineering PMB-020 roots blower (570 L s^{-1} at 0.1 Torr) backed by a large Japan Vacuum Engineering PKS-030 mechanical backing pump.

Two 102.6 mm (4″) Varian VHS-4 oil diffusion pumps (1500 L s^{-1} each) are used to maintain a high vacuum in the quadrupole during operation. Both are backed by Welch Scientific Company Duo Seal model 1397 two stage mechanical pumps. A 25 mm diameter bypass line connects the pumping system for the downstream quadrupole chamber to the flow tube during warm-up. A bellows valve is used to close the bypass

line and isolate the FT from the quadrupole during operation.

As with the upstream quadrupole the pressure in the quadrupole region is measured by a Duniway I-075-K vacuum ionisation gauge.

The backing pumps for both the upstream and downstream sections of the SIFT are located in a room separate to the main SIFT instrument referred to as the pump room. This significantly reduces audible noise in the laboratory.

2.3 Ancillary Systems

2.3.1 Helium Gas Flow System

A helium cylinder in the pump room supplies gas to both the flowing afterglow and the flow tube via 6.35 mm (¼″) diameter copper tubing. Impurities in the gas are removed by a molecular sieve trap cooled to ~ 77 K by liquid nitrogen. An MKS model 1179A mass flow controller (MFC) calibrated for helium with a maximum flow rate of 10000 sccm controls and meters the flow of gas to the FA. A 20000 sccm model 1179A MFC also calibrated for helium controls and meters the flow of gas to the FT. The MFCs are connected to an MKS type 247 4-channel readout on which gas flows are set manually.

When not in use the helium line is evacuated by a Hitachi 3VP-C mechanical pump. Four heating elements surrounding the molecular sieve trap allow it to be baked under vacuum at up to 80ºC. The trap is baked monthly to remove accumulated impurities that impair trap efficiency.

2.3.2 The Glass Gas Handling Line

Neutral reagents (gases or vapours of volatile liquids) are added to the SIFT from the glass gas handling line. Constructed from Pyrex, the line is designed in sections which can be isolated from both the rest of the glass line and the backing pump. This permits the use of multiple gases simultaneously.

A glass oil diffusion pump backed by a Jigtool SE 200 mechanical pump provides a background vacuum of 10^{-3} Torr in the glass line. The exhaust from the Jigtool pump is piped to the departmental fume-cupboard gas extraction system to prevent the release of noxious vapours into the laboratory. A 0 to 10 Torr MKS 122A capacitance manometer measures the pressure in the glass line as well as the flow tube. Gas taps either side of the

manometer in the glass line allow the measurement of pressure in each section independently.

The majority of the gases used in the laboratory are stored in portable glass bulbs. These bulbs attach to the line by B14 ground glass joints. More commonly used gases such as argon and oxygen are stored in 5 litre bulbs permanently connected to the glass line. The 5 litre bulbs are also utilised in the preparation and storage of gas mixtures such as the carbon monoxide in helium mixtures described in Chapter 3.

The flow of a neutral reactant admitted to the FT is determined by measuring the drop in pressure in a calibrated volume as a function of time. Three calibrated volumes are available in the glass line with the volume used depending on the reaction rate being measured. Slower reactions require larger gas flows and hence larger volumes. The pressure change in the calibrated volumes is measured by a Validyne DP15-20 differential pressure transducer. The response of the Validyne is fed directly to the PC lab card.

2.3.3 SIFT Protection Circuitry

Several of the key SIFT components are pressure sensitive. A sudden increase in pressure could cause significant damage to the quadrupoles, diffusion pumps and the particle multiplier. For this reason the SIFT has a system of protection circuits. These prevent 'operator' damage to the system in two ways. Firstly components cannot be turned on when it is not safe to do so i.e. the diffusion pumps can only be turned on when the backing pumps are running and cooling water is flowing. Secondly, if the pressure in the upstream quadrupole chamber (as measured by the cold cathode gauge) exceeds a certain preset limit (2×10^{-4} Torr), all pneumatic gate valves are automatically closed and power to all of the diffusion pumps (but not the backing pumps) and electronic components cut. This system can be set to by-pass during evacuation of the apparatus after opening to air when the pressure is well above the preset operating limit.

A shortcoming in the protection system is that the pressure around the downstream quadrupole is not measured as part of the circuit. Care must therefore be taken to ensure that the pressure is at a safe level before powering up the downstream quadrupole and the particle multiplier. It is particularly important in this respect to ensure

that the by-pass valve between the flow tube and the downstream diffusion pumps (which essentially connects the quadrupole to the flow tube) is closed (see Section 2.2.6.).

2.4 SIFT Kinetics

The following summary will demonstrate how the rate coefficient for a simple SIFT ion-molecule reaction can be determined.

2.4.1 Theory

Consider the determination of the rate constant for the generic bimolecular ion-molecule reaction **(2.1)**:

$$A^+ + B \rightarrow \text{Products} \qquad \textbf{(2.1)}$$

For SIFT kinetics the rate law for this reaction includes terms for both reactive and diffusive losses of A^+:

$$Rate = \frac{d[A^+]}{dt} = -k[A^+][B] - [A^+]\frac{D_i}{\Lambda^2} \qquad \textbf{(2.2)}$$

where $[A^+]$ and [B] are the reactant concentrations at time t, k is the (second order) rate constant, D_i is the free diffusion coefficient for the A^+ ions and Λ is the characteristic diffusion length of the flow tube. For all SIFT measurements the neutral reactant is in great excess of $[A^+]$ and pseudo-first order kinetics prevail. Allowing for this and ignoring the diffusive term (which is constant), integration of **(2.2)** yields:

$$\ln\left(\frac{[A^+]}{[A^+]_0}\right) = -k[B]t \qquad \textbf{(2.3)}$$

where $[A^+]$ is the reactant ion signal at time t, $[A^+]_0$ is the initial reactant ion signal (that is with no neutral reactant flowing), k is the rate coefficient for the reaction and [B] is the number density of reactant in the carrier gas (in molecules cm^{-3}) at time t. A plot of $\ln[A^+]$ against [B] should give a straight line with a slope of $-kt$.

First order reaction kinetics are usually measured by observing the decay of a reactant **with time** at a fixed ratio of reactants. For SIFT kinetics, however, $[A^+]$ is monitored as a function of neutral reactant over a **fixed time**. The reaction time is determined from the length over which the reaction occurs and the velocity of ions in the flow tube.

2.4.2 Carrier gas and ion velocity

The velocity of the helium carrier gas in a flow tube, v_g, is determined from the relationship:

$$v_g = \frac{\Phi_c}{p_g} \cdot \frac{4}{\pi D_t^2} \cdot \frac{T_g}{273} \qquad \textbf{(2.4)}$$

Here Φ_c represents the carrier gas flow rate, p_g the pressure in the flow tube, D_t the flow tube diameter and T_g the temperature in Kelvin. Typical values for the UC SIFT are Φ_c = 193 Torr L s^{-1}, p_g = 0.46 Torr and D_t = 73 mm which gives a carrier gas velocity of around 100 m s^{-1}.

Due to the radial profile of the fast flowing carrier gas, which the ions are at the head of, the velocity of the ions is greater than that of the carrier gas. The ion velocity for the UC SIFT has been experimentally determined to be $1.5v_g \pm 0.1$ in close agreement with the value of 1.45 obtained by Spanel and Smith for their SIFT [63, 66].

The reaction length is the distance from the showerhead ring inlet where the neutral reagent is introduced to the flow tube, to the downstream molybdenum disc through which the reactant and product ions are sampled for detection. In practice this distance (504 mm for the UC SIFT) must include a correction factor (ε) of a few centimetres to account for mixing effects as the neutral is injected against the carrier gas flow. Conventionally ε is determined by making multiple measurements of reaction **(2.5)** for which the rate coefficient is known accurately.

$$Ar^+ + O_2 \rightarrow O_2^+ + Ar \qquad k = 4.6 \times 10^{-11}\ cm^3\ s^{-1} \qquad \textbf{(2.5)}\ [67]$$

The reaction length used in determining the reaction time (in equation **(2.3)**) is adjusted accordingly. The value of ε so determined is approximately 20 mm for the UC SIFT. Under typical operating conditions the SIFT reaction time (reaction length divided by ion velocity) is 3.4 ms.

2.4.3 The Practical Measurement of Rate Coefficients

The velocity of ions is readily determined from the relationships given above. The reaction length is also known and hence the reaction time is easily calculated. From equation **(2.3)** the remaining unknown parameters required to determine k are the reactant ion signal and the concentration of neutral reactant.

Kinetics experiments begin with the observation of a mass spectrum. Reactant ions of a single mass are injected into the flow tube where a reasonably high flow of neutral reactant is added. The mass scan identifies the m/z values of the products of the reaction and gives an experienced operator a qualitative indication of the reaction rate (and hence the appropriate calibrated volume to use, Section 2.3.2).

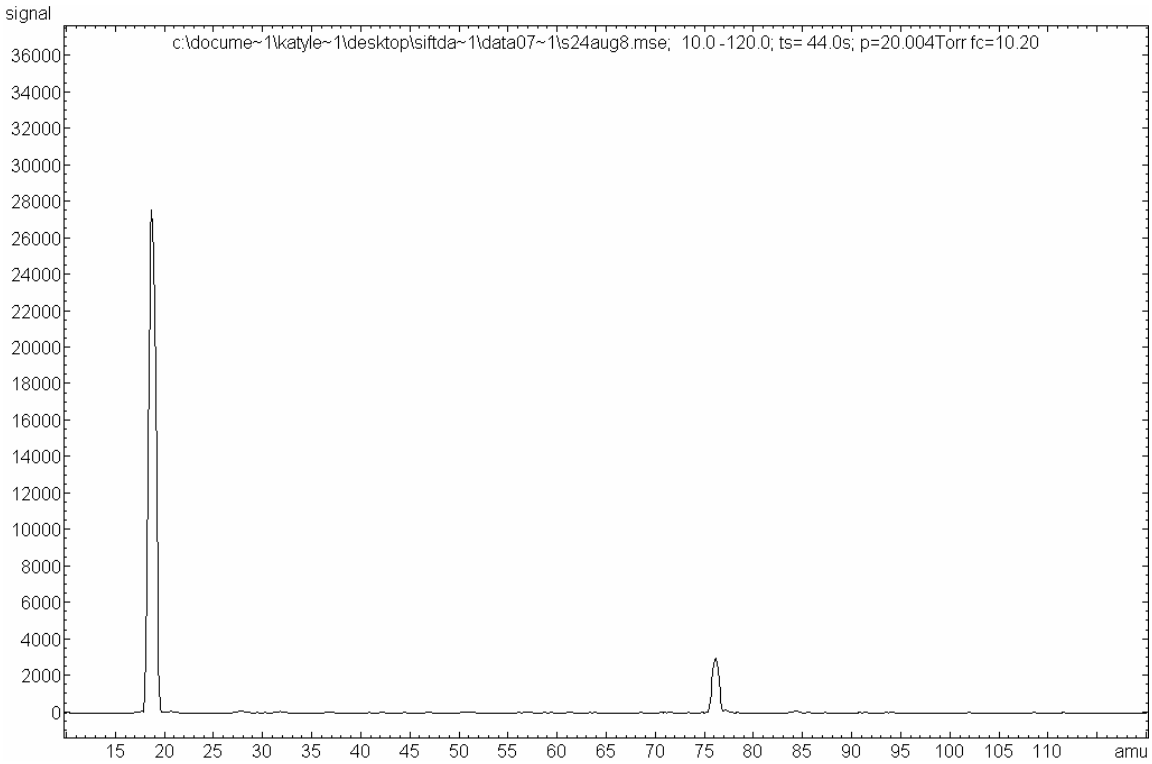

Figure 2.8. *Mass scan demonstrating the reaction of H_3O^+ (m/z 19) precursor ions with HC_5N which generates HC_5NH^+ (m/z 76).*

The precursor ion and product ion counts are then measured at a variety of neutral flow rates. It has already been shown that a plot of $\ln[A^+]$ vs [B] should give a straight line with slope $-kt$. A typical set of reaction data is presented in Figure 2.9. The rate of reaction is determined from the slope of the logarithmic decay in precursor ion signal divided by the reaction time. The SIFT set-up permits the determination of pseudo-bimolecular rate coefficients from ~ 5 x 10^{-13} cm^3 $molecule^{-1}$ s^{-1} up to collision rate reactions of ~ 5 x 10^{-9} cm^3 $molecule^{-1}$ s^{-1}.

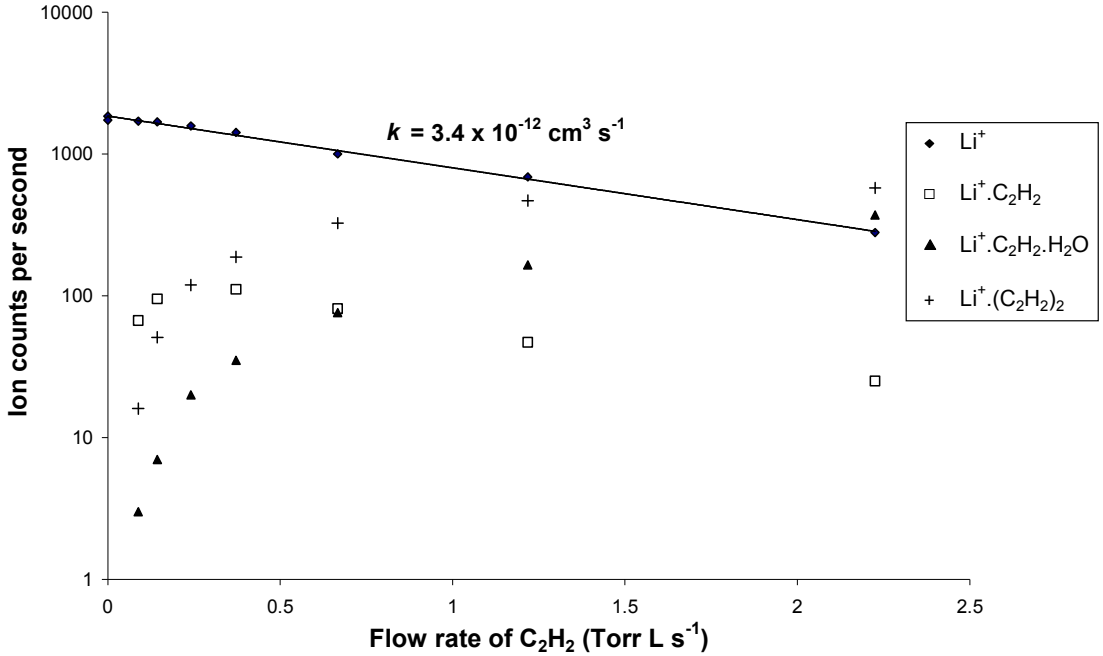

Figure 2.9. *Semi-logarithmic decay of lithium ion signal with increasing acetylene flow showing corresponding increase of product ions. Note that the primary product ion ($Li^+.C_2H_2$) signal increases initially before decreasing at higher flows due to secondary reactions with H_2O and C_2H_2.*

It is clear in Figure 2.9 that $Li^+.C_2H_2$ is the primary product of this reaction. Both $Li^+.(C_2H_2)_2$ and $Li^+.C_2H_2.H_2O$ are secondary products resulting from the reaction of $Li^+.C_2H_2$ with either excess C_2H_2 or H_2O impurities (which are typically less than 1 ppm). For many reactions it is not as obvious which are primary and which are secondary products. The procedure for determining the product branching ratios is straightforward. Each product ion signal is plotted as a percentage of total product ion counts at each neutral flow as shown in Figure 2.10.

Extrapolation of the percentage of each ion signal to zero neutral flow gives the product branching ratios for the reaction. Because there is only one primary product for this reaction, extrapolation of the $Li^+.C_2H_2$ signal to zero flow gives a branching ratio of 100%. Secondary products are characterised by the fact that they will always extrapolate to 0% at zero neutral flow.

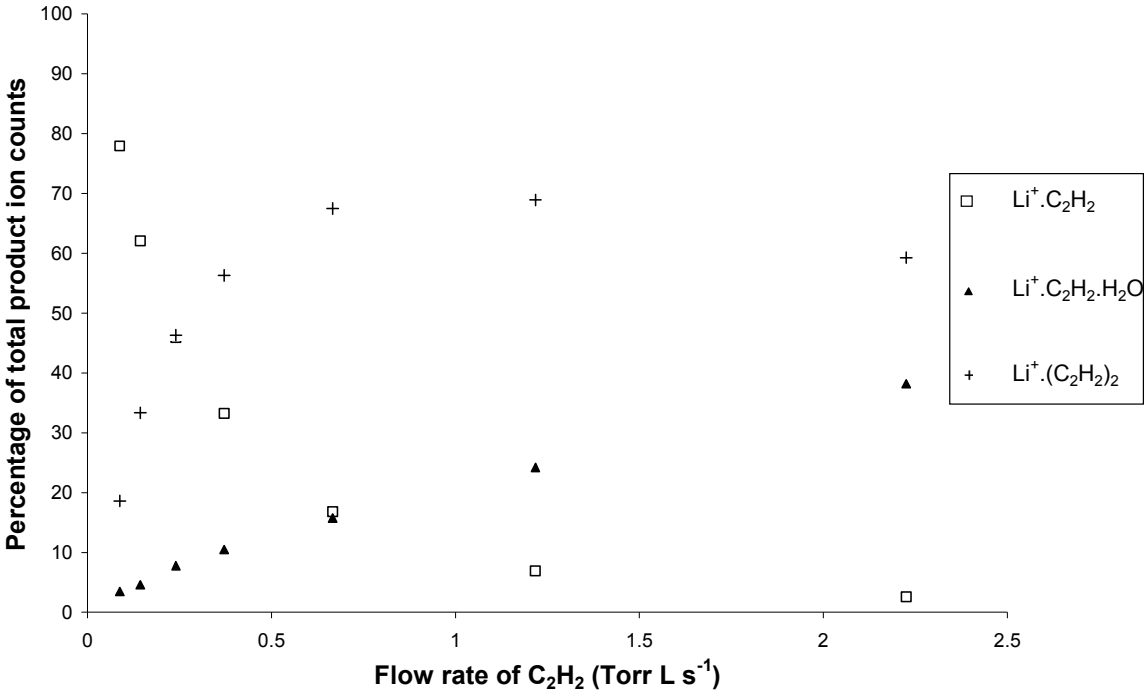

Figure 2.10. *Extrapolation of product ion signals as a percentage of total product ions to zero neutral flow confirms $Li^+.C_2H_2$ as the true primary product of the reaction. Because both $Li^+.(C_2H_2)_2$ and $Li^+.C_2H_2.H_2O$ form by secondary reactions with excess C_2H_2, they trend towards 0% of total ion count at zero neutral flow.*

2.4.4 Mass Discrimination and Diffusion Enhancement

A negative aspect of using quadrupole mass spectrometers is the variation in ion count which occurs as the m/z ratio is changed. Known as mass discrimination, this effect becomes important for masses greater than 100 amu for the UC SIFT instrument. Mass discrimination is specific to particular equipment settings including the voltages used in the detector assembly and the resolution setting of the quadrupole.

Ionic diffusion also causes unwanted variations in ion signal as the m/z ratio is changed. Heavier product ions diffuse more slowly to the FT walls than lighter ions as they are transported along the flow tube. This enhances the ion signal of the heavier ions relative to the lighter ions. This diffusion enhancement can affect product branching ratios when product ions have vastly different m/z ratios because the heavier ion's signal is erroneously boosted.

Mass discrimination and diffusion enhancement both occur in the UC SIFT and counteract each other. The overall effect is consequently small at m/z ratios less than 100, above which mass discrimination worsens.

Correction for mass discrimination and diffusion enhancement is made by calibration of the apparatus following the procedure of Španěl and Smith [68]. This method produces a mass specific correction (characterised by the mass discrimination factor or MDF) which includes correction for both effects. The separate contributions of diffusion enhancement and mass discrimination are determined experimentally. H_3O^+ is injected into the FT and the ion current on the downstream molybdenum disc (through which ions are sampled for detection) is measured as well as the ion signal detected by the particle multiplier. The detected ion signal should be proportional to the current on the molybdenum disc from the ratio of the size of the orifice in the disc to the disc's overall size. A neutral such as benzene is added to the H_3O^+ flow to produce a new ion ($C_7H_6^+$) having a higher mass and the ion current on the molybdenum disc and the ion signal re-measured. This process is repeated with a series of neutrals that form product ions (with H_3O^+) that cover the range of m/z ratios accessible by the instrument. This can usually be achieved with five or six judiciously chosen ketones which form protonated dimers with H_3O^+. It is important to this procedure that each reaction produces a single product ion and that total conversion of H_3O^+ to the new product ion is achieved.

A qualitative assessment of the effects of mass discrimination and diffusion enhancement can be made immediately from inspection of the results. Firstly, for species with higher m/z ratios than H_3O^+ the ion currents at the molybdenum disc are noticeably greater due to diffusion enhancement. Secondly, the ion signals measured by the detector increase slightly to begin with (the effect of diffusion enhancement slightly exceeds mass discrimination) but fall consistently above m/z 100 as the effect of mass discrimination begins to dominate. Analysis of the data following the procedure of Španěl and Smith leads to a plot of MDF against m/z ratio (see Figure 2.11).

For ions having m/z ratios less than 100 the MDF is close to unity. As the vast majority of reactions in the thesis are concerned with reactions having product ions with masses below 100, MDFs were largely ignored. However, mass discrimination and ionic diffusion are however the source of the largest error in product ion branching ratios

reported in this thesis. Product distribution ratios are considered to be accurate to ± 20% unless otherwise stated.

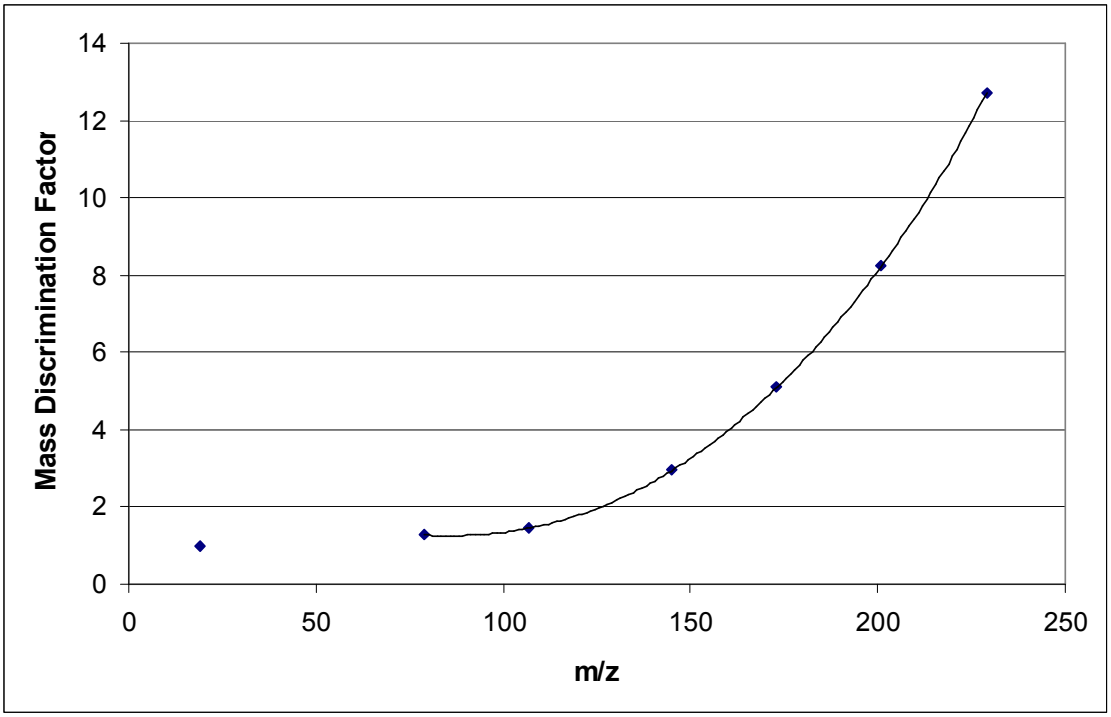

Figure 2.11. *A typical plot obtained from a mass discrimination experiment with the UC SIFT. These results were obtained at a resolution of 7.0. Correction for mass discrimination in kinetic experiments is made by multiplying the observed ion counts at each m/z by the mass-dependent mass discrimination factor, obtained from the curve in the above graph.*

2.5 Reagents and Physical Conditions

The gas supplied to the FA and FT was initially instrument grade helium (99.99% purity) obtained from BOC gases. During the course of this research the gas supplier was changed to Southern Gas Services Ltd who supplied helium with a stated purity of 99.995%. Sources of all other reagents used in this thesis are provided in the chapter where their use is described. All liquid reagents were further purified by multiple freeze-pump-thaw cycles.

Collision rate coefficients were calculated using the parameterised method of Su and Chesnavich [59]. Dipole moments and polarizabilities were taken from the CRC Handbook of Chemistry and Physics unless otherwise specified [69].

All measurements were made at a flow tube pressure of 0.46 Torr and at a room temperature of 294±4 K.

Rate coefficients determined in this work are considered to have an experimental uncertainty of ±20% for permanent gases and ±30% for vapours unless otherwise stated.

Thermodynamic quantities (at 298 K) were obtained from Gas Phase Ion and Neutral Thermochemistry [70] or the NIST Chemistry Webbook [71].

Table 2.1. *Typical regional standard operating pressures for the SIFT*

Region	During Pump Down	During Operation
Ion Source	2×10^{-6}	0.35
Ion Selection Chamber	2×10^{-6}	5×10^{-5}
Upstream Quadrupole	2×10^{-6}	1×10^{-5}
Flow Tube	6×10^{-7}	0.46
Analysing Assembly	6×10^{-7}	4×10^{-6}

CHAPTER 3.

ATTEMPTS TO GENERATE ATOMIC CARBON FOR REACTION

3.1 Introduction

Approximately 140 molecules have been identified in the interstellar medium [72] of which nearly three quarters contain at least one carbon atom. How this element is incorporated into so many interstellar molecules is of tremendous interest.

Carbon is the fourth most abundant atomic species in ISCs behind hydrogen, helium and oxygen, and has a typical fractional abundance (relative to H_2 = 1) of ~ 4 x 10^{-8} in dense ISCs at 10 K [6]. Higher fractional abundances are found in diffuse clouds where the carbon is less likely to be 'locked-up' in molecular species. Elevated levels of carbon can also be found near so-called C-rich giant stars [73].

At the temperature of interstellar clouds (10-100 K), reaction chemistry is dominated by exothermic ion-molecule reactions which require no activation energy and are rapid in this cold environment. Although some classes of neutral-neutral reaction can be rapid at interstellar cloud temperatures, models of interstellar clouds constructed entirely of ion-molecule reactions have been quite successful at predicting observed fractional abundances of ions and molecules [3, 74, 75]. The formation of H_2 is an exception which requires a different mechanism based on grain chemistry, described in Chapter 1. Ion-molecule reactions are considered the major route by which carbon-containing molecules are formed in the ISM.

Carbon is relatively easily ionised in the ISM by either cosmic rays or ultraviolet radiation and a reasonable fraction is converted to C^+ in ISCs. The reaction of C^+ with the most abundant interstellar molecule, hydrogen, was considered to be the starting point for hydrocarbon formation in ISCs for many years.

$$C^+ + H_2 \rightarrow CH_2^+ + h\upsilon \qquad \textbf{(3.1a)}$$

$$\rightarrow CH^+ + H \qquad \textbf{(3.1b)}$$

The ions produced by reaction **(3.1)** (CH^+ and CH_2^+) initiate a series of ion-molecule reaction pathways from which molecules of remarkable size and complexity are formed [3, 76]. Successful modeling of the chemistry occurring in diffuse and dense ISCs is highly dependent on the efficient formation of these ions. The radiative association reaction **(3.1a)** has been examined experimentally and found to be slow (k = 7.2 x 10^{-16} cm^3 s^{-1} at 80 K [77]) in close agreement with theory [78]. Reaction **(3.1b)** is endothermic by 37.4 kJ mol^{-1} [70] and therefore highly unlikely to be an efficient source of CH^+ in ISCs. Clearly then reactions **(3.1a)** and **(3.1b)** are not efficient sources of the primary hydrocarbon species CH^+ and CH_2^+ in the ISM. Indeed the most significant failing of early models of ISC chemistry was their inability to accurately predict the observed fractional abundance of CH^+ in diffuse ISCs, which was always considerably higher than permitted by reaction **(3.1b)** [75]. This issue is compounded by the rapid depletion of CH^+ by starlight (photo-destruction) and by reaction with abundant neutrals such as H_2 [79]. In order to sustain the observed fractional abundance of CH^+, an efficient route to its formation is essential.

In the absence of a viable alternative route to CH^+ production, it was proposed that shock waves travelling at high speed through ISCs could elevate cloud temperatures to greater than 1000 K, making reaction **(3.1b)** rapid, and thus a viable source of CH^+ [79]. The presence of shock waves in the ISM is well known, with possible sources including supernovae and cloud-cloud collisions. Although some evidence supported the shock wave hypothesis, the bulk of the evidence opposed the theory [80]. As shock waves are unlikely to be the source of the elevated CH^+ level in the ISM, an alternative source of CH^+ was required.

3.2 C + H_3^+ - A Key Reaction in Interstellar Space

It is now considered that the ion-atom reaction **(3.2)** is the key hydrocarbon-forming reaction in the ISM and that reaction **(3.2a)** is the major source of CH^+ in ISCs.

$$C + H_3^+ \rightarrow CH^+ + H_2 \qquad \textbf{(3.2a)}$$

$$\rightarrow CH_2^+ + H \qquad \textbf{(3.2b)}$$

Both reactants are abundant in the ISM. H_3^+ is the most common interstellar ion, formed by the reaction of H_2^+ (itself formed by stellar UV or cosmic ray ionisation of H_2) with H_2. H_3^+ is unreactive with H_2 but reactive with a variety of neutral species, readily undergoing proton transfer reactions, and is the starting point for a rich ion-molecule chemistry [3].

Reaction **(3.2a)** is exothermic and it is well known that when proton transfer reactions are exothermic they usually proceed rapidly [81]. Although the reaction appears straightforward, there is a problem with spin multiplicity. The ground state reactants approach on a triplet potential energy surface whilst ground state products are on a singlet potential energy surface. With ground state reactants, the lowest possible energy states of the products are excited CH^+ ($a^3\Pi$) and ground state H_2. It is therefore unclear if this exothermic reaction proceeds without an activation barrier. Any such energy requirement would make the reaction prohibitively slow at the temperature of ISCs. An experimental measurement of this reaction is therefore essential to clarify the effect of the multiplicity problem on the reaction rate. Reaction **(3.2a)** has not been studied experimentally in spite of its critical role in hydrocarbon formation.

Few studies of atomic carbon kinetics have been made because of the difficulty associated with producing a steady flow of neutral carbon atoms for reaction. The chemistry of H_3^+ has been investigated thoroughly and presents no impediment to the study of reaction **(3.2)**.

Two theoretical studies have produced useful insights into the reaction. Talbi *et al*. [12, 13] demonstrated with *ab initio* calculations that CH^+ could be formed **without** an activation barrier and calculated the rate coefficient for reaction **(3.2a)** to be 2.3 x 10^{-9} cm^3 s^{-1} at 300 K increasing to 2.9 x 10^{-9} cm^3 s^{-1} at 10 K. They were unable to find an intermediate that led to CH_2^+ formation (reaction **(3.2b)**) and concluded that CH_2^+ formation, although exothermic, would not occur.

A second theoretical investigation reaffirmed that reaction **(3.2a)** was likely to be rapid at low temperatures [10, 11] and calculated a reaction rate of 1.9 x 10^{-9} cm^3 s^{-1} at 10 K. The study also found a barrierless pathway leading to CH_2^+ formation (reaction **(3.2b)**) but determined this reaction to be slow (k = 3.4 x 10^{-11} cm^3 s^{-1}) at 10 K. Notwithstanding this slow rate, reaction **(3.2b)** would be a competitive source of CH_2^+ in the ISM with reaction **(3.1a)** which is also quite slow. The branching ratio for reaction **(3.2)** was estimated to be 0.98 : 0.02 in favour of CH^+ formation.

In order to incorporate an ion-neutral reaction in a model of ISC chemistry it is essential that conclusive evidence is available that the reaction occurs. The uncertainty with regard to the rate of reaction **(3.2)** and the product(s) formed accentuate the need for experimental confirmation of the viability of this reaction. The intention of this work was to make the first experimental measurement of the reaction between ground state carbon atoms and H_3^+. Atomic carbon is also likely to participate in ion-atom reactions with larger interstellar ions and this chemistry was also to be examined.

3.3 The Study of Ion-atom reactions

Few molecular species exist in diffuse ISCs. Ion-atom reactions therefore predominate with the principal reactive species being H, C, N and O atoms [82]. Although some ion-atom chemistry was investigated as long ago as the 1970s [83], until recently little data was available regarding ion-atom reactions in the large databases of ion-neutral reactions [67, 84]. A comprehensive experimental study of ion-atom chemistry relevant to ISCs was conducted in the UC SIFT laboratory in the 1990s by Scott [62]. In particular, rate coefficients and product branching ratios were determined for a large array of ions reacting with H, N and O atoms. Milligan also examined the reactivity of oxygen atoms during his time in the UC SIFT laboratory [85]. It is pertinent to discuss the methods used by these authors to provide an insight into the study of ion-atom reactions using a SIFT instrument and the major challenges involved.

3.4 Generating Atomic Species and Establishing their Concentration in the Gas Phase

Microwave discharges have been widely used to generate atomic species and were employed successfully by both Milligan and Scott [60, 62].

Hydrogen atoms can be produced from a microwave discharge in either pure hydrogen or a dilute mixture (~10%) of hydrogen in helium. A pure hydrogen discharge can yield up to 90% dissociation although rapid atom-atom and surface recombination reduces the initial 90% dissociation to between 30 and 60% (depending on the experimental set-up) [86]. Recombination (see Section 3.5) is one of the major obstacles associated with the examination of ion-atom chemistry.

Because the flow of atoms reaching the reaction region is dependent on the experimental arrangement and conditions, it cannot simply be related to the flow of gas through the discharge. The determination of reaction kinetics with the SIFT requires accurate knowledge of the neutral reactant concentration in the flow tube. The concentration of atoms in the gas flow must be determined experimentally before ion-atom kinetics can be determined. To date the most effective way to establish hydrogen atom flow rates is to utilise reactions **(3.3)** and **(3.4)**.

$CO_2^+ + H_2 \rightarrow HCO_2^+ + H$	$k = 6.2 \times 10^{-10}$ cm^3 s^{-1}	**(3.3)**
$CO_2^+ + H \rightarrow HCO^+ + O$	$k = 3.3 \times 10^{-10}$ cm^3 s^{-1}	~0.17 **(3.4a)** [67]
$\rightarrow H^+ + CO_2$		~0.83 **(3.4b)**

As accurate kinetics for these reactions have been established, the H atom flux (in the presence of undissociated molecular hydrogen) can easily be determined from the reaction of the discharge products with CO_2^+. In practice, the product ion count rates as well as the flow rate of hydrogen through the discharge are required to perform the necessary calculation. This approach to measuring the flow of atoms is convenient and easily applied to the SIFT instrument.

Nitrogen atoms can be produced by passing pure nitrogen through a microwave discharge. Depending on the experimental conditions, between 0.5% and 4% dissociation is observed [86]. This is a considerably lower degree of dissociation than for H_2, meaning that by far the dominant neutral entering the flow tube is N_2. It is therefore essential to

establish the kinetics and products for nitrogen molecules with each reactant ion (in the absence of nitrogen atoms) before nitrogen atom kinetics can be evaluated. Fortunately reaction rates for N_2 with interstellar ions are usually very slow and N atom products are easily distinguished.

A method analogous to that used for H atoms can be used to measure the N atom flow - examining the chemistry of the N/N_2 flow with a monitor ion for which the chemistry with both species is known. It is, however, more common to adopt a slightly different procedure to determine nitrogen atom flow rates (based on reaction **(3.5)**) which is known as the NO titration.

$$N + NO \rightarrow N_2 + O \qquad k = 3.4 \times 10^{-11}\ cm^3\ s^{-1} \qquad \textbf{(3.5)}$$

Nitric oxide is reacted with the products of a nitrogen discharge (N/N_2) prior to the SIFT flow tube. To establish the N atom concentration, the signal of a monitor ion (O_2^+ was used in Scott's thesis [62]) is measured at a series of NO flow rates. As the NO flow is increased the N atom flux is reduced to zero i.e. reaction **(3.5)** proceeds to completion – this is the endpoint of the titration. If the flow of NO is increased further, NO enters the flow tube and reduces the monitor ion signal. In a plot of logarithm of the monitor ion count against NO flow rate, the endpoint is readily visible as the intersection of two lines. From the known kinetics and the flow rate of NO at the titration endpoint, the N atom flow can be established. It is important that sufficient mixing time/volume is available for reaction **(3.5)** to go to completion for this method to be successful.

Oxygen atoms are typically produced for reaction by utilising reaction **(3.5)** which is greater than 98% efficient at producing oxygen atoms when optimised. The oxygen atom flow is easily determined from its relation to the nitrogen atom flow. Alternatively, O atoms can be generated by the application of a microwave discharge to a dilute mixture (~5%) of oxygen in helium. As with hydrogen and nitrogen atoms, the flow of atoms generated in this way can be determined by reaction of the products with a well chosen monitor ion, for which kinetics are known with both O and O_2.

3.5 Atom Recombination

Rapid atom recombination, either in the gas phase or on surfaces, is a major inhibiting factor in the study of ion-atom kinetics. The recombination of oxygen atoms

produced by reaction **(3.5)** prior to the reaction region can reduce apparent reaction rates by up to 20% [86].

Three body atom-atom recombination rates are available in the literature with helium the most important third body in the context of this research i.e. M = He in reactions **(3.6-3.9)**.

$H + H + M \rightarrow H_2 + M$ $\quad k = 8 \times 10^{-33}$ $\quad cm^6\ molec^{-2}\ s^{-1}$ **(3.6)** [86]

$N + N + M \rightarrow N_2 + M$ $\quad k = 1.05 \times 10^{-32}\ cm^6\ molec^{-2}\ s^{-1}$ **(3.7)** [87]

$O + O + M \rightarrow O_2 + M$ $\quad k = 8.4 \times 10^{-34}\ cm^6\ molec^{-2}\ s^{-1}$ **(3.8)** [88]

$C + C + M \rightarrow C_2 + M$ $\quad k = 5.46 \times 10^{-31}\ cm^6\ molec^{-2}\ s^{-1}$ **(3.9)** [89]

The rate coefficients for reactions **(3.6)** and **(3.7)** represent the recombination of atomic species flowing through quartz or Pyrex tubing. These values therefore include surface recombination as well as gas phase recombination. As such they must be treated with caution as the rate of surface recombination is dependent on the tube diameter and the nature of wall surfaces. Accurate surface recombination rates for these atoms are not available in the literature however they are likely to be significant.

It is clear from reactions **(3.6)** to **(3.9)** that carbon atoms recombine considerably more rapidly than H, N or O atoms. The difficulty in producing a continuous, stable flow atomic carbon in sufficient quantities for reaction is the principal reason that no experimental investigations of reaction **(3.2)** have been made to date.

3.6 Methods Which Can Be Used To Generate Atomic Carbon

Generating a flow of carbon atoms sufficient for reaction with ions in the SIFT constitutes the most challenging aspect of this work. This is made more difficult by the propensity of carbon atoms to recombine to form C_2 and larger carbon clusters. Numerous methods have been developed to produce carbon atoms in the gas phase, including: the carbon arc [90]; nuclear transformations [91]; flash photolysis [92, 93]; microwave discharges [89]; the evaporation of graphite rods [94, 95]; and the thermal decomposition of chemical precursors [96]. Of these methods, the microwave discharge generation of carbon atoms is the method best suited to a fast flow system such as the SIFT where a continuous high flow of carbon atoms is needed. Following the successful application of microwave discharge generated H, N and O atoms to the measurement of

ion-atom kinetics with the UC SIFT [60, 62], it was reasonable to attempt initially to produce carbon atoms for reaction in this way.

The generation of carbon atoms in a microwave discharge was first observed by Martinotti, Welch and Wolf in 1968 [89]. Atomic carbon emission lines were observed when carbon suboxide, carbon monoxide, benzene or allene were added to a microwave discharge in helium. Carbon atoms were produced when either a dilute mixture of a carbon-containing compound in helium was passed directly through a microwave discharge, or a carbon containing compound was added downstream from a helium discharge.

Hurt and Grable identified the major product channels for the reaction between metastable helium atoms (He 2^3S, created by a microwave discharge in helium) and carbon monoxide, reaction **(3.10)** [97].

$$\text{He}(2^3\text{S}) + \text{CO} \rightarrow (\text{CO}^+)^* + \text{He} + e \qquad 0.94 \textbf{ (3.10a)}$$

$$\rightarrow \text{C}^* + \text{O} + \text{He} \qquad 0.06 \textbf{ (3.10b)}$$

The electronically excited atomic carbon produced by reaction **(3.10b)** radiates to the ground state ^3P, and also to the ^1D and ^1S states by allowed transitions. Dorthe *et al*. have successfully utilised reaction **(3.10b)** to study atomic carbon kinetics in a fast flow system [98].

The study of reaction **(3.2b)** requires a source of ground state atomic carbon (^3P) to match the conditions in the ISM. It has been found that the ^3P, ^1D and ^1S states of atomic carbon react at different rates with neutral molecules [99]. As reaction **(3.10b)** produces all of the above states of carbon, it is not ideal for this work. Sekiya *et al*. demonstrated that metastable argon atoms $\text{Ar}(^3P_{2,0})$ were a useful alternative to metastable helium atoms for the generation of atomic carbon [100]. Because the energy of the Ar $^3P_2$ and $^3P_0$ atoms is insufficient to produce carbon atoms in the ^1S and ^1D states, only ground state $\text{C}(^3P)$ atoms are formed in reaction **(3.11)**. Argon was not used in this work due to difficulties in removing water impurities.

$$\text{Ar}(^3P_{2,0}) + \text{CO} \rightarrow \text{C}(^3P) + \text{O} + \text{Ar} \qquad \textbf{(3.11)}$$

For every carbon atom produced by reactions **(3.10b)** and **(3.11)**, an oxygen atom is also produced. The presence of oxygen atoms can be used as an indicator of the

presence of carbon atoms. The monitor ion used to detect the atomic carbon was chosen to take advantage of this, (see Section 3.7.1)

Both Scott and Milligan attempted to produce atomic carbon with a microwave discharge in quantities sufficient for reaction with the UC SIFT, and both were unsuccessful [60, 62]. Coincidentally both attempts were made near the end of their respective thesis projects, and neither spent a significant period of time attempting to make carbon atoms. In spite of their failure to produce and detect carbon atoms with a microwave discharge source, it was determined that further investigation was needed to prove whether or not this method could be applied to this system.

The purpose of this work was to make a concerted effort to produce carbon atoms with a microwave discharge in sufficient quantities to examine reaction **(3.2)**.

3.7 The Detection of Atomic Carbon

3.7.1 Introduction

A key concern in these experiments is how to detect the presence of carbon atoms. The presence of H, N and O atoms in the gas phase can be readily observed from the products of their reaction with ions for which reaction chemistry is known. At the time Milligan and Scott wrote their theses, no reactions between ions and carbon atoms were reported in the literature [67, 84]. Since then, Fujii has observed the reaction of lithium cations (Li^+) with carbon atoms [101]. Carbon atoms were thus identified as the major product of a microwave discharge acting on a dilute mixture of methane in hydrogen. As it is likely that only a small quantity of carbon atoms will be produced in this work, high ion counts are needed to improve the probability of observing a carbon atom generated product ion. Lithium ions can be produced for reaction with the SIFT (see Chapter 7) however they are not a convenient monitor ion for atomic carbon as they are difficult to produce in large quantities.

In the only other study of carbon atom-ion chemistry to be published, Gerlich *et al*. [95] measured the rate coefficient for the reaction between hot C atoms and D_3^+. The rate of deuteron transfer was estimated to be $4.7 \pm 2.35 \times 10^{-10}$ cm^3 s^{-1}. The key reaction to be studied in this work is reaction **(3.2)**. H_3^+ (being cheaper than and equally as effective as D_3^+) represents an ideal monitor ion for carbon atoms as its reactivity with

both the by-product of reaction **(3.10b)** (O atoms) and the precursor used to generate carbon atoms (CO) is known.

$H_3^+ + O \rightarrow OH^+ + H_2$ $\quad k = 1.2 \times 10^{-9}$ cm^3 s^{-1} $\quad$ ~0.70 **(3.12a)** [85]

$\rightarrow H_2O^+ + H$ $\quad$ ~0.30 **(3.12b)**

$H_3^+ + CO \rightarrow HCO^+ + H_2$ $\quad k = 1.9 \times 10^{-9}$ cm^3 s^{-1} $\quad$ **(3.13)** [67]

The products of these reactions would not interfere with the identification of carbon atom-H_3^+ reaction products.

3.7.2 Generating H_3^+ in the SIFT

Two methods can be used to generate H_3^+ for reaction in the UC SIFT. In the first, H_3^+ is generated in the FA ion source from H_2^+ produced in a microwave discharge on pure H_2. Ions produced in this way are mass selected and injected into the flow tube in the normal fashion.

$$H_2^+ + H_2 \rightarrow H_3^+ + H \qquad k = 2.0 \times 10^{-9} \text{ cm}^3 \text{ s}^{-1} \qquad \textbf{(3.14)}$$

A negative feature of reaction **(3.14)** is that the H_3^+ generated is predominantly vibrationally excited and vibrational quenching by H_2 is slow. Consequently, a fraction of the ions injected into the flow tube are not in their ground state [102]. This excitation is demonstrated by the detection of HeH^+ ions in the flow tube - the reaction between helium and H_3^+ is 244 kJ mol^{-1} endothermic for ground state H_3^+.

Alternatively, H_3^+ ions can be formed in the flow tube. This is achieved by injecting Kr^+ ions into the flow tube with hydrogen as the carrier gas instead of the usual helium. As the production of H_3^+ is in two steps from reactions **(3.15)** and **(3.16)**, and **(3.16)** is slightly endothermic, this method is far less likely to produce excited H_3^+.

$$Kr^+ + H_2 \rightarrow KrH^+ + H + 37 \text{ kJ mol}^{-1} \qquad \textbf{(3.15)}$$

$$KrH^+ + H_2 \rightarrow H_3^+ + Kr - 1.25 \text{ kJ mol}^{-1} \qquad \textbf{(3.16)}$$

Having hydrogen as the carrier gas will have a negative effect on the measurement of ion-neutral chemistry. Unlike inert helium, hydrogen is likely react with product ions and will interfere with the identification of reaction products. This is particularly pertinent to reaction **(3.2)** as both CH^+ and CH_2^+ are quite reactive with H_2. In practice it is necessary to measure the reactivity of a neutral with H_3^+ generated by both methods in order to accurately determine the rate coefficient and product branching ratios for ground state H_3^+ [60].

Because of the expense involved in using Kr^+ to generate H_3^+ it was decided that this was not a cost efficient way to produce the monitor ion whilst the carbon atom source was developed. Attempts to inject H_3^+ generated in the FA ion source were unsuccessful. The H_3^+ ions must be injected with quite different voltages on the FA nose cone and the Venturi than used for other ions, so that the ions do not become internally excited. The voltages are modified to reduce the potential gradient across the quadrupole region. This reduces the kinetic energy transferred to the ions but also reduces the transmission efficiency making it quite difficult to achieve a good flow of ions into the flow tube. Rather than persist with this approach alternative reagent ions were evaluated. The generation of H_3^+ would be revisited once a reliable carbon atom source had been developed.

Ideally the monitor ion should be produced easily in large quantities (to increase sensitivity) from a readily available precursor and should react rapidly with well defined chemistry with the target species. It has already been pointed out that only two ion-carbon atom reactions have been observed. Neither of the reagent ions employed (D_3^+ and Li^+) is suitable to this study and H_3^+ proved difficult to inject into the flow tube. An ion having unknown reactivity with C atoms needed to be employed. In this circumstance an ion should be chosen that is likely to react exothermically with carbon atoms and also has a well-defined chemistry with the by-product of reaction **(3.10b)** (oxygen atoms) as well as the C atom precursor (carbon monoxide).

3.7.3 $C_6H_6^+$ as a Monitor Ion for Atomic Carbon

The $C_6H_6^+$ ion is one of few ions that react with H, N and O atoms and does so more rapidly than other potential monitor ions [103]. This ion is easily produced in large quantities in the FA from benzene vapour and reacts with oxygen atoms to produce two easily identifiable ions [67].

$$C_6H_6^+ + O \rightarrow C_5H_6^+ + CO \qquad k = 1.4 \times 10^{-10}\ cm^3\ s^{-1} \qquad 0.90 \textbf{ (3.17a)}$$

$$\rightarrow C_4H_4O^+ + C_2H_2 \qquad 0.10 \textbf{ (3.17b)}$$

The undissociated CO present in the flow tube when CO is used to generate C atoms will not interfere with the $C_6H_6^+$ ions as CO is unreactive with this ion under SIFT operating conditions.

$$C_6H_6^+ + CO \rightarrow C_6H_5^+.CO + H \qquad k < 5 \times 10^{-13}\ cm^3\ s^{-1} \qquad \textbf{(3.18)}$$

In addition to these favourable ion-molecule reactions it is known that carbon atoms react rapidly with neutral benzene [104-106]. The products of this reaction are not well defined however there is consensus that the carbon insertion reaction **(3.19)** represents one of the major pathways [105, 107].

$$C + C_6H_6 \rightarrow C_7H_5 + H + 1.9 \text{ kJ mol}^{-1} \quad \textbf{(3.19)}$$

It was hoped that an analogous reaction with $C_6H_6^+$ would also occur, possibly producing an easily identifiable $C_7H_6^+$ ion.

$$C + C_6H_6^+ \rightarrow C_7H_6^+ + 470 \text{ kJ mol}^{-1} \quad \textbf{(3.20)}$$

$C_6H_6^+$ (produced from benzene) is an ideal monitor ion for atomic carbon and was used for the majority of this work. It is easily produced in large quantities, is known to react rapidly with atomic species including oxygen atoms and is unreactive with carbon monoxide.

3.8 The Design of the Carbon Atom Source

3.8.1 Introduction

For these studies the neutral inlet used to admit measured flows of neutral reactant to the flow tube had to be modified to incorporate apparatus capable of generating carbon atoms. Carbon atoms can be produced by applying a microwave discharge to a dilute mixture of CO in helium, or by adding CO downstream from a helium discharge plasma [89]. Both of these potential carbon atom production methods are easily incorporated into a single design. A diagram of the original design (including some minor modifications outlined in the following text) is shown in Figure 3.1. The position of the microwave discharge is adjustable and two CO inlet positions are available. The set-up attaches conveniently to any of the neutral inlet ports along the SIFT flow tube.

3.8.2 Operation

Pure helium or a dilute mixture of carbon monoxide in helium enters the Pyrex tubing and is subjected to a microwave discharge. Helium metastables thus produced react with CO either *in situ* or downstream at one of the CO inlets and any ions or atoms produced pass into the flow tube. Neutral species entering the flow tube may undergo reaction with the $C_6H_6^+$ monitor ion. Mass spectra were recorded with and without the discharge ignited. In this way product ions created from neutral species produced by the

discharge can be distinguished from product ions generated by carbon monoxide. Ionic species produced by the discharge can be identified by measuring spectra in the absence of the $C_6H_6^+$ monitor ion.

The products of reaction **(3.17)** were the key species used to identify in the product spectra. The identification of oxygen atoms would indicate concurrent carbon atom formation according to reaction **(3.10b)**.

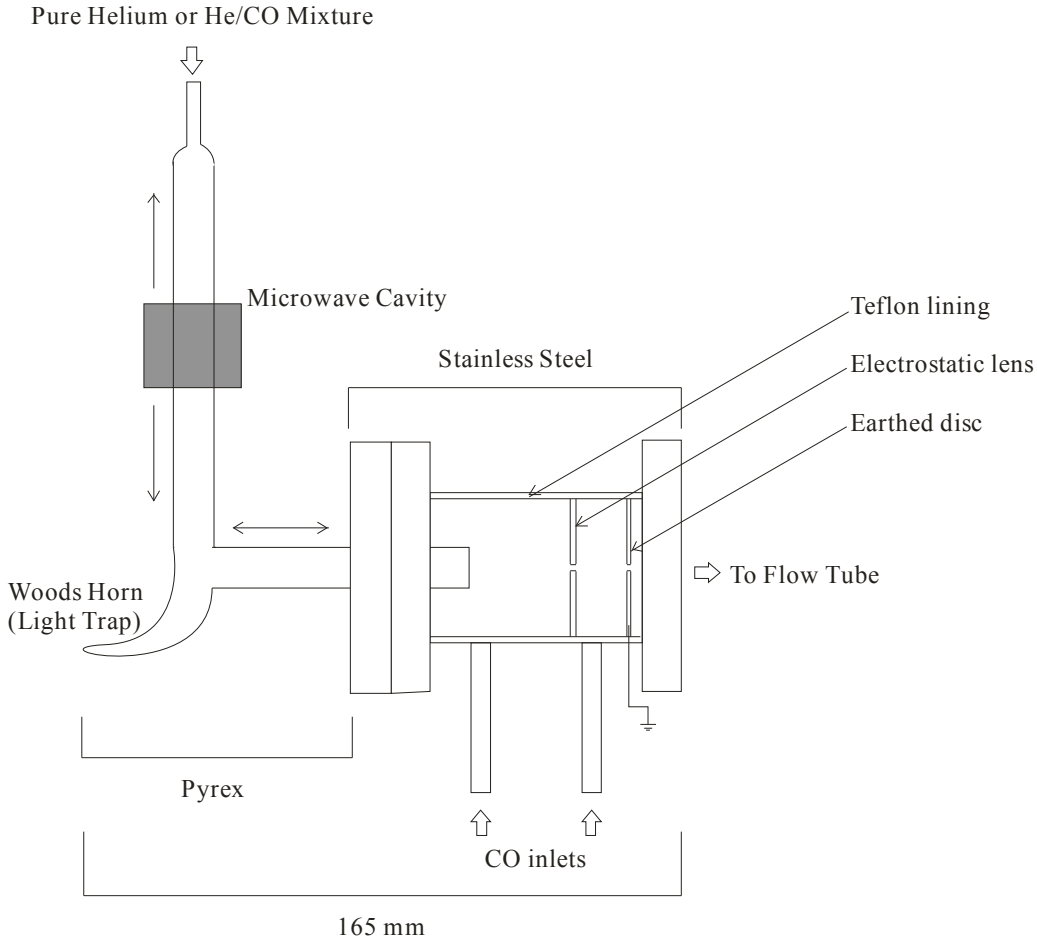

Figure 3.1. *The design of the first generation carbon atom source. The pressure in the atom source is measured through the vacant CO inlet. Double-headed arrows indicate adjustable sections in the design. Both the microwave cavity and the Pyrex sidearm can be moved to take the plasma closer to, or further from the flow tube. Photoionisation is minimized by the incorporation of a Wood's Horn (light trap) below the discharge.*

3.8.3 Early Modifications

When the discharge was ignited for the first time charged species produced in the atom source interrupted the flow of reactant ions in the flow tube and as a result no ion signal was detected at the downstream mass spectrometer. An electrostatic lens was introduced inside the carbon source prior to the entrance to the flow tube to prevent charged species from the atom source entering the flow tube. The addition of an earthed disc between the lens and the flow tube prevented this voltage from disrupting the flow of monitor ions in the flow tube. A 6 mm orifice in both the lens and the earthed disc allowed the passage of gas to the flow tube. At this point Teflon lining was also added to the stainless steel segment to minimise the surface removal of carbon atoms, mirroring the work of Dorthe *et al*. [98].

3.8.4 Experiments and Results

Having solved the initial design problems, attempts were made to generate carbon atoms from the addition of carbon monoxide **downstream** from a microwave generated helium plasma - hereafter referred to as Method 1. The position of the discharge relative to the flow tube was varied and the flows of both helium and CO manipulated whilst attempting to observe the production and reaction of oxygen atoms (indicative of carbon atom formation). Despite adjusting the available parameters, no evidence of either atomic oxygen (or atomic carbon) was observed.

Attempts were then made to generate carbon atoms by passing carbon monoxide **directly through the discharge** as a 2% mixture in helium – hereafter referred to as Method 2. Although no carbon atoms were observed, a significant amount of sooting occurred inside the apparatus around the discharge region. The build up of soot eventually extinguished the discharge. The ratio of CO to helium was then reduced to 1% to lessen the degree of soot formation. Significantly less soot was produced with the more dilute mixture but neither atomic carbon nor atomic oxygen was observed.

At this point it was unclear as to why no atoms were being observed so a new carbon atom source was constructed which was closer in design to previous atom generation systems used successfully to create H, N and O atoms [62]. Made entirely of glass, the new design is shown in Figure 3.2. It was hoped that some atomic products

would be observed if the length of time available for reaction between metastable helium atoms and CO prior to the flow tube was increased.

When carbon monoxide was added downstream from a helium discharge plasma (Method 1) the glass around the CO inlet became stained slightly brown but no evidence of carbon atom formation was found. No ions produced by the discharge were observed to reach the flow tube even with no voltage on the tungsten electrodes, possibly due to interactions with static charge on the Teflon lining.

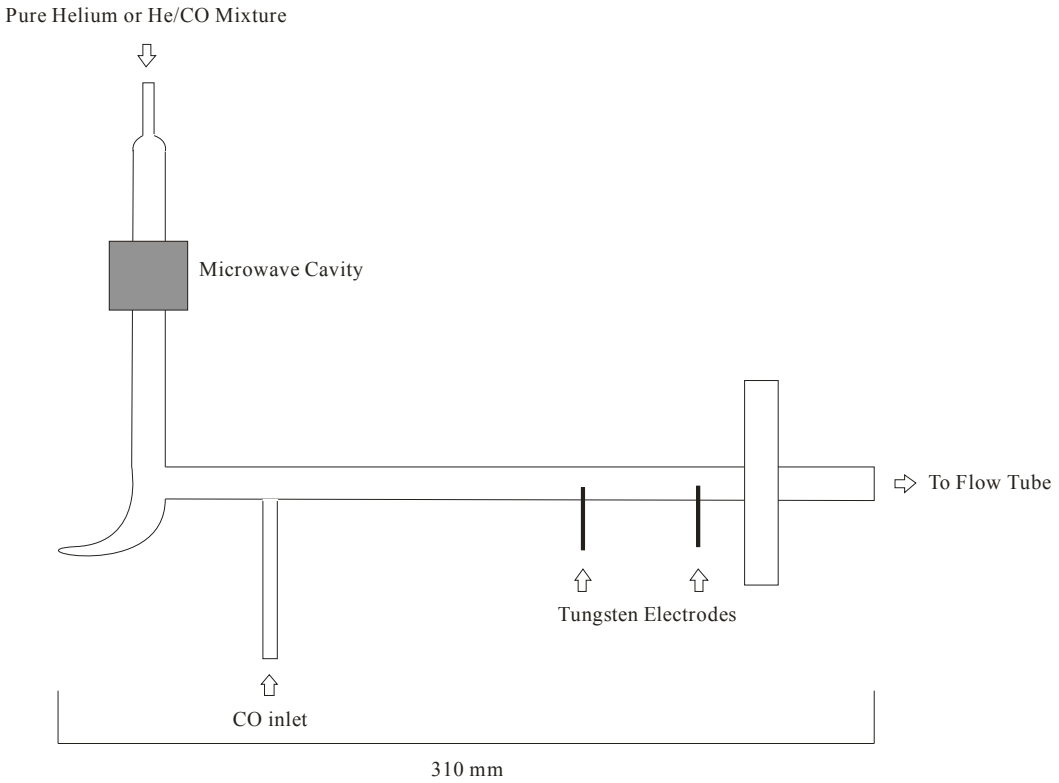

Figure 3.2. *Second generation carbon atom source made entirely of Pyrex. Tungsten electrodes are incorporated in order to remove charged species. The glass is lined with Teflon between the CO inlet and the flow tube to reduce C atom wall recombination.*

When Method 2 was applied with a 2% mixture of carbon monoxide in helium, oxygen atoms were produced and observed by their reaction with $C_6H_6^+$. For every oxygen atom produced from the decomposition of carbon monoxide by reaction **(3.10b)**, a carbon atom is also produced. No potential atomic carbon reaction product ions were observed in the product ion spectra (such as $C_7H_6^+$ from reaction **(3.20)**). This suggested that carbon atoms produced in the discharge did not survive sufficiently long to be seen

in the flow tube, presumably because of rapid recombination (Section 3.5). (This assumes that any reaction between atomic carbon and $C_6H_6^+$ is approximately as rapid as the reaction of atomic oxygen with $C_6H_6^+$). To maximise the probability of observing atomic carbon reaction products another series of experiments was conducted in order to optimise the oxygen atom product ion signal. The Pyrex carbon atom source was modified to allow greater flexibility of movement of the position of the microwave discharge relative to the flow tube (Figure 3.3) for these experiments.

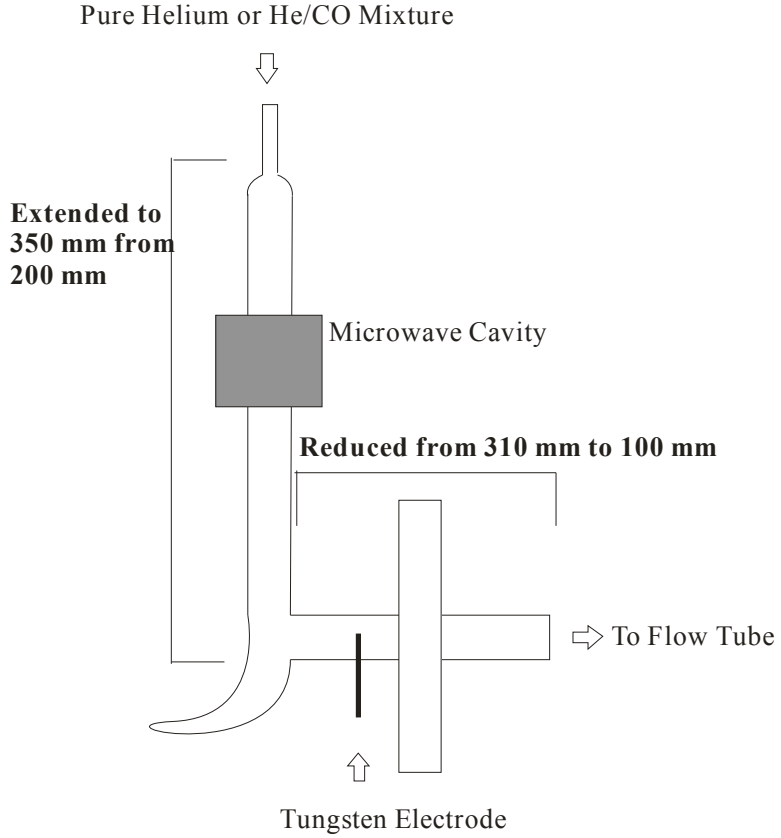

Figure 3.3. *The third generation carbon atom source was adapted from the second generation source to allow the microwave discharge to be positioned closer to the flow tube.*

Oxygen atom product ion peaks were measured relative to the reactant ($C_6H_6^+$) ion signal for a series of dilutions of carbon monoxide in helium ranging from 0.1 to 2.0%. The mixture of 1% CO in helium produced a significantly higher concentration of oxygen atoms than the other mixtures. Increasing the microwave power to 100 W from the usual operating power of 75 W had little effect on the flow of atoms. The oxygen

atom signal was enhanced by increasing the flow of gas through the discharge and by moving the discharge closer to the flow tube.

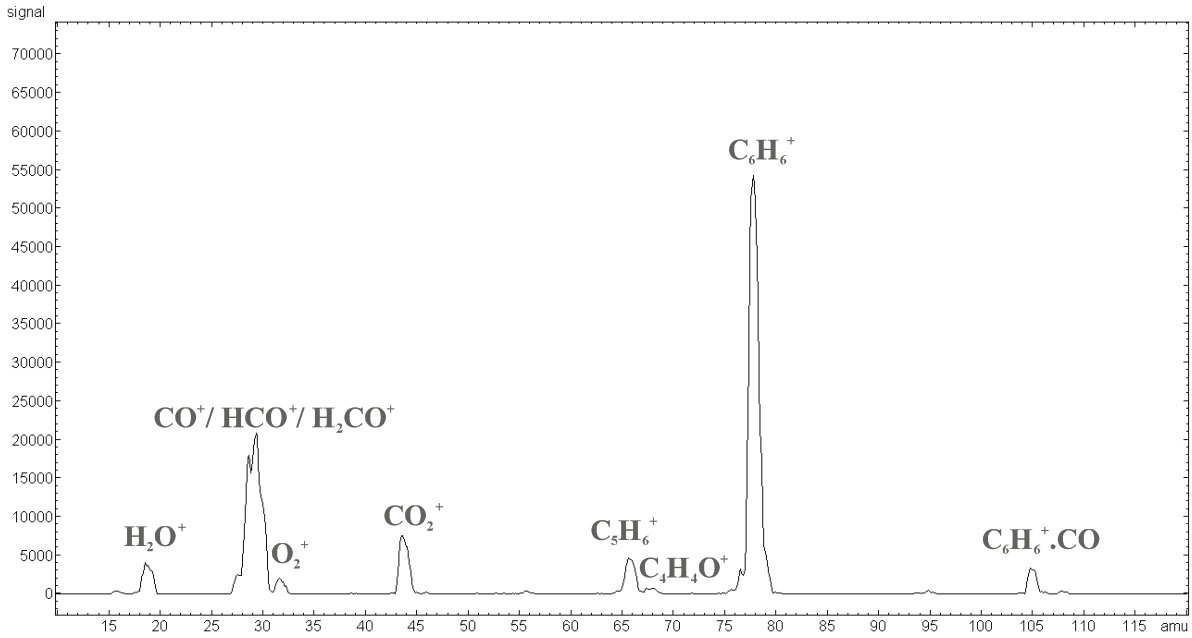

Figure 3.4 *Typical mass spectrum showing evidence of O atoms but not C atoms. Ions with m/z < 50 are produced in the carbon atom source and do not arise from reaction with $C_6H_6^+$. The peaks at m/z 66 and 68 represent the products of reaction* ***(3.17)*** *and indicate the presence of oxygen atoms. The peak at m/z 105 represents the product of reaction* ***(3.18)***.

There are deleterious side effects associated with having the discharge very close to the flow tube. If the discharge was placed within 150 mm of the flow tube, unreacted metastable helium atoms entered the main SIFT flow tube in large quantities, ionising impurities in the helium carrier gas and precluding the observation of ion-atom reactions. Higher He/CO flows also increased the metastable flux into the flow tube. The pressure inside the carbon atom source rose from 0.46 to 1.92 Torr when the flow rate was increased from 280 to 580 sccm. At 1.92 Torr the termolecular recombination rate of atomic carbon is four times greater than at 0.46 Torr (the pressure in the SIFT flow tube), which would negate any potential increase in the atomic carbon flux.

Increasing the diameter of the glass tubing directly after the discharge reduced the constriction caused by the narrower tubing (reducing the pressure difference) but in spite of doing this no potential product ions from the reaction of atomic carbon were observed.

3.8.5 Alternative Detection Methods

The observation of oxygen atoms and the profuse sooting in the Pyrex tube around the discharge region provided convincing evidence that carbon atoms were being formed in the discharge. However, no potential atomic carbon product ions were detected in the flow tube even when the atomic oxygen product ion signal and flow conditions were optimised.

$C_6H_6^+$ was employed as a monitor ion for atomic carbon based on the assumption that it may form $C_7H_6^+$ by reaction **(3.20)** or another easily identifiable ion. Reactions with alternative precursor ions (N_2O^+, $C_2H_2^+$, $C_3H_7^+$ and $C_4H_9^+$) were also examined in order to exclude the possibility that atomic carbon is simply unreactive with $C_6H_6^+$. These ions were chosen based on their reactivity with other atomic species. No potential atomic carbon reaction products were observed in these experiments.

An alternative method of carbon atom detection was also attempted. **Neutral** benzene was added 100 mm downstream from the microwave discharge under optimal He/CO flow conditions (Method 2). H_3O^+ was used as a reagent ion in the SIFT to establish whether a **protonated** species arising from the products of one of the following reactions could be observed:

$$C + C_6H_6 \rightarrow l\text{-}C_7H_4 + H_2 \qquad k = 4.8 \times 10^{-10}\ cm^3\ s^{-1} \textbf{ (3.21a)} [105]$$

$$\rightarrow C_7H_5 + H \qquad \textbf{(3.21b)}$$

$$\rightarrow C_5H_4 + C_2H_2 \qquad \textbf{(3.21c)}$$

No relevant product ions were detected.

All the experimental evidence described above indicates that carbon atoms were produced by the microwave discharge, but recombined before reaching the flow tube.

3.9 Radio Frequency Discharge

The rapid formation of soot around the microwave discharge indicated that surface recombination of carbon atoms was significant and was possibly charge-induced. To reduce the relative surface area available for surface recombination, the diameter of the Pyrex discharge tube needed to be increased significantly. Increasing the size of the microwave cavity to match the increased diameter tubing was not practicable so a radio frequency (RF) discharge was employed.

3.9.1 RF Experiments

An RF generator was coupled to the largest diameter Pyrex tubing that could be attached to the SIFT flow tube (50 mm outer diameter). The design of the atom source remained equivalent to that shown in Figure 3.3. The RF discharge produced significantly more ions than the microwave discharge, which interfered with the reagent ions in the SIFT flow tube. The flow of ions could not be reduced significantly by the introduction of two oppositely charged electrodes between the RF discharge and the flow tube, but could be reduced slightly by moving the RF discharge further from the flow tube.

Carbon deposition on the glass tubing around the discharge was significantly reduced by using the larger diameter tubing indicating a reduction in surface recombination but oxygen atom formation was not observed. Variations in the set-up (discharge position, flow rate through discharge, discharge power and mixture composition) did not affect this result.

When passed through a microwave discharge, a 5% oxygen in helium mixture can be used to generate copious amounts of oxygen atoms [60]. Such a mixture was passed through the RF discharge and the quantity of oxygen atoms reaching the flow tube examined. This experiment demonstrated that considerably fewer oxygen atoms were produced with the RF discharge than were with the microwave discharge. No further experiments were made with the RF discharge as it was highly unlikely that sufficient carbon atoms could be produced in this way.

3.10 Carbon Suboxide

3.10.1 Carbon Suboxide as a Source of Carbon Atoms

Critical for the study of reaction **(3.2)** is a clean source of atomic carbon with a minimum of interfering species. For this reason carbon monoxide is an ideal precursor. Carbon monoxide is unreactive with most ions and the only by-product of the decomposition to give atomic carbon is atomic oxygen, which is itself a useful aid to this study. Carbon monoxide is not the only organic substrate that can be used to generate carbon atoms, although it has the fewest by-products. Carbon suboxide, C_3O_2, was demonstrated by Braun *et al*. to decompose at wavelengths below 200 nm to produce two carbon monoxide molecules and one carbon atom [92].

$$C_3O_2 + h\upsilon\ (\lambda < 200\ nm) \rightarrow C + 2CO \qquad \textbf{(3.22)}$$

Carbon suboxide has also been shown to produce carbon atoms when added downstream from a helium discharge plasma [108].

Carbon monoxide was used in preference to carbon suboxide in initial experiments for several reasons. Carbon monoxide is readily available and produces fewer by-products under decomposition than does carbon suboxide. Unlike C_3O_2, CO does not react rapidly with the precursor ions chosen so far, allowing straightforward detection of trace quantities of atoms in the presence of high concentrations of carbon monoxide. A disadvantage of using carbon suboxide is its relatively rapid reaction with carbon atoms.

$$C_3O_2 + C \rightarrow \text{Products} \qquad k = 1.8 \times 10^{-10}\ cm^3\ s^{-1} \quad \textbf{(3.23)}\ [104]$$

Furthermore, carbon suboxide is not readily available as it is unstable at room temperature and must therefore be synthesized as it is required.

In its favour, carbon suboxide is more likely to dissociate by reaction with helium metastables when added downstream of a microwave discharge (Method 1) than carbon monoxide. The addition of carbon suboxide downstream of the discharge would mean carbon atom formation would occur closer to the flow tube, reducing the time available for atom recombination. This is a significant advantage over carbon monoxide which did not decompose in these experiments unless passed directly through the discharge.

The unsuccessful experiments with carbon monoxide meant that carbon suboxide was now a viable alternative.

3.10.2 Carbon Suboxide Synthesis

Because carbon suboxide polymerises rapidly at room temperature it must be prepared as it is required and used immediately (although it can be stored temporarily at -78 ºC). For the following experiments carbon suboxide was prepared by a method previously employed in the SIFT laboratory – the dehydration of malonic acid by phosphorous pentoxide under vacuum [109]. Dry sand was added to the solid reaction mixture to distribute heating and the mixture heated to approximately 115 °C for one hour. During heating the mixture was stirred mechanically to assist the escape of the gaseous product from the reaction mixture before it polymerises.

Under these experimental conditions malonic acid can also decarboxylate to give acetic acid and carbon dioxide. These must then be removed in order to obtain pure carbon suboxide. The gaseous products of the reaction pass through two cold traps, the first of which collects acetic acid impurities at dry-ice acetone temperature, whilst the product is collected in a second trap held at liquid nitrogen temperature. Carbon dioxide impurities present in the product trap are removed by subsequently warming the second trap to dry-ice acetone temperature and pumping away the vapour produced. This method was used repeatedly to produce carbon suboxide with reasonable success. The purity of the sample was found to be greater than 95% in most cases with carbon dioxide being the main impurity.

3.10.3 Results of Carbon Suboxide Experiments

If carbon atoms were produced by the decomposition of carbon suboxide by either Method 1 or 2, then carbon monoxide could be used as an indicator of carbon atom concentration (reaction **(3.22)**) assuming that the decomposition proceeds in a similar way. In most of the following experiments a small peak in the mass spectra collected at m/z 105 confirmed the presence of CO. This ion corresponds to the product of reaction **(3.18)** and was used as indirect evidence of carbon atom formation from the decomposition of C_3O_2.

Subjecting a 1% mixture of carbon suboxide in helium to a microwave discharge (Method 2, using the apparatus shown in Figure 3.3) produced significantly **more** soot around the discharge region than with analogous carbon monoxide mixtures. A much lower microwave power level (40W) was applied than was used for carbon monoxide (75W). Using $C_6H_6^+$ as a monitor ion no potential carbon atom products were observed. However, a peak was present in the mass spectra at m/z 105 corresponding to the product of the reaction **(3.18)**. This reaction is very slow and significant decomposition of carbon suboxide must have occurred for this peak to be observed but no evidence of carbon atoms was found. Similar variations in experimental set-up parameters to those tried when carbon monoxide was used (gas flow rate, discharge position and microwave power) yielded no useful results.

Experiments were also conducted where the suboxide was added downstream from the discharge rather than passing directly through it (Method 1). No neutral carbon

monoxide was produced by this method and there was no evidence of carbon deposition on the glass near the C_3O_2 inlet. It was concluded that carbon atoms were not being formed by this method.

3.11 Summary of Discharge Work

Thorough investigation has shown that producing atomic carbon from the decomposition of CO or C_3O_2 in or downstream of a microwave discharge on helium cannot be used to investigate the reactions of atomic carbon using the SIFT. Atomic carbon was produced from carbon suboxide more easily than it was from carbon monoxide, but carbon atoms did not reach the flow tube in either case. Electrostatic interactions between the ions produced in the discharge and neutral carbon atoms may have greatly increasing the rate of atom recombination in this region.

Following the unsuccessful attempts to produce carbon atoms by microwave (and RF) discharge, the relevance to this study of alternative carbon atom production methods was assessed.

3.12 Photolysis Experiments

3.12.1 VUV Flash Photolysis

It is possible to produce atomic carbon by the vacuum ultraviolet photolysis of carbon suboxide with xenon filled flash lamps [92]. This technique would produce fewer ions (some photo-ions would be produced) during the carbon suboxide decomposition than a microwave or RF discharge. Previous flash photolysis studies have focused on the rate of decay of carbon atoms in the presence of various organic reactants after a single photolysing flash. Husain has been particularly successful at investigating carbon atom kinetics by this method [93, 99].

To establish atomic carbon reaction kinetics using the SIFT instrument requires a continuous flow of atomic carbon. The repetition or ‘firing’ rate of UV flash photolysis equipment would not be sufficient to produce the continuous flow required for this experiment. Also, electrical noise created by the photolysing flash(es) would drastically affect the SIFT electronics.

3.12.2 Laser Photolysis

Carbon suboxide can be photo-dissociated with an excimer laser to produce atomic carbon [110]. At wavelengths below 200 nm, photolytic decomposition of carbon suboxide produces a carbon atom and two molecules of carbon monoxide, as described by reaction **(3.22)** [92].

Unlike flash photolysis equipment the pulse rate of an excimer laser should be sufficiently fast to produce a 'continuous' flow of carbon atoms (relative to the SIFT ion detection system). The laser dissociation could also be performed extremely close to the flow tube reducing the time available for atom-atom recombination. An argon-fluoride (ArF) excimer laser is ideally suited to this project as it emits an intense radiation beam at a wavelength of 193 nm. A Lumonics Pulsemaster EX-700 Argon-Fluoride (ArF) excimer laser was available within the chemistry department for this project, but because it was located on another level of the chemistry building and is quite large and difficult to shift, it was decided that preliminary experiments should be conducted before it was moved.

An experiment was devised which would permit the spectroscopic detection of carbon atoms produced by the laser photolysis of carbon suboxide. The atoms were to be detected indirectly by **absorption-emission** spectroscopy. A generalised scheme of the apparatus used for this experiment is shown in Figure 3.5.

The experiment involves irradiating a flow of carbon suboxide with the laser to generate carbon atoms; absorption (by these atoms) of radiation generated by a 'carbon lamp' (which provides intense monochromatic light at the wavelengths corresponding to the atomic lines of carbon); followed by the spontaneous emission of some of this absorbed radiation which is then detected by a monochromator-photomultiplier tube assembly. The intensity of the detected light would give some indication of the extent of carbon atom formation. This method of detection was used in preference to an absorption based experiment. The detection of atomic carbon by **absorption** would involve directing the atomic lines produced by the carbon lamp toward the monochromator aperture and measuring the attenuation of the light as atomic carbon flowed between the light source and the monochromator. This direct method of detection is less sensitive than an absorption-emission experiment as the signal-to-noise ratio is substantially higher.

For the absorption-emission experiment the carbon lamp must be perpendicular to the laser light, and the monochromator aperture perpendicular to both the laser light and the carbon lamp.

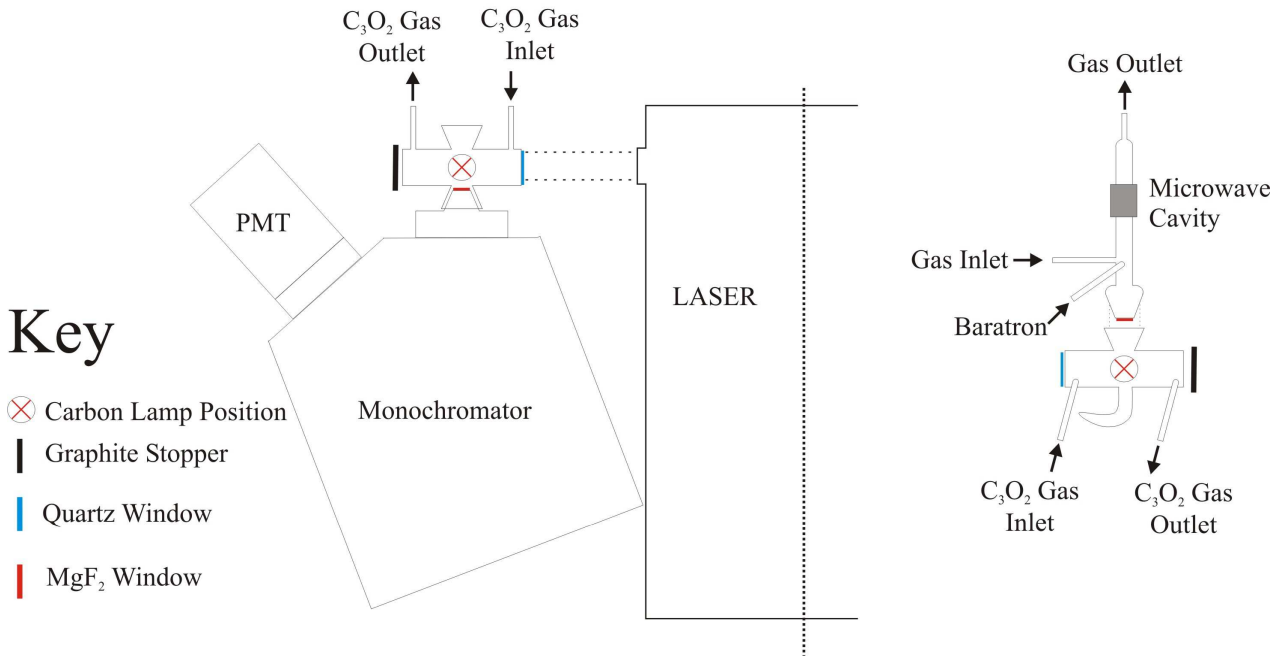

Figure 3.5. *Schematic diagram of the equipment designed to examine the laser photolysis of carbon suboxide. The image is not to scale and only part of the laser manifold is shown. There are five pieces of apparatus of which the laser, monochromator and photomultiplier tube (PMT) are commercial instruments. The rest of the apparatus was purpose built from Pyrex. Two views of the Pyrex assembly are given. The first is a bird's-eye view of the position of the photolysis tube relative to the monochromator and laser. The second view is a laboratory perspective of the position of the carbon lamp relative to the photolysis tube. Below the tube is a Wood's horn (light trap). The carbon lamp is positioned above the tube (as shown) during suboxide photolysis experiments, but can be moved to a second position (as marked) so the intensity of the atomic lines of carbon can be measured directly. The monochromator would be directly behind the photolysis tube as it is shown. A complete description of the apparatus is given in the following text.*

The photolysis tube was constructed from a 100 mm long section of 33 mm outer diameter (o.d.) Pyrex tube. A Suprasil quartz window was fixed to one end of the tube to allow the transmission of the 193 nm (UV) laser radiation along the length of the tube. Three ground glass fittings were integrated around the centre of the tube in a 'T' configuration. One of the fittings was used to connect the tube to the monochromator

whilst the other two (opposite and perpendicular to the monochromator aperture) were positions in which the carbon lamp could be placed. A pressure gauge was attached to the unused lamp position. A Wood's horn (light trap) was located below the carbon lamp position which was perpendicular to the monochromator, to draw stray light away from the monochromator. Short sections of 6.35 mm (¼ inch) o.d. Pyrex tube were connected at each end of the tube. These were the connections through which the carbon suboxide gas was to flow.

The carbon lamp is a simple piece of equipment and was made separately. Atomic carbon emission lines are generated when a microwave discharge is applied to a dilute sample of an appropriate organic substrate [111]. Many different source gases can be used including acetylene, ethylene, methane and carbon monoxide. A 0.5% mixture of carbon monoxide in helium was used in this research. To improve the chances of observing atomic carbon an intense beam of atomic carbon emission lines was needed. For this reason the apparatus used here incorporated a flow of carbon rather than a (more commonly used) static discharge set-up. The carbon lamp (Figure 3.5) was made from 13 mm o.d. Pyrex tube (this size matches our microwave cavity) with a 30 mm o.d. ground glass connection at one end. Three 6.35 mm (¼ inch) o.d. Pyrex tubes were incorporated as shown in Figure 3.5, two so that the source gas could be flowed through the tube with the internal pressure measured through the third. These experiments involve radiation which is in the vacuum ultraviolet (VUV) region of the spectrum. Pyrex does not transmit VUV light so a magnesium fluoride (MgF_2) window was built into the end of the carbon lamp. So that carbon produced in the discharge would not deposit on the MgF_2 window the gas supplied to the lamp was flowed away from the window.

Another MgF_2 window was used between the monochromator aperture and the photolysis tube. The Suprasil quartz window between the photolysis tube and the laser is sufficiently transparent at 193 nm to transmit the intense laser light. A piece of graphite was placed behind the opposite end of the photolysis tube to absorb the laser light and prevent it reflecting dangerously around the laboratory.

All of the ground glass fittings were made 'gas tight' with black wax. The Pyrex photolysis tube was painted black and the entire set-up shrouded with black plastic sheeting to reduce the effects of stray light.

The three lowest transitions for atomic carbon at wavelengths of 1657 Å, 1930 Å and 2479 Å correspond to the transitions $3s(^3P) \leftarrow 2p^2(^3P)$, $3s(^1P_1) \leftarrow 2p^2(^1D_2)$ and $3s(^1P_1) \leftarrow 2p^2(^1S_0)$ respectively [111]. Because these wavelengths are in the VUV region of the spectrum the McPherson 218-0.3 meter scanning monochromator used in this work had to be evacuated to prevent absorption of the VUV light by oxygen. An Edwards ED-200 two-stage backing pump was sufficient to reduce the pressure in the monochromator to a workable level, at below 0.15 Torr.

The detection of photons below 2000 Å cannot be achieved with the conventional photomultipliers that were available for this experiment. A large MgF_2 disc coated with sodium salicylate was placed in front of the photomultiplier tube to circumvent this problem. When irradiated with UV light at wavelengths between 275 Å and 2537 Å, sodium salicylate emits an intense fluorescence peaking at 4200 Å (the intensity of the emission is independent of the incident wavelength) [112]. The wavelength of the fluorescence peak coincides with the wavelength to which photomultipliers having an S11 cathode, like the EMI 9558 QB photomultiplier used in this work, are most sensitive [112].

To coat the MgF_2 disc, a saturated solution of sodium salicylate in methanol was sprayed onto the disc and the solvent allowed to evaporate. The process repeated until a coating of sufficient depth was formed.

The three lowest energy atomic carbon emission lines were observed when the carbon lamp was placed in line with the monochromator aperture and the discharge ignited. The flow of the helium/carbon monoxide mixture through the discharge was varied and the slit widths on the monochromator adjusted to maximise the intensity of the atomic carbon lines relative to the background radiation.

The next step was to examine the dissociation of carbon suboxide with the laser. Unfortunately the project was stalled at this point because the laser would not fire. Lasers are very sensitive to impurities in the laser gas mixture and will not fire if the impurities exceed certain levels. This appeared to be the reason that the laser would not operate. The fluorine gas used in the laser is supplied as a 5 % mixture in neon. Fluorine degrades over time and it is necessary to replace cylinders every few years to avoid the build up of impurities. The cylinder used to fill the laser for this work had not been replaced for over

five years. A cylinder of neon gas which was also used to fill the laser head was almost empty, and impurities may have also built up in this cylinder contributing to the problem. Due to the cost of replacing these cylinders and the limited time available to finish this work, the atomic carbon project was discontinued.

3.12 Conclusion

Unfortunately it has not been possible to generate atomic carbon from a microwave discharge in sufficient quantities for a reaction with an ion to be observed. This work confirms what has long been known, that carbon atoms are quite unwilling to be studied in the laboratory. The principal difficulty in this work appears to be the rate of recombination of carbon atoms both in the gas phase and on the walls of the discharge tube. The recombination of carbon atoms is known to be significantly faster than analogous reactions for other atomic species. There has been ample indirect evidence of carbon atom formation, including the formation of soot around the discharge; the detection of oxygen atoms from the decomposition of carbon monoxide (by their reaction with $C_6H_6^+$, see reaction **(3.10b)**); and similarly the detection of carbon monoxide from the decomposition of carbon suboxide (see reaction **(3.22)**). Because the soot formation occurred only very close to the discharge it was speculated that ions created by the discharge were influencing the rate of recombination. Moving the discharge closer to the flow tube was the next logical step. However, ions produced in the discharge began to influence the reactant ion flow in the main flow tube and this could not be mitigated by the introduction of electrodes between the discharge and the flow tube. It is apparent that a microwave discharge source of carbon atoms is not suited to a SIFT study of atomic carbon kinetics.

Carbon atoms could be produced in sufficient quantities for reaction in the SIFT by laser photolysis. This method was not explored earlier because it would have been difficult to integrate two large pieces of apparatus such as the SIFT and an ArF excimer laser in the limited space available in the UC SIFT laboratory. Although bulky, the laser has a significant advantage over microwave discharge methods in that it can be used much closer to the flow tube, reducing the time available for carbon atom recombination. It is unfortunate that the laser experiments described in Section 3.12.2 could not be completed. It should however be a starting point for future attempts to examine atomic

carbon kinetics where high flows of atomic carbon are needed, as they are in SIFT experiments.

CHAPTER 4.

CYANODIACETYLENE - HC_5N

4.1 Introduction

The cyanopolyynes are a series of molecules described by the formula $HC_{(2n+1)}N$. The first five members of the series (n = 1-5) have been detected in a variety of interstellar clouds including TMC-1 and Sgr B2 [113, 114]. $HC_{11}N$ (n = 5), identified in the circumstellar envelope of the carbon rich star IRC + 10º216, is to date the largest known interstellar molecule [114]. The observation of these long chain molecules in interstellar clouds implies that efficient synthetic routes to their formation are available. In early models of ISCs the larger members of the series were thought to form from the association of small cyanopolyynes with acetylene ions [115], for example:

$$C_2H_2^+ + HC_3N \rightarrow C_5H_3N^+ \qquad \textbf{(4.1)}$$

$$C_5H_3N^+ + e^- \rightarrow HC_5N + 2H \qquad \textbf{(4.2)}$$

and the reaction of nitrogen atoms with hydrocarbon ions [116]:

$$C_9H_2^+ + N \rightarrow C_9HN^+ + H \qquad \textbf{(4.3)}$$

$$C_9HN^+ + H_2 \rightarrow C_9H_2N^+ + H \qquad \textbf{(4.4)}$$

$$C_9H_2N^+ + e^- \rightarrow HC_9N + H \qquad \textbf{(4.5)}$$

Later, time-dependent simulations included neutral-neutral reactions between CN radicals and selected hydrocarbons [115, 117]. Most recently, Winstanley and Nejad gave three possible reaction routes to cyanopolyynes in their study of cyanopolyyne formation in the interstellar cloud TMC-1 [115]. Their reaction schemes follow (**(4.6)** to **(4.8)**). Two are based on neutral chemistry and one on ion chemistry.

$$C_nH_2 + CN \longrightarrow HC_{n+1}N + H, \quad n = 4,6 \text{ and } 8 \qquad \textbf{(4.6)}$$

$$C_nH^+ \xrightarrow{N} C_nN^+ \xrightarrow{H_2} HC_nN^+ \xrightarrow{H_2} H_2C_nN^+ \xrightarrow{e-} HC_nN,\ n = 5,7 \text{ and } 9 \qquad \textbf{(4.7)}$$

$$HCN \xrightarrow{C_2H} HC_3N \xrightarrow{C_2H} HC_5N \xrightarrow{C_2H} HC_7N \xrightarrow{C_2H} HC_9N \qquad \textbf{(4.8)}$$

The cyanopolyynes have been proposed as ideal probes of physical and chemical conditions in ISCs [115, 118] and it has also been suggested that the relative abundance of each cyanopolyyne in an ISC may be indicative of cloud age [119].

The atmosphere of Titan, Saturn's largest satellite, is principally nitrogen with a few percent methane. The minor atmospheric constituents include hydrocarbon and nitrile species formed in Titan's upper atmosphere by ion-neutral reactions. Large molecules diffuse to lower altitudes and condense between 50 and 100 km above Titan's surface forming a haze layer [22]. Cyanopolyynes are thought to contribute to the aerosol particles which give Titan its characteristic orange haze [120].

Laboratory simulations of Titan's atmosphere have produced a great variety of nitriles including the cyanopolyynes HC_3N and HC_5N [121, 122]. Cyanoacetylene, HC_3N, is the smallest cyanopolyyne and was detected in the atmosphere of Titan by the *Voyager* 1 spacecraft in 1980 [123]. It has since been detected in Titan's atmosphere by Earth based measurements [124, 125]. Cyanodiacetylene, HC_5N, has not been detected on Titan but is presumed to be present. This assumption is based on the identification of HC_5N in laboratory simulations of Titan's atmosphere [122] and its detection in many ISCs [113]. Researchers are hopeful that the improved sensitivity of the infrared spectrometer aboard the *Cassini* spacecraft will lead to its detection in Titan's atmosphere [120].

Titan's ionosphere is a reducing environment where ionisation flows from species with parent neutrals having low proton affinities to those with high proton affinities [126]. The composition of the ionosphere is therefore a function of the neutral composition weighted to the proton affinity of the neutral. Proton transfer reactions dominate the chemistry making protonated neutrals the most abundant ions [127]. The

three most common ions in Titan's ionosphere, CH_5^+, $C_2H_5^+$ and $HCNH^+$, are all derived from neutrals having proton affinities that are likely to be much lower than HC_5N. If HC_5N is present in Titan's atmosphere a small fraction is likely to be protonated. The existence of HC_5N in the upper atmosphere of Titan has been inferred from the occurrence of an ion at m/z 76 (corresponding to protonated HC_5N) in data recently obtained by the Ion and Neutral Mass Spectrometer (INMS) aboard the *Cassini* spacecraft [127].

Given its likely presence in Titan's atmosphere, the impact of HC_5N on Titan's ion chemistry must be included in models of the atmosphere.

There has been one theoretical study of the ion chemistry of HC_5N [128]. This was part of a broader investigation into the radiative association of metal ions with polyynes and cyanopolyynes in the ISM. The association of HC_5N with Na^+, Mg^+ and Al^+ was found to be highly efficient at the temperature of cold, dark interstellar clouds and in the outer regions of circumstellar envelopes and thus an important loss mechanism for these metal ions in cold environments [128].

Although the ion chemistry of the smaller cyanopolyyne HC_3N has been examined by several authors over many years [62, 129-131], the absence of a convenient synthetic route to HC_5N has precluded the study of its chemistry. The original synthetic route to HC_5N developed by Alexander *et al*. is a complex multi-step synthesis which is not feasible for undertaking a kinetic study [132]. Two alternative methods have been developed to generate HC_5N since the publication of this synthesis: the direct current discharge of a mixture of acetylene and cyanoacetylene [133]; and the pyrolysis of pyridine in the presence of trace amounts of phosphorous trichloride (PCl_3) [134]. Because these alternative methods produce significant quantities of by-products they are also unsuitable for use in a SIFT study of the ion chemistry of HC_5N.

Recently a new, uncomplicated synthetic route to HC_5N has become available which yields a small **pure** sample [135]. In the present work a pure sample of HC_5N was prepared by this newly published method. The chemistry of HC_5N was then examined with ions relevant to the chemistry occurring in Titan's atmosphere and in interstellar clouds.

Because Titan's ion chemistry is dominated by proton transfer reactions, an estimate of the proton affinity for HC_5N is of value to modellers of this environment. By employing selected reactant ions and examining the resultant chemistry the proton affinity of HC_5N was approximated. A theoretical calculation of the proton affinity was also undertaken to support this value.

4.2 Experimental

4.2.1 The Preparation of HC_5N

HC_5N was prepared following the recently published method of Guillemin and Trolez [135]. Pure cyanodiacetylene (**3**) can be isolated from the products of the reaction between butadiynyl tributyltin (**1**) and para-toluenesulfonyl cyanide (**2**).

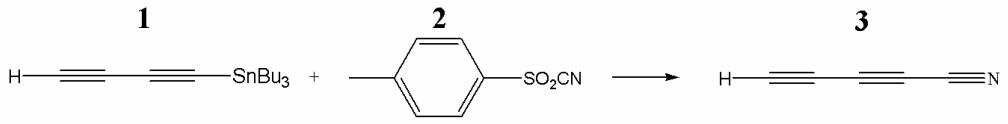

(4.9)

Para-toluenesulfonyl cyanide (**2**) is available from commercial sources and was obtained from Sigma-Aldrich. Butadiynyl tributyltin (**1**) was synthesized in two steps following literature methods [136]. In the first step diacetylene is prepared from the reaction of 1,4-dichlorobut-2-yne with KOH at 70 ºC and collected in two traps containing dry THF at -78 ºC. Next n-butyllithium is added drop-wise to the combined diacetylene in THF solutions. A large excess of diacetylene is necessary to inhibit the formation of unwanted di-substituted diacetylene which would generate dicyanodiacetylene (C_6N_2) if reacted with (**2**). Tributyltin chloride is then added to the mixture to generate the desired butadiynyl tributyltin product (**1**). Removal of the solvents under vacuum yields a viscous red-brown oil. It was found that the removal of remaining involatile solvents under a vacuum of 1-2 Torr took several hours and was important to the purity of cyanodiacetylene obtained from reaction **(4.9)**.

Cyanodiacetylene (**3**) was synthesized under vacuum from the reaction of 2.5g of p-toluenesulfonyl cyanide (**2**) with 1.75g of butadiynyl tributyltin (**1**) at 75-80 ºC for two hours. Gaseous products of the reaction were collected in two cold traps as described by Guillemin and Trolez: the first held at -30 ºC removing impurities and the second at -80

ºC selectively trapping cyanodiacetylene (**3**). The reaction yielded approximately 20 mg of HC_5N which was diluted in 200 Torr of helium. The diluted product remained stable at room temperature for several days. The cyanodiacetylene produced was introduced to the SIFT flow tube diluted in helium.

4.2.2 Characterization of HC_5N Preparation Products

The product(s) collected at -80 ºC were analyzed by their reaction with H_3O^+ and O_2^+ which generated the chemical ionisation spectra in Figures 4.1 and 4.2 respectively. These spectra demonstrate that a complex mixture of gases was collected. Although products derived from HC_5N were observed at m/z 76 (HC_5NH^+) in Figure 4.1 and m/z 75 (HC_5N^+) in Figure 4.2, they constituted only a minor fraction of the species present. The majority of the product peaks were attributed to residual solvents present in the butadiynyl tributyltin reagent, and diacetylene. The ions derived from solvent impurities were not observed in subsequent preparations of HC_5N where more time was allowed for the evaporation of the solvent residues at low pressure.

The products collected in the first cold trap at -30 ºC were analysed using the same method. Surprisingly, this cold trap (which was supposed to contain impurities) was found to contain essentially pure cyanodiacetylene (HC_5N), as shown in Figures 4.3 and 4.4.

The isolation of pure HC_5N at -30 ºC was reproducible and is inconsistent with the method reported by Guillemin and Trolez. This result is however in agreement with results published by Haas *et al*. [133]. In their work HC_5N was one of many species produced when a direct current discharge was applied to a mixture of C_2H_2 and HC_3N. The products of the discharge were collected at liquid nitrogen temperature and carefully distilled to obtain HC_5N. The purest HC_5N fraction was found to evaporate between -20 ºC and 0 ºC [133].

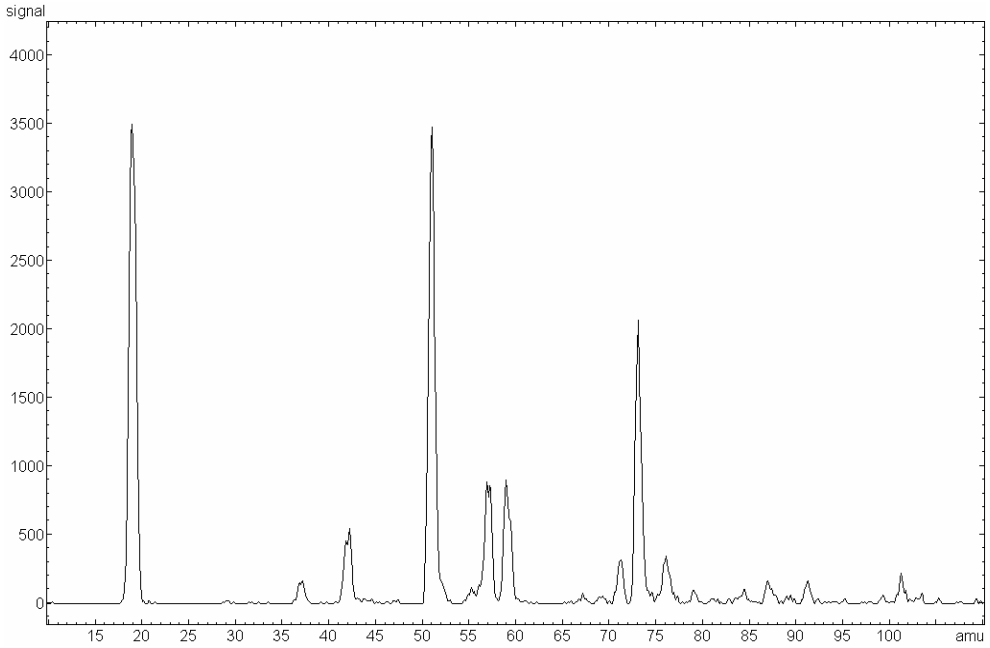

Figure 4.1. *Chemical ionisation spectrum generated from reaction of the products collected at -78 º C with H_3O^+. A small peak corresponding to protonated cyanodiacetylene (HC_5NH^+) is seen at m/z 76. The dominant impurity is diacetylene demonstrated by the large peak at m/z 51 ($C_4H_3^+$) with solvent residues (either pentane or THF) contributing to the m/z 73 peak.*

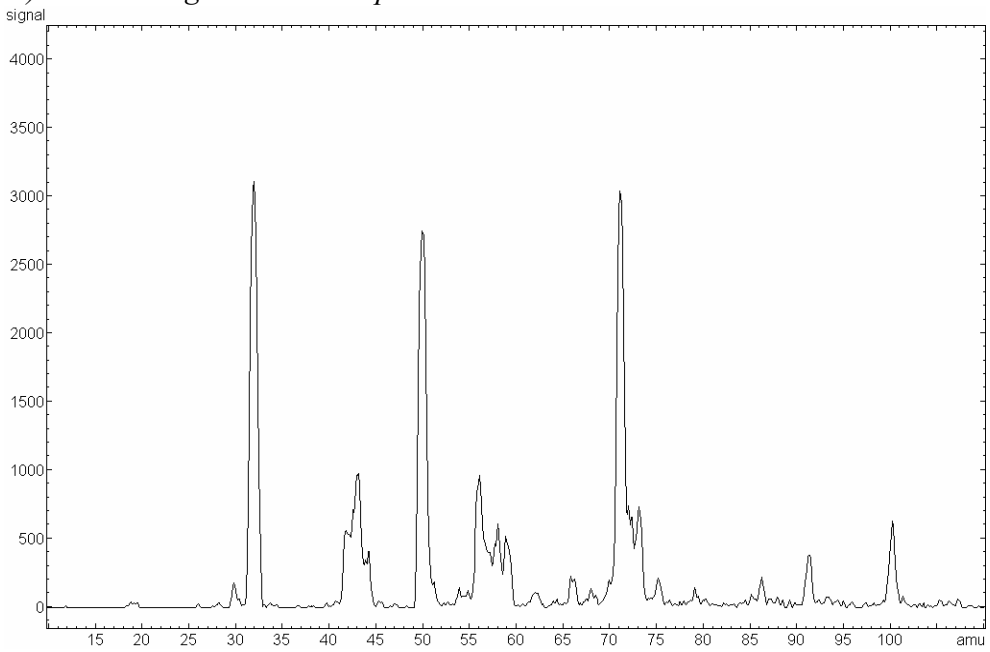

Figure 4.2 *Chemical ionisation spectrum generated from reaction of the products collected at -78 º C with O_2^+. Ionised cyanodiacetylene (HC_5N^+) is seen at m/z 75. The dominant impurities are diacetylene at m/z 50 ($C_4H_2^+$) and solvent residues at m/z 72 (either pentane or THF).*

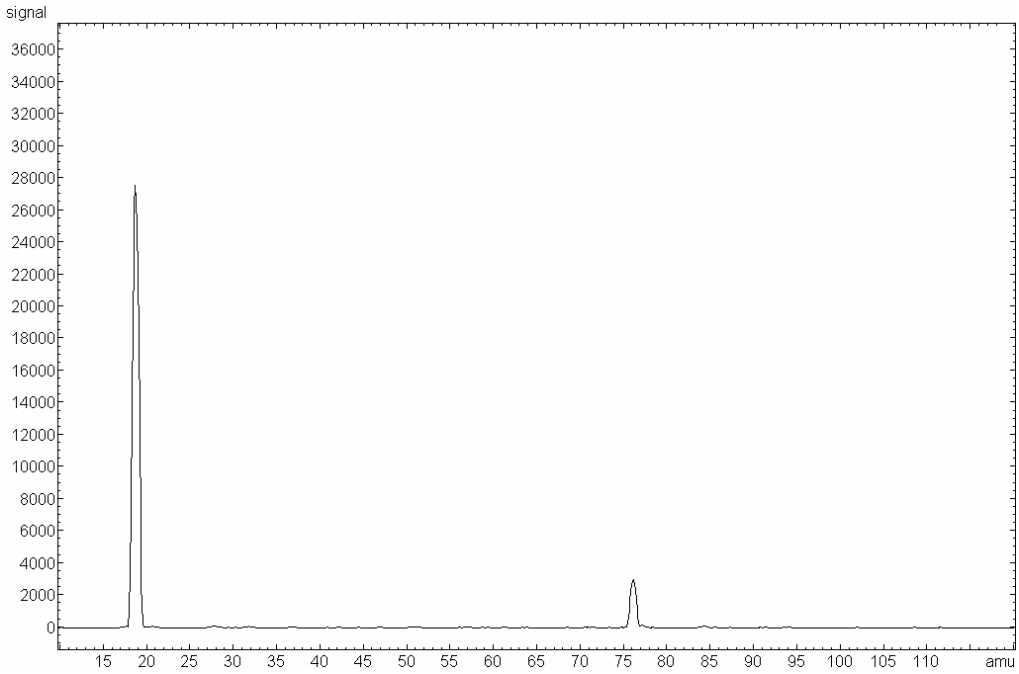

Figure 4.3. *Chemical ionisation spectrum generated from the reaction of HC_5N collected at -30 ° C with H_3O^+. A single product peak corresponding to protonated HC_5N is seen at m/z 76 (HC_5NH^+).*

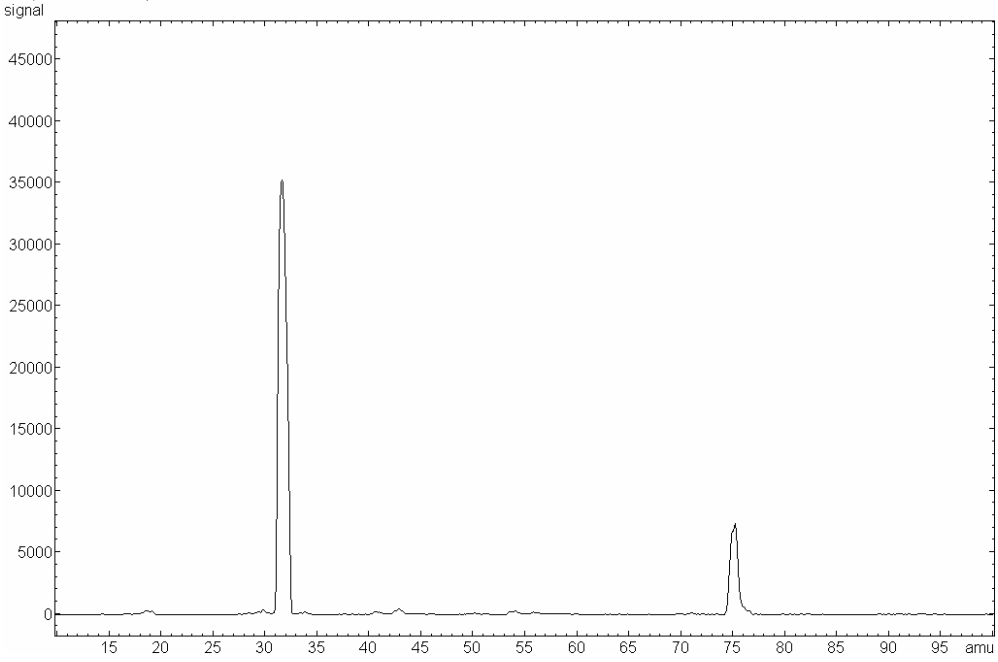

Figure 4.4. *Chemical ionisation spectrum generated from the reaction of HC_5N collected at -30 ° C with O_2^+. A single product peak corresponding to ionised HC_5N is seen at m/z 75 (HC_5N^+).*

4.2.3 Other Experimental Details

The ions examined in this study were generated from appropriate source gases obtained from commercial suppliers and were further purified by multiple freeze-pump-thaw cycles. Exceptions to this were HCN, HC_3N and C_4H_2 which were synthesized in the laboratory by standard methods. HCN was produced from the reaction of KCN with sulfuric acid and dried over P_2O_5 [137]. C_4H_2 was prepared by the same method outlined in the preparation of HC_5N [136]. HC_3N was synthesized in two steps. First, propiolamide was generated from the reaction of methyl propiolate and liquid ammonia. The propiolamide was then dehydrated with P_2O_5 to produce HC_3N [109, 138]. The synthesized gases were also purified by multiple freeze-pump-thaw cycles before use.

The ions used in this study were generated as follows: H_3O^+ from H_2O; CH_3^+ from CH_4; $C_2H_3^+$, $C_2H_5^+$ and $C_3H_5^+$ from C_2H_4; $C_3H_3^+$ from allene; $C_3H_7^+$ from C_3H_7Br; $C_4H_2^+$ and $C_4H_3^+$ from C_4H_2; $HCNH^+$ from HCN; HC_3NH^+ from HC_3N; CH_3CNH^+ from CH_3CN; CH_3CHOH^+ from CH_3CHO; $HCOOH_2^+$ from HCOOH; CO^+ from CO and $C_6H_6^+$ from benzene.

Ab initio calculations were performed with the Gaussian 03 program [139]. The molecular polarisability of HC_5N was calculated using a relatively high level of theory (RMP2-FC\Aug-CC-pVTZ) to be 10.77 x 10^{-24} cm^3. The capture collision rates were calculated with the parameterized method of Su and Chesnavich [59] using the experimental dipole moment of Kroto (4.33 Debye) [132] and the calculated molecular polarisability. G3 theory [140] was employed for the calculation of the proton affinity starting with the geometries of Botschwina [141].

4.3 Results

Reaction **(4.9)** produced insufficient HC_5N to permit a full kinetic investigation of each ion-molecule reaction. The HC_5N was diluted in helium in order that more chemistry could be examined with the small sample. Because kinetics could not be measured for all of the ions, the identification of reaction products became the main focus of the research. The experimental results are summarised in Table 4.1 for ions with a transferable proton.

Table 4.1. *A summary of the reactivity of HC_5N with ions having a transferable proton.*

Reagent Ion	PA (kJ mol^{-1})	Products	Branching Ratios[a]	k_c[b]
H_3O^+	691	$HC_5NH^+ + H_2O$	1.00	(5.6)
CH_3^+		$HC_5N.CH_3^+$	1.00	(6.1)
$C_2H_3^+$	641.4	$HC_5NH^+ + C_2H_2$	0.90	(4.9)
		$HC_5N.C_2H_3^+$	0.10	
$C_2H_5^+$	680.5	$HC_5NH^+ + C_2H_4$	1.00	(4.7)
$C_3H_3^+$	951	$HC_5N.C_3H_3^+$	1.00	(4.3) <0.001
$C_3H_5^+$	775[c]	$HC_5NH^+ + C_3H_4$	0.75[d]	(4.2) <4.2
		$HC_5N.C_3H_5^+$	0.20	
		$H_4C_8N^+ + H_2$	0.05	
$C_3H_7^+$	751.6	$HC_5NH^+ + C_3H_6$	0.90	(4.1)
		$HC_5N.C_3H_7^+$	0.10	
$C_4H_3^+$	737.2	$HC_5NH^+ + C_4H_2$	0.80	(3.9)
		$HC_5N.C_4H_3^+$	0.20	
$HCNH^+$	713	$HC_5NH^+ + HCN$	1.00	(4.8)
HC_3NH^+	751.2	$HC_5NH^+ + HC_3N$	1.00	(3.9)
CH_3CNH^+	779	$HC_5NH^+ + CH_3CN$	0.50[d]	(4.2) <4.2
		$HC_5N.CH_3CNH^+$	0.50	
CH_3CHOH^+	768.5	$HC_5NH^+ + CH_3CHO$	0.90[d]	(4.1) <4.1
		$HC_5N.CH_3CHOH^+$	0.10	
$HCOOHH^+$	742	$HC_5NH^+ + HCOOH$	1.00	(4.0)
$C_4H_2^+$		$HC_5N.C_4H_2^+$ (slow)	1.00	(4.0) <0.001
$C_6H_6^+$	884	No Reaction		(3.5) <0.001

a. Errors associated with branching ratios are ±30%.

b. The capture collision rates are in parenthesis. All reactions are estimated to proceed at the collision rate except when upper limits are given outside the parenthesis (see text). Units are 10^{-9} cm^3 s^{-1}.

c. For allene.

d. Upper limit due to the presence of H_3O^+ impurities that may also have produced this ion (see text).

The rate coefficient for the reaction of H_3O^+ with the **diluted** HC_5N was directly measured.

$$H_3O^+ + HC_5N/He \text{ mixture} \rightarrow HC_5NH^+ + H_2O \qquad k = 2.9 \times 10^{-11} \text{ cm}^3 \text{ s}^{-1} \quad \textbf{(4.10)}$$

Proton transfer reactions such as **(4.10)** are known to proceed at the collision rate when exothermic [142]. This measured rate is approximately 0.5% of the collision rate

($k = 5.6 \times 10^{-9}$ cm^3 s^{-1}). When the dilution of the HC_5N sample is taken into account (approximately 1-2 Torr of HC_5N in 200 Torr of helium) it is evident that the reaction does indeed proceed at or close to the collision rate.

A rate coefficient was also measured with $HCNH^+$.

$HCNH^+ + HC_5N/He\ mixture \rightarrow HC_5NH^+ + HCN \quad k = 2.6 \times 10^{-11}\ cm^3\ s^{-1}$ **(4.11)**

Reaction **(4.11)** also proceeds by proton transfer. When the measured rate is adjusted relative to the concentration of HC_5N in the mixture (~ 0.5%, based on the assumption that reaction **(4.10)** proceeds at the collision rate) it is clear that this reaction also proceeds at the collision rate. Most of the ions reacted by proton transfer only and were thus presumed to proceed at the calculated collision rates which are given in parenthesis in the fifth column of Table 4.1. Qualitative examination of each reaction supported this presumption. For reactions that were substantially slower than the collision rate an estimated upper limit for the reaction rate is given outside the parenthesis. The absolute uncertainty in the product branching ratios is ±30 % which is higher than the usual ±15 % because the branching ratios were estimated from mass spectra rather than the standard kinetic method.

A summary of results for ions without a transferable proton is listed in Table 4.2.

Table 4.2. *A summary of the reactivity of HC_5N with ions without a transferable proton.*

Reactant Ion	Neutral IE (eV)	Products	Branching Ratios[a]	k_c[b]
O_2^+	12.07	HC_5N^+	1.00	(4.6)
C^+	11.26	HC_5N^+	0.65	(6.7)
		$C_6N^+ + H$	0.35	
N^+	14.53	HC_5N^+	0.50	(6.3)
		$C_5H^+ + N_2$	0.50	
N_2^+	15.58	HC_5N^+	1.00	(4.8)
CO^+	14.01	HC_5N^+	1.00	(4.8)

a. Errors associated with branching ratios are ±30%.

b. The capture collision rates are in parenthesis. All of these reactions were estimated to proceed at the collision rate. Units are 10^{-9} cm^3 s^{-1}.

Of the ions examined in Table 4.2, only the rate coefficient for CO^+ was measured directly.

$CO^+ + HC_5N/He\ mixture \rightarrow HC_5N^+ + CO \quad k = 3.0 \times 10^{-11}\ cm^3\ s^{-1}$ **(4.12)**

Adjusting the measured rate relative to the dilution of the HC_5N (~0.5%) shows that this reaction proceeds at or close to the collision rate. The other ions were also observed to react rapidly with HC_5N and all of the reactions were thus estimated to proceed at their respective collision rates, given in parenthesis in the fifth column.

The IEs of the neutrals from which the reactant ions in Table 4.2 are derived are given in the second column of the table [71]. The charge transfer channels observed for each of the ions in Table 4.2 indicate that HC_5N has a comparatively low IE (< 11.26 eV).

4.4 Discussion

4.4.1 Ion Chemistry

A significant part of the chemistry outlined in Table 4.1 is unremarkable which is of little surprise given the reactants chosen. Proton transfer is the dominant reaction mechanism ensuring that almost all of the reactions proceed at the collision rate.

Not all of the ions reacted efficiently with HC_5N. Although some evidence of adduct formation was detected with $C_3H_3^+$ the reaction was very slow, giving an upper limit to the rate of reaction of ~1 x 10^{-11} cm^3 s^{-1}. $C_3H_3^+$ is an important interstellar ion which has two stable isomeric structures which exhibit contrasting reactivity. The linear isomer is considerably more reactive than the cyclic isomer. In this instance $C_3H_3^+$ was produced from allene (CH_2=C=CH_2). This source gas is expected to give a mixture of the two isomers. The exact ratio of reactive to unreactive isomer was established by reaction of the $C_3H_3^+$ with C_2H_2 and found to be 3:2 [143]. It is highly unlikely that the trace of adduct formed was generated by the c-$C_3H_3^+$ isomer which is almost universally unreactive in with interstellar ions [144]. The upper limit for the rate coefficient given in Table 4.1 is for linear $C_3H_3^+$ with cyclic $C_3H_3^+$ assumed to be unreactive. $C_4H_2^+$ also showed signs of adduct formation at very low levels and the same upper limit to the reaction rate coefficient was assigned to this species. $C_6H_6^+$ was found to be entirely unreactive under the conditions employed.

Collision rate charge transfer reactions were observed for each of the interstellar ions shown in Table 4.2. Two of the ions, C^+ and N^+, exhibited an additional product channel. Reaction **(4.13b)** may be an example of an insertion-elimination reaction which

is a well known reactive pathway for carbon ions and is the simplest way by which carbon chain lengths are increased in interstellar chemistry [3]. Highly unsaturated molecules are common in the ISM because of this type of reaction in which a hydrogen atom is eliminated.

$$C^+ + HC_5N \rightarrow HC_5N^+ + C \qquad 0.65 \qquad \textbf{(4.13a)}$$

$$\rightarrow C_6N^+ + H \qquad 0.35 \qquad \textbf{(4.13b)}$$

Reaction **(4.13)** appears typical of the cyanopolyynes with a comparable channel also observed in the reaction of C^+ with HCN, forming C_2N^+ [145], and with HC_3N producing C_4N^+ [129].

The reaction of N^+ with HC_5N generates equal portions of the charge transfer product HC_5N^+ and C_5H^+.

$$N^+ + HC_5N \rightarrow HC_5N^+ + N \qquad 0.50 \qquad \textbf{(4.14a)}$$

$$\rightarrow C_5H^+ + N_2 \qquad 0.50 \qquad \textbf{(4.14b)}$$

Reaction **(4.14b)** is interesting as the formation of C_5H^+ requires the rupture of the strong CN bond in HC_5N. The formation of N_2 is evidently sufficiently exothermic to make the overall process favourable and thus competitive with the charge transfer channel. This type of reaction is also observed for the reaction of N^+ with HC_3N, from which C_3H^+ is produced [129].

The first two cyanopolyynes, HC_3N and HC_5N, react in similar ways with C^+ and N^+ as outlined above. This chemistry is summarised in Tables 4.3 and 4.4. The chemistry of HCN is included in both tables for comparison.

Table 4.3. *Trends in reaction chemistry for C^+ with cyanopolyynes*.

Reactant	Products	Rate Coefficient[a]	Reference
HCN	$C_2N^+ + H$	2.95	[145]
HC_3N	$C_4N^+ + H$	1.40[b]	[129]
HC_5N	$C_6N^+ + H$	~ 2.3[c]	This work

a. In units of 10^{-9} cm^3 s^{-1}.

b. From the branching ratio. Occurs in competition with $C_3H^+ + CN$ channel.

c. From the branching ratio. Occurs in competition with an electron transfer channel.

Table 4.4. *Trends in reaction chemistry for N^+ with cyanopolyynes.*

Reactant	Products	Rate Coefficient[a.]	Reference
HCN	$HCN^+ + N$	3.7	[146]
HC_3N	$C_3H^+ + N_2$	2.1[b]	[129]
HC_5N	$C_5H^+ + N_2$	~ 3.1[b]	This work

a. In units of 10^{-9} cm^3 s^{-1}.

b. From the branching ratio. Occurs in competition with an electron transfer channel.

4.4.2 The Proton Affinity of HC_5N

One of the main objectives in this work was to obtain an approximate value for the proton affinity of HC_5N. Estimates of the PA were made experimentally and theoretically.

It is known that if proton transfer is exothermic then a reaction generally proceeds at the capture collision rate [142]. This has already been exploited to estimate the reaction rates for the ions listed in Table 4.1. As the exothermicity of proton transfer approaches zero other reaction channels are likely to become favourable. It is also probable that the reaction rate will be slower when a proton transfer channel is unavailable. Once proton transfer is more than a few kJ mol^{-1} endothermic HC_5NH^+ cannot be produced. The PA of HC_5N can be inferred by reaction with a set of judiciously chosen protonated ions. The resultant chemistry is indicative of the difference in PA between HC_5N and the neutral from which the protonated ions are derived.

Firstly it was assumed the PA of HC_5N would be similar to or slightly greater than the PA of the smaller cyanopolyyne HC_3N of 753.5 kJ mol^{-1} [147]. A series of neutrals having proton affinities between 730 kJ mol^{-1} to 780 kJ mol^{-1} were then selected. These species are listed in Table 4.5. The protonated neutrals were reacted with HC_5N and the resultant chemistry is included in Table 4.1.

Table 4.5. *Neutrals employed to investigate the proton affinity of HC_5N.*

Neutral	Proton Affinity (kJ mol^{-1})[a]
C_4H_2	737.2
HCOOH	742
HC_3N	751.2
CH_3CHO	768.5
C_3H_4 [b]	775
CH_3CN	779

a. Reference [148].

b. For allene.

Rapid proton transfer was observed with $C_4H_3^+$, $HCOOHH^+$, HC_3NH^+, CH_3CHOH^+ and $C_3H_5^+$. Slow proton transfer was observed for CH_3CNH^+ in addition to adduct formation. The reactions of CH_3CHOH^+, $C_3H_5^+$ and CH_3CNH^+ were complicated by the presence of small quantities of H_3O^+ which may have contributed to the formation of HC_5NH^+. For this reason the proton transfer branching ratios for these species in Table 4.1 are given as upper limits.

In spite of the problem caused by the H_3O^+ impurities the fact that all of the reactions except for CH_3CNH^+ were rapid, indicates that the PA of HC_5N is probably greater than 765 kJ mol^{-1}. The slow reaction with CH_3CNH^+ and competitive adduct formation effectively prevent the PA from being much greater than 779 kJ mol^{-1}.

A theoretical calculation with the Gaussian 03 program using the G3 level of theory gave a value for the PA of HC_5N of 775.5 kJ mol^{-1}. Combined with the experimental results outlined above the proton affinity of HC_5N is thus estimated to be 770 ± 20 kJ mol^{-1}.

4.5 Conclusion

A pure sample of cyanodiacetylene, HC_5N, was successfully prepared following the recently published method of Trolez and Guillemin [135]. A slight alteration to the collection method was implemented after pure HC_5N was unexpectedly found in the first cold trap held at -30 ºC rather than the second cold trap held at -78 ºC. The HC_5N collected was insufficient to permit a complete kinetic investigation with each of the ions listed in Tables 4.1 and 4.2. Consequently the focus of the research was directed to the

identification of reaction products. The results reveal that HC_5N readily accepts a proton from a variety of hydrocarbon and nitrile ions which are present in the ionosphere of Titan. All of the reactions having proton transfer as the dominant reaction pathway were presumed to proceed at the collision rate. Less reactive ions including $C_4H_2^+$ and $C_3H_3^+$ exhibited only slow association with HC_5N. A mixture of cyclic and linear $C_3H_3^+$ was formed from allene in this work. It is presumed that c-$C_3H_3^+$ is unreactive with HC_5N in keeping with its chemistry with other neutrals on Titan.

Proton transfer reactions are thought to be the dominant reaction mechanism in Titan's upper atmosphere and the results obtained here uphold this. Moreover the inferred presence of HC_5N in Titan's atmosphere based on the observation of an ion at m/z 76 (corresponding to protonated HC_5N) by the *Cassini* INMS is supported by this work. HC_5N has a relatively high proton affinity and is likely to be found as HC_5NH^+ in Titan's ionosphere. HC_5NH^+ has been identified as the principal product of several of the reactions in this work. The abundance of this ion in Titan's upper atmosphere will be dependent on the abundance of neutral HC_5N and the reactivity of HC_5NH^+ with the most abundant neutral species in Titan's atmosphere. The chemistry of HC_5NH^+ was not examined in this study as there was insufficient HC_5N (the precursor to HC_5NH^+) for such an investigation.

The proton affinity of HC_5N determined in this work has been used by Vuitton *et al*. to estimate the mole fraction of HC_5N in Titan's upper atmosphere as 1.0×10^{-6} at 1100 km [127].

CHAPTER 5.

METHYLENIMINE AND PROPIONITRILE

5.1 Introduction

5.1.1 Results of the *Cassini-Huygens* Mission

The dense atmosphere of Titan is distinctive in the solar system in that it is nitrogen-based like Earth. Photochemical processes initiate a complex ion and neutral chemistry which generates a unique mix of ions and molecules in Titan's upper atmosphere. The ion-molecule reactions occur primarily between 1000 and 1200 km above Titan's surface and the ion chemistry is complex. Following the discovery of a dense atmosphere on Titan, researchers have striven to identify and predict the atmospheric constituents. Advanced models of Titan's atmosphere have been developed which attempt to replicate the observed atmospheric abundances [34, 46, 149]. The accuracy of these models can now be tested following the successful *Cassini-Huygens* mission.

On 16 April 2005 the *Cassini Orbiter* passed through the night-side atmosphere of Titan at altitudes between 1027 and 1200 km. *In situ* measurements of the atmosphere by the Ion and Neutral Mass Spectrometer (INMS) aboard the spacecraft identified a substantial ionosphere and showed that a complex ion chemistry was occurring [51]. The INMS results have recently been published and a comparison made between the recorded ion densities and the expected ion densities (based on models of Titan's atmosphere) [51]. Many of the features of the ionospheric models were validated by the data. Clusters of ion peaks separated by 12 mass units can be seen in the *Cassini* INMS spectra (Figure 5.1, taken from Cravens *et al*. [51] and Figure 1.7 from reference [52]). This periodicity

was predicted by mass spectra generated from model data although the observed spectra were more complete than expected. The dominant ionic species, $HCNH^+$ (m/z 28), was anticipated to be one of the terminal ions in the atmosphere because it has few reactive pathways [26, 34, 149].

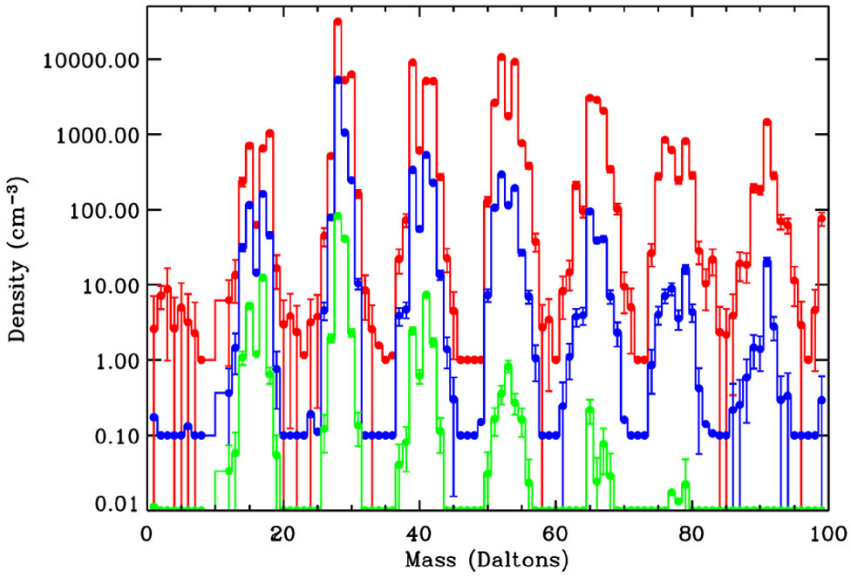

Figure 5.1 *Ion mass spectra recorded by the Cassini spacecraft in Titan's upper atmosphere taken from reference* [51]. *The spectra were measured over three altitude ranges. The (average) ion density scale is logarithmic and the spectra have been displaced vertically as follows: red: 1027 – 1200 km, multiplied by a factor of 100; blue: 1200 – 1400 km, multiplied by a factor of 10; green: 1400 -1600 km, not scaled. The peaks will all have the same scale heights.*

The scarcity of the primary ions formed in Titan's upper atmosphere (N_2^+, CH_3^+ and CH_4^+) emphasises the importance of chemistry to Titan. Overall the observed spectra matched model data well but some ions observed in the *Cassini* data were under-represented or not produced at all in the models. Of these, the ions at m/z 18, 30, 42, 54, 56 and 66 made important contributions to the overall ion density on Titan but were not in pre-*Cassini* models [51]. If the pre-*Cassini* models are to be made accurate these ions must be identified and the ion chemistry of the parent neutrals measured and included.

Titan's ionosphere is a reducing environment in which proton transfer reactions predominate. This means that hydrocarbons and oxygen-bearing hydrocarbon species are represented by ions having odd masses. Molecules such as nitriles containing a single nitrogen atom are represented by ions having even masses. The m/z values for the

unidentified species listed above are all at even masses which suggests that Titan's atmosphere accommodates many more nitrogen containing molecules than previously thought.

5.1.2 Methylenimine - CH_2NH

The unidentified ion at m/z 30 in the *Cassini* INMS spectrum has recently been identified as $CH_2NH_2^+$, produced from the protonation of neutral methylenimine, CH_2NH, which is also known as methanimine and formaldimine [127]. This designation is based on the likely fate of other sources of ions having m/z 30. For example, the molecular ion of ethane ($C_2H_6^+$) could also be responsible for this ion peak as ethane is abundant in Titan's atmosphere. This possibility can however be discounted as the radical cation $C_2H_6^{+\cdot}$ is highly reactive and would be depleted rapidly by reaction with other hydrocarbons in the atmosphere. Given its high reactivity, the formation routes available for $C_2H_6^{+\cdot}$ could not sustain the ion density at m/z 30 observed by the *Cassini* INMS. $C_2H_6^{+\cdot}$ can thus be discounted as the source of this ion density. NO^+ could also provide some of ion density at m/z 30 although Vuitton, Yelle and Anicich argue that this could not be more than ~ 2% [127]. From a consideration of the prevailing atmospheric chemistry, protonated methylenimine is the most plausible candidate for the ion density occurring at m/z 30.

Methylenimine was first identified in the interstellar medium in 1973 in the emission spectrum of the largest known interstellar cloud, Sagittarius B2 (normally abbreviated to Sgr B2) [150]. It has since been observed in numerous other interstellar and circumstellar environments [151]. It has been proposed that methylenimine is formed in the interstellar medium from the following bimolecular reactions:

$$N(^2D) + CH_4 \rightarrow CH_2NH + H \qquad \textbf{(5.1)}\ [152]$$

$$NH + CH_3 \rightarrow CH_2NH + H \qquad \textbf{(5.2)}\ [153]$$

The reactant species involved in **(5.1)** and **(5.2)** are abundant in the upper atmosphere of Titan, making CH_2NH formation likely. Ion-molecule pathways may also generate CH_2NH [154]:

$$CH_3^+ + NH_3 \rightarrow CH_3NH_3^+ \qquad \textbf{(5.3a)}$$

$$\rightarrow NH_4^+ + CH_2 \qquad \textbf{(5.3b)}$$

$$\rightarrow CH_2NH_2^+ + H_2 \qquad \textbf{(5.3c)}$$

Neutral methylenimine is presumed to form from the dissociative recombination of atmospheric electrons with protonated methylenimine produced by channel **(5.3c)**.

Laboratory studies of methylenimine have focused on spectroscopic measurements [155-159] and on establishing accurate enthalpies of formation for CH_2NH, CH_2NH^+ and $CH_2NH_2^+$ [160-163]. No kinetic investigations of methylenimine ion chemistry are reported in the literature.

5.1.3 Propionitrile – C_2H_5CN

The m/z 56 peak in the *Cassini* INMS data has been confidently attributed to $C_2H_5CNH^+$, generated by the protonation of propionitrile, C_2H_5CN, which is also known as ethyl cyanide or propanenitrile [127]. This assignment was made using the same rationale as employed to identify methylenimine: viz. that the hydrocarbon and oxygen-bearing hydrocarbon ions that could also contribute to m/z 56 are reactive radical cations which would not survive sufficiently long in the atmosphere to sustain the observed ion density.

Propionitrile has been detected in the Orion nebula (OMC-1) and in Sgr B2 by Earth-based radio astronomy [164] and has a typical fractional abundance of 10^{-10} in dense ISCs (relative to H_2) [6]. Propionitrile is one of many nitrile species predicted by laboratory simulations of Titan's atmosphere that have not been conclusively identified in the atmosphere [122]. Khanna recently proposed that an IR emission previously attributed to HC_3N (and possibly H_2O ices) in an IR spectrum of Titan's atmosphere recorded by *Voyager* 1 in 1980, was actually emitted by crystalline propionitrile in Titan's stratosphere [165]. This proposal is yet to be verified.

Protonated propionitrile is thought to be formed in ISCs via ion-molecule association reactions; with neutral propionitrile resulting from dissociative recombination reactions with electrons. Wilson *et al*. completed a thorough investigation of two such association reactions [166].

$$H_2CN^+ + C_2H_4 \rightarrow C_3H_6N^+ \qquad \textbf{(5.4)}$$

$$CH_3^+ + CH_3CN \rightarrow C_3H_6N^+ \qquad \textbf{(5.5)}$$

Both reactions generate ions having the same empirical formula as protonated propionitrile although many possible isomers of this ion could be formed in each reaction. By comparing the reactivity of the $C_3H_6N^+$ ions with the reactivity of protonated

propionitrile ($C_2H_5CNH^+$) and protonated ethyl isocyanide ($C_2H_5NCH^+$), the authors were able to show that neither **(5.4)** nor **(5.5)** led to protonated propionitrile.

Propionitrile has been the subject of three further ion-molecule chemistry investigations by Prodnuk *et al*. [167], Bowie and Williams [168] and Franklin *et al*. [169]. Bowie and Williams conducted an ICR study of the reactivities of alkyl and aryl cyanides with some hydrocarbon and nitrile ions [168]. Kinetics were not measured. Only two ions were reacted with propionitrile and neither is common in the ISM or the atmosphere of Titan. Franklin *et al*. measured reaction kinetics for propionitrile with a series of hydrocarbon and nitrile ions including two ions also examined in this study [169]. Their measurements are included in the results of this work for comparison (Table 5.3). The SIFT study of Prodnuk *et al*. measured kinetics for the reactions of linear and cyclic $C_3H_2^+$ with propionitrile [167]. The chemistry of $C_3H_3^+$ was part of the current study but $C_3H_2^+$ was not.

5.1.4 Summary

Several ion peaks were observed by the *Cassini* INMS that were not predicted by pre-*Cassini* models of Titan's atmosphere. Methylenimine and propionitrile have been proposed as the neutral species which, when protonated, give rise to ion densities at m/z 30 and m/z 56 respectively. Both molecules have been positively identified in ISCs and propionitrile has been tentatively identified in the atmosphere of Titan.

To update the pre-*Cassini* models of Titan's ion chemistry, the reactivity of methylenimine and propionitrile with ions important to Titan's ionosphere must be determined. Rather than performing a complete survey of ion chemistry for these species, reactivity was only measured for the small hydrocarbon and nitrile ions that dominate Titan's ion chemistry. The reactions likely to have the most influence on the atmosphere were identified by Roger Yelle and Veronique Vuitton of the *Cassini-Huygens* mission [170].

5.2 Experimental

There have been many laboratory studies of methylenimine and numerous production methods are available. These methods have been summarised by Bock and Dammel [171]. SIFT reaction kinetics are most easily measured using a pure neutral

reactant. A synthetic route to pure CH_2NH has been developed but was unfortunately too complex for this work [172]. The synthesis was likely to be impractical anyway as methylenimine is a transient species which readily polymerises at temperatures greater than -80 °C [172]. Once a sample is collected at a temperature less than -80 °C, warming that sample to room temperature for reaction would probably result in rapid polymerisation.

Of the remaining production methods the thermal decomposition (pyrolysis) of an organic precursor was the most easily incorporated with the SIFT. Methyl*amine* (CH_3NH_2) was chosen as the most suitable precursor from which methyl*enimine* (CH_2NH) can be obtained by pyrolysis. Methylamine is readily available and H_2 is the main by-product of the pyrolysis. This is fortunate as pyrolysis methods usually produce by-products which can interfere with the ion chemistry in the flow tube. H_2 is unreactive with many ions and did not interfere with the chemistry examined.

Methylenimine (CH_2NH) was first produced from the pyrolysis of methylamine (CH_3NH_2) by Johnson and Lovas who flowed CH_3NH_2 through a 4 mm i.d. (internal diameter) quartz tubing with a 20 mm section heated to very near the melting point of quartz (~1600 ºC) [158]. The imine product was detected by microwave spectroscopy. These authors, and several others since, have noted the concurrent formation of HCN and NH_3 at lower concentrations than CH_2NH [157-159, 173]. Bock and Dammel found that the onset of HCN formation occurred at 1300 ºC [173].

For the present work a pyrolysis tube was constructed from a 150 mm section of 10 mm i.d. quartz tube. The heating element consisted of 27 gauge nichrome wire wound into a tight coil around the exterior of the quartz. Thin strands of fibreglass were initially placed between the wire and the quartz tube to prevent the heating coil from slipping when the tube was cooled from high temperatures. During the first experiments the fibreglass strands melted, binding the wire to the quartz. Contraction of the immobilised wire during cooling caused the quartz tube to break. To avoid future breakages the fibreglass strands were not included in the next pyrolysis tube. The tightly wound coil did not appear to slip or to deform during further experiments without the fibreglass strands. The tube was tightly swathed in fibreglass wool to insulate the heating element in all experiments.

The temperature of the tube was measured **externally** with a 'Type K' (chromel/alumel) thermocouple in conjunction with a Fluke digital thermometer. The maximum temperature reached by electrical heating of the element was 1425 ºC.

As data available on the lifetime of the transient CH_2NH is unreliable [150, 158], positioning the production region as close to the reaction zone was desirable. The pyrolysis tube was thus inserted into the glass section of the neutral inlet line between the Varian leak valve and the main SIFT flow tube (described in Section 2.2.5 of this thesis). This positioning means that the pyrolysis occurs less than 250 mm from the flow tube.

5.2.1 The Generation of Methylenimine

Methylenimine was produced by passing a dilute (1%) mixture of methylamine in helium through the pyrolysis tube at temperatures between 1380 and 1420 °C. The precursor gas was diluted in helium to enhance the efficiency of the heating. The pressure inside the pyrolysis tube was not measured directly but was estimated to be between 0.5 and 2 Torr.

The proton affinity of CH_2NH (852.9 kJ mol^{-1} [148]) is considerably larger than that of water (691 kJ mol^{-1} [174]) making H_3O^+ an ideal monitor ion for this species. A small flow of the methylamine/helium mixture was passed through the pyrolysis tube into the flow tube and the products of the pyrolysis monitored with H_3O^+. The onset of methylenimine formation was observed at around 1000°C by the appearance of an ion at m/z 30 corresponding to protonated methylenimine, $CH_2NH_2^+$. Below 1000°C protonated methylamine ($CH_3NH_3^+$) at m/z 32 was the only product ion observed. The identification of methylenimine was confirmed by the observation of a product ion at m/z 29, corresponding to CH_2NH^+ when O_2^+ was used as the reactant ion. Raising the temperature further increased the size of the methylenimine signal at m/z 30 (from H_3O^+) relative to the methylamine signal at m/z 32 and at the limit of the apparatus' capability (around 1400°C) the quantity of methylenimine produced was still increasing.

HCN and NH_3 were also produced by the pyrolysis. The low proton affinity of HCN (713 kJ mol^{-1} [174]) relative to the reagent ions studied meant that it did not interfere with measurements. On the other hand, NH_3 has a high proton affinity (854 kJ mol^{-1} [174]). Very small quantities of protonated ammonia were observed in all of the experiments but did not significantly interfere with the reactions observed.

Because the pyrolysis of CH_3NH_2 occurs downstream from the leak valve in the neutral inlet system, the flow of CH_2NH to the reaction region could not be measured directly. It was hoped that an estimate of the CH_2NH flow could be made based on the CH_3NH_2 flow. However, this was complicated because only partial decomposition of methylamine was possible and the observed production of methylenimine did not increase linearly with CH_3NH_2 flow. By assuming that the reaction of CH_2NH with H_3O^+ proceeded at the collision rate, the maximum degree of decomposition of amine to imine was estimated to be 15 ± 3 %. Methylamine was thus always present in the flow tube along with methylenimine. For this reason the reactivity of methylamine was measured separately so that the chemistry of the two neutrals could be distinguished.

Having established the reactivity of pure methylamine the quartz tube was heated to 1400 °C and the chemistry of methylenimine examined. For each reagent ion all precursor and product ion count rates were measured at a variety of flow rates. Initial experiments showed that whilst the CH_3NH_2 reaction products increased linearly with flow the reaction products for CH_2NH did not, initially increasing with flow, then becoming constant. If the flow of CH_2NH had increased linearly i.e. if the degree of decomposition remained constant as the flow rate was increased, absolute rate coefficients for methylenimine could have been calculated by comparing the ratio of product peak heights with the various reactants to those for methylamine (CH_3NH_2). Although absolute rate coefficients could not be determined, relative rates could be estimated.

The ions examined were produced from the following neutral reagents: H_3O^+ from H_2O; $C_2H_5^+$ from methane; $C_3H_3^+$ from allene, $C_3H_5^+$ from C_2H_4; $HCNH^+$ from HCN; CH_3CNH^+ from CH_3CN; $C_2H_3CNH^+$ from C_2H_3CN; HC_3NH^+ from HC_3N; $C_5H_5^+$ and $C_7H_7^+$ from cycloheptatriene and $C_4H_3^+$ from C_4H_2. All of these reagents were obtained from commercial sources and purified by multiple freeze-pump-thaw cycles. Exceptions to this were HCN, HC_3N and C_4H_2 which were synthesized in the laboratory by standard methods outlined in Chapter 4 (Cyanodiacetylene - HC_5N).

No attempt was made to determine the nature of the reagent ions produced where the formation of isomers was possible. Previous experience using these methods of ion generation would suggest that a mixture of $C_5H_5^+$ and $C_7H_7^+$ isomers were produced from

cycloheptatriene, that a mixture of linear and cyclic $C_3H_3^+$ was generated from allene and that the lowest energy allyl form of $C_3H_5^+$ was produced from ethene.

Propionitrile (99%) was obtained from Aldrich and further purified by vacuum distillation. A dilute mixture (1%) of propionitrile in helium was admitted to the flow tube (without the need for the heated section) for this work and kinetics measured in the usual way.

5.3 Results

The reactivity of methylamine with each of the ions investigated in this study was measured separately; so that it could be separated from the chemistry of methylenimine when both were present. The results for methylamine are summarized in Table 5.1. A summary of the chemistry observed for methylenimine is given in Table 5.2. The collision rate calculations were made using the parameterized theory of Su and Chesnavich [59] using a dipole moment of 1.97 Debye [157] and a polarisability of 3.20 x 10^{-24} cm^3 [175]. All of the reactions were estimated to proceed at their respective collision rates except for $C_5H_5^+$ and $C_7H_7^+$.

Table 5.1. *The reactivity of methylamine, CH_3NH_2, with selected ions.*

Reagent Ion	Neutral	Products[a]	Branching Ratio	k_o[b]	k_c[c]	k_{lit}	$-\Delta H_r$[d]
H_3O^+	CH_3NH_2	$CH_3NH_3^+ + H_2O$	1.00	2.1	2.4		199
$C_2H_5^+$	CH_3NH_2	$CH_3NH_3^+ + C_2H_4$	0.80	1.9	2.1	1.8[e]	216
		$CH_3NH_2.C_2H_5^+$	0.20				
$C_3H_5^+$	CH_3NH_2	$CH_3NH_3^+ + C_3H_4$	0.40	1.9	1.9		121
		$CH_2NH_2^+ + C_3H_4 + H_2$	0.25				158
		$CH_3NH_2.C_3H_5^+$	0.35				
$HCNH^+$	CH_3NH_2	$CH_3NH_3^+ + HCN$	1.00	2.0	2.10	~1.0[f]	178
CH_3CNH^+	CH_3NH_2	$CH_3NH_3^+ + CH_3CN$	1.00	1.8	1.9		109
$C_2H_3CNH^+$	CH_3NH_2	$CH_3NH_3^+ + C_2H_3CN$	1.00	1.7	1.8		102
HC_3NH^+	CH_3NH_2	$CH_3NH_3^+ + HC_3N$	1.00	1.6	1.8		143
O_2^+	CH_3NH_2	$CH_3NH_2^+ + O_2$	0.65	1.9	2	~1.0[g]	531
		$CH_2NH_2^+ + O_2 + H$	0.35				179
$C_5H_5^+$	CH_3NH_2	$CH_3NH_3^+ + C_5H_4$	0.80	0.25	1.8		-7
		$CH_2NH_2^+ + C_5H_4 + H_2$	0.10				26
		$CH_3NH_2.C_5H_5^+$	0.10				
$C_7H_7^+$	CH_3NH_3	$CH_3NH_3^+ + C_7H_6$	0.90	0.018	1.6		
		$CH_3NH_2.C_7H_7^+$	0.10				
$C_4H_3^+$	CH_3NH_2	$CH_3NH_3^+ + C_4H_2$	0.65	2.0	1.8		143
		$CH_2NH_2^+ + C_4H_2 + H_2$	0.25				9
		$CH_3NH_2.C_4H_3^+$	0.10				

a. Neutral reaction products were not identified. See text.

b. Observed rate coefficient in units of 10^{-9} cm^3 s^{-1}.

c. Collision rates calculated with variational transition state theory of Su and Chesnavich [59]. Units are 10^{-9} cm^3 s^{-1}.

d. Reaction enthalpy in kJ mol^{-1}

e. Reference [176].

f. Reference [177].

g. Reference [178, 179].

Table 5.2. *The reactivity of methylenimine, CH_2NH, with selected ions.*

Reagent Ion	Neutral	Products[a]	Branching Ratio	k_o[b]	k_c[c]	$-\Delta H_r$[d]
H_3O^+	CH_2NH	$CH_2NH_2^+ + H_2O$	1.00	~3.0	3.0	223
$C_2H_5^+$	CH_2NH	$CH_2NH_2^+ + C_2H_4$	0.95	~2.7	2.7	240
		$CH_2NH.C_2H_5^+$	0.05			
$C_3H_5^+$	CH_2NH	$CH_2NH_2^+ + C_3H_4$	0.70	~2.5	2.5	145
		$CH_2NH.C_3H_5^+$	0.30			
$HCNH^+$	CH_2NH	$CH_2NH_2^+ + HCN$	1.00	~2.7	2.7	202
CH_3CNH^+	CH_2NH	$CH_2NH_2^+ + CH_3CN$	1.00	~2.5	2.5	133
$C_2H_3CNH^+$	CH_2NH	$CH_2NH_2^+ + C_2H_3CN$	1.00	~2.4	2.4	126
HC_3NH^+	CH_2NH	$CH_2NH_2^+ + HC_3N$	1.00	~2.4	2.4	167
O_2^+	CH_2NH	$CH_2NH^+ + O_2$	1.00	~2.6	2.6	555
$C_5H_5^+$	CH_2NH	$CH_2NH_2^+ + C_5H_4$	1.00	~0.32	2.3	17
$C_7H_7^+$	CH_2NH	$CH_2NH_2^+ + C_7H_6$	1.00	~0.034	2.2	
$C_4H_3^+$	CH_2NH	$CH_2NH_2^+ + C_4H_2$	0.80	~2.4	2.4	167
		$CH_2NH.C_4H_3^+$	0.20			

a. Neutral reaction products were not identified. See text.

b. Observed rate coefficient in units of 10^{-9} cm^3 s^{-1}.

c. Collision rates calculated with variational transition state theory of Su and Chesnavich [59]. Units are 10^{-9} cm^3 s^{-1}.

d. Reaction enthalpy in kJ mol^{-1}. Calculated using ΔH_f° $CH_2NH_2^+$ = 751 kJ mol^{-1} [162].

For the propionitrile experiments the pyrolysis reactor was removed from the neutral inlet line. The results of this investigation are given in Table 5.3.

Table 5.3. *The reactivity of propionitrile, C_2H_5CN, with selected ions.*

Reagent Ion	Neutral	Products[a]	Branching Ratio	k_{obs}[b]	k_c[c]	k_{lit}	$-\Delta H_r$[d]
N^+	C_2H_5CN	$N_2^+ + C_3H_5$	0.55	4.2	4.5		262
		$C_3H_3^+ + N_2 + H_2$	0.20				748
		$C_2H_4CN^+ + NH$	0.25				630
N_2^+	C_2H_5CN	$C_2H_4CN^+ + N_2 + H$	0.65	3.4	5.8		416
		$CH_3^+ + CH_2CN + N_2$	0.20				216
		$C_2H_2^+ + CH_2NH + N_2$	0.15				92
$HCNH^+$	C_2H_5CN	$C_2H_5CNH^+ + HCN$	1.00	4.2	4.5		88
CH_3CNH^+	C_2H_5CN	$C_2H_5CNH^+ + CH_3CN$	0.95	4.3	4.0		20
		$C_2H_5CN.CH_3CNH^+$	0.05				
H_3O^+	C_2H_5CN	$C_2H_5CNH^+ + H_2O$	1.00	4.6	5.2		110
$C_2H_2^+$	C_2H_5CN	$C_3H_5^+ + CH_2CN$	> 0.95	4.2	4.6	~2.2[e]	189
		$C_2H_5CNH^+ + C_2H$	< 0.05				39
$C_2H_4^+$	C_2H_5CN	$C_2H_5CNH^+ + C_2H_3$	1.00	4.5	4.5	1.8[e]	77
$C_2H_5^+$	C_2H_5CN	$C_2H_5CNH^+ + C_2H_4$	0.95	4.3	4.5		126
		$C_2H_5CN.C_2H_5^+$	0.05				
$C_3H_3^+$	C_2H_5CN	$C_2H_5CN.C_3H_3^+$	1.00	~0.3	4.0		
$C_3H_4^+$	C_2H_5CN	$C_2H_5CNH^+ + C_3H_3$	0.95	3.9	4.0		120
		$C_2H_5CN.C_3H_4^+$	0.05				
$C_3H_5^+$	C_2H_5CN	$C_2H_5CNH^+ + C_3H_4$	0.65	4.1	4.0		59
		$C_2H_5CN.C_3H_5^+$	0.35				
$C_4H_2^+$	C_2H_5CN	$C_2H_5CN.C_4H_2^+$	1.00	3.6	3.8		

a. Neutral reaction products were not identified. See text.

b. Observed rate coefficient in units of 10^{-9} cm^3 s^{-1}.

c. Collision rates calculated with variational transition state theory of Su and Chesnavich [59]. Units are 10^{-9} cm^3 s^{-1}.

d. Reaction enthalpy in kJ mol^{-1}.

e. Reference [169].

It should be noted that none of the neutral products of the reactions summarised in Tables 5.1, 5.2 and 5.3 were observed directly. The neutral products listed are based on previously observed ion chemistry, thermochemistry and also ‘chemical commonsense’. The reaction enthalpies given in the last column of each table are for the most likely products.

5.4 Discussion

5.4.1 Methylamine

Of the reactant ions in Tables 5.1 and 5.2, only O_2^+ does not have a transferable proton. The proton affinity of methylamine (899 kJ mol^{-1} [174]) is very high and it is therefore of little surprise that proton transfer reactions dominate the chemistry in Table 5.1. Proton transfer reactions are known to proceed at the collision rate when exothermic and this is what is observed [142]. $C_5H_5^+$ and $C_7H_7^+$ reacted at considerably less than the collision rate with methylamine which is indicative of endoergic proton transfer. The reaction enthalpy for proton transfer from $C_5H_5^+$ to methylamine was slightly endothermic based on the presumed structure of the neutral reaction product (the lowest energy isomer listed in reference [180]). The structure of the $C_7H_7^+$ ion formed from cycloheptatriene is unknown hence the reaction enthalpy could not be calculated.

Proton transfer was the only reaction observed for the nitrile ions. The hydrocarbon ions $C_2H_5^+$, $C_3H_5^+$, $C_5H_5^+$, $C_7H_7^+$ and $C_4H_3^+$, exhibited termolecular association in competition with proton transfer with $C_3H_5^+$, $C_5H_5^+$ and $C_4H_3^+$, having an additional channel leading to $CH_2NH_2^+$. The formation of $CH_2NH_2^+$ from methylamine complicates the identification of methylenimine as $CH_2NH_2^+$ is the proton transfer product of CH_2NH.

5.4.2 Methylenimine

The proton affinity of methylenimine (852.9 kJ mol^{-1}) is close to methylamine and this similarity is illustrated in the observed chemistry which is nearly equivalent to that of methylamine. The products of the methylenimine reactions were easily identified, as they were identical to those for methylamine except for being two m/z units lower in the mass spectra.

The identification of products with $C_3H_5^+$, $C_5H_5^+$ and $C_4H_3^+$ was complicated by the fact that the key CH_2NH proton transfer product ion ($CH_2NH_2^+$) ion was also a product of the reaction of CH_3NH_2 with these ions. The large excess of amine ensured that the $CH_2NH_2^+$ derived from methylenimine was not easily distinguished from the methylamine generated $CH_2NH_2^+$. By assuming that both reactions proceeded at the collision rate and that 15% of the methylamine had decomposed to methylenimine (see Section 5.2.1); the chemistry was modelled iteratively to give the best match with the

observed data at a series of neutral flow rates. This was moderately successful however the product branching ratios for methylenimine reacting with these three ions are considered to have a greater uncertainty than for the other ions at ± 50%.

As with methylamine, the nitrile-based reactant ions transferred a proton to methylenimine at the collision rate and no other reaction channels were observed.

5.4.3 The Estimation of Relative Rates for Methylenimine

The rate coefficients for the methylenimine reactions could not be measured directly because increasing the flow of methylamine did not lead to a linear increase in the flow of methylenimine into the flow tube. It was possible to estimate the rate coefficients for the majority of the ions based on the following logic.

During the experiments the methylenimine products were always observable despite the large excess of methylamine. Because methylamine reacted at the collision rate with all but two of the ions it was assumed that the reactions of methylenimine would also proceed at the collision rate. This assumption is warranted as most were proton transfer reactions which are known to be fast when exothermic [142].

The degree of decomposition of CH_3NH_2 to CH_2NH was estimated using the data collected for each reagent ion and calculations were performed to give the best fit with the data at **low** flows of neutral (where the degree of decomposition was observed to be independent of flow rate). The calculations consistently showed that 15 ± 3% of the CH_3NH_2 flow was pyrolysed to give CH_2NH. The assumption that the CH_2NH reactions would proceed at the collision rate appears valid given that all of the mass spectra collected were similar to that recorded with $HCNH^+$, as shown in Figure 5.2. Figure 5.3 is included for comparison and shows a mass spectrum obtained for the reaction of pure methylamine with $HCNH^+$.

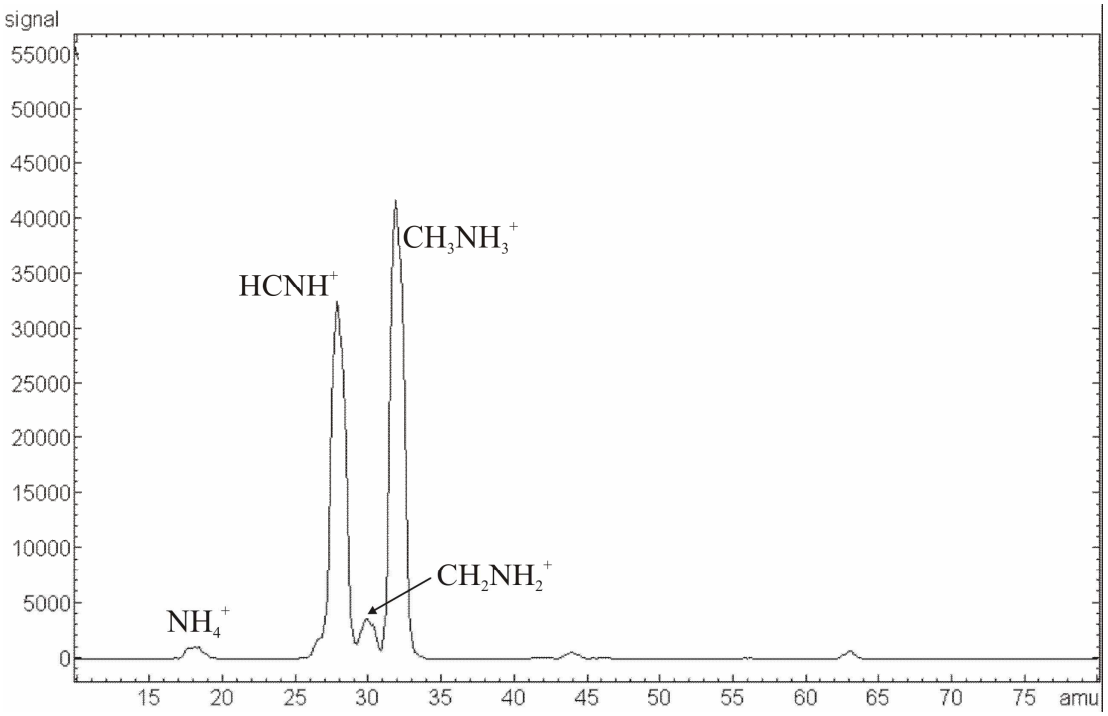

Figure 5.2. *Mass spectrum illustrating the reaction of methylenimine (in the presence of methylamine) with $HCNH^+$. The $CH_2NH_2^+$ peak is small by comparison with the $CH_3NH_3^+$ peak because only a fraction of the methylamine is decomposed to methylenimine. Note also the small NH_4^+ peak at m/z 18 which was observed in all of the methylenimine experiments.*

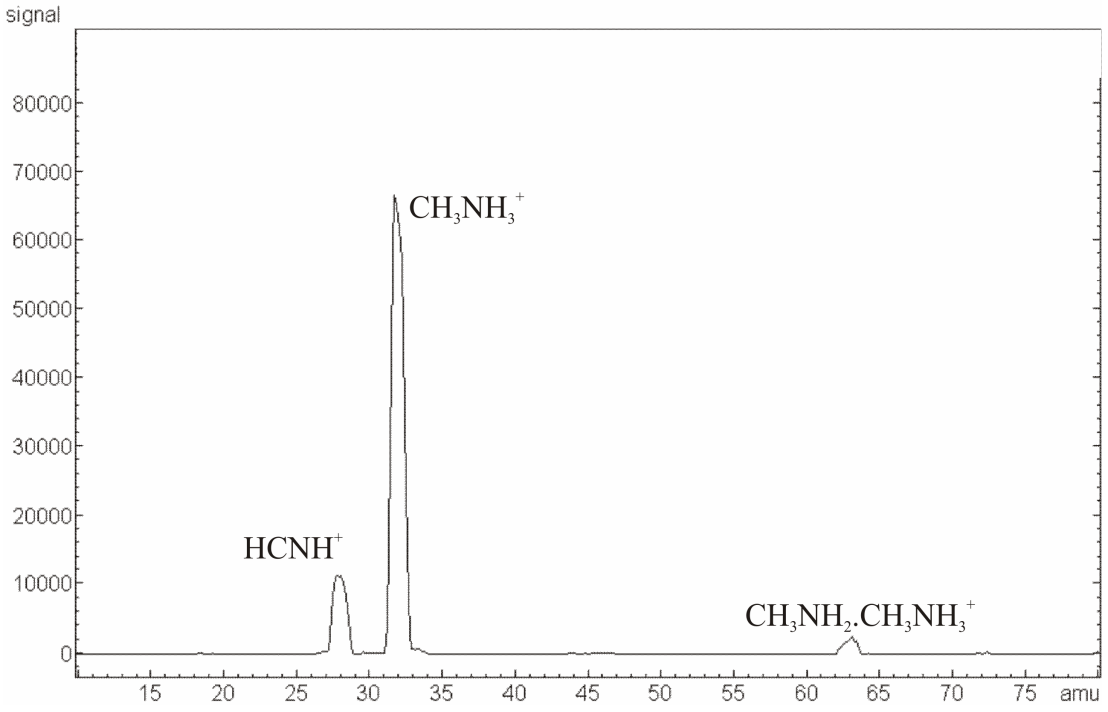

Figure 5.3. *Mass spectrum illustrating the reaction of pure methylamine with $HCNH^+$.*

If the methylenimine reaction rates were slower, say 20% of the collision rate, 70% methylamine decomposition would be needed to match the data. If the level of dissociation was this high the methylamine product ion signals would decrease considerably above 1000 °C as most of the methylamine decomposed to methylenimine. This is entirely inconsistent with the results. The methylamine product ion signals were always much greater than the methylenimine product signals and did not decrease drastically as the temperature was increased from room temperature to 1400 °C. From this observation it was concluded that methylenimine reacted at approximately the collision rate with each of the ions as listed in the fifth column of Table 5.2.

$C_5H_5^+$ and $C_7H_7^+$ did not react at the collision rate with methylamine. For methylenimine their rate of reaction was qualitatively the same as methylamine, based on the relative intensities of the respective product ions. The rate of reaction for these ions with methylenimine was therefore estimated from the ratio of the calculated collision rates and the measured methylamine reaction rate using the simple expression below.

$$\frac{k_c(CH_2NH)}{k_c(CH_3NH_2)} \times k_{meas}(CH_3NH_2) = k_{est}(CH_2NH) \qquad \textbf{(5.6)}$$

5.4.4 Propionitrile

With the exception of $C_3H_3^+$, propionitrile reacted at the calculated collision rate with each of the ions listed in the first column of Table 5.3. $C_3H_3^+$ reacted with propionitrile at less than one tenth of the collision rate to form the adduct $C_2H_5CN.C_3H_3^+$. This product is presumably formed from a reaction with the linear $C_3H_3^+$ isomer as the cyclic isomer is known to be quite unreactive [143].

Propionitrile has a proton affinity of 794.1 kJ mol^{-1} [174] and reacted by proton transfer with ions for which the reaction was exothermic: H_3O^+, $C_2H_4^+$, $C_2H_5^+$, $C_3H_4^+$, $C_3H_5^+$, $HCNH^+$ and CH_3CNH^+. Although proton transfer was exothermic for $C_2H_2^+$ the dominant reaction pathway generated the highly stable $C_3H_5^+$ ion rather than $C_2H_5CNH^+$. $C_2H_5^+$, $C_3H_4^+$, $C_3H_5^+$ and CH_3CNH^+ also exhibited varying degrees of adduct formation in competition with proton transfer channels. An adduct ion was the sole product for both $C_3H_3^+$ and $C_4H_2^+$.

A more diverse chemistry was exhibited with the N^+ and N_2^+ ions. Multiple product ions were created from their rapid reactions with C_2H_5CN. Both ions exhibit a

hydride abstraction/transfer channel creating $C_2H_4CN^+$ and this was the major product channel for N_2^+. The remaining reaction channels for N^+ (**(5.4a)** and **(5.4b)**) appear to break the highly stable CN triple bond in propionitrile. This seemingly unfavourable pathway is presumably made possible by the formation of a nitrogen molecule with its associated thermodynamic stability. The highly stable $C_3H_3^+$ ion produced by reaction **(5.4b)** would also make such a transformation favourable.

$$N^+ + C_2H_5CN \rightarrow N_2^+ + C_3H_5 \qquad 0.55 \textbf{ (5.4a)}$$

$$\rightarrow C_3H_3^+ + N_2 + H_2 \qquad 0.20 \textbf{ (5.4b)}$$

This type of reaction where a CN bond is broken in favour of N_2 formation has been observed elsewhere in this thesis (see Chapter 4, Section 4.4.1).

It must be stressed that the neutral products were not directly identified in any of these reactions and the exothermicities listed for the reactions in all three tables of results are based on the presumed identity of the neutral fragments.

5.5 Conclusions

The data obtained by the INMS aboard the *Cassini* spacecraft has recently been published [51, 127]. This data indicated that more nitrogen-containing ions were present in Titan's upper atmosphere than previously thought [51, 127]. Two of the more abundant ions observed that were not predicted to be significant by models of Titan's ionosphere, m/z 30 and 56, have been proposed to be derived from the neutral species methylenimine (CH_2NH) and propionitrile (C_2H_5CN) [127]. A detailed investigation of the ion chemistry of these neutrals has been performed for the first time. The relatively high proton affinities of methylenimine and propionitrile ensure that their chemistry in this environment is governed by proton transfer reactions. Protonated methylenimine ($CH_2NH_2^+$, m/z 30) and protonated propionitrile ($C_2H_5CNH^+$, m/z 56) are the principal products of most of the reactions. In some cases association products were observed in competition with the proton transfer channels as a result of collisional stabilization. These channels would not be expected to occur at the pressures encountered in the upper atmosphere of Titan.

Provided $CH_2NH_2^+$ and $C_2H_5CNH^+$ react only slowly with the most abundant neutral species in Titan's atmosphere, they may be considered a viable source of the ion

density at m/z 30 and m/z 56 in the *Cassini* INMS data. An investigation of the chemistry of $CH_2NH_2^+$ and $C_2H_5CNH^+$ with the neutral components of Titan's atmosphere would complement the results reported here.

CHAPTER 6.

MINOR PROJECTS

6.1 $C_3H_3^+$

$C_3H_3^+$ is a highly stable and somewhat interesting ion. It has been attributed as having a key role in soot formation within the field of flame chemistry [181] and it is also an omnipresent fragment ion in mass spectra of hydrocarbons. This ion is also widespread in the interstellar medium and is presumed to be the precursor to several neutral molecules including cyclopropenylidene, C_3H_2, the first cyclic molecule to be discovered in interstellar clouds [182]. The pervasive nature of this ion in a broad range of environments has prompted many investigations of its ion chemistry [143, 167, 181-183].

It has been established that two low-energy $C_3H_3^+$ isomers exist and that their reactivities are often quite distinct [143]. The acyclic propargyl ion ($HCCCH_2^+$) has an enthalpy of formation of 1179 kJ mol^{-1} [184] and is the more reactive isomer. The isomeric cyclic ion (c-$C_3H_3^+$) is more stable, having a lower enthalpy of formation of 1075 kJ mol^{-1} [184], and is quite unreactive. There is a considerable energy barrier to interconversion of the two $C_3H_3^+$ isomers [143].

As well as being a common interstellar ion, $C_3H_3^+$ is expected to be present in the atmosphere of Titan, formed *in situ* via a series of ion-molecule reactions between small hydrocarbon ions and neutrals [45]. Current models of Titan's atmosphere cannot account for the different participation by the isomeric forms because the ratio of each isomer (formed by ion-molecule reactions) is unknown. In this work the contrasting reactivities of the isomers with C_2H_2 under the high pressure conditions of the SIFT have been used to establish the ratio of linear $C_3H_3^+$ to cyclic $C_3H_3^+$ produced in four ion-molecule reactions which occur in Titan's ionosphere.

6.1.1 Experimental

Because the isomers react at different rates with neutral species in Titan's atmosphere it is important that the percentage each isomer contributes to the total $C_3H_3^+$ ion density is established. The four ion-molecule reactions which are known to produce $C_3H_3^+$ in Titan's atmosphere are summarised in Table 6.1.

Table 6.1. *Ion-molecule reactions occurring in the atmosphere of Titan of which $C_3H_3^+$ is a product.*

					Reaction Enthalpy[b]	
Reactant Ion	**Neutral**	**Products**	**Branching**	**k_{meas}[a]**	**$-\Delta H^\circ_r(HCCCH_2^+)$**	**$-\Delta H^\circ_r(c\text{-}C_3H_3^+)$**
CH_3^+	C_2H_2	$C_3H_3^+ + H_2$	1.00[c]	1.15[c]	142	246
$C_2H_2^+$	C_2H_4	$C_3H_3^+ + CH_3$	0.48[c]	1.38[c]	55	159
		$C_4H_5^+ + H$	0.23			
		$C_2H_4^+ + C_2H_2$	0.30			
CH_3^+	C_2H_4	$C_2H_3^+ + CH_4$	~0.46[c]	1.06[c]		
		$C_3H_5^+ + H_2$	~0.51			
		$C_3H_3^+ + 2H_2$	0.04		-34	71
$C_2H_5^+$	C_2H_2	$C_4H_7^+$	0.94[d]	1.30[d]		
		$C_3H_3^+ + CH_4$	0.04		26	130
		$C_4H_5^+ + H_2$	0.02			

a. Observed rate coefficient in units of 10^{-9} cm^3 s^{-1}.

b. Reaction enthalpy in kJ mol^{-1} [184].

c. Reference [67].

d. This work, see Section 6.1.2.

The reactivity of $C_3H_3^+$ with some neutral molecules is reported in Chapters 4 and 5 of this thesis. In those chapters, $C_3H_3^+$ ions were generated in the flowing afterglow from allene (CH_2CCH_2). Propyne (CH_3CCH) could also have been used. Neither precursor gas produces a flow of a single $C_3H_3^+$ isomer, so a mixture of linear and cyclic $C_3H_3^+$ is always present. Identifying the proportion each isomer contributes to the total ion signal is straightforward. At the pressure encountered in the SIFT flow tube, C_2H_2

associates rapidly with linear $C_3H_3^+$ to form $C_5H_5^+$ (M = He in the reactions below) whereas the cyclic isomer is essentially unreactive [143].

$$HCCCH_2^+ + C_2H_2 \xrightarrow{M} C_5H_5^+ \qquad k = 1.2 \times 10^{-9}\ cm^3\ s^{-1} \quad \textbf{(6.1)}\ [143]$$

$$c\text{-}C_3H_3^+ + C_2H_2 \xrightarrow{M} \text{No Reaction} \qquad k < 5 \times 10^{-12}\ cm^3\ s^{-1} \quad \textbf{(6.2)}\ [143]$$

It is therefore easy to differentiate the isomers simply by reacting the $C_3H_3^+$ with C_2H_2. This method was utilised here to determine the isomeric ratio of $C_3H_3^+$ formed from the reactions in Table 6.1.

The ions examined were produced from the following neutral reagents: CH_3^+ and $C_2H_5^+$ from methane and $C_2H_2^+$ from C_2H_2). These reagents were obtained from commercial sources and purified by multiple freeze-pump-thaw cycles. The reactant ions were generated in the flowing afterglow and injected into the SIFT flow tube as usual. The neutral reactant (column 2 in Table 6.1) was added through the upstream neutral inlet (78.4 cm upstream of the downstream ion sampling orifice) in sufficient quantity to complete the $C_3H_3^+$ forming reaction. C_2H_2 was then added to the reaction mixture at the second neutral inlet (50.4 cm upstream of the ion sampling orifice) and the reactivity of the $C_3H_3^+$ produced upstream was examined.

For two of the reactions, C_2H_2 was also a reactant. For these reactions it was necessary to add sufficient C_2H_2 at the first neutral inlet to completely deplete the reactant ion signal. This prevented the formation of $C_3H_3^+$ at the second neutral inlet where C_2H_2 was also added, which would have affected the results. Because high flows of C_2H_2 were used at the upstream inlet secondary reactions were observed. For the first reaction listed in Table 6.1, much of the linear $C_3H_3^+$ formed upstream reacted with the excess C_2H_2 to form $C_5H_5^+$ before the second neutral inlet. This chemistry did not inhibit the estimation of the quantity of each isomer formed in this reaction.

6.1.2 Results and Discussion

The first reaction in Table 6.1 has only $C_3H_3^+$ as its product. The $C_3H_3^+$ thus produced reacted with C_2H_2 to generate a large $C_5H_5^+$ ion signal, indicating the linear $HCCCH_2^+$ isomer to be the dominant product of the reaction. Based on the extent of the $C_5H_5^+$ formation at high downstream flows of C_2H_2, it was estimated that greater than 75% of the $C_3H_3^+$ was the linear isomer. This agrees well with the results of an earlier

study in which it was estimated that 85% of the $C_3H_3^+$ was the linear propargyl form [143].

The second reaction, between $C_2H_2^+$ and C_2H_4, generates more than one product ion. The mass spectrum became cluttered with ion peaks when C_2H_2 was added at the second neutral inlet downstream. This did not disrupt the examination of the $C_3H_3^+$ signal and it was quite clear that the $C_3H_3^+$ produced in this reaction was not reactive and greater than 90% was estimated to be cyclic.

The next reaction provided a good test for the methodology. The formation of the reactive $HCCCH_2^+$ isomer is endothermic by 34 kJ mol^{-1} and none of this species should have been evident. This is precisely what was observed with the $C_3H_3^+$ produced being completely unreactive with C_2H_2.

In the absence of a reliable literature value for the branching ratio of the final reaction examined, between $C_2H_5^+$ and C_2H_2, kinetics for the reaction were measured in addition to the isomeric branching ratio. The results indicated $C_3H_3^+$ to be a very minor product (4%). The $C_3H_3^+$ ion signal generated was insufficient for an estimate of the isomer ratios to be made by further reaction with C_2H_2.

6.1.3 Summary

$C_3H_3^+$ is a product of four of the ion-molecule reactions which occur in the atmosphere of Titan. The isomers of $C_3H_3^+$ exhibit contrasting reactivity but this has not been accounted for in models of Titan's atmosphere. This oversight can now be remedied for three of the four reactions for which the ratio of the two isomers has now been estimated. The ratio could not be determined for the fourth reaction because insufficient $C_3H_3^+$ was produced for its reactivity to be examined. Because $C_3H_3^+$ was only a minor product of the fourth reaction this should not introduce a significant error to models.

6.2 Proton Affinities

6.2.1 Introduction

A common theme in the ion-molecule reactions examined in this thesis is the proton transfer (PT) reaction which may be described by the generic equilibrium **(6.3)**.

$$AH^+ + B \leftrightarrow BH^+ + A \qquad \textbf{(6.3)}$$

The degree to which this reaction proceeds in the forward or reverse direction is determined by the relative proton affinities of the neutrals A and B - the neutral with the higher proton affinity being more likely to accept the proton. The proton affinity (PA) of a neutral is defined as the negative of the reaction enthalpy change for the standard gas phase association reaction between a neutral (A) and a proton:

$$A_{(g)} + H^+_{(g)} \rightarrow AH^+_{(g)} \qquad \textbf{(6.4)}$$

$$PA = \Delta H°_f(A_{(g)}) + \Delta H°_f(H^+_{(g)}) - \Delta H°_f(AH^+_{(g)}) \qquad \textbf{(6.5)}$$

Another commonly utilised thermodynamic value, the gas phase basicity (GB) of a neutral, is defined as the negative of the Gibbs free energy change for reaction **(6.4)**. Proton affinities and gas phase basicities are linked by the standard relation:

$$\Delta G_T = \Delta H_T - T\Delta S \qquad \textbf{(6.6)}$$

PAs typically range from 500 to 900 kJ mol^{-1} for simple organic molecules [148].

If each of the formation enthalpies in equation **(6.5)** are known then an absolute value can be obtained for the PA of A. It is common for the enthalpy of formation of AH^+ to be the only unknown quantity. The direct measurement of $\Delta H°_f(AH^+)$ can be made by 'threshold ionization' experiments. The absolute enthalpy of formation can be found from either the ionization energy of AH:

$$AH \rightarrow AH^+ + e^- \qquad \textbf{(6.7)}$$

or from the appearance energy of AH^+ from a larger molecule,

$$ABH \rightarrow AH^+ + B + e^- \qquad \textbf{(6.8)}$$

Absolute values are not solely derived from experimental results and *ab initio* calculations have been shown to give PAs with a high degree of accuracy [148].

Unfortunately the determination of $\Delta H°_f(AH^+)$ from the methods described by **(6.7)** and **(6.8)** (and hence an absolute value for the PA of A) is not possible for many molecules. Instead proton affinity scales (also known as ladders) have been developed from **relative** PAs (which are easily determined from a combination of experimental ΔG values and calculated ΔS values) which are anchored to one or several **absolute** values.

Relative PA scales are derived from GB scales, which are created from the experimental measurement of the equilibrium constant for the gas phase reaction **(6.3)**. The equilibrium constant K is found from the relative abundance of AH^+ and BH^+ under conditions where thermal equilibrium has been reached:

$$K = \frac{BH^+ \cdot P(A)}{AH^+ \cdot P(B)} \qquad \textbf{(6.9)}$$

In equation **(6.9)**, *P(A)* and *P(B)* are the partial pressures of the neutrals A and B. Equilibrium constants like this can be measured with an ICR instrument. Having measured the equilibrium constant the Gibbs free energy for the reaction is easily calculated using $\Delta G_T = -RT \ln K$, which is equivalent to the difference in GB of the two neutrals:

$$\Delta GB_T = GB_T(B) - GB_T(A) \qquad \textbf{(6.10)}$$

The difference in GB from the equilibrium measurement is linked to the difference in PA (standard enthalpy) by the entropy change in the reaction. It is not possible to obtain a value for ΔPA without a reliable estimate for the entropy of protonation. By measuring the equilibrium constant K over a range of temperatures, a van't Hoff plot (ln K against T^{-1}) will provide the entropy and enthalpy changes for the equilibrium from the slope and intercept of a line of best fit through the data.

$$\ln K = \frac{-\Delta H^\circ}{RT} + \frac{\Delta S^\circ}{R} \qquad \textbf{(6.11)}$$

This treatment is possible because the relative protonation enthalpies and entropies can be assumed to be independent of temperature (provided the equilibrium constants were measured between 298 K and 600 K) [148].

For smaller molecules, such as those considered in this thesis, entropy changes are small and to a good approximation ΔGB ≈ ΔPA with the difference between these quantities unlikely to be more than a few kJ mol^{-1}. It is frequently assumed that if a proton transfer reaction is exothermic it will proceed at the collision rate. Because of the approximate equivalence of ΔPAs and ΔGBs this is essentially true, even though it would be more correct to say that an exoergic PT reaction will proceed at the collision rate.

Relative PAs are usually derived from the thermodynamic equilibrium constants measured for a series of proton transfer reactions at one or more temperatures [142, 185]. Practically this means that it is the GBs which are evaluated first and from these values the PAs can be calculated. Equilibrium constants can be obtained by two methods: either from measurement of the equilibrium concentrations of AH^+ and BH^+, which are then put into equation **(6.9)**; or from the ratio of the rate coefficients (measured independently) for

the forward and reverse reactions in **(6.3)** [148, 185]:

$$K = \frac{k_f}{k_r} \qquad \textbf{(6.12)}$$

Equilibrium constants measured by the two different methods are remarkably consistent [142].

The SIFT is ideally suited to the measurement of rate coefficients for the forward and reverse reactions because the chemistry is evaluated under thermal conditions. Reaction rates show consistently high efficiency for exoergic proton transfer reactions with rates decreasing as PT approaches thermoneutrality [142].

By measuring large numbers of relative PAs, comprehensive ladders of PAs (referenced to absolute values) have been formed [184, 186]. The latest values are available on the NIST website for many hundreds of neutral molecules and radicals [174]. Most of the PA values listed are derived from **relative** PAs. The PA of those compounds which have been referenced to many neutrals is better defined and their position in the scale more assured. The accuracy of the scale is improved as the number of compounds to which each neutral is referenced is increased. Continual improvements are made to the NIST database as more equilibrium constants are measured.

The PAs for propyne (CH_3CCH) and acetylene (C_2H_2) are not well defined in the proton affinity scale. For acetylene only one relative PA value exists, derived from its PT equilibrium constant with cyanogen (C_2N_2) [187]. The PA of cyanogen is itself also not tied well to the PA scale. Although the PA of acetylene is not reliably placed, the current GB value (616.7 kJ mol^{-1} [148]), from which the PA is derived, is in very good agreement with a value recently calculated by *ab initio* methods (618 kJ mol^{-1} [188]). Like acetylene, propyne has only one equilibrium constant value from which its position in the PA scale is derived [148]. In this case however the GB value of 723 kJ mol^{-1} [148] differs significantly from the theoretically calculated value (which is usually very reliable) of 705.3 mol^{-1} [188].

The objective of this work was to determine equilibrium constants for PT reactions between propyne and acetylene and appropriate reference compounds by measuring the rate coefficients for the forward and reverse reactions described by **(6.3)**.

The equilibrium constants are used to enhance the precision of the GBs (and hence the relative PAs) for these two compounds.

6.2.2 Experimental

To establish an equilibrium constant from the ratio of rate coefficients (k_f / k_r), for a proton transfer equilibrium **(6.3)**, it is desirable that the GBs (≈ relative PAs) of the target and reference compounds have values close to each other. This ensures that the difference in rate coefficient for the forward and reverse reactions is minimal [142]. As the PAs of reference compounds are similar to the PA being determined, most of the reactions approach thermoneutrality. This means that other reaction channels can become more facile than PT, however this is not usually a problem. The reference compounds should have well established PAs in order to provide a sound benchmark for PA comparison. Unless specified all of the GBs and PAs given in the following are taken from the NIST database [174].

The currently listed PA of acetylene is 641.4 kJ mol^{-1} making methyl chloride (CH_3Cl, PA 647.3 kJ mol^{-1}) a suitable reference compound. The ions created when these species are protonated, $C_2H_3^+$ and CH_3ClH^+, each have only one stable isomeric form, so no problems arise from different ion structures being formed in either the forward or reverse reactions.

For propyne (PA 748 kJ mol^{-1}), methanol (CH_3OH, PA 754.3 kJ mol^{-1}) is a suitable reference compound as the PAs are fairly similar and protonated methanol has only one stable isomer. Kinetics were also measured for propyne with H_2S as it was mistakenly noted that the PA of H_2S was 750 kJ mol^{-1} (close to that of propyne) when in fact the value is 705 kJ mol^{-1}. The results with H_2S were of surprising value and are described later.

Care must be taken in the production of protonated propyne as the $C_3H_5^+$ ion has two isomeric forms. Ideally it would be made from the ionisation and fragmentation of CH_3CClCH_2 in the FA ion source as the $C_3H_5^+$ ion produced would have the desired propenyl ($CH_3CCH_2^+$) structure [189]. A barrier exists to the conversion of the propenyl isomer to the allyl isomer $CH_2CHCH_2^+$ resulting in an isomerically pure ion signal [189]. This precursor species was not available so the propenyl cation was instead produced by proton transfer from H_3O^+ to propyne. According to Bowers *et al.* this generates a

mixture of the two $C_3H_5^+$ isomers with 86% being the desired propenyl form [189]. The error introduced by the presence of some allyl isomer should not greatly affect the equilibrium constant determination [188]. The reactant ions for the reverse reactions ($CH_3OH_2^+$ and H_3S^+) should generate mostly the propenyl cation [189].

Apart from H_3S^+, none of the protonated ions could be generated in the FA and injected directly into the SIFT flow tube. Instead they were produced in the flow tube by reaction of the neutral with a protonated precursor ion. $CH_3CCH_2^+$ and $CH_3OH_2^+$ were generated from the reaction of H_3O^+ with propyne and methanol respectively, whilst $C_2H_3^+$ and CH_3ClH^+ were generated from the reaction of HCO^+ (produced in the FA from H_2CO) with acetylene and methyl chloride respectively. The neutrals were added to either H_3O^+ or HCO^+ at the neutral inlet located 78.4 cm upstream of the ion sampling orifice. The protonated reactant ions thus generated were reacted with the appropriate neutral species which was added through the neutral inlet 50.4 cm upstream of the ion sampling orifice and reaction kinetics measured in the usual way. To prevent HCO^+ or H_3O^+ from reaching the second neutral inlet and generating unwanted reaction products, sufficient neutral was added at the first neutral inlet to saturate the injected ion signals. The high flows used to accomplish this caused some secondary ion clustering. In all of the reactions examined the secondary cluster ions were unreactive and presented no problem to the measurement of kinetics or branching ratios. Measurements were made at a temperature of 298 ± 4 K and a helium pressure of 0.46 Torr.

6.2.3 Results and Discussion

The results of the measurements are summarised below for the six reactions examined.

$C_2H_3^+ + CH_3Cl$	$\rightarrow CH_3ClH^+ + C_2H_2$	$k = 1.4 \times 10^{-9}$ cm^3 s^{-1}	0.95	**(6.13a)**
	$\rightarrow C_2H_3^+.CH_3Cl$		0.05	**(6.13b)**
$CH_3ClH^+ + C_2H_2$	$\rightarrow C_2H_3^+ + CH_3Cl$	$k = 5.9 \times 10^{-10}$ cm^3 s^{-1}	0.50	**(6.14a)**
	$\rightarrow CH_3ClH^+.C_2H_2$		0.50	**(6.14b)**

The product branching ratio for reaction **(6.13)** was derived from the ion signal for the $CH_3{}^{35}ClH^+$ isotopomer only as the $CH_3{}^{37}ClH^+$ ion peak coincided with a secondary ion formed at the upstream neutral inlet. The forward and reverse rate coefficients (for the protonation reactions, derived from the overall rate coefficients and the branching ratios) yield an equilibrium constant K = $k_{(6.13a)}$ / $k_{(6.14a)}$ = 4.5 making ΔG_{298} = -3.7 kJ mol^{-1}. With $GB_{298}(CH_3Cl)$ listed as 621.1 kJ mol^{-1} in the NIST database [174] $GB_{298}(C_2H_2)$ was calculated to be 617.4 kJ mol^{-1}. This value agrees well with the recently calculated $GB_{298}(C_2H_2)$ of 618 kJ mol^{-1} [188] and with the previous equilibrium measurement of 618.7 kJ mol^{-1} [187].

$H_3S^+ + CH_3CCH \rightarrow CH_3CCH_2^+ + H_2S$ $\quad k = 1.7 \times 10^{-9}$ cm^3 s^{-1} $\quad$ 1.00 **(6.15)**

$CH_3CCH_2^+ + H_2S \rightarrow H_3S^+ + CH_3CCH$ $\quad k = 2.3 \times 10^{-10}$ cm^3 s^{-1} $\quad$ 0.40 **(6.16a)**

$\rightarrow CH_3CCH_2^+.H_2S$ $\quad$ 0.60 **(6.16b)**

As was observed for the CH_3Cl/C_2H_2 system, some termolecular association occurred in competition with proton transfer for reaction **(6.16)**. The equilibrium constant from the ratio of the forward and reverse PT reactions was K = $k_{(6.15)}$ / $k_{(6.16a)}$ = 18.5 which gives ΔG_{298} = -7.2 kJ mol^{-1}. From the tabulated $GB_{298}(H_2S)$ (673.8 kJ mol^{-1}) [148], $GB_{298}(CH_3CCH_2)$ = 681.0 kJ mol^{-1}. This is considerably less than the value derived from an appearance potential measurement which put the GB at 723 kJ mol^{-1} [148]. The value reported here does however agree with one previous equilibrium-based measurement of 682.6 kJ mol^{-1} [190].

$CH_3CCH_2^+ + CH_3OH \rightarrow CH_3OH_2^+ + CH_3CCH$ $\quad k = 3.1 \times 10^{-9}$ cm^3 s^{-1} $\quad$ 0.85 **(6.17a)**

$\rightarrow CH_3CCH_2^+.CH_3OH$ $\quad$ 0.15 **(6.17b)**

$CH_3OH_2^+ + CH_3CCH \rightarrow CH_3OH_2^+.CH_3CCH$ $\quad k = 6.1 \times 10^{-10}$ cm^3 s^{-1} $\quad$ **(6.18)**

No proton transfer was evident for the reverse reaction of **(6.17a)** (i.e. reaction **(6.18)**) indicating that the GB of propyne is over 20 kJ mol^{-1} less than the GB of methanol

(724.5 kJ mol^{-1}). This is consistent with the results obtained with H_2S for even though H_2S was initially 'wrongly' chosen as a reference compound for propyne, the results show that the GBs of these species are sufficiently close for the method to work. Very recent [188] high level calculations put the GB of propyne intermediate between the value reported by Hunter and Lias (723 kJ mol^{-1} [148]) and the value presented here, at 705.3 kJ mol^{-1} [188].

6.2.4 Conclusions

These results indicate that the GB of propyne (and hence PA) is poorly defined in the scales of relative gas phase basicity. The currently listed NIST value for $GB_{298}(CH_3CCH_2)$ is over 40 kJ mol^{-1} greater than the equilibrium value determined here of 681.0 kJ mol^{-1}. Clearly it would be useful if more PT equilibrium constants for propyne were to be determined with compounds having GBs covering the range of reported GBs for propyne i.e. 681.0 to 723.0 kJ mol^{-1}. It would also be advantageous if the experimental error created by the formation of some allyl ($CH_2CHCH_2^+$) isomer from the reaction of H_3O^+ with propyne could be eliminated. A simple solution to this would be to generate the propenyl ion from CH_3CBrCH_2 from which the formation of the allyl isomer is thermodynamically disallowed.

The results for acetylene were consistent with previous measurements and *ab initio* calculations and its position in the scale of relative GBs (and PAs) can therefore be treated with some confidence. The accuracy of these values could be improved by further equilibrium constant measurements.

6.3 Miscellaneous Ion-molecule Reactions

6.3.1 Introduction

During analysis of the data recorded by the *Cassini* INMS it became clear that several nitrogen-bearing molecules were present that were not predicted or included in pre-*Cassini* models [51, 191]. The chemistry of three of the neutrals thought to contribute to these discrepancies (methylenimine, propionitrile and cyanodiacetylene) has been reported in Chapters 4 and 5 of this thesis. In addition to the thorough analysis of the chemistry of these neutrals, the need for data on a number of individual ion-molecule reactions of potential significance has become apparent [192]. This section examines a

series of ion-molecule reactions for which laboratory data is needed in order to plug gaps in the existing models of Titan's atmosphere. The chemistry examined does not comprise a systematic study but rather a collection of individual reactions whose chemistry is unknown but whose relevance may have been underestimated in pre-*Cassini* models.

6.3.2 Experimental

No special apparatus or ion preparation schemes were necessary for the reactions examined, making the measurements straightforward. The ions examined were produced from the following neutral reagents: CH_5^+ from CH_4; $C_2H_5^+$ from methane; $C_3H_5^+$ from ethene; $HCNH^+$ from HCN; HC_3NH^+ from HC_3N; CH_3CNH^+ from CH_3CN and $C_2N_2H^+$ from C_2N_2 diluted in H_2. All of these reagents were obtained from commercial sources and purified by multiple freeze-pump-thaw cycles. An exception to this was HC_3N which was synthesized in the laboratory by a standard method outlined in Chapter 4 (HC_5N). No attempt was made to determine the nature of the reagent ions produced where the formation of isomers was possible. Previous experience using these methods of ion generation would suggest that the lowest energy allyl form of $C_3H_5^+$ was produced from ethane.

6.3.3 Results and Discussion

The chemistry detailed in Table 6.2 was examined at the request of Roger Yelle and Veronique Vuitton of the *Cassini-Huygens* mission who identified the reactions as potentially important omissions in models of Titan's atmosphere [192].

As with previous tables of reactions given in this thesis none of the neutral products of the reactions summarised in Table 6.2 were measured directly. The neutral products listed are inferred from previously observed ion chemistry and the thermochemistry. The reaction enthalpies given in the last column of Table 6.2 are for the most likely products.

The most common neutral for which chemistry was examined (in Table 6.2) was ammonia, NH_3. Ammonia has been observed in a laboratory simulation of Titan's atmosphere [193] but was not expected to be a significant atmospheric component [26]. The data provided by the *Cassini* INMS produced evidence which conflicts with this prediction. A large ion signal at m/z 18 was observed and confidently attributed to NH_4^+. Ammonia has a very high PA (853.6 kJ mol^{-1}) and will react by proton transfer with the

important Titanian ions, including the dominant $HCNH^+$ ion, to generate the ammonium ion, NH_4^+.

$$HCNH^+ + NH_3 \rightarrow NH_4^+ + HCN \qquad k = 2.4 \times 10^{-9}\ cm^3\ s^{-1} \qquad \textbf{(6.19)}\ [45]$$

The high PA of NH_3 ensures that its reactivity in Table 6.2 is dominated by collision rate PT reactions. Collision stabilised association competes with PT in the reaction of $C_3H_5^+$ with NH_3 although this is of little consequence to Titan's upper ionosphere where only bimolecular reactions are possible.

Table 6.2. *The reactivity of selected hydrocarbon and nitrile species with ions important to the chemistry of Titan.*

Reactant Ion	Neutral	Products	Branching	k_{obs} [a]	k_c [b]	$-\Delta H_r$ [c]
CH_5^+	C_4H_2	$C_4H_3^+ + CH_4$	0.85	1.6	1.6	203
		$C_3H_3^+ + C_2H_4$	0.15			114
	HCN	$HCNH^+ + CH_4$	1.00	4.1	4.3	168
$C_2H_5^+$	C_4H_2	$C_4H_3^+ + C_2H_4$	0.60	0.36	1.3	73
		$C_6H_5^+ + H_2$	0.40			215
	C_2H_3CN	$C_2H_3CNH^+ + C_2H_4$	> 0.95	4.2	4.3	114
		$C_2H_5^+.C_2H_3CN$	< 0.05			
$C_3H_5^+$	CH_3CN	$CH_3CNH^+ + C_3H_4$	0.55	3.5	4.1	39
		$C_3H_5^+.CH_3CN$	0.45			
	NH_3	$NH_4^+ + C_3H_4$	0.50	2.2	2.2	107
		$C_3H_5^+.NH_3$	0.50			
$HCNH^+$	NH_3	$NH_4^+ + HCN$	1.00	2.4	2.4	136
HC_3NH^+	NH_3	$NH_4^+ + HC_3N$	1.00	2.2	2.2	317
	C_2H_3CN	$C_2H_3CNH^+ + HC_3N$	1.00	3.8	3.7	41
CH_3CNH^+	NH_3	$NH_4^+ + CH_3CN$	1.00	2.2	2.2	67
	C_2H_3CN	$C_2H_3CNH^+ + CH_3CN$	> 0.95	3.5	3.9	7
		$CH_3CNH^+.C_2H_3CN$	< 0.05			
$C_2N_2H^+$	HCN	$HCNH^+ + C_2N_2$	1.00	3.3	3.3	42
	C_4H_2	$C_4H_3^+ + C_2N_2$	1.00	0.28	1.1	77

a. Observed rate coefficient in units of $10^{-9}\ cm^3\ s^{-1}$.

b. Collision rates calculated with variational transition state theory of Su and Chesnavich [59]. Units are $10^{-9}\ cm^3\ s^{-1}$.

c. Reaction enthalpy in $kJ\ mol^{-1}$ [184].

All of the reactions outlined in Table 6.2 exhibited a proton transfer channel. Adduct formation was competitive with proton transfer for the reaction of $C_3H_5^+$ with

both ammonia and acrylonitrile. Just two of the reactions exhibited channels other than proton transfer or association. In the first of these, the highly stable $C_3H_3^+$ ion was a minor product channel for the reaction of CH_5^+ with diacetylene (C_4H_2). The second example, which was perhaps the most interesting reaction observed, was that between $C_2H_5^+$ and diacetylene. A secondary channel occurred in competition with proton transfer with $C_6H_5^+$ contributing 40% of the product ions.

$$C_2H_5^+ + C_4H_2 \rightarrow C_4H_3^+ + C_2H_4 \qquad k = 3.6 \times 10^{-10}\ cm^3\ s^{-1} \qquad 0.60 \quad \textbf{(6.20a)}$$

$$\rightarrow C_6H_5^+ + H_2 \qquad 0.40 \quad \textbf{(6.20b)}$$

Reaction **(6.20b)** is interesting because the carbon chain length is increased by two and the reaction is (pseudo-)bimolecular rather than a termolecular association.

Given that all of the reactions exhibited a proton transfer channel it is unsurprising that almost all proceeded at or close to the collision rate. It is difficult, however, to explain the values of the rate coefficients for reaction **(6.20)** and reaction **(6.21)** below.

$$C_2N_2H^+ + C_4H_2 \rightarrow C_4H_3^+ + C_2N_2 \qquad k = 2.8 \times 10^{-10}\ cm^3\ s^{-1} \qquad \textbf{(6.21)}$$

Both of these reactions exhibit an exothermic proton transfer channel. The proton affinities of each of the species involved (C_2H_4, 680.5 kJ mol^{-1}; C_2N_2, 674.7 kJ mol^{-1}; C_4H_2, 737.2 kJ mol^{-1}) are sufficiently different to make proton transfer highly exothermic and therefore (presumably) rapid, with rate coefficients approaching the collision rate [142]. A possible explanation for the observed low k values is that the proton affinity of one or more of the species is poorly defined (see Section 6.2.3 regarding C_2N_2) and that proton transfer is in fact not as thermodynamically favourable as it appears.

6.3.4 Summary

The kinetics and product branching ratios summarised in Table 6.2 are straightforward and should prove useful to models of Titan's atmosphere. The measurement of reactions such as these is ongoing as species are continually being identified for which laboratory kinetics have not been measured.

CHAPTER 7.

LITHIUM ION CHEMISTRY

7.1 SIFT-MS and the Quantification of Analytes

Throughout this thesis the SIFT has been used to measure the products and rate coefficients of ion-molecule reactions. Rate coefficients are established from the semi-logarithmic decay of reactant ion signal with increasing neutral reactant flow. Remarkably, this procedure can be reversed – a known rate coefficient can be used to measure an unknown concentration of neutral reactant. The technique developed to measure unknown concentrations of neutrals based on this principle is known as Selected Ion Flow Tube Mass Spectrometry which is abbreviated to SIFT-MS.

The experimental procedure for SIFT-MS is straightforward and requires no modification to the existing apparatus. A flow of gas containing an analyte is admitted to the flow tube where the analyte reacts with the reagent ion. The sum of the product ion signals generated by the analyte is proportional to the partial pressure (concentration) of the analyte in the flow tube. Provided the rate coefficient and products of the ion-analyte reaction are known, the exact proportionality can be calculated and the absolute concentration of analyte in the original gas sample determined.

The greatest advantage SIFT-MS has over rival analyte detection methods is that quantification occurs in real time without the need for pre-concentration of the analyte. Product ion signals appear as soon as the analyte containing gas is admitted to the flow tube. The experiment takes seconds and requires only the flow of analyte containing gas into the flow tube and product ion count rates to be measured. No pre-concentration of the analyte is necessary. Individual analyte concentrations can be established in multi-component mixtures even at very low levels simply by looking at the ion count for (unique) products of that particular analyte. SIFT-MS and has been exploited by a

number of researchers to measure analytes **quantitatively** in air and breath samples **in real time** [194, 195].

Whereas the reactant ion signal is essential to the measurement of rate coefficients using the SIFT (Chapter 2), for the detection and quantification of volatile compounds it is both the reactant and product ions and their count rates that are measured. It is therefore essential that the products and product branching ratios for an ion-analyte reaction and the rate coefficient are known before quantification can be attempted.

SIFT-MS is most sensitive to analytes which react at close to the collision rate with the reactant ion with parts per trillion (by volume) detection limits being possible for some species [194, 196]. The proportionality between product ion count rates and analyte concentration becomes non-linear when the precursor ion signal is depleted by more than 10%. This means that at analyte concentrations above 20 parts per million (by volume) SIFT-MS cannot provide accurate analyses. The working range can be increased if higher reactant ion currents can be generated – lower levels of analytes may then have acceptable signal to noise ratios.

Clearly the reagent ion (commonly referred to as the precursor ion) plays an important role in this system. To be applicable to SIFT-MS, the reagent ion must be reactive with the analyte and **unreactive** with the major components of the sample (which is almost always air): N_2, O_2, H_2O, CO_2 and Ar. Of these H_2O is perhaps the most important as the most commonly analysed sample media, air and breath, contain varying degrees of humidity. The three precursor ions most commonly used for SIFT-MS are H_3O^+, O_2^+ and NO^+ although other ions have been used for specific analytes [197]. Most volatile organic compounds react rapidly with at least one of these ions. H_3O^+ reacts by proton transfer with a broad range of volatile molecules and is the most frequently used reactant ion.

The use of three precursor ions enables the detection of a huge array of analytes and lends a high level of specificity to SIFT-MS. If a sample contains two analytes that react with H_3O^+ to give product ions with the same nominal mass, their individual concentrations cannot be determined. Because analytes invariably react in different ways with each reactant ion, switching to another precursor ion effectively solves such

problems. This is not possible with similar techniques such as PTR-MS which relies solely on H_3O^+ proton transfer reactions to identify analytes [198].

Increasing the number of precursor ions available to SIFT-MS should broaden the range of detectable analytes and enhance specificity in cases where reaction products are indistinguishable for two analytes. Lithium ions, Li^+, may be a useful additional reactant ion to the three current SIFT-MS precursor ions. Lithium ions are known to attach to a range of molecules forming a single quasi-molecular ion for each species [199]. The suitability of lithium ions for SIFT-MS was assessed by first examining what is known of their reaction chemistry.

Hodges and Beauchamp were the first to utilise the attachment of lithium ions to molecules as a way of obtaining a mass spectrum of quasi-molecular ions [200]. Having observed the ability of lithium ions to attach to a wide range of radicals and molecules, Fujii developed a novel technique which he calls Lithium Ion Attachment Mass Spectrometry. The technique utilises lithium ions, Li^+, to identify volatile constituents in air in real time from their attachment reactions in the gas phase [201]. Because lithium ion attachment is a soft ionisation method, fragmentation is avoided and analytes are identified in mass spectra as quasi-molecular ions. Fujii's method can be used to detect volatile species in air at concentrations as low as 52 pptv (1-bromopropane) although this represents the optimal case [201]. The method, which is non-quantitative, is most sensitive to compounds for which lithium ions have the highest affinity – namely polar or polarisable molecules.

There have been two previous kinetic investigations into lithium ion chemistry. Spears and Ferguson surveyed the termolecular association kinetics of Li^+ with a series of molecules using a flowing afterglow [202]. Included in this study were some species also investigated in this work. This early investigation was motivated by a desire to obtain a greater understanding of termolecular kinetics and to improve theoretical models of association reactions. Lithium ion association is generally described by the following two

step mechanism (where M is any molecule which can remove energy in a collision):

$$Li^+ + X \rightarrow (Li^+.X)^* \qquad \textbf{(7.1)}$$

$$(Li^+.X)^* + M \rightarrow Li^+.X + M \qquad \textbf{(7.2)}$$

making the overall reaction:

$$Li^+ + X + M \rightarrow Li^+.X + M \qquad \textbf{(7.3)}$$

All of the alkali metal ions are known to react by this mechanism, with lithium cations having the highest attachment affinities [199].

Woodin and Beauchamp examined bimolecular association between Li^+ and a series of aldehydes and ketones using ion cyclotron resonance (ICR) spectroscopy [203]. They investigated the fate of the excited collision complex generated by reaction **(7.1)** in the lower pressure environment of the ICR. Radiative stabilization was assumed to be the dominant mechanism by which stable $Li^+.X$ adducts were formed at low pressures and the authors estimated rates for this process.

In the present work the suitability of lithium ions as an additional SIFT-MS reagent ion is appraised. This involved the development of a lithium ion source that could be incorporated with the SIFT and the measurement of kinetics for Li^+ reacting with a variety of neutral reagents. The rate coefficients and products given in the present work (Table 7.1) were measured during my Honours year at the University of Canterbury. During the measurement of the rate coefficients, some unusual chemistry was observed when water was also present (as an impurity). Because the overall suitability of Li^+ as a reagent ion for SIFT-MS requires a complete understanding of the chemistry occurring, the effect of water on the chemistry of Li^+ attachment to neutral species was critically examined and it is this further investigation that is presented here.

7.2 Experimental

7.2.1 Lithium Ion Source

The principal modification made to the SIFT for this work was the alteration of the ion source. The flowing afterglow ion source was removed to accommodate the new lithium ion source based on thermionic emission from a coated iridium filament. The ion source (Figure 7.1) consists of an iridium filament welded across two molybdenum rods.

The ion source fits neatly in front of the first electrostatic lens in the upstream quadrupole chamber. Lithium ions generated from the filament coating by thermionic emission are propelled into an Einzel lens array by a large positive voltage on the repeller. The electrostatic lenses focus the ions into the upstream ion-selection quadrupole.

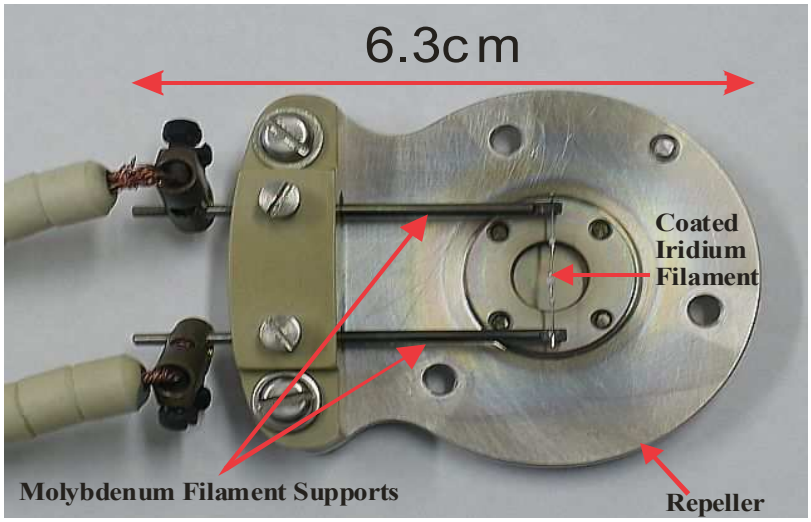

Figure 7.1. *Lithium ion source based on thermionic emission from a coated filament.*

Two filament coatings were used during the course of this research. Lithium β-eucryptite, a naturally occurring mineral having the formula $Li_2O.Al_2O_3.2SiO_2$, is widely reported as the most efficient source of lithium ions in emission based experiments [204, 205]. Lithium oxide, Li_2O, was also used and was found to be an equally efficient source of Li^+.

Figure 7.2. *A mineral sample of lithium β-eucryptite in a quartz matrix. The lithium β-eucryptite is fluorescent under UV light.*

It is possible to produce lithium β-eucryptite in the laboratory by heating a mixture of Li_2CO_3, Al_2O_3 and SiO_2 [206]. The furnace required for this was not available so a natural mineral sample was obtained instead. Lithium β-eucryptite

fluoresces under UV light (Figure 7.2) and was identified and separated from its rock matrix by utilising this property.

The procedure adopted for coating the filament is as follows. The lithium-containing compound is ground to a fine powder and mixed with a small amount of amyl acetate to form a slurry. This slurry is then painted onto the filament and the solvent evaporated by resistive heating of the filament. The lifetime of coated filaments ranged from one to ten hours. A typical emission spectrum from a lithium β-eucryptite coated filament is shown in Figure 7.3 (with the ion-selection quadrupole detuned so that all ions produced by the filament were transmitted to the flow tube). Stable lithium ion currents were generated with ion count rates varying from 2000 to 100000 cps. Continuous operation at very high count rates reduced the lifetime of the filament.

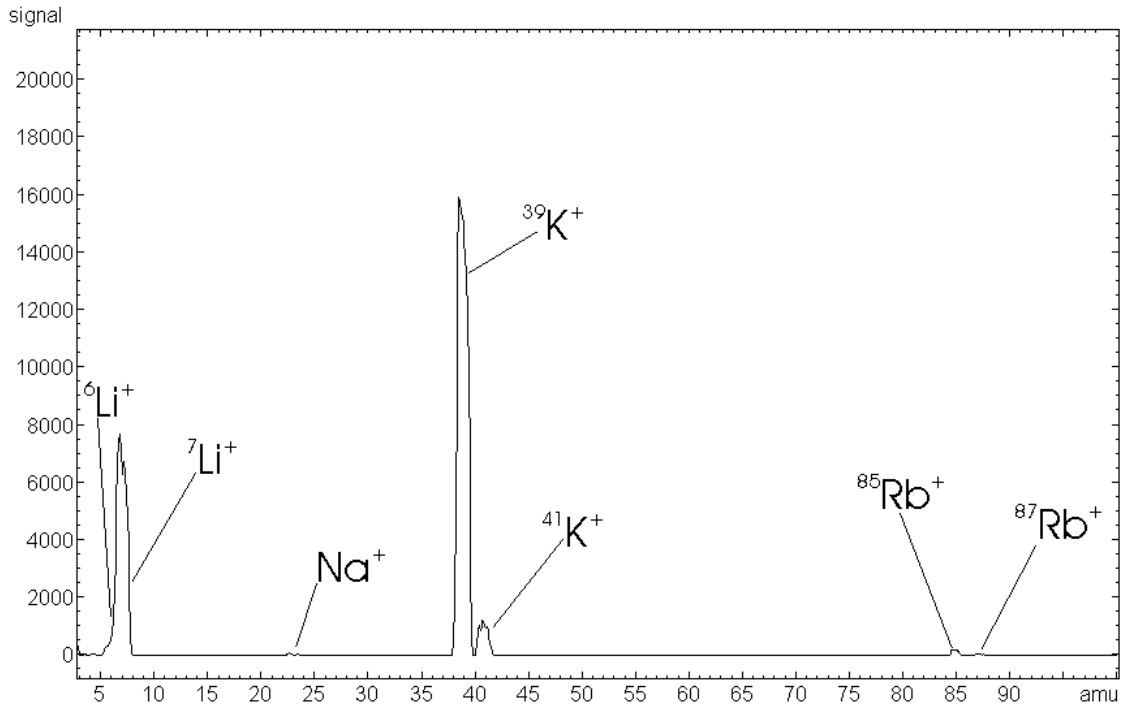

Figure 7.3. *Typical emission spectrum obtained from a filament coated with lithium β -eucryptite illustrating the presence of other alkali metal ions in the mineral sample.*

Lithium has two naturally occurring isotopes – ^{6}Li (7.4%) and ^{7}Li (92.6%). The ion selection quadrupole was set to transmit $^{7}Li^{+}$ and it is the kinetics for this isotopic species which are reported here.

All neutral reagents used were obtained from commercial sources and where possible purified by multiple freeze-pump-thaw cycles. For the measurement of kinetics, the neutral was added through the usual SIFT inlet port, 504 mm upstream of the sampling orifice for the downstream analysing quadrupole mass spectrometer. To analyse the chemistry of the products of these reactions with water, the products were first created by adding the neutral species through a neutral inlet located 280 mm upstream of the usual inlet. Products thus generated were reacted with a mixture of 1.5% H_2O in helium added downstream through the usual inlet (which is 504 mm upstream of the sampling orifice).

7.3 Results and Discussion

The reaction kinetics measured during my Honours year are included here as a reference for the subsequent work in which the ion chemistry in the presence of water was evaluated and the overall suitability of Li^+ as a SIFT-MS precursor ion assessed. The results of the initial Li^+ investigation are presented in Table 7.1.

The rate coefficients were measured at a single pressure (0.46 Torr) and are reported as pseudo-bimolecular rate coefficients. The nature of termolecular association reactions such as these for Li^+ means that the pseudo-bimolecular rates will vary linearly with pressure, in particular this applies to those where association is slow, $k < 1 \times 10^{-11}$ cm^3 s^{-1}. For reactions where the rate coefficient approaches the collision rate ($k \sim 1 \times 10^{-9}$ cm^3 s^{-1}) the bimolecular rate coefficients would not be expected to vary much with pressure. For these rapid reactions almost all of the products are stabilized by collision before they can dissociate back to reactants. For the purposes of comparison with literature values those reactions having rate coefficients less than 1×10^{-10} cm^3 s^{-1} have been converted to termolecular rate coefficients. As these represent only a single point in a plot of rate coefficient against pressure these values should be considered approximate.

Association rates for methane (CH_4) and carbon monoxide (CO) were measured near the lower limit of the SIFT's working range which may account for the disparity between the approximated termolecular and literature rate coefficients. In the only other

case where there is a significant divergence between the approximate termolecular rate coefficient and the literature value (for CO_2) it is possible that water impurities may have contributed to the difference.

Table 7.1. *Measured pseudo-bimolecular rate coefficients for the association of Li^+ with the given reactant at 294 K.*

Reactant	Product	Rate coefficient[a]	Approximate k_3[b]	Literature k_3[b,c]	k_c [d]
CH_4	$Li^+.CH_4$	2.2×10^{-13}	1.4×10^{-29}	5.1×10^{-30}	1.7
H_2O	$Li^+.H_2O$	9.8×10^{-11}	6.5×10^{-27}		4.0
C_2H_2	$Li^+.C_2H_2$	3.4×10^{-12}			1.8
HCN	$Li^+.HCN$	2.5×10^{-12}	1.7×10^{-28}		5.9
CO	$Li^+.CO$	2.7×10^{-13}	1.8×10^{-29}		1.4
C_2H_4	$Li^+.C_2H_4$	4.6×10^{-12}	3.0×10^{-28}	1.9×10^{-28}	2.0
NO	$Li^+.NO$	3.3×10^{-13}	2.2×10^{-29}		1.4
C_2H_6	$Li^+.C_2H_6$	6.1×10^{-12}	4.0×10^{-28}	2.3×10^{-28}	2.1
CH_2CCH_2	$Li^+.CH_2CCH_2$	9.3×10^{-11}	6.4×10^{-27}	$\sim 1.2 \times 10^{-26}$	2.3
CH_3CCH	$Li^+.CH_3CCH$	2.9×10^{-10}			2.9
c-C_3H_6	$Li^+.$ c-C_3H_6	9.8×10^{-11}	6.5×10^{-27}		2.6
CO_2	$Li^+.CO_2$	7.4×10^{-13}	4.9×10^{-29}	1.6×10^{-29}	1.6
C_3H_8	$Li^+.C_3H_8$	9.7×10^{-11}	6.5×10^{-27}	$\sim 7.2 \times 10^{-27}$	2.4
i-C_4H_{10}	$Li^+.$ i-C_4H_{10}	3.4×10^{-10}			2.7
SO_2	$Li^+.SO_2$	7.6×10^{-12}	5.1×10^{-28}	1.8×10^{-28}	3.7
C_5H_{12}	$Li^+.C_5H_{12}$	1.6×10^{-9}			2.9
C_6H_6	$Li^+.C_6H_6$	3.2×10^{-9}			3.0
C_5H_5N	$Li^+.C_5H_5N$	3.6×10^{-9}			5.2
C_6H_{12}	$Li^+.C_6H_{12}$	2.0×10^{-9}			2.0
C_6H_{14}	$Li^+.C_6H_{14}$	2.7×10^{-9}			3.2
CH_3Br	$Li^+.CH_3Br$	2.2×10^{-11}	1.4×10^{-27}	8.0×10^{-28}	4.1

a. Pseudo-bimolecular rate coefficient in units $cm^3\ s^{-1}$.

b. Estimated termolecular rate coefficient in units of $cm^6\ s^{-1}$.

c. Reference [202].

d. Collision rate calculated using the variational transition state model in reference [59]. Units are $10^{-9}\ cm^3\ s^{-1}$.

SIFT-MS is most sensitive to analytes for which rate coefficients are rapid. The results summarised in Table 7.1 show that for smaller reactants (less than 6 atoms) association is generally slow, $k < 1 \times 10^{-10}$ cm^3 s^{-1} and only for reactants with 12 or more atoms do the rate coefficients approach the collision limit, $k \sim 10^{-9}$ cm^3 s^{-1}. Two factors contribute to the termolecular association rate and in combination account for these observations. The first is supplied by the RRKM model which predicts that the lifetime of the association adduct is directly related to the number of degrees of freedom of the complex [203]. Larger complexes have many degrees of freedom and dissociation back to reactants is slow, increasing the time available for collisional stabilisation. The second contribution arises from the Li^+-X binding energy. A stronger bond energy (characterised by a deeper potential well) generally increases the transitory lifetime of a complex thus reducing the likelihood of unimolecular dissociation prior to stabilisation.

During the measurement of the kinetics, some observations were made that were at odds with the slow rate measured for the reaction between lithium ions and water. In reactions with molecules for which the rate coefficients approached the collision rate, significant $Li^+.(H_2O)_n$ peaks were observed in spite of the vast difference in reaction rate. This peculiar chemistry was investigated by reacting selected products from Table 7.1 with H_2O.

7.4 The Reactivity of $Li^+.X$ in the presence of H_2O

For many of the reactions studied, secondary clustering occurred in the absence of H_2O, producing $Li^+.(X)_n$ clusters. A typical mass spectrum showing this type of clustering is shown in Figure 7.4, for the reaction of Li^+ with acetylene.

When H_2O was present mixed clusters of the form $Li^+.X.H_2O$ as well as $Li^+.(H_2O)_n$ ions were observed instead. This indicated that water molecules were replacing the analyte molecules in the clusters. The unusual chemistry observed has been reported in the literature before for lithium and other alkali metal cations [207, 208]. Reactions in which one molecule replaces another in an adduct or cluster are known as **cluster switching** or **ligand exchange** reactions [208].

Reaction **(7.4)** is an example of a cluster switching reaction. Cluster switching reactions are almost always rapid ($k \geq 10^{-10}$ cm^3 s^{-1}) when exothermic [209].

$$Na^+.H_2 + H_2O \rightarrow Na^+.H_2O + H_2 \qquad k = 1 \times 10^{-9}\ cm^3\ s^{-1} \qquad \textbf{(7.4)}\ [207]$$

The reaction mechanism is intuitive. The association of a water molecule to $Li^+.X$ forms an excited mixed cluster $(Li^+.X.H_2O)^*$. The mixed cluster may be stabilized by collision, or if the exothermicity of the association exceeds the $Li^+.X$ bond dissociation energy, the $Li^+.X$ bond may be broken leaving $Li^+.H_2O$ [207]. The displacement of a ligand by water implies that a stronger bond is formed between the incoming water molecule and the lithium ion than the bond between the lithium ion and the ejected molecule. The relative binding energies of $Li^+.X$ and $Li^+.H_2O$ determine the outcome of the reaction. Spears and Ferguson [202] have observed these effects in an experimental investigation of alkali cations including Li^+. In their work the rapid switching out of sulfur dioxide by water demonstrated the $Li^+.H_2O$ bond to be stronger than the $Li^+.SO_2$ bond.

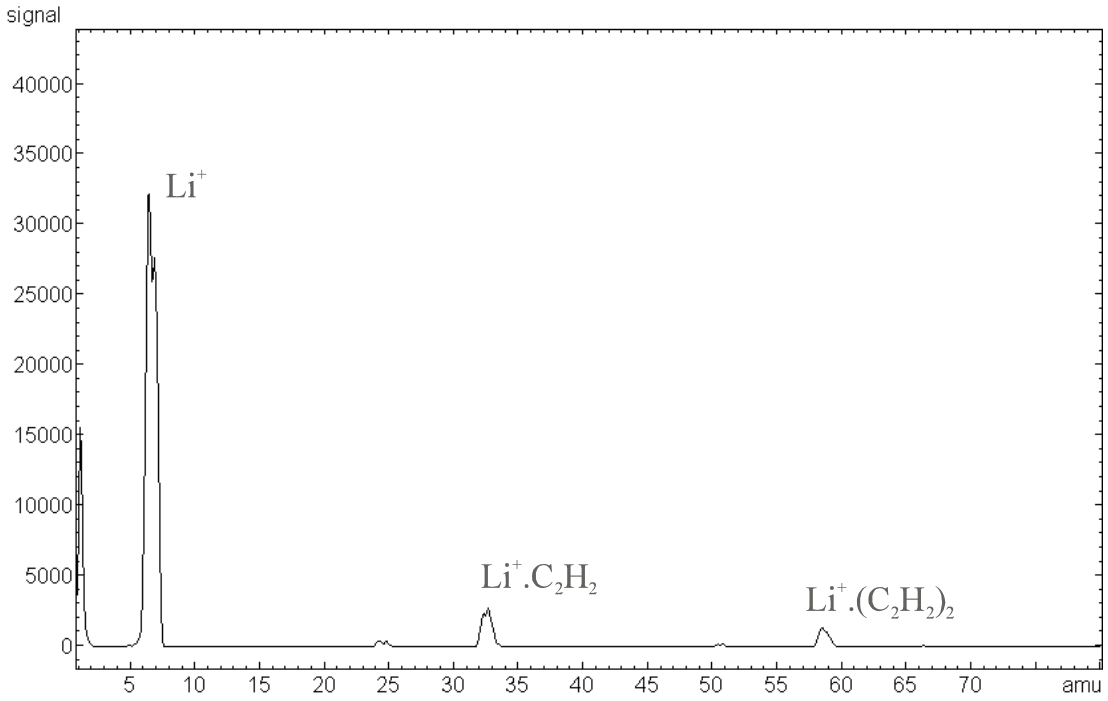

Figure 7.4. *Product mass spectrum for the reaction of Li^+ with acetylene showing secondary clustering.*

The bond dissociation energies (BDEs) of a wide range of Li^+ complexes (often described as 'lithium ion affinities') have been published [210-212]. Most of the BDEs available were measured or calculated as part of investigations into solvation effects.

Alkali metal ions are useful gas phase models of solvation as the ions are easy to produce and up to six water molecules can be clustered around each ion.

The BDEs for $Li^+.(H_2O)_n$ for n = 1-6 have been measured by Rodgers and Armentrout in threshold collision-induced dissociation experiments [213]. As expected the binding energy decreases for each additional ligand. The BDEs for the first three water clusters are given in Table 7.2 as well as those for other $Li^+.X$ adducts for which the chemistry with water was examined in this project.

Table 7.2. *$Li^+.X$ bond dissociation energies (for the loss of one ligand) for $Li^+.(H_2O)_n$ and a selection of $Li^+.X$ products from Table 7.1.*

Cluster	Bond Dissociation Energy (kJ mol^{-1})
$Li^+.H_2O$	137[a]
$Li^+.(H_2O)_2$	114[a]
$Li^+.(H_2O)_3$	94[a]
$Li^+.C_6H_6$	164.4[b]
$Li^+.(C_6H_6)_2$	103.7[b]
$Li^+.C_2H_2$	82.8[c]
$Li^+.C_2H_4$	82[c]
$Li^+.C_5H_5N$	185[d]
$Li^+.HCN$	141[e]

a. Reference [213].
b. Reference [214].
c. Reference [215].
d. Reference [216].
e. References [202, 217].

The presence of $Li^+.H_2O$ complexes in the preliminary kinetic measurements was unexpected because the direct rate of reaction between Li^+ and water is slow. The water clusters observed do not arise from the direct reaction of lithium ions with water but from cluster switching reactions. As these reactions may have a palpable effect on the ultimate usefulness of Li^+ as a precursor ion for SIFT-MS, the chemistry was investigated in detail. A selection of neutral reagents for which kinetics had been measured (Table 7.1), was chosen to cover a range of $Li^+.X$ bond dissociation energies (BDEs) relative to H_2O. The experimental results are summarised below. The observed trends in chemistry correlate well with the relationship between the $Li^+.(H_2O)_n$ BDEs and the Li^+-X BDE.

$Li^+ + C_2H_4$

The BDE of Li^+-C_2H_4 has been calculated as 82 kJ mol^{-1} [215]. The pseudo-bimolecular association rate was measured as 4.6 x 10^{-12} cm^3 s^{-1} corresponding to an approximate termolecular association rate coefficient of $k_3 \sim 3 \times 10^{-28}$ cm^6 s^{-1}. The second and third cluster ions $Li^+.(C_2H_4)_2$ and $Li^+.(C_2H_4)_3$ also formed prior to the downstream inlet where the water was added.

$Li^+ + C_2H_4 + M \rightarrow Li^+.C_2H_4 + M$ $\quad k \sim 3 \times 10^{-28}$ cm^6 s^{-1} **(7.5)**

$Li^+.C_2H_4 + C_2H_4 + M \rightarrow Li^+.(C_2H_4)_2 + M$ $\quad k \sim 3 \times 10^{-28}$ cm^6 s^{-1} **(7.6)**

$Li^+.(C_2H_4)_2 + C_2H_4 + M \rightarrow Li^+.(C_2H_4)_3 + M$ **(7.7)**

In the presence of added water, each of these ethene clusters is switched out at close to the collision rate with the resultant ions being $Li^+.(H_2O)_n$.

$Li^+.C_2H_4 + H_2O \rightarrow Li^+.H_2O + C_2H_4$ $\quad k = 1.6 \times 10^{-9}$ cm^3 s^{-1} **(7.8)**

$Li^+.(C_2H_4)_2 + H_2O \rightarrow Li^+.C_2H_4.H_2O + C_2H_4$ $\quad k = 2.6 \times 10^{-9}$ cm^3 s^{-1} **(7.9)**

$Li^+.C_2H_4.H_2O + H_2O \rightarrow Li^+.(H_2O)_2 + C_2H_4$ $\quad k \sim 1.8 \times 10^{-9}$ cm^3 s^{-1} **(7.10)**

The results for many of the other small hydrocarbons are similar. The BDE for Li^+-C_2H_2 has been calculated as 82.8 kJ mol^{-1} [215]. A very similar kinetics reaction sequence to ethene was observed for acetylene except that acetylene reacts more slowly than ethene.

$Li^+ + H_2O$

Water associates slowly with Li^+ forming $Li^+.H_2O$ with a pseudo-bimolecular rate coefficient of k = 9.8x10^{-11} cm^3 s^{-1}. Reaction of the $Li^+.H_2O$ adduct with water produced clusters with up to five water molecules bonded to a single lithium ion.

$Li^+ + H_2O + M \rightarrow Li^+.H_2O + M$ $\quad k = 9.8 \times 10^{-11}$ cm^3 s^{-1} **(7.11)**

$Li^+.(H_2O)_n + H_2O + M \rightarrow Li^+.(H_2O)_{n+1} + M$ $\quad (n = 1\text{-}4)$ **(7.12)**

$Li^+ + HCN$

The binding energy of Li^+ and HCN has been calculated as being slightly larger than water at 141 kJ mol^{-1} [217]. Slow association was observed to form the Li^+-HCN adduct with a pseudo-bimolecular rate coefficient of k = 2.5 x 10^{-12} cm^3 s^{-1} corresponding to an approximate termolecular rate coefficient of $k_3 \sim 1.6 \times 10^{-28}$ cm^6 s^{-1}. Further clustering was observed with up to four HCN molecules attached to the lithium ion.

$Li^+ + HCN + M \rightarrow Li^+.HCN + M \qquad k = 2.5 \times 10^{-12}\ cm^3\ s^{-1}$ **(7.13)**

$Li^+.(HCN)_n + HCN + M \rightarrow Li^+.(HCN)_{n+1} + M \quad (n = 1\text{-}3)$ **(7.14)**

At higher concentrations of HCN the dominant peak observed was $Li^+.(HCN)_3$. The reaction of $Li^+.(HCN)_n$ with H_2O was too slow to be measured with a 1.5% mixture of water in helium, giving a maximum possible reaction rate of ~ 1×10^{-11} $cm^3\ s^{-1}$. Slow reactions were observed at very high flows as shown by the following reactions:

$Li^+.(HCN)_3 + H_2O \rightarrow Li^+.(HCN)_2.H_2O + HCN \quad k < 1 \times 10^{-11}\ cm^3\ s^{-1}$ **(7.15)**

$Li^+.(HCN)_4 + H_2O \rightarrow Li^+.(HCN)_3.H_2O + HCN. \quad k < 1 \times 10^{-11}\ cm^3\ s^{-1}$ **(7.16)**

Li^+ + Benzene

Li^+ associates rapidly with benzene at the collision rate which is consistent with association rates for large molecules having significant binding energies. The BDE of $Li^+.C_6H_6$ has been measured as 164.4 kJ mol^{-1} and for $Li^+.(C_6H_6)_2$ as 103.7 kJ mol^{-1} [214]. The reaction sequence observed for the Li^+/C_6H_6 system is as follows. Results are shown for benzene addition up to the second cluster only.

$Li^+ + C_6H_6 \rightarrow Li^+.C_6H_6 \qquad k = 3.2 \times 10^{-9}\ cm^3\ s^{-1}$ **(7.17)**

$Li^+.C_6H_6 + C_6H_6 \rightarrow Li^+.(C_6H_6)_2 \qquad k \sim 8.5 \times 10^{-10}\ cm^3\ s^{-1}$ **(7.18)**

$Li^+.C_6H_6 + H_2O + M \rightarrow Li^+.C_6H_6.H_2O + M \qquad k = 7.1 \times 10^{-26}\ cm^6\ s^{-1}$ **(7.19)**

$Li^+.(C_6H_6)_2 + H_2O \rightarrow Li^+.C_6H_6.H_2O + C_6H_6 \quad k = 1.1 \times 10^{-9}\ cm^3\ s^{-1}$ **(7.20)**

$Li^+ + H_2O + M \rightarrow Li^+.H_2O + M \qquad k = 6.5 \times 10^{-27}\ cm^6\ s^{-1}$ **(7.21)**

$Li^+.C_6H_6.H_2O + H_2O \rightarrow Li^+.(H_2O)_2 + C_6H_6 \quad k \sim 2.3 \times 10^{-9}\ cm^3\ s^{-1}$ **(7.22)**

$Li^+.(H_2O)_2 + H_2O + M \rightarrow Li^+.(H_2O)_3 + M$ **(7.23)**

$Li^+.(C_6H_6)_2.H_2O + H_2O \rightarrow Li^+.C_6H_6.(H_2O)_2 + C_6H_6$

$k \geq 4 \times 10^{-10}\ cm^3\ s^{-1}$ **(7.24)**

$Li^+.C_6H_6.(H_2O)_2 + H_2O \rightarrow Li^+.(H_2O)_3 + C_6H_6 \quad k \geq 5 \times 10^{-10}\ cm^3\ s^{-1}$ **(7.25)**

In spite of the strong $Li^+.C_6H_6$ BDE, the resultant ions from this reaction sequence were $Li^+.(H_2O)_2$ and $Li^+.(H_2O)_3$.

Li^+ + Pyridine

Li^+ has a higher binding energy with pyridine than it does for benzene. The $Li^+.C_5H_5N$ BDE has been calculated to be 185 kJ mol^{-1} in a study that estimated the BDE of $Li^+.C_6H_6$ as 151 kJ mol^{-1} [216]. As noted previously, the BDE for benzene was measured as164 kJ mol^{-1} and therefore the BDE for $Li^+.C_5H_5N$ may be even higher than

this calculation suggests [216]. The reactions were initiated with a collision rate reaction between Li^+ and pyridine and multiple clusters were seen.

$Li^+ + C_5H_5N \rightarrow Li^+.C_5H_5N$ $k = 3.6 \times 10^{-9}$ cm^3 s^{-1} **(7.26)**

$Li^+.C_5H_5N + C_5H_5N + M \rightarrow Li^+.(C_5H_5N)_2 + M$ $k = 2.5 \times 10^{-10}$ cm^3 s^{-1} **(7.27)**

$Li^+.C_5H_5N + H_2O + M \rightarrow Li^+.C_5H_5N.H_2O + M$ $k = 7.6 \times 10^{-10}$ cm^3 s^{-1} **(7.28)**

$Li^+.(C_5H_5N)_2 + H_2O \rightarrow Li^+.C_5H_5N.H_2O + C_5H_5N$ $k = 1.9 \times 10^{-10}$ cm^3 s^{-1} **(7.29)**

$Li^+.(C_5H_5N)_2 + H_2O + M \rightarrow Li^+.(C_5H_5N)_2.H_2O + M$ $k = 1.9 \times 10^{-10}$ cm^3 s^{-1} **(7.30)**

$Li^+.C_5H_5N.H_2O + H_2O + M \rightarrow Li^+.C_5H_5N.(H_2O)_2 + H_2O$

$k = 1.8 \times 10^{-10}$ cm^3 s^{-1} **(7.31)**

As with the previous reagents, the reactions with background water occur simultaneously with the reactions with pyridine except that here the pyridine cluster ions $Li^+.(C_5H_5N)_2.H_2O$ and $Li^+.C_5H_5N.(H_2O)_2$ are 'terminal' ions rather than the water cluster ions.

Reaction Chemistry Summary

The outcome of these reactions is determined by the bond energy of the $Li^+.X$ adduct. Both $Li^+.C_2H_2$ and $Li^+.C_2H_4$ have BDEs which are considerably lower than $Li^+.H_2O$. When water is present, ethylene or acetylene is efficiently 'switched out' by water molecules leaving only $Li^+.(H_2O)_n$ clusters. HCN has a slightly higher BDE than water with Li^+. In this system mixed clusters were observed as the terminal ions in the presence of water. The $Li^+.C_6H_6$ BDE is considerably higher than that for water. The reaction of the Li^+/benzene clusters with water generated mixed cluster $Li^+.C_6H_6.H_2O$ which was then converted to either $Li^+.(H_2O)_2$ or $Li^+.C_6H_6.(H_2O)_2$ and then $Li^+.(H_2O)_3$. $Li^+.(H_2O)_2$ and $Li^+.(H_2O)_3$ were the terminal ions at high water concentrations. The $Li^+.C_5H_5N$ cluster has an even higher BDE than benzene (185 kJ mol^{-1}). Again mixed clusters were formed with water but pyridine was not subsequently switched out. The mixed clusters formed were the terminal ions.

7.5 The Suitability of Li^+ as a SIFT-MS Reagent

For Li^+ to be a useful reagent ion in addition to the three currently used in SIFT-MS, several criteria must be met. Firstly, a reliable, stable source of lithium ions in high

yield must be available. Secondly, lithium ions must not react at appreciable rates with the major components of air, and thirdly, the ions must react rapidly with the analytes.

A lithium ion source based on thermionic emission from a coated filament provided adequate lithium ion currents for this work. Both the lithium β-eucryptite and lithium oxide filament coatings gave stable Li^+ signals under constant heating power. Unfortunately the lifetime of the filaments was relatively short - between one and ten hours depending on the operating conditions. This would need to be improved considerably if the ion source was to be incorporated in a commercial SIFT-MS instrument. One option (not pursued here) would be to convert the pasty lithium β-eucryptite filament coatings to a glassy form by melting the coating onto the filament. Significant enhancements to ion signal have been reported for 'glassy' lithium β-eucryptite filament coatings [218]. Glassy coatings also have the advantage of being more durable as compared to the pasty coating used here which can easily flake off the filament.

Lithium ions were found to be unreactive with the major components of air. The reactions of N_2, O_2 and Ar were too slow to observe ($k < 1 \times 10^{-13}$ cm^3 s^{-1}) and are not included in Table 7.1. CO_2 reacts only very slowly with Li^+ with a bimolecular rate coefficient of 7.4×10^{-13} cm^3 s^{-1}. The most important component of air for which reactivity was measured is H_2O. This reaction is relatively slow with $k = 9.8 \times 10^{-11}$ cm^3 s^{-1} which means that water should not greatly affect the detection of species with rate coefficients greater than $k = 1 \times 10^{-10}$ cm^3 s^{-1}.

The kinetic investigation revealed that lithium ions would not be a sensitive reagent ion for the detection of small molecules (with less than 6 atoms) as they associate very slowly with Li^+. SIFT-MS is most sensitive to species that react with the precursor ion at close to the collision rate. Larger molecules (12 or more atoms) do react rapidly with the lithium ions. However, because of cluster switching reactions with water, quantification by SIFT-MS is ultimately controlled by the Li^+.X bond dissociation energy. The bond dissociation energy determines the chemistry that occurs when water is also present – as it would be in all environmental samples subjected to SIFT-MS analysis. The chemistry of a selection of Li^+.X products (covering a range of BDEs) with H_2O was investigated to clarify this.

The BDE for $Li^+.H_2O$ is 137 kJ mol^{-1}. For clusters with BDEs less than this, ($Li^+.C_2H_2$, $Li^+.C_2H_4$), water rapidly replaces the analyte in the adduct by a simple switching reaction leaving only $Li^+.(H_2O)_n$ clusters. Hydrogen cyanide has a BDE slightly greater than water. The reaction of water with $Li^+.(HCN)_n$ clusters was very slow and generated mixed clusters of the form $Li^+.H_2O.(HCN)_n$ which were the terminal ions. Because HCN is not switched out by water, HCN could be detected by lithium ions however because the association of Li^+ and HCN is very slow, Li^+ would not be an ideal monitor ion for this species. $Li^+.C_6H_6$ has a much higher BDE than $Li^+.H_2O$. This species exhibited the most intriguing chemistry with water. The benzene molecule cannot be directly displaced by a water molecule so initially the mixed cluster $Li^+.C_6H_6.H_2O$ forms. The addition of second water molecule (three ligands are now bound to a single lithium ion) reduces the $Li^+.C_6H_6$ BDE in the cluster to the point where the excess energy in the cluster is sufficient to displace the benzene molecule, leaving $Li^+.(H_2O)_2$. In spite of the strength of the $Li^+.C_6H_6$ bond, the rapid reaction of $Li^+.C_6H_6$ and $Li^+.(C_6H_6)_2$ with H_2O generates both $Li^+.(H_2O)_2$ and $Li^+.(H_2O)_3$ clusters as the terminal ions under conditions of high humidity. At still higher $Li^+.X$ BDEs such as for pyridine, water does not switch out the analyte and the terminal ions are mixed clusters.

These results show that Li^+ has very limited applicability to the detection of volatile compounds by SIFT-MS in spite of lithium ions being reactive with a wide variety of molecules and unreactive with the major components of air. Lithium ion SIFT-MS would be insensitive to small molecules as the association reactions are too slow. Ultimately the use of Li^+ is restricted to species for which the $Li^+.X$ BDE is very high, otherwise the analyte is rapidly switched out by water.

CHAPTER 8.

LABVIEW

8.1 Introduction

When the UC SIFT instrument was first commissioned in the 1980s, all data was recorded manually making the task of data acquisition time consuming and laborious. SIFT data acquisition was transformed during the 1990s by the development of computer software capable of performing this task. Computer-controlled data acquisition massively increased the number of ion-molecule reactions that could be measured in a single day. Currently, data acquisition and analysis is performed by the purpose-written software *Sift for Windows*. This software controls the downstream analysing quadrupole (selection of mass number), measures the response of the particle multiplier (signal intensity at selected mass) and measures the flow rate of neutral reactant to the flow tube. Data is analysed and displayed graphically as it is acquired and complete mass spectra and kinetic data for a given reaction can be recorded and saved in minutes. The installation of this software represented a revolution in SIFT data collection and analysis. It should be noted that all other parts of the SIFT instrument are still controlled manually.

Sift for Windows is written in the Borland Pascal language and is run on a computer with a Windows ’95 operating system. *Sift for Windows* is not compatible with newer versions of Windows and continues to be operated on an outdated computer. Recently this computer has become unreliable and requires frequent repairs. The computer has been increasingly difficult to fix as the technology is obsolete and some components are no longer available. Replacement of the computer is a matter of urgency. Because *Sift for Windows* is not compatible with a modern desktop computer, the SIFT operating software must be re-written in a format compatible with a modern Windows operating environment.

As part of this thesis project new software has been developed with the LabVIEW™ programming suite. The essential features of *Sift for Windows* are replicated in the new program and it has been successfully applied to the measurement of kinetics with the SIFT.

8.2 The Operation of *Sift for Windows*

The original *Sift for Windows* program was written by Dr Patrik Španěl to control a SIFT instrument at the University of Innsbruck in Austria. In 1994 Dr Španěl generously donated a copy of the software to the University of Canterbury SIFT laboratory and spent time at the university customising the software to our instrument. An updated version of the software was purchased and installed in 1996 and it is this version of the program that has been used to collect the data presented in other chapters of this thesis. *Sift for Windows* is a complete data acquisition and analysis package.

Sift for Windows performs exceptionally well and reliably and has been used successfully ever since its installation. It has all the basic functions required to examine the kinetics of ion-molecule reactions as well as having many advanced attributes that are rarely exploited. It would be very difficult to develop a superior program to *Sift for Windows* for the examination of SIFT kinetics. For this reason the new SIFT operating software has been designed to replicate the operating characteristics of *Sift for Windows* as closely as possible. Before giving details of the development of the new software it will be valuable to give an overview of the function of *Sift for Windows*. Although the software is primarily designed to measure rate coefficients for ion-molecule reactions it also includes a mode in which mass spectra can be recorded. This is an essential feature of the program as before a kinetic investigation can be made, the ionic products of the reaction must be identified.

8.2.1 Mass Spectra

Sift for Windows records a mass spectrum by sweeping the downstream quadrupole through a range of masses whilst simultaneously measuring the ion signal reaching the detector. The acquired data is plotted as it is measured. Any selected range of masses can be swept over a time specified by the operator and the resultant spectra displayed with either a linear or a logarithmic scale for the ion signal. Having manually

initiated an ion-molecule reaction in the SIFT flow tube the user need only input the minimum and maximum masses of the range to be measured and the time over which to scan. Pressing 'Enter' then initiates the mass scan. In this respect the program is very simple. A sample mass spectrum is shown in Figure 8.1.

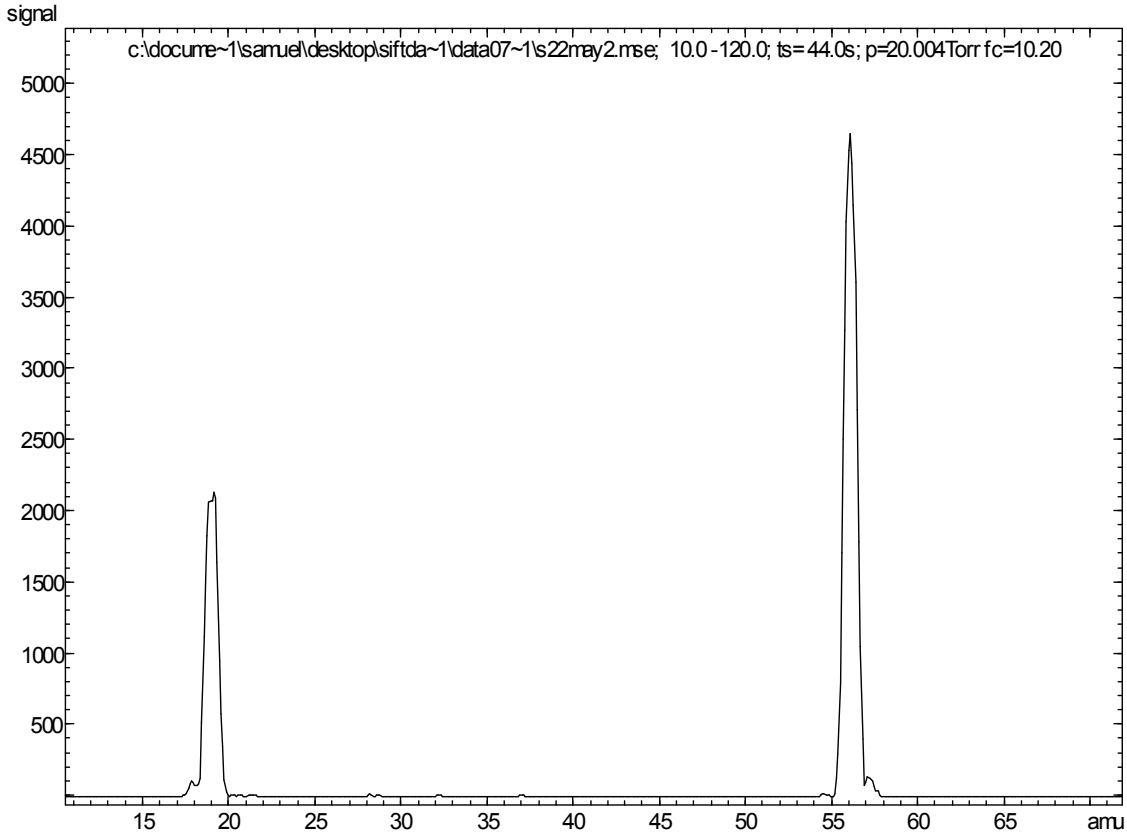

Figure 8.1. *A mass spectrum recorded by Sift for Windows for the reaction between H_3O^+ (m/z 19) and C_2H_5CN generating $C_2H_5CNH^+$ (m/z 56).*

The mass spectrum function allows for the qualitative examination of ion-neutral reactions. As a neutral is injected and its flow varied, the primary ion peaks are observed to decrease with the simultaneous evolution of product ions. Before a rate coefficient can be measured it is essential to obtain accurate mass assignments for the reactant and product ions from a mass spectrum.

8.2.2 Rate Coefficient Determination

The quantitative examination of ion-molecule reactions is performed by the second facet of *Sift for Windows*. Ion-molecule rate coefficients are determined from the semi-logarithmic decay of reactant ion signal with increasing neutral flow. Product

branching ratios are determined by extrapolating product ion ratios to zero neutral flow. A complete investigation of ion-molecule kinetics therefore requires the measurement of all reactant and product ion signals over a series of neutral flow rates.

To complete a kinetics measurement the experimentalist first provides *Sift for Windows* with details of the reaction to be measured. This includes identifying the ions to be counted and recording the experimental conditions such as the pressure in the flow tube and temperature. The ions to be counted are designated as primary (reactant), product or other (spectator). Having input these values a simple keystroke is all that is required to begin collecting data. The program instructs the quadrupole to transmit one of the ions and to count the ion signal for a designated period. At the end of this period the next ion is transmitted and its ion signal measured. Each ion is counted at a particular neutral flow rate (which is measured simultaneously). After all of the ions have been measured at a pre-set flow (usually zero to begin with) the program stops to allow the operator to adjust the flow of neutral. The data collection process is then repeated. Ion counts are measured at a succession of neutral flows until sufficient data is acquired to give accurate results.

Data acquisition and analysis occur synchronously allowing the user to continuously assess the progress of an experiment. The *Sift for Windows* program generates and displays three panels of data during rate coefficient measurements. The first is a semi-logarithmic plot of the ion signals against neutral flow. A straight line representing a least squares fit is plotted over the decay of reactant ion signal and the rate coefficient for the reaction (calculated from the slope of the decay divided by the reaction time) displayed adjacent to the line of best fit. The second panel displays the product ion ratios at each neutral flow and gives an estimate of the product branching ratios for the reaction by extrapolating the ratios to zero neutral flow. The third panel gives a table of the raw data collected in the experiment and includes details of the experimental conditions. Data is saved at the end of a measurement and can be printed, transferred directly to documents or exported to Excel for further analysis.

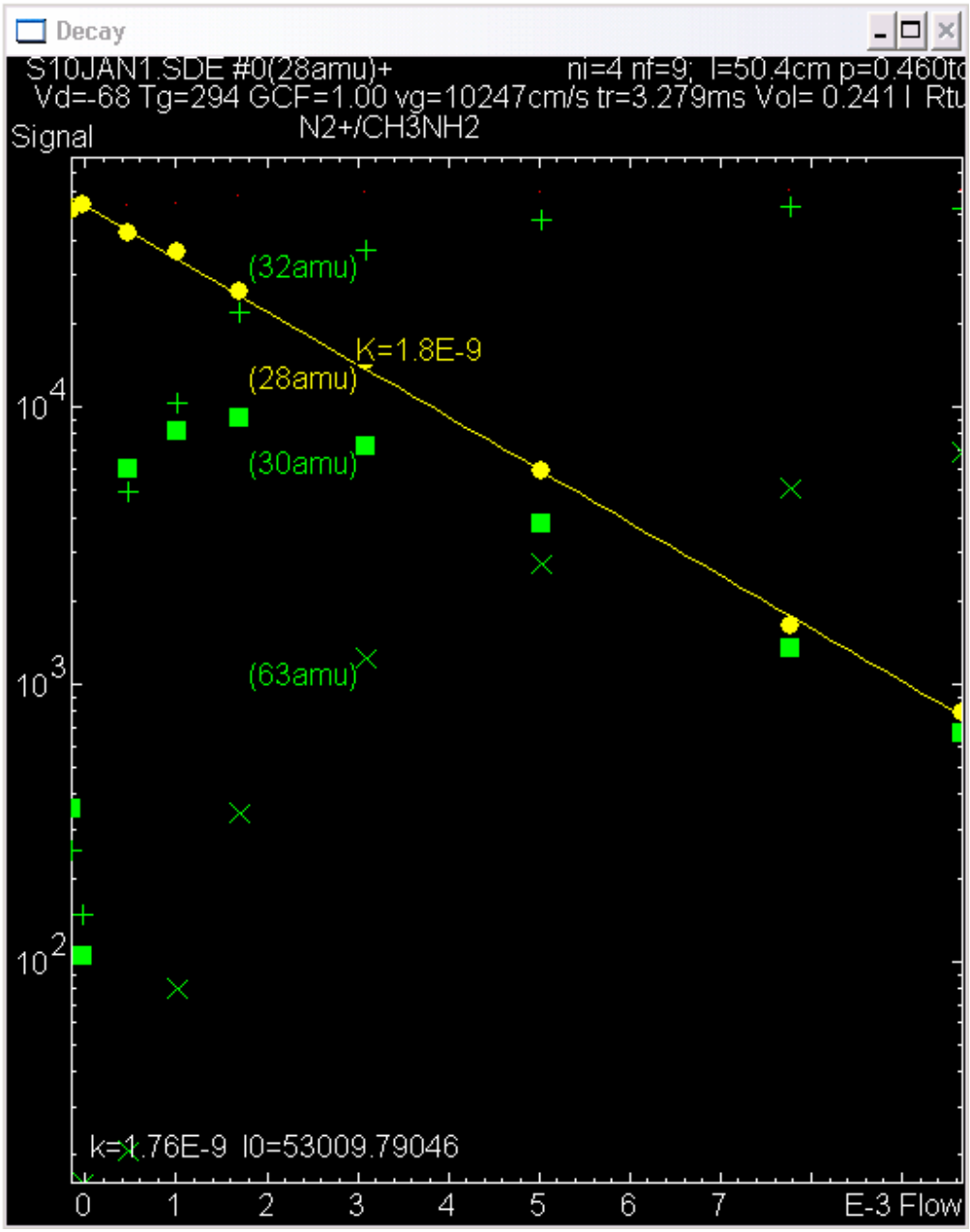

Figure 8.2. *The first panel of data displayed by Sift for Windows during a rate coefficient measurement is a semi-logarithmic plot of ion signal against neutral flow. The example provided is for the reaction of N_2^+ with methylamine (CH_3NH_2). The rate coefficient for the reaction - 1.8 x 10^{-9} of cm^3 s^{-1} - is displayed adjacent to the semi-log decay.*

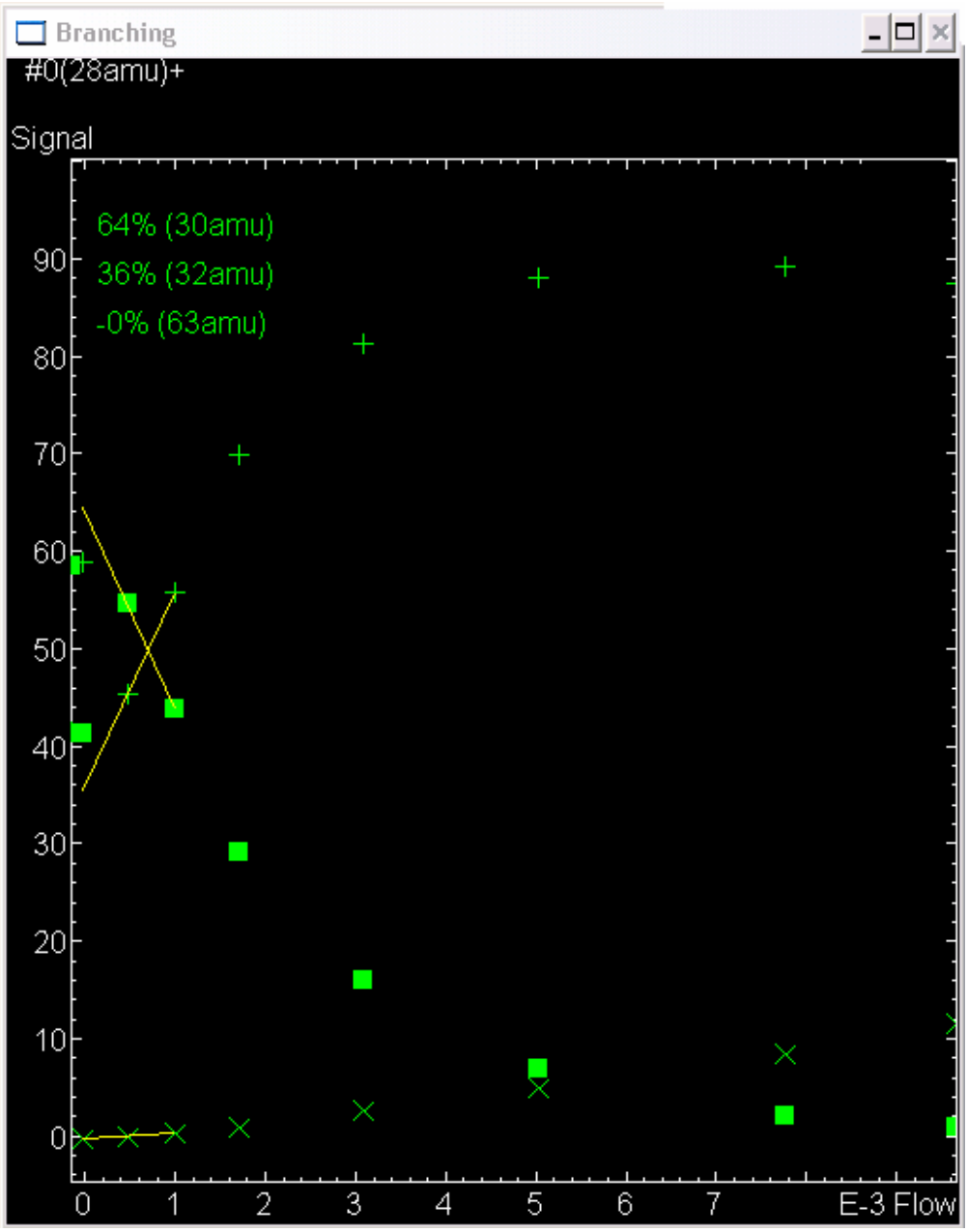

Figure 8.3. *The second panel displays a plot of the product ion ratios at each neutral flow. Extrapolation of the ratios to zero neutral flow gives the branching ratio for the reaction. A value of 0% shown here for m/z 63 indicates that this ion is the product of a secondary reaction.*

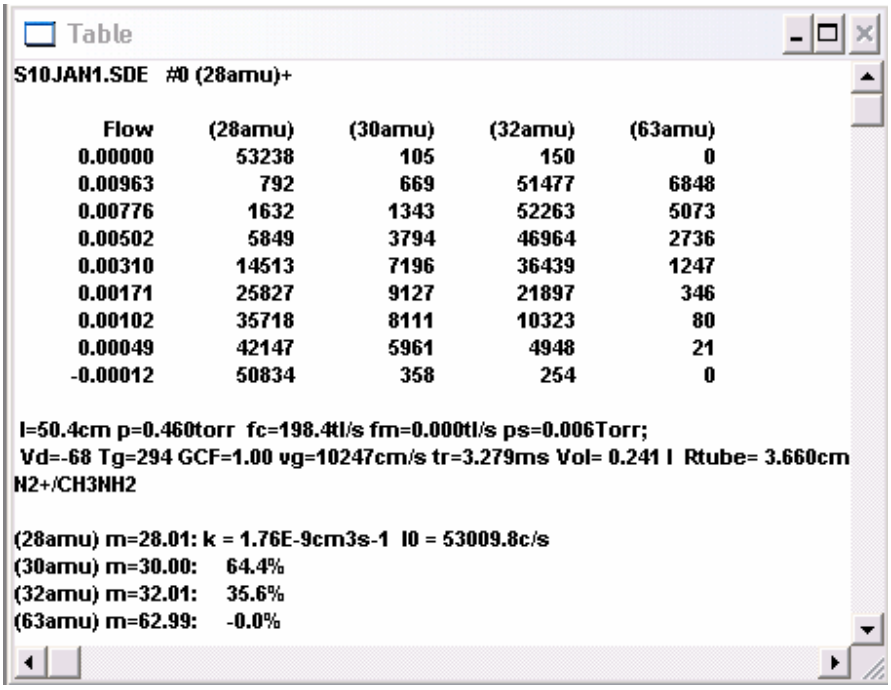

Figure 8.4. *The third panel provides a summary of the data collected, the experimental conditions and the calculated results.*

Sift for Windows is an elegant program that incorporates the key data acquisition requirements for the measurement of SIFT kinetics. The instant analysis and presentation of results is particularly advantageous as the success of an experiment can immediately be gauged. There is no problem with the functionality of the *Sift for Windows* except that it cannot be transferred to a new computer with a modern Windows operating system. To update the computer, the software had to be rewritten in a format compatible with later versions of Windows. Although the software was rewritten in a different programming language, it was designed to closely replicate *Sift for Windows*.

8.3 Experimental

The SIFT operating software has been rewritten in LabVIEW version 7.1, a software package produced by National Instruments (NI).

Hardware

Complimentary hardware was purchased from NI to provide the interface between the SIFT instrument and the software. The software operates on a new computer which runs a Windows XP operating system. The model PCI-6221 plug-in data acquisition

(DAQ) board purchased from NI comes with compatible (NI DAQ-mx) driver software. The board slots inside the computer case and is connected directly to the computer. The DAQ board has 16 analogue input channels, two analogue output channels, twenty four digital input/output (I/O) channels and two counter/timers. The board can receive or output up to ±10 V and has a maximum current drive of 5 mA. Its counters can detect TTL pulses with a minimum width of 12.5 ns.

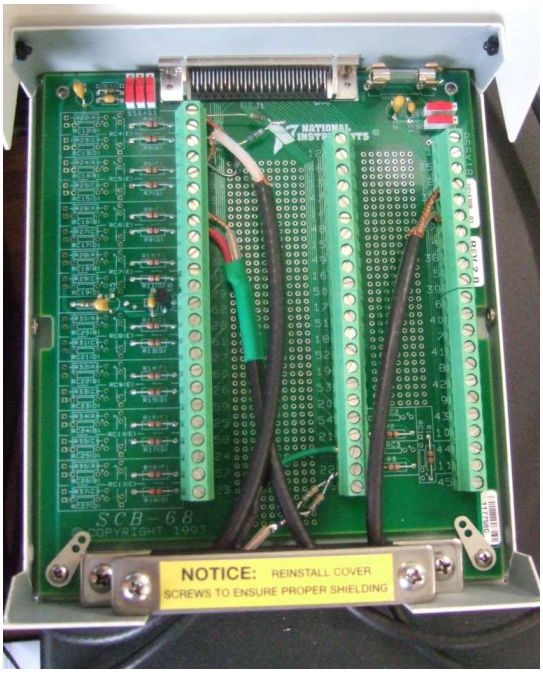

Figure 8.5. *The SCB-68 connector block with four input/output wires connected.*

Also purchased was an NI SCB-68 pin shielded I/O block connector (pictured) for DAQ devices and a compatible cable to link this to the DAQ board. The SCB-68 is the point of physical connection between the SIFT instrument and the computer. Input and output wires screw directly into the numbered pins of the SCB-68 breadboard.

Software

LabVIEW is a graphical programming language in which applications are created with icons rather than lines of text. The language employs 'dataflow programming' where the flow of data guides program execution. This differs from text-based programs where instructions dictate program execution. Programs written in LabVIEW are called visual instruments (abbreviated to VIs). A combination of simple VIs is usually used to build a complete program.

When programming with LabVIEW the programmer is presented with two panels on the screen. The 'Front Panel' is the user interface on which the display of the final program is constructed. The programmer is provided with a set of tools and objects which can be selected and placed on the interface. These include program controls and numerical or graphical indicators. Code is then added on the second panel, called the 'Block Diagram', using graphical representations of functions. Each function is linked to

other parts of the program on the block diagram by a series of ‘wires’ connected by the programmer. The data flows along these wires from one function to the next. In this graphical format the program resembles a flow chart. This is why LabVIEW programming is described as dataflow programming. A very basic working program illustrates these principles in Figures 8.6 and 8.7. The program generates a random number once every second which is displayed in the ‘Output’ **indicator** on the front panel, until the user selects the ‘Stop’ **control**.

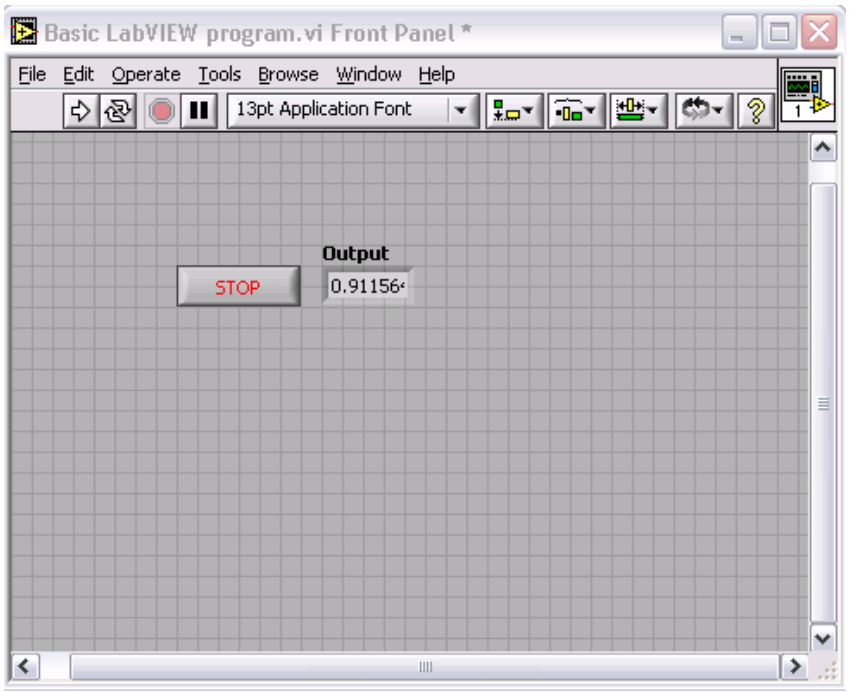

Figure 8.6. *Front panel as seen in the LabVIEW development environment.*

To create this program, a stop button and a numerical indicator are first placed on the front panel. An icon representing each object on the front panel appears on the block diagram. Code is then added to the block diagram to complete the program. Code added to the block diagram is not shown on the front panel. Until icons from the front panel are connected to an appropriate function on the block diagram they are inactive. In this example the ‘Output’ indicator will not display the random number until the output of the random number generator is wired to the ‘Output’ icon on the block diagram.

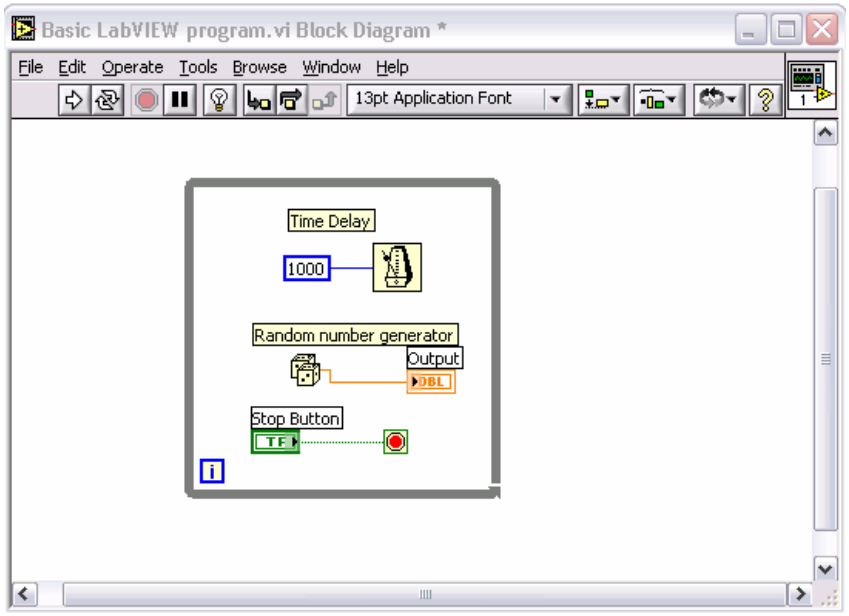

Figure 8.7. *Block Diagram as seen in the LabVIEW development environment. Here code (graphical representations of functions which are then wired in place) is added to activate operational controls and send data to indicators that have been placed on the front panel. The dark grey loop is the graphical representation of a while loop.*

Simple programs or VIs such as these can be saved and given an icon of their own. The program may then be incorporated as a sub-program (sub-VI) within a much larger framework simply by placing the icon on a block diagram and wiring it in place. This feature of LabVIEW prevents complex programs from becoming cluttered with wires and icons. It is much easier identify the overall flow of data and pin-point problems when aspects of a program are compressed into a single icon.

The handling of data acquisition with LabVIEW is made easy by the DAQ Assistant Express VI. Express VIs are ready-made programs (provided as part of the LabVIEW package) designed for specific tasks such as data acquisition. Placing the DAQ Assistant express VI icon on a block diagram opens a control panel containing parameters which are used to configure the VI for a specific task. These tasks include providing an output voltage and signal counting. Once configured, the DAQ Assistant need only be wired in place on the block diagram. The DAQ Assistant is a very useful time saving device for simple DAQ measurements. For more complex procedures the DAQ Assistant is often not ideal as only a limited number of parameters can be modified. To enhance its utility it can be transformed into a sub-VI which allows the programmer to

access to the underlying LabVIEW code from which it was created. It can then be modified as necessary. This can save a lot of time as building a DAQ program from scratch can be time consuming.

LabVIEW programs are simple to construct and can be trialled at any time during their construction. The built-in error-handling software identifies the location of problems that will affect execution and gives detailed information regarding possible solutions. The LabVIEW software also comes with extensive libraries of example code. In addition the NI website provides a forum where novice programmers can obtain advice and example code from professional LabVIEW programmers [219].

8.4 Program Development

The essential features of *Sift for Windows* have been replicated in the new SIFT software. This includes a mass scanning function and a separate function for the measurement of reaction kinetics. Many aspects of the program were developed independently before consolidation into a complete SIFT operating software package. A description of the program's development, features and operation follows.

8.4.1 DAQ Considerations

The three data input/output requirements that form the basis of experimental SIFT kinetics measurements must be considered before the analysis and presentation of data. How the program completes the input/output controls is detailed below. This is followed by a summary of the operation of the mass scanning function and the measurement of reaction kinetics.

Quadrupole Control

The downstream quadrupole is controlled by an Extrel model 270-9 quadrupole power supply. Current directs the quadrupole to transmit ions of a particular mass. The driving current can be set manually with a dial on the front of the quadrupole control or alternatively a suitable mass programmer can supply a driving current through the 'External Command' BNC connector at the rear of the quadrupole control chassis. The mass meter on the front of the quadrupole power supply is deflected full scale (transmitting ions of approximately 200 amu when the supply is set to low mass range) when a current of 1 mA is supplied.

The new software drives the quadrupole to transmit ions of a single mass using a 0 to 10 V output from the DAQ board. The incorporation of a 10 kΩ resistor between the SCB-68 connector board and the external command connector at the rear of the quadrupole power supply produces the appropriate driving current for the quadrupole. For example, a 10 V output passing through the 10 kΩ resistor produces a 1 mA driving current. The full range of output voltages that can be produced by the DAQ board is utilised to maximise the sensitivity of the program to small changes in mass.

Ion Counting

Ions attracted into the particle multiplier generate electrical pulses which are passed to an Advanced Research Instruments F-100T preamplifier/ discriminator. The preamplifier/discriminator outputs standard TTL signals. The frequency of the TTL signals indicates the ion count rate. The signals are fed directly to a counter input on the SCB-68 block connector. The new software measures the TTL signal by edge counting over a very short period. This measurement is scaled to obtain the ion signal in counts per second.

Neutral Reactant Flow Rate

Neutral reactants are added from a calibrated volume in the glass gas handling line to the flow tube through a variable leak valve. Three different calibrated volumes are employed, the choice depending on the rate of the reaction to be measured. The volume used in a kinetics experiment is input by the operator. The flow rate is determined from the change in pressure in the calibrated volume measured by a Validyne model DP 15-20 differential pressure transducer over a measured time. The change over time in the Validyne output voltage is converted to a flow rate by a series of simple calculations performed by the program created with LabVIEW. The response of the Validyne to changes in pressure is calibrated periodically and is included in the calculation of flow rate by the software. The calibration factor can be adjusted by the operator as necessary. It does not need to be input each time an experiment is conducted.

Programmatic control of these above three aspects of the SIFT is relatively simple. What is more complex is the amalgamation of each into a single piece of software which can be used to make SIFT measurements.

8.4.2 Operation of the Mass Scanner

Before a mass spectrum can be measured a reaction must be initiated manually. All of the SIFT's electronic components must be turned on including the high voltage power supply for the particle multiplier and the quadrupole power supply. To complete the measurement of a mass scan the program performs the following sequence. Beginning with the primary screen of the new LabVIEW program, the user selects the control button for the measurement of a mass spectrum (the alternative is to initiate a rate coefficient measurement). Selecting 'Mass Scan' opens the 'Input Parameters' panel shown in Figure 8.8. The user enters the mass range to be examined as well as the time over which this range is to be scanned. The scan time determines the number of data points collected over the range of the scan. Ion counts are usually measured over a very short time and must therefore be scaled to give true count per second values. The mass range will be scanned repeatedly from the lowest to the highest mass unless 'Scan Once' is selected. Several consecutive spectra can be averaged by selecting the 'Average Scans' check box and inputting the number of scans over which to average. This feature is useful for slow reactions which have very low product ion counts - averaging the ion counts over several runs helps to distinguish real ion signals from background noise. The measurement of a mass spectrum is initiated by clicking 'OK' or pressing enter on the keyboard.

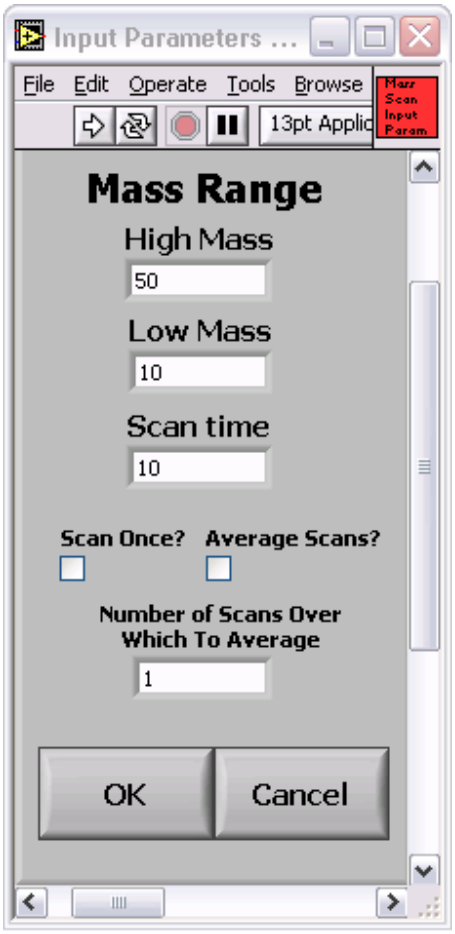

Figure 8.8. *User inputs required to initiate the measurement of a mass spectrum.*

The program outputs a current to drive the quadrupole to transmit ions of a certain mass and the ion counts are measured at that mass. The program then steps to a higher mass and repeats the ion count measurement. This process is continued until the full

range of masses has been scanned with the rate of stepping determined by the scan time input by the operator.

The user interface for the mass spectrum function is shown in Figure 8.9. The mass spectrum is displayed as it is recorded with both the x and y axes automatically scaled to fit the data. Although it is expected that most users will operate the controls by mouse, all of the controls are linked to a key on the keyboard. As an example, by pressing F1 or clicking the Linear Scale control the user can switch between a linear and a logarithmic scale on the ion counts axis.

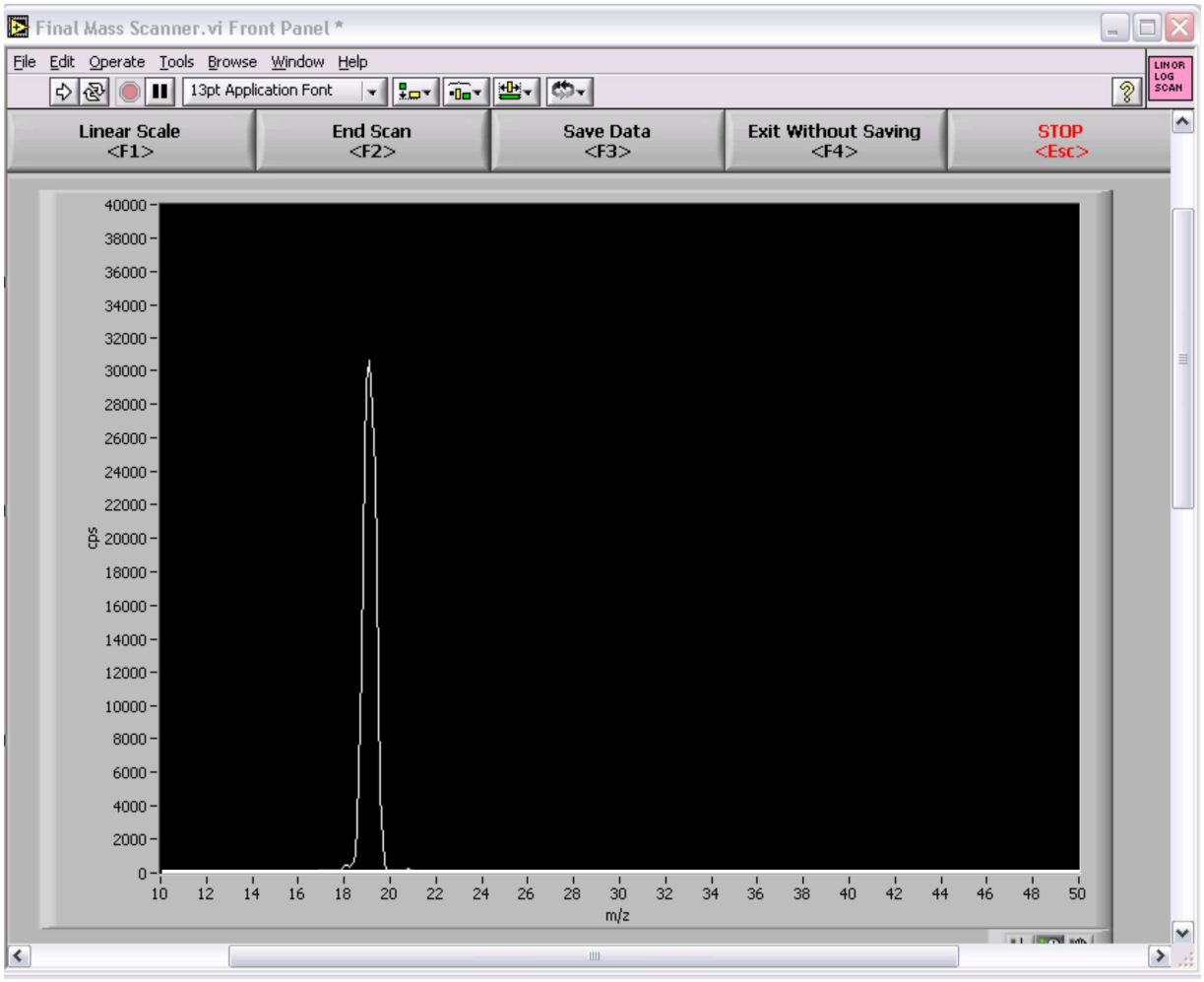

Figure 8.9. *The GUI of the mass spectrum function. The key controls are displayed above the mass spectrum and can be selected by either clicking with the mouse or by using the designated function keys.*

Spectra can be saved as a data file at any time by stopping the scan (F2) and selecting save (F3). The program can be exited at any time by pressing Escape. Exiting the program returns the operator to the initial screen which offers the choice between the measurement of a mass spectrum and a rate coefficient measurement.

A mass spectrum obtained with the new software is shown in Figure 8.10.

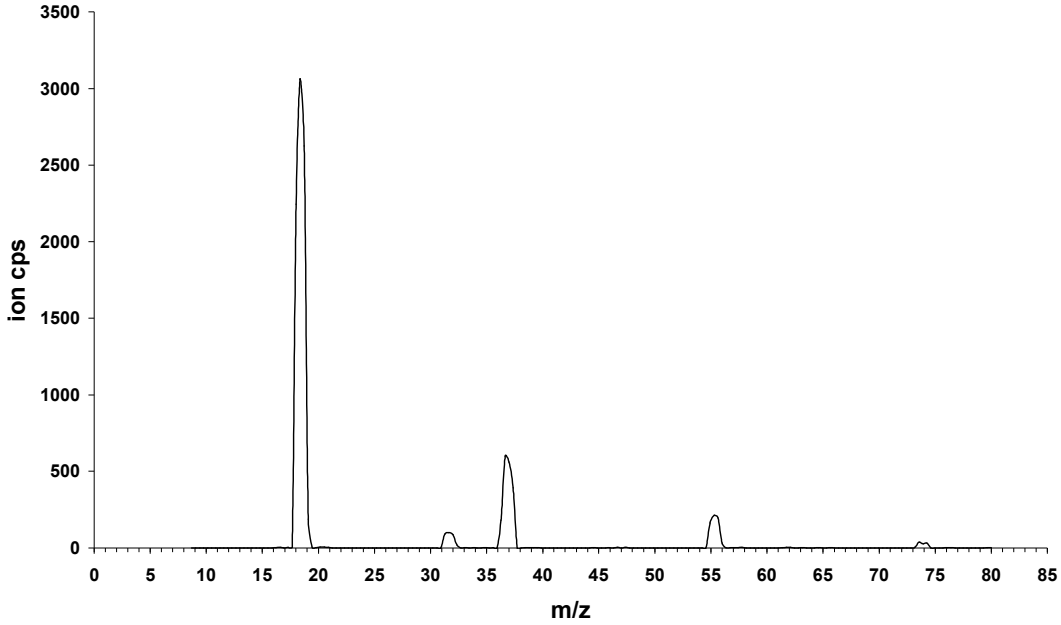

Figure 8.10. *Mass spectrum obtained with the new LabVIEW software. The spectrum shows the reaction of H_3O^+ with air generating water cluster ions $H_3O^+.(H_2O)_n$ at m/z 37, 55 and 73.*

During the measurement of mass scans with the program it was found that the H_3O^+ m/z 19 signal was centred at m/z 18.8. This is not unexpected as the resolution setting of the quadrupole has a significant effect on nominal ion mass. The mass range from m/z 19 to m/z 180 was calibrated by reacting H_3O^+ with compounds that generate products at known masses across this range. A plot of observed mass against true mass demonstrated a clear linear correlation and is shown in Figure 8.11.

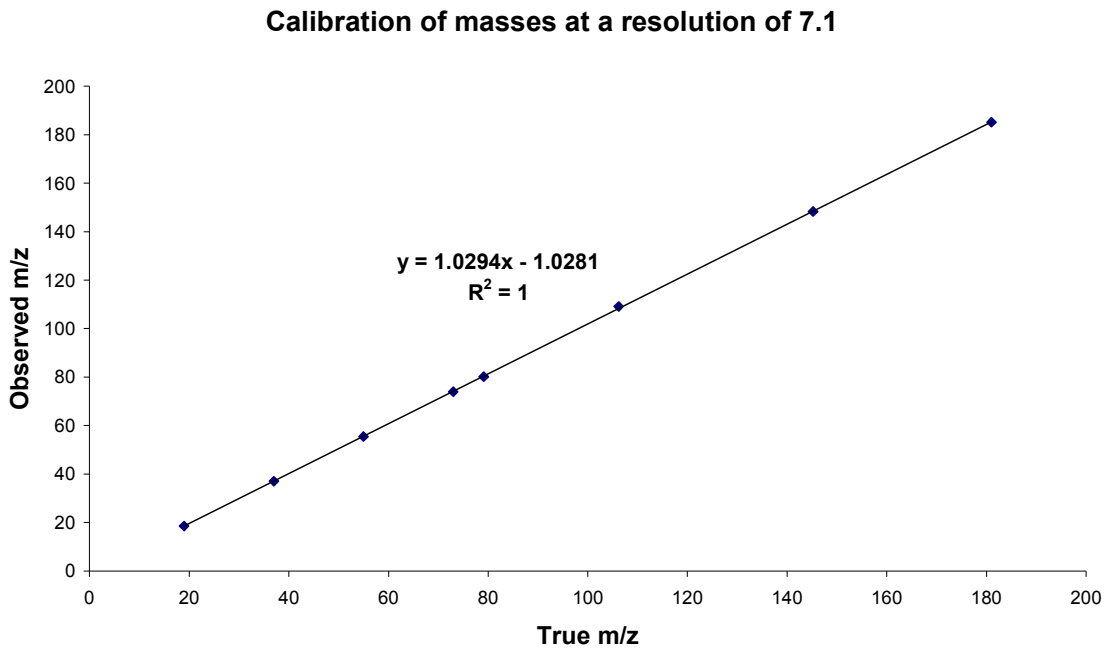

Figure 8.11. *Correlation between nominal ion position measured by the LabVIEW program and the expected ion mass.*

The slope of this plot is used as an adjustment factor to calibrate the mass scale in the final version of the program. Whenever the quadrupole resolution is changed the adjustment factor must be modified accordingly. The parameters for this are embedded within the program but are accessible to the user by selecting the Mass Calibration button (not shown in Figure 8.9).

8.4.3 The Measurement of Kinetics

Before ion-molecule kinetics can be measured, the nominal masses of the reactant ion and product ions must be identified with the mass spectrum function. To calculate the rate coefficient and product branching ratios, ion counts for each of the identified ions are then measured at a series of measured neutral reactant flow rates. In addition to driving the downstream quadrupole and measuring the ion count rates, the flow of neutral reactant must also be measured.

The program is initiated by the user by selecting ‘Measure Rate’ on the initial display screen of the program. A pop-up window (Figure 8.12) invites the user to input the key parameters for the reaction including the nominal primary and product ion

masses. Apart from the ion masses, most of the inputs are usually constant and default values are used as shown in the left hand column of Figure 8.12.

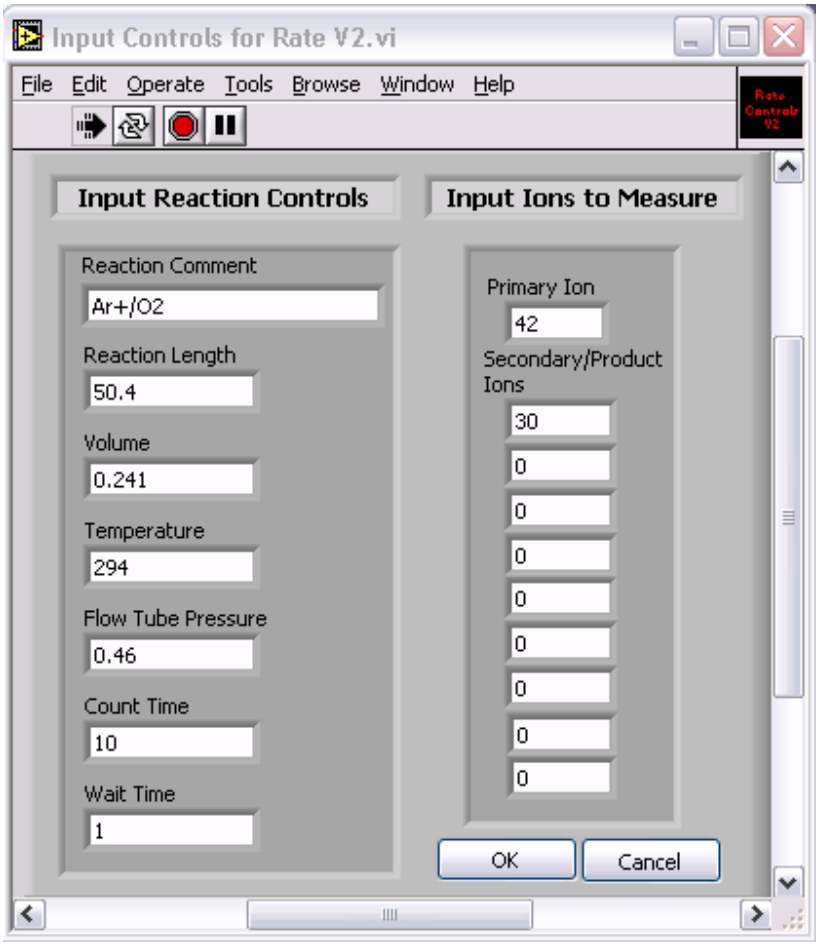

Figure 8.12. *The control panel for a kinetics experiment. The user inputs the parameters necessary for the measurement and calculation of a rate coefficient and product ion branching ratios. Usually the ion and neutral species being examined are input as part of the reaction comment e.g.* Ar^+/O_2.

Having entered these parameters the first data points are measured (the ion counts in the absence of added neutral) by selecting 'OK' or pressing enter on the keyboard. The graphical user interface (GUI) for the rate coefficient program opens (Figure 8.13) and the first results are plotted.

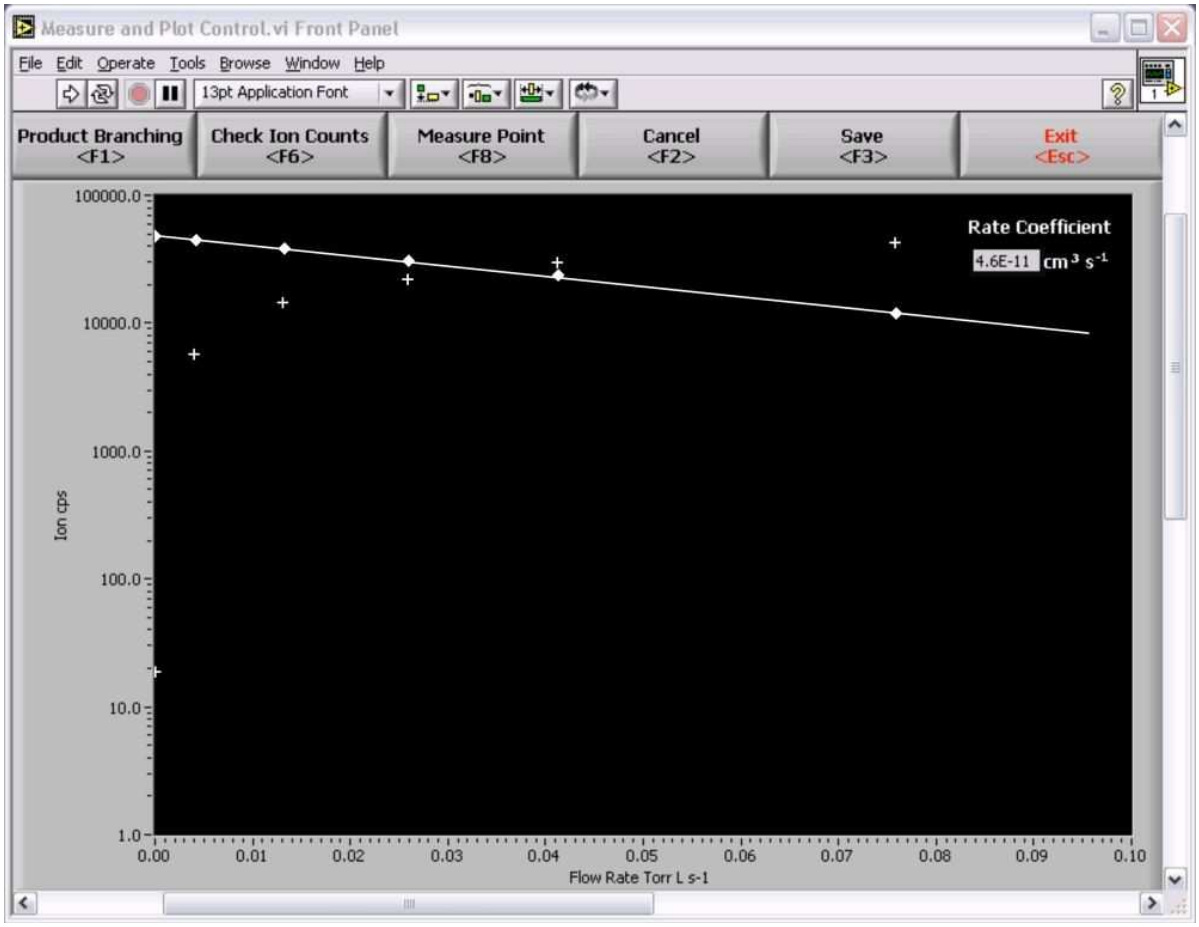

Figure 8.13. *The GUI of the rate coefficient program. The controls for 'Check Ion Counts' and 'Measure Point' (F6 and F8 respectively) are the same as those used for the analogous functions in Sift for Windows. When data are recorded a straight line is fitted through the semi-logarithmic decay of reactant ion signal with increasing neutral flow. The rate coefficient is calculated from the slope of this line and displayed in the upper corner of the GUI.*

The program stops once each ion count has been measured to allow the operator to add the neutral reactant. It is usual to add, initially, sufficient neutral to deplete the primary ion count by ~ 50% by easing open the Varian adjustable leak valve whilst observing the primary ion signal. The ion signal (in counts per second) for any of the ions can be checked at any time (except during the measurement of data, when ion counts are displayed as they are measured) by selecting 'Check Ion Counts' (F6) and then selecting an ion from the list that appears in the pop-up window. The ion signal for the selected ion is displayed. Once sufficient neutral has been added to deplete the primary ion signal, the complete set of ion signals is re-measured by pressing F8. As with *Sift for Windows* the

ion counts are plotted against the neutral flow rate at which they were measured as they are recorded. The neutral flow is then **reduced** and further data collected. This process is repeated until sufficient data is recorded. A control (F1) allows the user to switch between the rate coefficient plot and the plot of product ion ratios. A line of best fit is plotted through the semi-logarithmic decay of primary ion signal with increasing neutral flow and the calculated rate coefficient displayed adjacent to this line. At the completion of data collection the data can be saved (as a data file) by selecting 'Save' (F3). The measurement of data can be stopped at any time by selecting Cancel (F2) and the program closed by pressing 'Exit' (the Escape key). Some data collected with the program is shown in Figure 8.13.

8.5 A Summary of the New Software

The *Sift for Windows* software has been re-written into the LabVIEW programming environment. The new software runs on a modern computer running the Windows XP operating system. The software and associated DAQ hardware have been used to successfully measure mass spectra and rate coefficients for a series of ion-molecule reactions. Although the GUI of the new software is quite different from the original *Sift for Windows* program, the functionality of the new program is essentially the same. The new program can perform all of the tasks necessary to obtain experimental SIFT data.

One of the major advantages of the new mass spectrum recorder is that a data file is now available as output as well as an image of the spectrum. This data file (not available with *Sift for Windows*) will allow spectra to be plotted in styles and formats appropriate to the demands of a publication.

Reaction kinetics are measured and displayed in a manner almost identical to *Sift for Windows*. A control allows an operator to choose whether to view the rate coefficient or product branching ratio measurements. The data file produced when an experimental run is saved includes all of the experimental parameters including temperature, pressure and which of the three calibrated volumes was used, as well as the recorded results.

The basic SIFT operating program created here works well but could be improved. One feature that has not yet been introduced that would be useful is a function

that allows measured data to be re-opened and displayed by the program. Currently saved data can only be re-opened and displayed in certain programs such as Microsoft Excel although images of mass spectra can be opened in a wide variety of programs. It may also be useful if it were possible to delete individual data points during a measurement when a mistake is made by the user.

Although only the important features of *Sift for Windows* have been replicated in the new LabVIEW program, many modifications could potentially be made in the future to enhance its capability and utility (see Section 9.2, Suggestions for Further Work).

CHAPTER 9.

CONCLUSION

9.1 Summary of Results

The original discovery of molecules in the interstellar medium was a surprise as this environment was thought to be too harsh for the formation of stable molecular species. The abundance and complexity of the molecules observed suggested that there were efficient routes to their formation even at very low temperatures and pressures. Ion-neutral chemistry has now been identified as providing the principal molecule-forming chemistry in ISCs [6, 15]. Ion-molecule chemistry also occurs in Titan's atmosphere.

Models of the ion chemistry in ISCs and Titan's atmosphere rely heavily on the laboratory data from which they are constructed, including reaction kinetics and product branching ratios. In this thesis the ion chemistry of several neutral species of relevance to the atmosphere of Titan and ISCs has been examined in the laboratory for the first time. The results of each project are briefly summarised here and some suggestions are given later for further work.

9.1.1. Atomic Carbon

An attempt was made to study the reaction between the most common interstellar ion, H_3^+, and atomic carbon. Extensive attempts to introduce atomic carbon (generated by the application of a microwave discharge to an organic substrate) to the SIFT flow tube were unsuccessful. This was disappointing, especially because carbon atom kinetics have been examined previously using this type of atom source [89, 98, 100]. An RF discharge was also tried but found to be less effective than the microwave discharge. The deposition of soot on the walls of the discharge tube provided indirect evidence of carbon atom formation but the atoms were not observed to reach the flow tube just centimetres away. Given that the soot formation was concentrated around the microwave discharge

plasma, it was thought that ions from the discharge plasma may have affected (increased) the rate of atom recombination.

At this point it was decided that another method of atom generation should be attempted. Photolysis of carbon suboxide using an ArF excimer laser was proposed as an alternative method of carbon atom formation. A laser would not produce large quantities of ions in the region of the decomposition (although some photo-ions would be expected) and as such the dissociation could be performed much closer to the flow tube, reducing the time available for atom recombination. This method was not employed earlier because the laser apparatus is large and much more difficult to couple with the SIFT than the simple equipment used in the microwave discharge experiments. Unfortunately the laser photolysis experiments were not completed due to a lack of the necessary gases needed for the operation of the laser.

The lack of success in generating carbon atoms by microwave discharge reinforces previous reports that carbon atoms are difficult to study in the laboratory. It is regrettable that the laser photolysis method could not be pursued further as it presented the best chance of producing sufficient carbon atoms for reaction.

9.1.2. Titan's Ion Chemistry

The successful *Cassini-Huygens* mission to Titan has provided new data on the composition of Titan's atmosphere and ionosphere. These results have demonstrated that many more nitrogen-containing species are present in Titan's atmosphere than had been predicted by pre-*Cassini* models. In order to improve models of the atmosphere, the ion chemistry of three of the newly-identified molecules (cyanodiacetylene, methylenimine and propionitrile) has been examined in the laboratory for the first time. The same three molecules have been identified in ISCs and thus this chemistry is also relevant to these environments.

The results of the *Cassini-Huygens* mission also identified several (miscellaneous) individual reactions as being of potential importance to Titanian models. Kinetics for this disparate mix of reactions were studied during this thesis as they were requested by Roger Yelle and Veronique Vuitton of the *Cassini-Huygens* mission [170]. These reactions are summarised in Chapter 6.

The reactivity of cyanodiacetylene (HC_5N) with the principal ions present in Titan's atmosphere and with some key interstellar ions, is described in Chapter 4. A pure sample of HC_5N was successfully produced for this work following the newly published method of Guillemin and Trolez [135]. A slight modification to the published method was necessary after it was discovered that the pure sample was obtained in a cold trap cooled to -30 °C rather than -78 ºC as reported.

Proton transfer reactions dominated the chemistry that has been examined and this was not unexpected. As the chemistry of Titan's ionosphere is governed by proton transfer reactions, the fate of HC_5N in this environment is determined by its proton affinity (PA). No value for the PA of HC_5N was available in the literature [174]. For this reason an estimate of this value has been determined. Bracketing experiments were performed in addition to a theoretical investigation of the PA. From the combined results of these investigations, the PA of HC_5N has been estimated to be 770 ± 20 kJ mol^{-1}.

Chapter 5 examines the fate of methylenimine (CH_2NH) and propionitrile (C_2H_5CN) with ions relevant to Titan's ionospheric chemistry. Propionitrile is a stable liquid under standard conditions and a sample was obtained from a commercial source and the relevant ion chemistry examined. Again proton transfer reactions were predominant with association channels also evident with many of the hydrocarbon ions.

Methylenimine is unavailable from commercial sources because it is a transient species and it must therefore be produced as it is required. In this work methylenimine (CH_2NH) was produced from the pyrolysis of methylamine (CH_3NH_2) at around 1400 ºC. Because the flow of CH_2NH could not be established, absolute rate coefficients could not be measured. They have instead been estimated relative to the corresponding values for rates of reaction of CH_3NH_2, based on an iterative method. As the vast majority of the reactions examined included an exothermic proton transfer channel it was with confidence that the rate coefficients for methylenimine have been estimated as proceeding at the respective collision rates. Like C_2H_5CN, association reactions were observed in competition with proton transfer with many of the hydrocarbon ions.

Some of the most interesting chemistry observed was that with ions not having a transferable proton. The reaction of N^+ with HC_5N and the reactions of N^+ and N_2^+ with C_2H_5CN were observed to have product channels in which it was apparent that the strong

CN bond in the neutral was broken. The stability of the (presumed) neutral products of these reactions clearly makes the reactions sufficiently exothermic to permit the thermodynamically unfavourable CN bond breakage.

9.1.3 Other Topics

Some proton transfer equilibrium studies are included in Chapter 6. The results of this work have provided new estimates for the gas phase basicities of propyne and acetylene from which their relative PAs can be estimated. The position of both of these species in scales of gas phase basicities (and relative proton affinities) was uncertain and these experiments should make these values more reliable. The GB of propyne was determined to be 681 kJ mol^{-1} and the GB of acetylene 617.4 kJ mol^{-1}.

Chapter 7 represents a slight digression from the theme of planetary and interstellar ion chemistry. The discovery that SIFT chemistry can be made to work in reverse has opened a new field in analytical chemistry for the SIFT technique. If reaction kinetics are known for a particular ion-analyte reaction, the absolute concentration of the analyte can be calculated from the intensity of the product ion signal(s) generated by the analyte. The choice of reagent ion plays a key role in this procedure. Optimal quantitation is achieved when the trace gas reacts rapidly with the ion to produce a unique ion product. Specificity is improved by having more than one reagent ion to choose from. As part of this thesis, lithium ions (Li^+) were investigated to determine if they would be a useful addition to the three currently used reagent ions, H_3O^+, O_2^+ and NO^+.

Li^+ ions were found to associate with each of the analytes studied forming adduct ions. These association reactions were observed to be rapid with large hydrocarbons (having more than 12 atoms) but much slower with smaller species. Many of the adduct ions (Li^+.X, where X is the analyte molecule) were observed to react rapidly with water. Because the binding energy of water with Li^+ was greater than the binding energy of many of the other analytes examined, water tended to ‘switch out’ the trace gas in the adduct leaving only $Li^+.H_2O$. Because trace gas samples always contain varying degrees of humidity it has been concluded that Li^+ would not be a suitable precursor ion for SIFT-MS trace gas analysis.

Finally, the software used to operate the UC SIFT was rewritten as part of this work. The new software has been used successfully to record mass spectra and to obtain and plot rate coefficient data. This is described in Chapter 8.

9.2 Suggestions for Further Work

Interstellar chemistry is a substantial topic and whilst ion-chemistry is just one branch of this, it is considered the most important route by which molecules are formed in interstellar clouds [15]. Carbon is the fourth most abundant species in the interstellar medium yet our understanding of the role of neutral carbon atoms in interstellar ion chemistry is limited. This is principally because of the there have been very few laboratory studies atomic carbon kinetics because of difficulties associated with generating atomic carbon in the gas phase. Although theoretical calculations have been reported there is no substitute for a laboratory measurement. It is essential that further attempts to examine ion-carbon atom kinetics in the laboratory are pursued to establish the importance of carbon in interstellar ion chemistry.

The only impediment to a SIFT study of ion-atomic carbon reactions is the lack of a method capable of producing a continuous flow of atoms in sufficient quantity for reaction. Whilst it has been established in this thesis that a microwave discharge cannot be used as a convenient source of carbon atoms for SIFT experiments, the same cannot be said of photolysis methods. Following on from the work presented in this thesis, a concerted effort to synchronize a laser carbon atom source with a SIFT should provide the best chance of measuring atomic carbon kinetics at thermal temperatures with the SIFT.

Our understanding of Titan has advanced considerably in the three decades since the *Voyager* spacecraft first revealed the true nature of Titan's atmosphere. The updated data provided by the recent *Cassini-Huygens* mission has highlighted just how complex the chemistry occurring in the ionosphere is, with many more species identified than were predicted. Following analysis of the data, three neutral species have been proposed as the source of some of the unexpected ion density in Titan's ionosphere: methylenimine, cyanodiacetylene and propionitrile. The chemistry of these species has been examined to determine the reactivity of these neutrals with ions in Titan's ionosphere. As more of the

previously unidentified neutrals are recognized, their ion-chemistry (if not already known) must be established. The process of identifying new neutral molecules in Titan's atmosphere and examining their reactivity is on-going. The chemistry of each species must be established if a greater understanding of this unique environment is to be achieved. This should provide a considerable source of work in the future for scientists in the field of ion-molecule kinetics. Exactly the same situation exists regarding molecules in interstellar clouds, with new molecules continually being identified. Future workers in the SIFT laboratory should not have to wait long for more such neutrals to be identified.

The quantitation of trace gases by a technique known as SIFT-MS was touched on only briefly in this thesis. In the future it may be necessary to develop more precursor ions than the current three, particularly for specific applications. Negative ions have been proposed as prime candidates for the detection of molecules used as fumigants that contain halogen atoms. Databases of ion-molecule chemistry contain mostly positive ion-molecule reactions [67, 84]. If negative ions are found to be useful it is likely that a significant amount of negative ion-molecule chemistry will need to be studied so that analytes can be detected and quantified.

SIFT-MS can be applied to the detection of volatile analytes in diverse applications that include food and flavour chemistry, the environment including air, metabolites on human breath and the detection of fumigants. The number of analytes is continually increasing as new applications are found; so there is a constant demand kinetic analysis of the new analytes with H_3O^+, O_2^+ and NO^+ so that quantification can be performed. This will provide many opportunities for research in the future.

The demand for laboratory measurements of ion-neutral kinetics by investigators of ISC chemistry, Titan's atmosphere and practitioners of SIFT-MS is endless. The details of potential future work in these areas described above are intentionally non-specific, as most of the chemistry required is identified by other scientists. More specific proposals for future work can be given regarding the newly-written SIFT operating software. Currently the software performs the basic functions required to record mass spectra and measure reaction kinetics. The most pressing issue is that neither mass spectra nor kinetic data can be re-opened with the program once saved as a data file. This would be a useful feature for mass spectra as the LabVIEW graphing function has

controls which allow the user to zoom in on the mass spectra, possibly revealing obscured details. A re-open function would also be useful for kinetics data as presently the data must be re-plotted using a program such as Excel before observation of the data can be made. It would also be useful if kinetics data could be manipulated during an experiment. Sometimes an operator will make an error such as forgetting to open a gas tap in the neutral inlet line, resulting in an erroneous measurement of a neutral flow rate. The result is usually a disorderly plot and an inaccurate rate coefficient. Currently the only way to rectify this is to delete such points when working up the data in another program, usually Excel. It is likely that other minor adjustments will be necessary as the functionality of the program is tested in the future.

REFERENCES

[1]. C. Y. Johnson, E. B. Meadows and J. C. Holmes, *J. Geophys. Res.*, **63**, (1958) 443-444

[2]. E. E. Ferguson, F. C. Fehsenfeld and D. L. Albritton, *Gas Phase Ion Chemistry Volume 1*, M. T. Bowers, Ed; Academic Press, New York, (1979)

[3]. E. Herbst, *Ann. Rev. Phys. Chem.*, **46**, (1995) 27-53

[4]. T. P. Snow and V. M. Bierbaum, *Ann. Rev. Anal. Chem.*, **1**, (2008) 229-259

[5]. T. P. Snow and B. J. McCall, *Ann. Rev. Astron. Astrophys.*, **44**, (2006) 367-414

[6]. W. W. Duley and D. A. Williams, *Interstellar Chemistry*, Academic Press Inc. (London) Ltd, London, (1984)

[7]. E. Herbst, *Chem. Soc. Rev.*, **30**, (2001) 168-176

[8]. H.-H. Lee, R. P. A. Bettens and E. Herbst, *Astron. Astrophys. Supp. Ser.*, **119**, (1996) 111-114

[9]. M. C. McCarthy, C. A. Gottlieb, H. Gupta and P. Thaddeus, *Astrophys. J. Lett.*, **652**, (2006) L141-144

[10]. R. P. A. Bettens and M. A. Collins, *J. Chem. Phys.*, **108**, (1998) 2424-2433

[11]. R. P. A. Bettens and M. A. Collins, *J. Chem. Phys.*, **114**, (2001) 6490

[12]. D. Talbi and D. J. DeFrees, *Chem. Phys. Lett.*, **179**, (1991) 165-168

[13]. D. Talbi, D. J. DeFrees, D. A. Egolf and E. Herbst, *Astrophys. J.*, **374**, (1991) 390-393

[14]. J. Semaniak, A. Larson, A. Le Padellec, C. Stromholm, M. Larsson, S. Rosen, R. Peverall, H. Danared, N. Djuric, D. H. Dunn and S. Datz, *Astrophys. J.*, **498**, (1998) 886-895

[15]. E. Herbst and W. Klemperer, *Astrophys. J.*, **185**, (1973) 505-533

[16]. D. A. Williams and E. Herbst, *Surface Sci.*, **500**, (2002) 823-827

[17]. D. C. B. Whittet, W. A. Schutte, A. G. G. M. Tielens, A. C. A. Boogert, T. de Graauw, P. Ehrenfreund, P. A. Gerakines, F. P. Helmich, T. Prusti and E. F. van Dischoeck, *Astron. Astrophys.*, **315**, (1996) L357

[18]. J. H. Black and A. Dalgarno, *Astrophys. J. Suppl. Ser.*, **34**, (1977) 405-423

[19]. I. W. M. Smith, *Int. J. Mass Spec. Ion Proc.*, **149**, (1995) 231-249

[20]. E. F. van Dischoeck and J. H. Black, *Astrophys. J. Suppl. Ser.*, **62**, (1986) 109-145

[21]. G. P. Kuiper, *Astrophys. J.*, **100**, (1944) 378

[22]. A. Coustensis and F. Taylor, *Titan: The Earth-Like Moon*, World Scientific, Singapore, (1999)

[23]. cassini-huygens.jpl.nasa.gov/science/titan.cfm

[24]. J. Caldwell, *Planetary Satellites*, J. A. Burns, Ed; The University of Arizona Press, Tucson, (1977)

[25]. D. M. Hunten, *Planetary Satellites*, J. A. Burns, Ed; The University of Arizona Press, Tucson, (1977)

[26]. E. H. Wilson and S. K. Atreya, *J. Geophys. Res.*, **109**, (2004) E06002

[27]. Y. Yung, M. Allen and J. P. Pinto, *Astrophys. J. Suppl. Ser.*, **55**, (1984) 465-506

[28]. M. Fulchignoni, F. Ferri, F. Angrilli, A. J. Ball, A. Bar-Nun, M. A. Barucci, C. Bettanini, G. Bianchini, W. Borucki, G. Colombatti, M. Coradini, A. Coustenis, S. Debei, P. Falkner, G. Fanti, E. Flamini, V. Gaborit, R. Grard, M. Hamelin, A. M. Harri, B. Hathi, I. Jernej, M. R. Leese, A. Lehto, P. F. L. Stoppato, J. J. Lopez-Moreno, T. Makinen, J. A. M. McDonnell, C. P. McKay, G. Molina-Cuberos, F. M. Neubauer, V. Pirronello, R. Rodrigo, B. Saggin, K. Schwingenschuh, A. Seiff, F. Simoes, H. Svedhem, T. Tokano, M. C. Towner, R. Trautner, P. Withers and J. C. Zarnecki, *Nature*, **438**, (2005) 785-791

[29]. L. M. Lara, E. Lellouch, J. J. Lopez-Moreno and R. Rodrigo, *J. Geophys. Res.*, **101**, (1996) 261

[30]. D. Toublanc, J. P. Parisot, J. Brillet, D. Gautier, F. Raulin and C. P. McKay, *Icarus*, **113**, (1995) 2-26

[31]. C. N. Keller, T. E. Cravens and L. Gan, *J. Geophys. Res.*, **97**, (1992) 12117-12135

[32]. G. F. Lindal, G. E. Wood, H. B. Hotz and D. N. Sweetman, *Icarus*, **53**, (1983) 348

[33]. A. F. Nagy and T. E. Cravens, *Planet. Space Sci.*, **46**, (1998) 1149

[34]. C. N. Keller, V. G. Anicich and T. E. Cravens, *Planet. Space Sci.*, **46**, (1998) 1157

[35]. M. K. Bird, R. Dutta-Roy, S. W. Asmar and T. A. Rebold, *Icarus*, **130**, (1997) 426-436

[36]. L. A. Capone, R. C. Whitten, J. Dubach, S. S. Prasad and W. T. J. Huntress, *Icarus*, **28**, (1976) 367-378

[37]. L. A. Capone, S. S. Prasad, W. T. J. Huntress, R. C. Whitten, J. Dubach and K. Santhanam, *Nature*, **293**, (1981) 45-46

[38]. M. J. McEwan and V. G. Anicich, *Mass Spec. Rev.*, **26**, (2007) 281-319

[39]. D. F. Strobel, *Icarus*, **21**, (1974) 466

[40]. Y. Yung, M. Allen and J. P. Pinto, *Icarus*, **72**, (1987) 468

[41]. W.-H. Ip, *Astrophys. J.*, **362**, (1990) 354-63

[42]. V. G. Anicich and W. T. J. Huntress, *Astrophys. J. Suppl. Ser.*, **62**, (1986) 553

[43]. J. L. Fox and R. V. Yelle, *Geophys. Res. Lett.*, **24**, (1997) 2179-2182

[44]. D. F. Strobel and M. Summers, *Icarus*, **100**, (1992) 512

[45]. V. G. Anicich and M. J. McEwan, *Planet. Space Sci.*, **45**, (1997) 897-921

[46]. M. Banaszkiewicz, L. M. Lara, R. Rodrigo, J. J. Lopez-Moreno and G. J. Molina-Cuberos, *Icarus*, **147**, (2000) 386-404

[47]. J.-P. Lebretton, O. Witasse, C. Sollazzo, T. Blancquaert, P. Couzin, A.-M. Schipper, J. B. Jones, D. L. Matson, L. I. Gurvits, D. H. Atkinson, B. Kazeminejad and M. Perez-Ayucar, *Nature*, **438**, (2005) 758-764

[48]. E. R. Stofan, C. Elachi, J. I. Lunine, R. D. Lorenz, B. Stiles, K. L. Mitchell, S. Ostro, L. Soderblom, C. Wood, H. Zebker, S. Wall, M. Janssen, R. Kirk, R. Lopes, F. Paganelli, J. Radebaugh, L. Wye, Y. Anderson, M. Allison, R. Boehmer, P. Callahan, P. Encrenaz, E. Flamini, G. Francescetti, Y. Gim, G. Hamilton, S. Hensley, W. T. K. Johnson, K. Kelleher, D. Muhleman, P. Paillou, G. Picardi, F. Posa, L. Roth, R. Seu, S. Shaffer, S. Vetrella and R. West, *Nature*, **445**, (2007) 61-64

[49]. J. H. J. Waite, W. S. Lewis, W. T. Kasprzak, V. G. Anicich, B. P. Block, T. E. Cravens, G. G. Fletcher, W.-H. Ip, J. G. Luhmann, R. L. McNutt, H. B. Niemann, J. K. Parejko, J. E. Richards, R. L. Thorpe, E. M. Walter and R. V. Yelle, *Space Sci. Rev.*, **114**, (2004) 113-231

[50]. *Preliminary Cassini Results*, *Science*, **308**, (2005) 969-992

[51]. T. E. Cravens, T. P. Robertson, J. H. J. Waite, R. V. Yelle, W. T. Kasprzak, C. N. Keller, S. A. Ledvina, H. B. Niemann, J. G. Luhmann, R. L. McNutt, W.-H. Ip, V. De La Haye, I. Mueller-Wodarg, J.-E. Wahlund, V. G. Anicich and V. Vuitton, *Geophys. Res. Lett.*, **33**, (2006) L07105

[52]. photojournal.jpl.nasa.gov/catalog/PIA07865

[53]. F. C. Fehsenfeld, A. L. Smeltekopf, P. D. Goldan, H. I. Schiff and E. E. Ferguson, *J. Chem. Phys.*, **44**, (1966) 4087

[54]. F. C. Fehsenfeld, A. L. Smeltekopf, P. D. Goldan, H. I. Schiff and E. E. Ferguson, *J. Chem. Phys.*, **44**, (1966) 4095

[55]. J. K. Kim, V. G. Anicich and W. T. J. Huntress, *J. Phys. Chem.*, **81**, (1977) 1798-1805

[56]. D. Smith and N. G. Adams, *Gas Phase Ion Chemistry Volume 1*, M. T. Bowers, Ed; Academic Press, New York, (1979)

[57]. M. Mautner, *Gas Phase Ion Chemistry Volume 1*, M. T. Bowers, Ed; Academic Press, New York, (1979)

[58]. T. Su and M. T. Bowers, *Gas Phase Ion Chemistry Volume 1*, M. T. Bowers, Ed; Academic Press, Inc., New York, (1979)

[59]. T. Su and W. J. Chesnavich, *J. Chem. Phys.*, **76**, (1982) 5183

[60]. D. B. Milligan, *Ph.D. Thesis*, University of Canterbury, (2000).

[61]. S. A. H. Petrie, *Ph.D. Thesis*, University of Canterbury, (1991).

[62]. G. B. I. Scott, *Ph.D. Thesis*, University of Canterbury, (1997).

[63]. D. A. Fairley, *Ph.D. Thesis*, University of Canterbury, (1998).

[64]. N. G. Adams and D. Smith, *Int. J. Phys. B*, **9**, (1976) 1439

[65]. N. G. Adams and D. Smith, *Int. J. Mass. Spec. Ion Phys.*, **21** (1976) 349

[66]. D. Smith and N. G. Adams, *Adv. At. Mol. Phys.*, **24**, (1988) 1

[67]. V. G. Anicich, *J. Phys. Chem. Ref. Data*, **22**, (1993) 1469

[68]. P. Španěl and D. Smith, *J. Am. Soc. Mass. Spec.*, **12**, (2001) 863-72

[69]. D. R. Lide, *Handbook of Chemistry and Physics 80th Edition*, Chemical Rubber Company Press, Boca Raton, (1999)

[70]. S. G. Lias, J. E. Bartmess, J. F. Liebman, J. L. Holmes, R. D. Levin and W. G. Mallard, *J. Phys. Chem. Ref. Data.*, **17**, Supplement #1 (1998)

[71]. http://webbook.nist.gov/chemistry/

[72]. T. P. Snow and V. M. Bierbaum, *Ann. Rev. Anal. Chem.*, **1**, (2006) 229-259

[73]. A. G. G. M. Tielens, *Dust and Chemistry in Astronomy*, T. J. Millar and D. A. Williams, Ed; Institute of Physics, Philadelphia, (1993)

[74]. E. Herbst and C. M. Leung, *Astrophys. J. Supp. Ser.*, **69**, (1989) 271

[75]. J. H. Black and A. Dalgarno, *Astrophys. J. Supp. Ser.*, **34**, (1977) 405-423

[76]. D. Smith, *Chem. Rev.*, **92**, (1992) 1473-85

[77]. D. Gerlich and S. Horning, *Chem. Rev.*, **92**, (1992) 1509-1539

[78]. E. Herbst, J. G. Schubert and P. R. Certain, *Astrophys. J.*, **213**, (1977) 696

[79]. M. Elitzur and W. D. Watson, *Astrophys. J.*, **222**, (1978) L141-L144

[80]. R. Gredel, E. F. v. Dishoeck and J. H. Black, *Astron. Astrophys.*, **269**, (1993) 477-495

[81]. D. K. Bohme, *Interactions between Ions and Molecules*, P. Ausloos, Ed; Plenum, New York, (1975)

[82]. A. A. Viggiano, F. Howorka, D. L. Albritton, F. C. Fehsenfeld, N. G. Adams and D. Smith, *Astrophys. J.*, **236**, (1980) 492-497

[83]. F. C. Fehsenfeld, *Astrophys. J.*, **209**, (1976) 628

[84]. Y. Ikezoe, S. Matsuoka, M. Takebe and A. A. Viggiano, *Gas Phase Ion-Molecule Rate Constants Through 1986*, Maruzen, Tokyo, (1987)

[85]. D. B. Milligan and M. J. McEwan, *Chem. Phys. Lett.*, **319**, (2000) 482-485

[86]. M. Sablier and C. Rolando, *Mass Spec. Rev.*, **12**, (1993) 285-312

[87]. W. Brennen and E. C. Shane, *J. Phys. Chem.*, **75**, (1971) 1552-1564

[88]. J. E. Morgan and H. I. Schiff, *J. Chem. Phys.*, **38**, (1963) 1495-1500

[89]. F. F. Martinotti, M. J. Welch and A. P. Wolf, *Chem. Comm.*, (1968) 115-116

[90]. P. S. Skell and R. R. Engel, *JACS*, **87**, (1965) 1334

[91]. A. P. Wolf, *Adv. Phys. Org. Chem.*, **2**, (1964) 201

[92]. W. Braun, A. M. Bass, D. D. Davis and J. D. Simmons, *Proc. Roy. Soc. A.*, **312**, (1969) 417-434

[93]. D. Husain and L. J. Kirsch, *Trans. Faraday Soc.*, **67**, (1971) 2025-2035

[94]. R. I. Kaiser and A. G. Suits, *Rev. Sci. Instrum.*, **66**, (1995) 5405-5411

[95]. D. Gerlich, I. Savić and I. Čermák, *Int. J. Mass. Spec.*, **240**, (2005) 139-147

[96]. P. B. Shevlin, *JACS*, **94**, (1972) 1379-1380

[97]. W. B. Hurt and W. C. Grable, *J. Chem. Phys.*, **57**, (1972) 734-737

[98]. G. Dorthe, P. Caubet, T. Vias, B. Barrère and J. Marchais, *J. Phys. Chem.*, **95**, (1991) 5109-5116

[99]. D. Husain and L. J. Kirsch, *J. Photochem.*, **2**, (1973/74) 297-308

[100]. H. Sekiya, T. Masaharu and Y. Nishimura, *J. Chem. Phys.*, **83**, (1985) 2857-2859

[101]. T. Fujii and M. Kareev, *J. Appl. Phys.*, **89**, (2001) 2543-2546

[102]. D. Smith and P. Španěl, *Int. J. Mass. Spec. Ion. Proc.*, **129**, (1993) 163

[103]. T. P. Snow, V. Le Page, Y. Keheyan and V. M. Bierbaum, *Nature*, **391**, (1998) 259-260

[104]. N. Haider and D. Husain, *Int. J. Chem. Kin.*, **25**, (1993) 423-435

[105]. A. Bergeat and J.-C. Loison, *Phys. Chem. Chem. Phys.*, **3**, 2038-2042 (2001)

[106]. J. L. Sprung, S. Winstein and W. F. Libby, *JACS*, **87**, (1965) 1812-1813

[107]. H. F. Bettinger, P. v. R. Schleyer, H. F. Schaefer III, P. R. Schreiner, R. I. Kaiser and Y. T. Lee, *J. Chem. Phys.*, **113**, (2000) 4250-4264

[108]. E. Y. Y. Lam, P. Gaspar and A. P. Wolf, *J. Phys. Chem.*, **75**, (1971) 445-7

[109]. F. A. Miller and D. H. Mellon, *Spectrochim. Acta*, **23A**, (1967) 1415-1423

[110]. J. McFarlane, J. C. Polanyi, J. G. Shapter and J. M. Williamson, *J. Photochem. Photobio. A: Chem.*, **46**, (1989) 139-58

[111]. N. Washida, H. Akimoto and I. Tanaka, *App. Optics*, **9**, (1970) 1711-1712

[112]. J. A. R. Samson, *Techniques of Vacuum Ultraviolet Spectroscopy*, John Wiley & Sons, Inc., New York, (1967)

[113]. G. Winnewisser and C. M. Walmsley, *Astrophys. & Space Sci.*, **65**, (1979) 83-93

[114]. M. B. Bell, P. A. Feldman, S. Kwok and H. E. Matthews, *Nature*, **295**, (1982) 389-391

[115]. N. Winstanley and L. A. M. Nejad, *Astrophys. & Space Sci.*, **240**, (1996) 13-37

[116]. E. Herbst and C. M. Leung, *Astrophys. J. Suppl. Ser.*, **69**, (1989) 271

[117]. E. Herbst and C. M. Leung, *Astron. Astrophys.*, **233**, (1990) 177-180

[118]. G. Winnewisser, M. Winnewisser and J. J. Christiansen, *Astron. Astrophys.*, **109**, (1982) 141-144

[119]. S. W. Stahler, *Astrophys. J.*, **281**, (1984) 209-18

[120]. A. Jolly, Y. Benilan and A. Fayt, *Molecules in Space and Laboratory Conference*, Paris, France, (2007)

[121]. G. J. Molina-Cuberos, K. Schwingenschuh, J. J. Lopez-Moreno, R. Rodrigo, L. M. Lara and V. Anicich, *J. Geophys. Res.*, **107**, (2002)

[122]. P. Coll, D. Coscia, N. Smith, M.-C. Gazeau, S. I. Ramirez, G. Cernogora, G. Israel and F. Raulin, *Planet. Space Sci.*, **47**, (1999) 1331-1340

[123]. R. Hanel, B. Conrath, F. M. Flasar, V. Kunde, W. Maguire, J. C. Pearl, J. Pirraglia, R. Samuelson, L. Herath, M. Allison, D. P. Cruikshank, D. Gautier, P. J. Gierasch, L. Horn, R. Koppany and C. Ponnamperuma, *Science*, **212**, (1980) 192-200

[124]. B. Bezard, A. Marten and G. Paubert, *Bull. Am. Astron. Soc.*, **24**, (1992) 953

[125]. A. Marten, T. Hidayat, Y. Biraud and R. Moreno, *Icarus*, **158**, (2002) 532-544

[126]. J. L. Fox and R. V. P. Yelle, *Geophys. Res. Lett.*, **24**, (1997) 2179-2182

[127]. V. Vuitton, R. V. Yelle and M. J. McEwan, *Icarus*, **191**, (2007) 722-42

[128]. R. C. Dunbar and S. Petrie, *Astrophys. J.*, **564**, (2002) 792-802

[129]. J. S. Knight, C. G. Freeman, M. J. McEwan, N. G. Adams and D. Smith, *Int. J. Mass Spec. Ion Phys.*, **67**, (1985) 317-330

[130]. A. B. Raksit and D. K. Bohme, *Int. J. Mass Spec. Ion Proc.*, **57**, (1984) 211-224

[131]. A. Fox, A. B. Raksit, S. Dheandhandoo and D. K. Bohme, *Can. J. Chem.*, **64**, (1986) 399-403

[132]. A. J. Alexander, H. W. Kroto and D. R. M. Walton, *J. Molec. Spec.*, **62**, (1976) 175-180

[133]. S. Haas, G. Winnewisser and K. M. T. Yamada, *Can. J. Chem.*, **72**, (1994) 1165-1178

[134]. L. Bizzocchi, C. Degli Eposti and P. Botschwina, *J. Molec. Spec.*, **225**, (2004) 145-151

[135]. Y. Trolez and J.-C. Guillemin, *Angew. Chem. Int. Ed.*, **44**, (2005) 7224-7226

[136]. L. Brandsma, *Preparative Acetylinic Chemistry*, Elsevier Science Publishing BV, New York, (1988)

[137]. H. Melville and B. G. Gowenlock, *Experimental Methods in Gas Reactions*, Macmillan, London, (1964)

[138]. A. D. Sen, W. D. Huntress, V. Anicich, M. J. McEwan and A. B. Denison, *J. Chem. Phys.*, **94**, (1991) 5462-5470

[139]. Gaussian 03, Revision C.02, M. J. Frisch, G. W. Trucks, H. B. Schlegel, G. E. Scuseria, M. A. Robb, J. R. Cheeseman, J. A. Montgomery, T. V. Jr, K. N. Kudin, J. C. Burant, J. M. Millam, S. S. Iyengar, J. Tomasi, V. Barone, B. Mennucci, M. Cossi, G. Scalmani, N. Rega, G. A. Petersson, H. Nakatsuji, M. Hada, M. Ehara, K Toyota, R. Fukuda, J. Hasegawa, M. Ishida, T. Nakajima, Y. Honda, O. Kitao, H. Nakai, M. Klene, X. Li, J. E. Knox, H. P. Hratchian, J. B. Cross, C. Adamo, J. Jaramillo, R. Gomperts, R. E. Stratmann, O. Yazyev, A. J. Austin, R. Cammi, C. Pomelli, J. W. Ochterski, P. Y. Ayala, K. Morokuma, G. A. Vot, P. Salvador, J. J. Dannenberg, V. G. Zakrzewski, S. Dapprich, A. D. Daniels, M. C. Strain, O. Farkas, D. K. Malick, A. D. Rabuck, K. Raghavachari, J. B. Foresman, J. V. Ortiz, Q. Cui, A. G. Baboul, S. Clifford, J. Cioslowski, B. B. Stefanov, G. Liu, A. Liashenko, P. Piskorz, I. Komaromi, R. L. Martin, D. J. Fox, T. Keith, M. A. Al-Laham, C. Y. Peng, A. Nanayakkara, M. Challacombe, P. M. W. Gill, B. Johnson, W. Chen, M. W. Wong, C. Gonzalez and J. A. Pople, Gaussian Inc., Wallington CT, 2004.

[140]. L. A. Curtiss, K. Raghavachari, P. C. Redfern, V. Rassalov and J. A. Pople, *J. Chem. Phys.*, **109**, (1998) 7764-7776

[141]. P. Botschwina, A. C. Heyl, M. Oswald and T. Hisano, *Spectrochim. Acta*, **53A**, (1997) 1079-1090

[142]. D. K. Bohme, G. I. Mackay and H. I. Schiff, *J. Chem. Phys.*, **73**, 4976-4986 (1980)

[143]. M. J. McEwan, C. L. McConnell, C. G. Freeman and V. G. Anicich, *J. Phys. Chem.*, **98**, (1994) 5068-5073

[144]. D. Smith and N. G. Adams, *Int. J. Mass Spec. Ion Proc.*, **76**, (1987) 307-317

[145]. D. Clary, D. Smith and N. G. Adams, *Chem. Phys. Lett.*, **119**, (1985) 320-326

[146]. D. Clary, C. E. Dateo and D. Smith, *Chem. Phys. Lett.*, **167**, (1990) 1-6

[147]. C. A. Deakyne, M. Mautner, T. J. Buckley and R. Metz, *J. Chem. Phys.*, **86**, (1987) 2334-2342

[148]. E. P. L. Hunter and S. G. Lias, *J. Phys. Chem. Ref. Data*, **27**, (1998) 413-656

[149]. J. L. Fox and R. V. Yelle, *Geophys. Res. Lett.*, **21**, (1997) 2179-2182

[150]. P. D. Godfrey, R. D. Brown, B. J. Robinson and M. W. Sinclair, *Astrophys. Lett.*, **12**, (1973) 119-121

[151]. J. E. Dickens, W. M. Irvine, C. H. DeVries and M. Ohishi, *Astrophys. J.*, **479**, (1997) 307-312

[152]. N. Balucani, L. Cartechini, A. Bergeat, P. Casavecchia and G. G. Volpi, *European Space Agency Special Publication*, **SP496**, (2001) 159-162

[153]. P. Redondo, F. Pauzat and Y. Ellinger, *Planet. Space Sci.*, **54**, (2006) 181-187

[154]. M. J. McEwan, A. B. Denison, W. T. Huntress, V. G. Anicich, J. Snodgrass and M. T. Bowers, *J. Phys. Chem.*, **93**, (1989) 4064-4068

[155]. L. Halonen and G. Duxbury, *J. Chem. Phys.*, **83**, (1985) 2091-2096

[156]. G. Duxbury, H. Kato and M. Le Lerre, *Faraday Discuss.*, **71**, (1981) 97-110

[157]. M. Allegrini, J. W. C. Johns and A. R. W. McKellar, *J. Chem. Phys.*, **70**, (1979) 2829-2833

[158]. D. R. Johnson and F. J. Lovas, *Chem. Phys. Lett.*, **15**, (1972) 65-68

[159]. G. Duxbury and M. L. Le Lerre, *J. Molec. Spec.*, **92**, (1982) 326-348

[160]. D. J. DeFrees and W. J. Hehre, *J. Phys. Chem.*, **82**, (1978) 391-393

[161]. J. L. Holmes, F. P. Lossing and P. M. Mayer, *Chem. Phys. Lett.*, **198**, (1992) 211-213

[162]. G. De Oliveira, J. M. L. Martin, I. K. C. Silwal and J. F. Liebman, *J. Comput. Chem.*, **22**, (2001) 1297-1305

[163]. P. Burgers, J. L. Holmes and J. K. Terlouw, *JACS*, **106**, (1984) 2762-2764

[164]. D. R. Johnson, F. J. Lovas, C. A. Gottlieb, E. W. Gottlieb, M. M. G. Litvak, M and P. Thaddeus, *Astrophys. J.*, **218**, (1977) 370-376

[165]. R. K. Khanna, *Icarus*, **177**, (2005) 116-121

[166]. P. F. Wilson, C. G. Freeman and M. J. McEwan, *Int. J. Mass Spec. Ion Proc.*, **128**, (1993) 83-89

[167]. S. D. Prodnuk, S. Gronert, V. M. Bierbaum and C. H. DePuy, *Org. Mass Spec.*, **27**, (1992) 416-422

[168]. J. H. Bowie and B. D. Williams, *Aust. J. Chem.*, **27**, (1974) 769-775

[169]. J. L. Franklin, Y. Wada, P. Natalis and P. M. Hierl, *J. Phys. Chem.*, **70**, (1966) 2353-2361

[170]. R. V. Yelle and V. Vuitton, *Private Communication*,

[171]. H. Bock and R. Dammel, *Chem. Ber.*, **120**, (1987) 1961-1970

[172]. B. Braillon, M. C. Larne and J. M. Denis, *Nouveau J. Chim.*, **6**, (1982) 121

[173]. H. Bock and R. Dammel, *Angew. Chem. Int. Ed.*, **26**, (1987) 504-526

[174]. NIST Chemistry Webbook, webbook.nist.gov/chemistry/

[175]. J. M. Stout and C. E. Dykstra, *JACS*, **117**, (1995) 5127-5132

[176]. T. Su and M. T. Bowers, *Int. J. Mass Spec. Ion Phys.*, **12**, (1973) 347

[177]. J. A. Herman, K. Herman and T. B. McMahon, *J. Am. Soc. Mass Spec.*, **2**, (1990) 220

[178]. D. M. Jackson, N. J. Stibrich, N. G. Adams and L. M. Babcock, *Int. J. Mass Spec.*, **243**, (2005) 243

[179]. P. Spanel and D. Smith, *Int. J. Mass Spec.*, **176**, (1998) 203

[180]. S. G. Lias, J. E. Bartmess, J. F. Liebman, J. L. Holmes, R. D. Levin and W. G. Mallard, *J. Phys. Chem. Ref. Data*, **17**, (1988) Suppl. 1

[181]. G. Baykut, F. W. Brill and J. R. Eyler, *Comb. Sci. Tech.*, **45**, (1986) 233-243

[182]. E. Herbst, N. G. Adams and D. Smith, *Astrophys. J.*, **269**, (1983) 329

[183]. D. Smith and N. G. Adams, *Int. J. Mass Spec. Ion. Proc.*, **76**, 307-317 (1987)

[184]. S. G. Lias, J. E. Bartmess, J. F. Liebman, J. L. Holmes, R. D. Levin and W. G. Mallard, *J. Phys. Chem. Ref. Data*, **17**, (1998) Suppl. 1

[185]. M. Mautner, *Int. J. Mass Spec.*, **227**, (2003) 525-554

[186]. J. E. Szulejko and T. B. MacMahon, *Int. J. Mass Spec. Ion. Proc.*, **109**, (1991) 279

[187]. D. B. M. Milligan, D. A. Fairley, M. Mautner and M. J. McEwan, *Int. J. Mass Spec.*, **179/180**, (1998) 285-291

[188]. M. Mautner, *Private Communication*, (2008)

[189]. M. T. Bowers, L. Shuying, P. Kemper, R. Stradling, H. Webb, D. H. Aue, J. R. Gilbert and K. R. Jennings, *JACS*, **102**, (1980) 4830-4832

[190]. D. H. Aue, W. R. Davidson and M. T. Bowers, *JACS*, **98**, (1976) 6700

[191]. V. Vuitton, R. V. Yelle and V. G. Anicich, *Astrophys. J.*, **647**, (2006) L175-L178

[192]. R. V. Yelle and V. Vuitton, *Private Communication*, (2007)

[193]. J.-M. Bernard, P. Coll, A. Coustensis and F. Raulin, *Planet. Space Sci.*, **51**, (2003) 1003-1011

[194]. P. Spanel and D. Smith, *Med. & Biol. Eng. & Computing*, **34**, (1996) 409-419

[195]. C. G. Freeman and M. J. McEwan, *Aust. J. Chem.*, **55**, (2002) 491-494

[196]. D. B. Milligan, G. J. Francis, B. J. Prince and M. J. McEwan, *Anal. Chem.*, **79**, (2007) 2537-2540

[197]. P. F. Wilson, D. B. Milligan, L. W. Lam, C. G. Freeman and M. J. McEwan, *J. Am. Soc. Mass. Spec.*, **13**, (2002) 1028

[198]. W. Lindinger, A. Hansel and A. Jordan, *Int. J. Mass. Spec. Ion. Proc.*, **173**, (1997) 191

[199]. T. Fujii, *Mass Spec. Rev.*, **19**, (2000) 111-138

[200]. R. V. Hodges and J. L. Beachamp, *Anal. Chem.*, **48**, (1976) 825-829

[201]. T. Fujii, *Anal. Chem.*, **64**, (1992) 775-778

[202]. K. G. Spears and E. E. Ferguson, *J. Chem. Phys.*, **59**, (1973) 4174-4183

[203]. R. L. Woodin and J. L. Beauchamp, *Chem. Phys.*, **41**, (1979) 1-9

[204]. J. P. Blewett and E. J. Jones, *Phys. Rev.*, **50**, (1936) 464-468

[205]. T. Fujii and M. Ohta, *J. Phys. D: Appl. Phys.*, **28**, (1995) 1268-72

[206]. S. K. Allison and M. Kamegai, *Rev. Sci. Instrum.*, **32**, (1961) 1090-1092

[207]. B. R. Rowe, A. A. Viggiano, F. C. Fehsenfeld, D. W. Fahey and E. E. Ferguson, *J. Chem. Phys.*, **76**, (1982) 742-743

[208]. D. Smith, N. G. Adams, E. Alge and E. Herbst, *Astrophys. J.*, **272**, (1983) 365-368

[209]. A. W. Castleman and R. G. Keesee, *Chem. Rev.*, **86**, (1986) 589-618

[210]. R. W. Taft, F. Anvia, J.-F. Gal, S. Walsh, M. Capon, M. C. Holmes, K. Hosn, G. Oloumi, R. Vasanwala and S. Yazdani, *Pure Appl. Chem.*, **62**, (1990) 17

[211]. P. Burk, I. A. Koppel, I. Koppel, R. Kurg, J.-F. Gal, P.-C. Maria, M. Herreros, R. Notario, J.-L. M. Abboud, F. Anvia and R. W. Taft, *J. Phys. Chem. A*, **104**, (2000) 2824-2833

[212]. R. H. Staley and J. L. Beachamp, *JACS*, **97**, (1975) 5920

[213]. M. T. Rodgers and P. B. Armentrout, *J. Phys. Chem. A*, **101**, (1997) 1238-49

[214]. J. C. Amicangelo, *J. Phys. Chem. A*, **104**, (2000) 11420-11432

[215]. T. Kar, R. Ponec and A. B. Sannigrahi, *J. Phys. Chem. A*, **105**, (2001) 7737-7744

[216]. T. Fujii, H. Tokiwa, H. Ichikawa and H. Shinoda, *Theochem*, **277**, (1992) 251-262

[217]. S. Petrie, *J. Phys. Chem. A*, **107**, (2003) 10441-10449

[218]. M. Ueda, R. R. Silva, R. M. Oliveira, H. Iguchi, J. Fujita and K. Kadota, *J. Phys. D: Appl. Phys.*, **30**, (1997) 2711-2716

[219]. forums.ni.com/ni/